

**Autonomous Driving Control Strategies for Multi-Trailer Articulated
Heavy Vehicles with Active Safety System**

by

Amir Rahimi

A thesis submitted to the
School of Graduate and Postdoctoral Studies in partial
fulfillment of the requirements for the degree of

**Doctor of Philosophy
in Mechanical Engineering**

Faculty of Engineering and Applied Science
University of Ontario Institute of Technology (Ontario Tech University)
Oshawa, Ontario, Canada
May 2023

© Amir Rahimi, 2023

THESIS EXAMINATION INFORMATION

Submitted by: **Amir Rahimi**

Doctor of Philosophy in Mechanical Engineering

Thesis title: Autonomous Driving Control Strategies for Multi-Trailer Articulated Heavy Vehicles with Active Safety System

An oral defense of this thesis took place on May 19th, 2023 in front of the following examining committee:

Examining Committee:

Chair of Examining Committee	Prof. Bale Reddy
Research Supervisor	Prof. Yuping He
Examining Committee Member	Prof. Moustafa El-Gindy
Examining Committee Member	Prof. Xianke Lin
University Examiner	Prof. Mohamed Youssef
External Examiner	Prof. Bruce Minaker, University of Windsor

The above committee determined that the thesis is acceptable in form and content and that a satisfactory knowledge of the field covered by the thesis was demonstrated by the candidate during an oral examination. A signed copy of the Certificate of Approval is available from the School of Graduate and Postdoctoral Studies.

ABSTRACT

This study aims to develop automated driving strategies and integrated active control system for multi-trailer articulated heavy vehicles (MTAHVs) to enhance road transport efficiency, directional performance, and safety. To this end, a MTAHV with the configuration of A-train double was selected to be the subject vehicle, and the required vehicle models were generated. The corresponding nonlinear TruckSim model was employed as the virtual for co-simulations. The original contributions of the thesis in autonomous driving control of MTAHVs include: 1) a lateral preview driver model for MTAHVs was developed using the optimal preview control method; 2) a longitudinal motion-planning and control strategy using fuzzy sets was also devised; 3) an integrated control system was designed for coordinating autonomous driving and active trailer and dolly steering (ATDS) using a model predictive control (MPC) technique; and 4) a model-based predictive motion planning method was developed using the Frenet-Serret frame. The proposed lateral preview driver model may operate in two modes according to varied forward speed: i) in high-speed operations, the lateral stability is prioritized, and the high-speed and stability-oriented mode is activated; ii) while in low-speed curved path negotiations, the path-following off-tracking performance is emphasized, and the low-speed path-following mode is activated. It also takes benefits of the vehicle units' body-fixed reference frames for lateral deviation calculations to mimic the driver's local perception of vehicle position and reference path. If the so-called driver neuromuscular delay is set to zero, the driver model may perform as an autonomous human-like controller for vehicle lateral motion control. The devised longitudinal motion planner considers the road curvature over a preview horizon to regulate vehicle forward speed. It is featured with

the predictive and compensatory throttle/brake actuations to assure all the vehicle units' lateral stability. The MPC-based control method integrates the ATDS into the automated tractor steering and speed control, while the ATDS is activated to operate in either high-speed or low-speed mode, thereby improving the directional performance. The developed trajectory planner benefits from a model-based predictive approach to customize the generated trajectory to enhance the lateral stability in high-speed evasive maneuvers. The innovative findings of this dissertation will contribute to the advancement and development of autonomous driving control for MTAHVs.

Keywords: multi-trailer articulated heavy vehicles; autonomous driving; active trailer steering; motion planning; driver model

AUTHOR'S DECLARATION

I hereby declare that this thesis consists of original work of which I have authored. This is a true copy of the thesis, including any required final revisions, as accepted by my examiners.

I authorize the University of Ontario Institute of Technology (Ontario Tech University) to lend this thesis to other institutions or individuals for the purpose of scholarly research. I further authorize University of Ontario Institute of Technology (Ontario Tech University) to reproduce this thesis by photocopying or by other means, in total or in part, at the request of other institutions or individuals for the purpose of scholarly research. I understand that my thesis will be made electronically available to the public.



Amir Rahimi

STATEMENT OF CONTRIBUTIONS

Part of this dissertation have been published or to be published as:

A. Rahimi and Y. He, “A Review of Essential Technologies for Autonomous and Semi-autonomous Articulated Heavy Vehicles”, *Progress in Canadian Mechanical Engineering*. Volume 3, Jun. 2020, <https://doi.org/10.32393/csme.2020.1203>

Rahimi, A., Huang, W., Sharma, T., He, Y. (2022). An Autonomous Driving Control Strategy for Multi-trailer Articulated Heavy Vehicles with Enhanced Active Trailer Safety. In: Orlova, A., Cole, D. (eds) *Advances in Dynamics of Vehicles on Roads and Tracks II*. IAVSD 2021. *Lecture Notes in Mechanical Engineering*. Springer, Cham. https://doi.org/10.1007/978-3-031-07305-2_72

Shenjin Zhu, Zhituo Ni, Amir Rahimi & Yuping He (2022) On dynamic stability evaluation methods for long combination vehicles, *Vehicle System Dynamics*, 60:12, 3999-4034, <https://doi.org/10.1080/00423114.2021.1986223>

A. Rahimi, W. Huang, and Y. He, “A Longitudinal Speed Controller for Autonomous Multi-Trailer Articulated Heavy Vehicles”, *Progress in Canadian Mechanical Engineering*. Volume 4, Jun. 2021, <https://doi.org/10.32393/csme.2021.219>

Wei Huang, Mehdi Ahmadian, Amir Rahimi & Luke Steinginga (2023) Dynamics performance of long combination vehicles with active control systems, *Vehicle System Dynamics*. <https://doi.org/10.1080/00423114.2023.2194545>

A. Rahimi, W. Huang, and Y. He, “A lateral preview driver model for multi-trailer articulated heavy vehicles”, *IEEE/ASME Transactions on Mechatronics*. 2023. (to be submitted)

A. Rahimi, and Y. He, “A Longitudinal motion-planning for Autonomous Multi-Trailer Articulated Heavy Vehicles”, *International journal of heavy vehicle systems*. 2023 (to be submitted)

ACKNOWLEDGEMENTS

I am deeply grateful to my supervisor, Prof. Yuping He, for his invaluable guidance and unwavering support throughout my PhD journey. His expertise, insightful feedback, and encouragement have been instrumental in shaping my research and helping me to overcome challenges. I would also like to express my heartfelt appreciation to Dr. Wei Huang, who has been a friend and mentor to me throughout my studies. His wisdom, expertise, and generosity have been instrumental in shaping me into the researcher and person I am today.

I would like to take this opportunity to acknowledge my late father, who instilled in me a love of learning and a deep curiosity about the world. Though he is no longer with us, his memory lives on in my work. I am also grateful to my mother, who has always been a source of consistent encouragement. Her sacrifices have enabled me to pursue my dreams and achieve my goals. I would like to thank my wife for her love, patience, and unshakable solidarity throughout my PhD journey. Her understanding has been a great source of strength for me, and I am so grateful to have her by my side. Last but not least, I would like to thank my little daughters, NilaRose and Elara, who have brought so much joy and happiness to my life. Their boundless energy, curiosity, and love have been a constant source of inspiration.

TABLE OF CONTENTS

Thesis Examination Information	ii
Abstract	iii
Authors Declaration	v
Statement of Contributions.....	vi
Acknowledgements	vii
Table of Contents	viii
List of Tables	xii
List of Figures.....	xiii
List of Abbreviations and Symbols	xviii
Chapter 1. Introduction.....	1
1.1 Background	1
1.2 Motivations.....	5
1.3 Objectives of the research	7
1.3.1 Develop effective lateral preview driver models.....	7
1.3.2 Develop driver models for longitudinal motion control	8
1.3.3 Develop effective active trailer and dolly steering	8
1.3.4 Develop trajectory planning strategy for highway automated driving	8
1.4 Research methodologies.....	8
1.4.1 Develop vehicle dynamics model.....	8
1.4.2 Driver model development	9
1.4.3 Customized longitudinal driver model	9
1.4.4 Active trailer steering control	10
1.4.5 Highway automated driving trajectory planning;	10
1.5 Research contributions	10
1.5.1 A new lateral preview driver model for MTAHV automated driving.....	10
1.5.2 Global speed planner and controller for MTAHVs	11
1.5.3 Automated model-based driving for MTAHVs with ATDS	11
1.5.4 MPC-based optimal trajectory planning and automated driving for MTAHVs on highway driving scenarios	12
1.6 Thesis organization.....	12
Chapter 2. Literature review	13
2.1 Introduction	13

2.2 Types of MTAHVs.....	13
2.3 Dynamic performance of AHVs.....	16
2.3.1 Directional performance measures	17
2.4 Active trailer control systems	24
2.4.1 Active trailer steering for AHVs, control methods and performance improvements	24
2.5 Autonomous driving for AHVs	28
2.5.1 Lateral motion and stability control.....	28
2.5.2 Longitudinal motion control	32
2.6 Driver models for MTAHVs	33
Chapter 3. MTAHV modelling and validation.....	36
3.1 Introduction	36
3.2 Fundamental linear yaw-plane model	37
3.2.1 Linear vehicle model extension	39
3.2.2 Non-linear yaw-plane model	42
3.2.3 TruckSim model	46
3.3 5-DOF-based linear vehicle model verification	48
3.3.1 Vehicle model verification under high-speed maneuver	50
3.3.2 Vehicle model verification under low-speed maneuver	55
3.4 Summary	59
Chapter 4. Driver model development	60
4.1 Introduction	60
4.2 Preview/predictive driver models.....	64
4.3 Lateral preview driver model methodology	66
4.3.1 Low-speed path-following mode (First mode):.....	68
4.3.2 High-speed lateral stability mode (Second mode):.....	73
4.4 Driver model validation.....	78
4.5 Summary	91
Chapter 5. A longitudinal speed control strategy for MTAHVs	93
5.1 Introduction	93
5.2 Longitudinal Motion Control Methodology	95
5.3 Fuzzy controller.....	103
5.4 Simulation results and discussion.....	105

5.5 Summary	113
Chapter 6. Model-based predictive autonomous driving control strategies for MTAHVs with active trailer and dolly steering.....	114
6.1 Introduction	114
6.2 Autonomous driving and active trailer and dolly steering control method	116
6.2.1 Model predictive control method	117
6.2.2 Non-linear model predictive control design	117
6.2.3 Autonomous driving control.....	122
6.2.4 Active Trailer and Dolly Steering	122
6.3 Simulation results	124
6.4 Summary	132
Chapter 7. Model-predictive-based motion planning for highway operations of autonomous MTAHVs.....	133
7.1 Introduction	133
7.2 Frenet-Serret coordinate system.....	135
7.3 Coordinates transformation between Frenet and Cartesian frames	137
7.4 Local trajectory generation for highway scenario	140
7.4.1 Cruise control behavior	143
7.4.2 Lane-change behavior.....	144
7.4.3 Vehicle-following behavior	145
7.5 Trajectory evaluation.....	147
7.6 Collision checking.....	148
7.7 Trajectory generation methods and case studies	155
7.8 Basic trajectory planning method (case study 1).....	156
7.9 Improving the vehicle lateral dynamics using ATDS controller (case study 2).....	161
7.10 Improving the basic trajectory generation considering the MTAHV unique dynamics using model-based predictive methodology (case study 3)	165
7.11 Trajectory generation with reduced lateral jerk (case study 4)	171
7.11.1 Incorporating the ATDS (case study 5)	176
7.11.2 Incorporating the trajectory optimization (case study 6)	180
7.12 Adaptive vehicle speed control results	185
7.13 Summary	192
Chapter 8. Conclusion and future work	193

8.1 Conclusion.....	193
8.2 Future work	196
References.....	198
Appendices.....	215
Appendix A	215
A.1 A-train double parameters	215
A.2 Fundamental linear model state-space matrices	216
A.3 State-space matrices of fundamental linear model extension.....	217
A.4 State-space matrices of non-linear extension of fundamental linear model	219

LIST OF TABLES

CHAPTER 1

Table 1.1 The U.S. and Canada motor vehicle crashes and human factor involvement [1][2]	1
Table 1.2. Levels of driving automation, reproduced from [14].....	4

CHAPTER 2

Table 2.1. Longitudinal and directional performance issues of AHVs.....	17
Table 2.2 The improvements achieved by the controller that was created for different heavy vehicle combinations are summarized in [48].	27

CHAPTER 7

Table 7.1. The case studies developed by combining the ATDS, optimization and preview time required for trajectory generation	155
--	-----

LIST OF FIGURES

CHAPTER 1

Figure 1.1 Past and future evolution of driving assistance functions from market perspective, reproduced from [5]	2
Figure 1.2. Vehicles automated driving timeline.....	3

CHAPTER 2

Figure 2.1. Different types of vehicle units and couplings used in AHVs [25].....	14
Figure 2.2. Three common LCV configurations in North America [27].....	15
Figure 2.3. different ways that two trailers are hooked to one another in North America [30].....	15
Figure 2.4. Swept path width performance measure [35].....	18
Figure 2.5. Frontal swing performance metric perspective illustration (right image), tail swing performance measure illustration (left image) [35].....	19
Figure 2.6. A diagram depicting the HSTO performance measure and the overshoot/undershoot conditions [11], [21].....	23
Figure 2.7. A diagram illustrating the high-speed steady-state off-tracking (HSSO) performance measure [21].	23

CHAPTER 3

Figure 3.1. A schematic representation of the A-train double.....	37
Figure 3.2. Global and body-fixed coordinates schematics depicted for the tractor.	42
Figure 3.3. Open-loop steering input for linear model verification through high-speed lane-change maneuver.....	47
Figure 3.4. Open-loop steering input for linear model verification through high-speed lane-change maneuver.....	51
Figure 3.5. Simulation results achieved under high-speed lane-change maneuver for linear vehicle model with nominal tires cornering stiffness values (dashed lines) and the TruckSim model (solid lines): (a) side-slip angle, (b) yaw rate, (c) lateral acceleration...52	
Figure 3.6. Simulation results achieved under high-speed lane-change maneuver for the linear vehicle model with optimal tire cornering stiffness values (dashed lines) and the TruckSim model (solid lines): (a) side-slip angle, (b) yaw rate, (c) lateral acceleration...54	
Figure 3.7. Open-loop steering input for linear model verification under a low-speed maneuver.....	55
Figure 3.8. Simulation results achieved under low-speed maneuver for the linear vehicle model with the nominal tire cornering stiffness values (dashed lines) and the TruckSim (solid lines): (a) side-slip angle, (b) yaw rate, (c) lateral acceleration.....	57

Figure 3.9. Simulation results achieved under low-speed maneuver for the linear vehicle model with the optimal tire cornering stiffness values (dashed lines) and the TruckSim results (solid lines): (a) side-slip angle, (b) yaw rate, (c) lateral acceleration.58

CHAPTER 4

Figure 4.1 Schematic representation of preview driver model for A-train double MTAHV67

Figure 4.2 Simple representation of the flowchart of the proposed lateral preview driver model.....67

Figure 4.3 Geometrical method used to calculate the lateral position of the target point on the desired path described in the tractor’s body-fixed coordinate system73

Figure 4.4 Geometrical method used to calculate the 1st trailer deviation from the tractor delayed preview path described in the 1st trailer body-fixed coordinate system75

Figure 4.5 Flowchart of the algorithm used for the lateral preview driver model.....78

Figure 4.6. High-speed lane change maneuver: (a) target path geometry, (b) lateral position of vehicle units using the unified lateral preview driver model, (c) lateral position of vehicle units using the proposed driver model.81

Figure 4.7. High-speed turn: (a) target path geometry, (b) absolute values of the TFAC lateral deviation from the target path based on different driver models.84

Figure 4.8. Steering wheel angle time history: (a) proposed driver model, (b) MacAdam driver model, (c) unified driver model.....86

Figure 4.9. Comparison of the simulation results of the two modes the proposed driver model under the high-speed turn maneuver: (a) lateral displacement for path-following mode, (b) lateral displacement for lateral stability mode, (c) lateral acceleration for path-following mode, (d) lateral acceleration for lateral stability mode.87

Figure 4.10. Simulation results of the proposed driver model under the low-speed 90° turn maneuver: (a) target path, (b) TFAC and 2nd trailer RAC positions with $k_1 = 0.6, k_2 = 0.1$ and $k_3 = 0.3$, (c) TFAC and 2nd trailer RAC positions with $k_1 = k_2 = k_3 = 0$, (d) swept path width of TFAC and 2nd trailer RAC positions with $k_1 = 0.6, k_2 = 0.1$ and $k_3 = 0.3$, (e)) swept path width of TFAC and 2nd trailer RAC positions with $k_1 = k_2 = k_3 = 0$88

Figure 4.11. Simulation results under the low-speed 360° roundabout turn: (a) target path, (b) TFAC and 2nd trailer RAC trajectories with $k_1 = 0.6, k_2 = 0.1$ and $k_3 = 0.3$, (c) TFAC and 2nd trailer RAC trajectories with $k_1 = k_2 = k_3 = 0$, (d) swept path width between TFAC and 2nd trailer RAC trajectories with $k_1 = 0.6, k_2 = 0.1$ and $k_3 = 0.3$, (e) swept path width between TFAC and 2nd trailer RAC trajectories with $k_1 = k_2 = k_3 = 0$90

CHAPTER 5

Figure 5.1. Schematic diagram representing the anticipatory and compensatory control points for MTAHV speed planning.99

Figure 5.2. MTAHV performance envelope diagram	102
Figure 5.3. Speed planning and control strategy flowchart.	103
Figure 5.4. Membership functions: (a) acceleration demand as input variable, (b) throttle as first output, (c) pedal brake force as second output.	105
Figure 5.5. Lateral displacement for HSLC maneuver: (a) with controller, (b) without controller.	106
Figure 5.6. A-train double HSLC maneuver results: (a) lateral acceleration with controller (solid line) and without controller (dashed line), (b) Longitudinal speed.	108
Figure 5.7. Longitudinal and lateral accelerations shown in the g-g diagrams for HSLC maneuver: (a) with controller, (b) without controller.	109
Figure 5.8. The target path curvature diagram for a U-turn negotiation maneuver	110
Figure 5.9. U-turn negotiation results: (a) lateral acceleration, (b) longitudinal velocity, and (c) g-g diagram.	112

CHAPTER 6

Figure 6.1. Architecture of integrated autonomous driving and active safety/ maneuverability control system.	121
Figure 6.2. Schematic representation of the low-speed path-following mode (first mode).	123
Figure 6.3. Schematic representation of the high-speed lateral stability mode (second mode).	124
Figure 6.4. A-train double low-speed 90° turn maneuver results: (a) time history of the vehicle units' rear end lateral deviation from the target path, (b) vehicle's longitudinal speed time history versus the target speed, (c) required steering angles for the trailing units' axles when the ATDS is active.	126
Figure 6.5. A-train double low-speed 360° turn maneuver results: (a) time history of the vehicle units' rear end lateral deviation from the target path; (b) vehicle's longitudinal speed time history versus the target speed; (c) required steering angles for the trailing units' axles when the ATDS is active.	128
Figure 6.6. A-train double HSLC maneuver results when ATDS is inactive: (a) vehicle units' rear end lateral deviation from the target path, (b) vehicle units' CG lateral acceleration.	129
Figure 6.7. A-train double HSLC maneuver results when ATDS is active and the controller is set to operate in either the first mode or the second mode: (a) vehicle units' rear end lateral deviation from the target path, (b) vehicle units' CG lateral acceleration, (c) required steering angles for the trailing units' axles, (d) vehicle's longitudinal speed time history versus the target speed.	131

CHAPTER 7

Figure 7.1. The difference between vehicle coordinate representation in Cartesian frame versus Frenet frame, regenerated from [114].	135
---	-----

Figure 7.2 The Frenet frame representation of a sample point on the trajectory	137
Figure 7.3. Vehicle position transformation from the Cartesian frame to the Frenet frame.	138
Figure 7.4. The trajectory generated for cruise control.....	144
Figure 7.5. The trajectory generated for lane-change.	145
Figure 7.6. The trajectory generation for adaptive cruise control behavior.....	147
Figure 7.7. The vehicle shape approximation methods for collision checking: (a) multiple discs approximation, (b) box or point approximation, and (c) proposed approximation method.....	149
Figure 7.8. The trajectory generation for adaptive cruise control behavior.....	152
Figure 7.9. A-train double autonomous lane-change maneuver behavior on highway driving scenario with the preview time of 2 s (the red rectangles represent obstacle vehicles, the blue, orange and yellow rectangles represent the tractor, first trailer and second trailer respectively).....	157
Figure 7.10 A-train double's steering inputs and forward speed over the triple lane-change maneuver with the preview time of 2 sec: (a) steering input, and (b) forward speed.....	158
Figure 7.11 A-train double's dynamic responses for each vehicle unit over the triple lane- change maneuver with the preview time of 2 sec: (a) lateral displacement versus longitudinal displacement, (b) time history of lateral acceleration, (c) time history of tractor's lateral jerk, and (d) time history of yaw-rate.....	161
Figure 7.12 A-train double's steering angle input and forward speed over the triple lane- change maneuver with ATDS activated and the preview time of 2 sec: (a) steering input time history, and (b) forward speed time history.	162
Figure 7.13. A-train double's dynamic responses of each vehicle unit over the triple single lane change maneuver with ATDS activated and the preview time of 2 sec: (a) lateral displacement versus longitudinal displacement, (b) time history of lateral accelerati on, (c) time history of tractor's lateral jerk, and (d) time history of yaw-rate.....	164
Figure 7.14. Time history of required steering angle for ATDS controller during the highway autonomous driving scenario.	165
Figure 7.15. The optimized trajectory versus the initial quintic polynomial trajectory...166	166
Figure 7.16. A-train double's steering input and forward speed over the triple lane-change maneuver with the preview time of 2 sec: (a) time history of steering input, and (b) time history of longitudinal speed.....	168
Figure 7.17. A-train double's dynamic responses under the triple lane change maneuver for the model predictive-based trajectory optimization with the preview time of 2 sec: (a) lateral displacement versus longitudinal displacement, (b) time history of lateral acceleration, (c) time history of tractor's lateral jerk, and (d) time history of yaw-rate time.	171
Figure 7.18. Reserved trajectory approach for reducing lateral jerk under lane-change maneuvers.	172
Figure 7.19. A-train double's steering input and forward speed under the triple single lane- change maneuver with 1+2 sec preview time: (a) time history of steering angle input, and (b) time history of longitudinal speed.	173

Figure 7.20. A-train double’s dynamic responses under the triple lane change maneuver for the 1+2 sec preview time method: (a) lateral displacement versus longitudinal displacement, (b) time history of lateral acceleration, (c) time history of tractor’s lateral jerk, (d) time history of yaw-rate.175

Figure 7.21. A-train double’s steering angle input and forward speed under the triple single lane change maneuver for the joint effort with the 1+2 preview time and ATDA control: (a) time history of steering input, and (b) time history of forward speed.177

Figure 7.22. A-train double’s dynamic responses under the triple single lane change maneuver for the joint effort of the 1+2 sec preview time and the ATDS control: (a) lateral displacement versus longitudinal displacement, (b) time history of lateral acceleration, (c) time history of tractor’s lateral jerk, (d) time history of yaw-rate, and (e) time history of trailing units’ axles steering angle.179

Figure 7.23. A-train double autonomously executing the triple lane-change maneuver in a highway operation with the joint effort of 1+2 sec preview time and optimized trajectory generation (red rectangles representing obstacle vehicles; blue, orange and yellow rectangles representing the tractor, first trailer and second trailer, respectively).180

Figure 7.24. A-train double’s steering angle input and forward speed under the triple single lane change maneuver with the joint effort of 1+2 preview time and optimized trajectory generation method: (a) time history of steering angle input, and (b) time history of forward speed.181

Figure 7.25. A-train double’s dynamic responses under the triple lane-change maneuver with the joint effort of 1+2 preview time and optimized trajectory generation method: (a) lateral displacement versus longitudinal displacement, (b) time history of lateral acceleration, (c) time history of tractor’s lateral jerk, and (d) time history of yaw-rate..184

Figure 7.26. Performance measures of the A-train double under the triple lane-change maneuver for six combinations of trajectory generation strategies and ATDS safety system.185

Figure 7.27. A-train double autonomous adaptive cruise control in highway driving scenario for joint effort of 1+2 preview time and optimized trajectory generation (red rectangles representing obstacle vehicles; blue, orange and yellow rectangles representing tractor, first trailer, and second trailer, respectively).187

Figure 7.28. A-train double’s steering angle input and forward speed over the double lane-change maneuver for the joint effort of 1+2 preview time, optimized trajectory generation and adaptive cruise control: (a) time history of steering input, and (b) time history of forward speed.....188

Figure 7.29. A-train double’s dynamic responses over the specified maneuver for the joint effort of 1+2 preview time, optimized trajectory generation, and adaptive cruise control: (a) lateral displacement versus longitudinal displacement, (b) time history of longitudinal acceleration, (c) time history of longitudinal jerk, (d) time history of lateral acceleration, (e) time history of tractor’s lateral jerk, and (f) time history of yaw-rate.....191

LIST OF ABBREVIATIONS AND SYMBOLS

AAR	Active anti-roll
AARB	Active anti-roll bar
ACC	Adaptive cruise control
ADAS	Advanced driver assistance systems
AGV	Autonomous ground vehicle
AHV	Articulated heavy vehicle
ARC	Active roll control
ATDS	Active trailer and dolly steering
ATS	Active trailer steering
AVSS	Active vehicle safety system
CG	Center of gravity
DOF	Degrees of freedom
DLC	Double-lane-change
HIL	Hardware-in-the-loop
HSLC	High-speed lane change
HST	High-speed turn
LCV	Long combination vehicle
LQR	Linear quadratic regulator
LST	Low-speed turn
MPC	Model predictive control
MTAHV	Multi-trailer articulated heavy vehicle
NLMPC	Non-linear model predictive control
PFOT	Path-following off-tracking
PBS	Performance-based standard
PSS	Predictive safety system
RAC	Rear axle center

RSS	Reactive safety system
RWA	Rearward amplification
SLC	Single lane change
SMC	Sliding mode control
TDB	Tractor differential braking
TFAC	Tractor front axle center
TJA	Traffic jam assistant
YDC	Yaw damping coefficient

Chapter 1. Introduction

1.1 Background

The automotive industry is moving towards a new era of autonomous ground vehicles (AGVs). The term AGV refers to a vehicle that can travel under all operating conditions on and off-road without human intervention. With software, computers, sensors and wireless communications being increasingly used, the design of such vehicles is undergoing significant changes.

Table 1.1 The U.S. and Canada motor vehicle crashes and human factor involvement [1][2]

Classification	U.S.	Canada
Total crashes per year	5.5 million	0.29 million
Human causes as main factor	93%	80%
Economic costs of crashes	\$277 billion	\$37 billion
Total fatal and injurious crashes per year	2.22 million	0.16 million
Fatal crashes per year	32,367	1,895
Total fatal and injurious crashes per year involving a heavy truck	96,129	12,000

Worldwide around 1.25 million people are killed per year in road vehicle accidents [1].

Table 1.1 lists the statistical data regarding the car/truck crashes occurred only in the US and Canada in 2016. Approximately 93% of serious crashes are because of human errors.

In 2016 more than 37,000 people were killed in around 32,000 fatal motor vehicle accidents in North America [2]. Additionally, the economic costs of crashes are unbelievably high (277 billion dollars in the US). Considering these facts, the lifesaving and financial benefits of driving assistance technologies become undeniable. Autonomous ground vehicles have the potential to decline human errors from the accidents, thereby increasing the safety of passengers, drivers and pedestrians and reducing the financial costs, considerably.

Furthermore, utilizing Advanced Driver Assistance Systems (ADAS), e.g. Adaptive Cruise Control (ACC), Traffic Jam Assistant (TJA) and Collision Avoidance Systems, fatal car crashes decreased in Europe between 2001 and 2015 by 48% [3]. Figure 1.1 presents the evolution of driving assistance functions application and their potential future evolution.

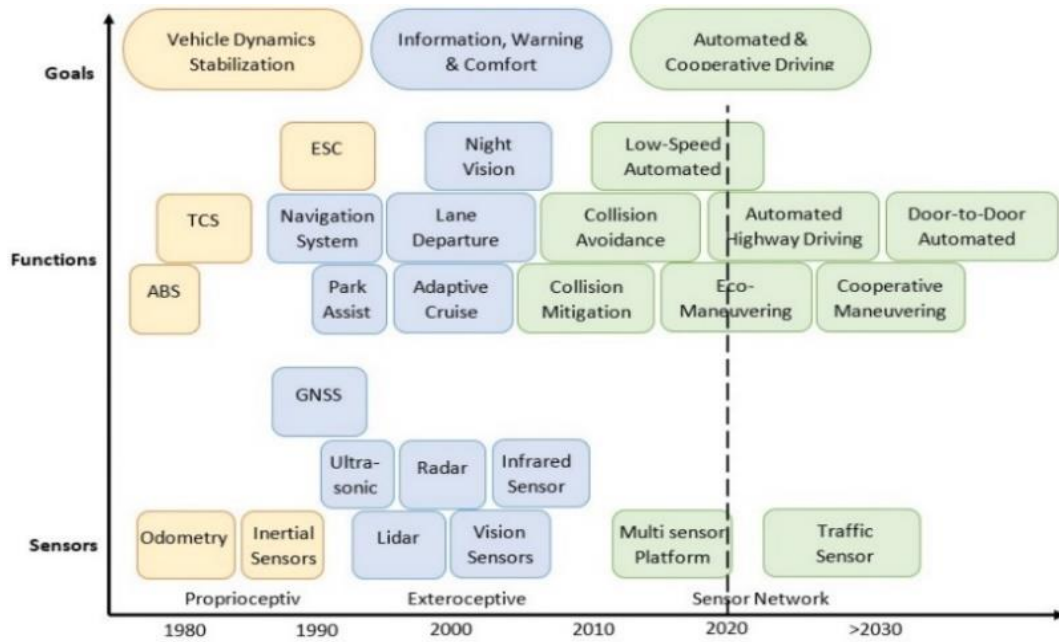


Figure 1.1 Past and future evolution of driving assistance functions from market perspective, reproduced from [5]

As the safety merits of automated driving are paramount, governments urgently need to develop vehicle safety guidelines for the design of AGVs [4]. The guidelines are expected to identify design aspects for manufacturers to consider when developing, testing and deploying such vehicles. Recently, many design methods for autonomous vehicles have been proposed, but the literature mainly focuses on semiautonomous and autonomous driving of single-unit vehicles, e.g., cars. Heavy vehicles exhibit unique high-speed lateral dynamics and low-speed maneuverability characteristics. For example, the static roll-over threshold for heavy trucks can be as low as 0.35g, whereas the rollover threshold for

passenger cars is typically 1.1g [5]. In 1997, the US National Highway Traffic Safety Administration reported more than 15,000 rollover accidents of commercial vehicles, of which 9400 were rollovers of articulated heavy vehicles (AHVs) [6]. On the other hand, mortality due to AHV accidents in the US in 2017 rose to 5.8% compared with 2016 [7]. However, little attention has been paid to autonomous driving for these large vehicles.

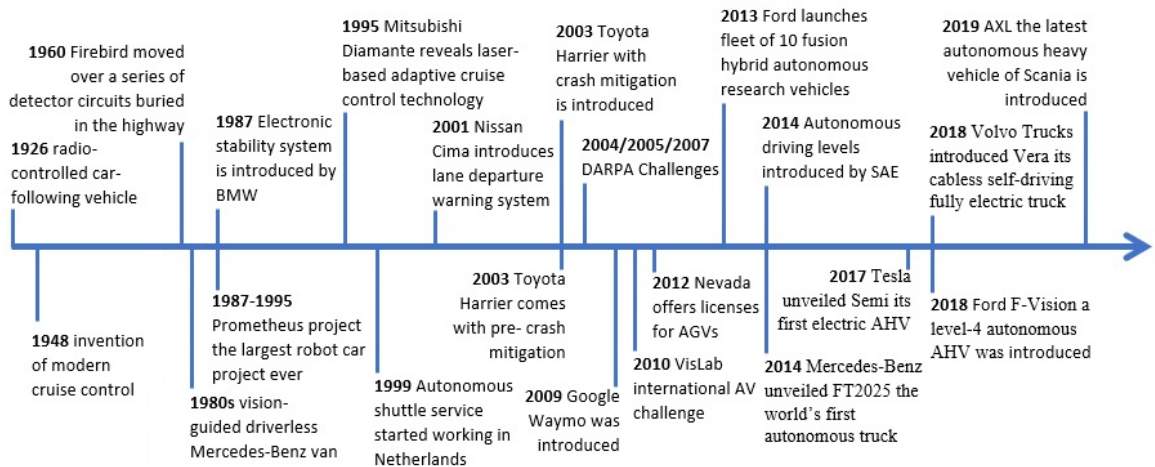


Figure 1.2. Vehicles automated driving progress timeline.

To increase vehicle safety, active vehicle safety systems (AVSSs), e.g., vehicle stability control, have been proposed, studied, and commercialized [8]. These AVSSs can be classified as reactive safety systems (RSSs), designed to react to the current vehicle state [9]. Although RSSs are effective in increasing safety, they do not consider the effect of driver mistakes. As noted earlier, human errors cause the vast majority of traffic collisions [4], and the potential resolution to the human error problem is autonomous driving [10], removing human factors from the control loop. The mass deployment of autonomous driving systems has been hindered due to the lack of effective approaches for verifying the safety of such systems in arbitrary situations [7][8]. The automated driving industry has come a long distance so far, and still there will be a long transition period, in which most

vehicles have some capabilities of autonomous driving. Figure 1.2 depicts a brief timeline of vehicles automated driving and safety functions development. Since the late 1990s, advanced driver assistance systems (ADASs), e.g., lane departure prevention, have been developed. These systems are classified as 'predictive safety systems' (PSSs), considering not only current vehicle state, but also predicted vehicle state and hazards.

The ground vehicle automation needs a standard set of terminology and regulations with a taxonomy and definitions to coordinate all the efforts made in this field. In 2014 SAE International introduced a standard J3016 to facilitate collaboration and simplify communication within technical and policy domains. Table 1.2 summarizes the levels of driving automation based on this standard. The last two decades have witnessed extensive research of semi-autonomous vehicles, which are human driven vehicles with autonomous driving capabilities [11]. These vehicles are level 2/3 automated vehicles [12].

Table 1.2. Levels of driving automation, reproduced from [14].

Level	Name	Dynamic Driving Task (DDT)		DDT Fallback	Operational Design Domain (ODD)
		Sustained lateral and longitudinal vehicle motion control	Object and Event Detection and Response (OEDR)		
Driver performs part or all of the DDT					
0	No Driving Automation	Driver	Driver	Driver	N/A
1	Driver Assistance	Driver and System	Driver	Driver	Limited
2	Partial Driving Automation	System	Driver	Driver	Limited
Automated Driving System (ADS "System") performs the entire DDT (while engaged)					
3	Conditional Driving Automation	System	System	Fallback-ready user	Limited
4	High Driving Automation	System	System	System	Limited
5	Full Driving Automation	System	System	System	Unlimited

To date, the research activities in semi-autonomous and autonomous driving have mainly been dedicated to passenger cars. Heavy goods vehicles represent a 7.5 times higher risk

than passenger cars in highway operations [13]. However, much less attention has been paid to exploring the PSSs for articulated vehicles and in particular, MTAHVs. Recently, few studies tackled autonomous driving for articulated construction vehicles [14]–[16], articulated vehicles with automated reverse parking [15], and construction truck [16]. These autonomous systems were designed only considering low-speed trajectory planning and tracking based on kinematic control, neglecting the high-speed dynamic behaviors of articulated vehicles, e.g. trailer sway, jackknifing, and rollover. The interactions of human-machine have been explored for improving the ADAS of articulated vehicles [17][18]. But few attempts have been made to explore semi-autonomous and full autonomous driving for AHVs and, in particular, MTAHVs.

1.2 Motivations

The main design objectives of autonomous driving systems for road vehicles are to increase the safety of operations and improve transportation efficiency. Multi-trailer articulated heavy vehicles are being increasingly used on highways. In comparison with a single-trailer AHV, the application of the MTAHV with the structure of A-train double can reduce the mileage travelled by 44%, decrease the fuel consumption and the greenhouse emission by 32% and reduce the tire-road wear by 40% [19]. Despite these benefits, MTAHVs exhibit poor low-speed maneuverability and low high-speed lateral stability due to their multi-unit structures, large sizes and high CGs. In high-speed transient curved path negotiations, MTAHVs generally experience exaggerated lateral/yaw motions of trailing vehicle units when performing an evasive maneuver. This dynamic phenomenon is known as rearward amplification (RWA) [20]. The trailer positioned at the back of a tractor-trailer combination typically experiences greater lateral acceleration than the tractor, and as a

result, may be more susceptible to rolling over. It's possible that this rear trailer could be the first to tip over. Unfortunately, drivers may not become aware of the rollover until it's too late to make any necessary corrective maneuvers. [21]. The human driver controls the MTAHV mainly based on the motion cues of the leading vehicle unit, since the perceived motion cues from trailing vehicle units are very weak due to the filtering function of the suspension of tractor cabin, articulation joints, etc. [22]. Multi-trailer articulated heavy vehicle driving poses stringent requirements on drivers in terms of training, skills, and experience.

Multi-trailer articulated heavy vehicles play an important role in freight transport, particularly for the movement of goods and supplies over long distances. Thus, improving the safety and efficiency of MTAHVs can have a significant impact on the economy, as well as on the lives of people who rely on the goods that these vehicles transport. Autonomous and semi-autonomous driving technologies have the potential to revolutionize the transportation industry by making it safer, more efficient, and more sustainable. By automating the driving process either entirely or partially, MTAHVs could operate more smoothly and with fewer accidents, improving safety for both drivers and other road users.

With the growing demand for MTAHVs, it is becoming increasingly important to develop technologies that can improve their safety and performance. Active safety systems such as active trailer steering (ATS) that integrate sensors, control algorithms, and other technologies can help prevent accidents and improve the overall safety of MTAHVs.

The current MTAHV safety technology is limited, and there is a need for more research in this area to better understand the safety challenges and develop effective solutions. Autonomous driving and active safety control of MTAHVs is a critical research area that

can address these challenges and pave the way for more advanced and safer MTAHVs in the future.

The development of autonomous driving and active safety control technologies for MTAHVs can achieve significant economic benefits in terms of reducing transportation costs and improving the overall efficiency of the transportation industry. By reducing fuel consumption, tire wear, and other costs associated with MTAHVs, these technologies can make the industry more competitive and sustainable.

Autonomous driving and active safety control systems developed for MTAHVs can also address the problem of driver fatigue, which is a common issue for drivers of these vehicles. By automating the driving process, drivers can focus on other tasks, reducing the risk of fatigue-related accidents and improving overall driver well-being.

1.3 Objectives of the research

The specific objectives of the present study regarding the motion control of MTAHVs are described as follows:

1.3.1 Develop effective lateral preview driver models

An effective lateral preview driver model for MTAHVs based on the conventional MacAdam driver model, which was originally designed for single-unit vehicles, will be developed. This driver model will be adapted to the unique dynamics of the MTAHVs including the high-speed lateral instability and low-speed maneuverability to perform the path-following task accordingly. Furthermore, a model predictive-based driver model will be developed considering the aforementioned dynamics features of MTAHVs. These two driver models could be implemented for automated driving of MTAHVs.

1.3.2 Develop driver models for longitudinal motion control

A longitudinal global speed planning and control strategy customized for MTAHVs considering their distinctive dynamics and multi-unit structures for lateral stability improvement will be proposed. Additionally, a non-linear model predictive-based longitudinal speed controller integrated into the lateral MPC control strategy will be developed to present a comprehensive driver model for MTAHVs' automated motion control in various driving scenarios.

1.3.3 Develop effective active trailer and dolly steering

An integrated driving and safety control strategy including the previously noted lateral and longitudinal autonomous motion control and a model predictive-based active trailer and dolly steering (ATDS) controller will be developed and tailored for MTAHVs.

1.3.4 Develop trajectory planning strategy for highway automated driving

A motion planning method considering the vehicle speed and acceleration for local speed planning and control will be developed for MTAHVs. Similarly, this control strategy which includes vehicle speed maintaining, obstacle avoidance and adaptive speed control behaviors, will be customized for an A-train double AHV so as to improve the path-following performance and reduce the lateral instability in highway evasive driving scenarios such as lane-change maneuver.

1.4 Research methodologies

1.4.1 Develop vehicle dynamics model

In order to design the model-based controllers, vehicle dynamics models should be developed. Hence, the equations of motion for an A-train double AHV, which is the only configuration considered for all the controller designs in this dissertation, were generated

and then coded in MATLAB and the basic linear vehicle model was developed. Two linear and non-linear extensions of the fundamental linear model were also developed. To make the vehicle model performance close to the TruckSim non-linear model an optimization method involving a cost function consists of yaw-rates and side-slip angles of the vehicle units was generated. Minimizing the cost function results in proper cornering stiffness values that makes the linear model performance response similar to the TruckSim non-linear high-fidelity model. In order to verify the vehicle model's accuracy, open-loop co-simulations were conducted by giving the same steering input to the vehicle model and the non-linear high fidelity TruckSim A-train double model under high-speed and low-speed maneuvers, and the critical vehicle states were then compared.

1.4.2 Driver model development

To develop the first lateral preview driver model, the optimal preview control technique was implemented using a 5-DOF linear vehicle model. To design the second lateral driver model, a non-linear model predictive control method (NLMPC) was employed. As the model-predictive-based driver model also controls the longitudinal acceleration by setting the desired speed, a simple dynamics approximation of the vehicle longitudinal motion was also integrated into the dynamics state-space equations.

1.4.3 Customized longitudinal driver model

As the upper layer of the longitudinal motion controller for the A-train double, a simple kinematical method was utilized for the global speed planning and a fuzzy control strategy was used in order to implement the throttling and braking. Co-simulation with TruckSim was performed to verify the controller capabilities in various driving scenarios.

1.4.4 Active trailer steering control

The steering demand for the trailers' and dolly's wheels of the A-train double was also calculated using the NLMPC. The required vehicle dynamics equations which are the same as the model predictive-based driver model, as well as the controller itself were coded in MATLAB. The ATDS performance was then investigated through various maneuvers via co-simulations with TruckSim.

1.4.5 Highway automated driving trajectory planning;

In order to carry out the trajectory planning for A-train double AHV, a quintic polynomial was generated frequently at each time step, using the current and the desired final states of the vehicle over the preview horizon of the planning, in the Frenet-Serrete coordinate system. Then the developed optimal driver model was employed to follow the path and a model predictive longitudinal controller adjusted the acceleration according to the desired speed. A model predictive strategy was also applied to enhance the trajectory generated to reduce the rearward amplification in obstacle avoidance maneuvers.

1.5 Research contributions

1.5.1 A new lateral preview driver model for MTAHV automated driving

A novel lateral preview driver model considering the motion cues of all vehicle unit's in order to find the optimal tractor steering is introduced. The optimal preview-based controller uses the vehicle body-fixed coordinate systems of all the vehicle units and as a result can perform well over a wide range of driving scenarios. The driver model has two modes, namely high-speed lateral stability and low-speed path-following. The superior performance of the low-speed operation of this driver model in sharp turns is one of the features distinguishing this driver model from the others.

1.5.2 Global speed planner and controller for MTAHVs

A new autonomous speed planner/controller mimicking a skilled driver and taking advantage of the vehicle performance envelope is proposed for an A-train double AHV. The controller makes use of a compensatory approach considering all the vehicle units' states to tackle the vehicle's inaccurate states prediction over the preview horizon estimated by the anticipatory strategy. The proposed speed planner/controller uses both previewed and real-time MTAHV states, and the main goal is to limit the lateral acceleration within a desirable range based upon the curvature of the road, by adjusting the vehicle speed well in advance. Hence, it also operates as a predictive safety system to improve the lateral stability.

1.5.3 Automated model-based driving for MTAHVs with ATDS

A novel automated driving strategy for MTAHVs is proposed, which is integrated with ATDS safety system. A non-linear model predictive control strategy is used to control the MTAHV longitudinally and laterally. It also simultaneously determines the required steering for the trailers' and dolly's wheels to maintain the lateral stability and improve the maneuverability, accordingly. The controller considers all the vehicle units' states in order to determine the required steering for the towing and trailing units. The controller is characterized in a way that over high-speed driving scenarios maintaining the lateral stability has the highest priority, while during the low-speed scenarios the maneuverability matters more. Hence, the proposed controller features two operating modes.

1.5.4 MPC-based optimal trajectory planning and automated driving for MTAHVs on highway driving scenarios

Similarly, the trajectory planning also features a tailored strategy for the A-train double AHV. It distinguishes itself by introducing an MPC-based trajectory improvement for the initial trajectory generated for the vehicle. The proposed method considers the yaw rates and lateral accelerations of the last vehicle unit in order to reduce the rearward amplification under evasive high-speed maneuvers such as obstacle avoidance scenario. The proposed global speed planning and control strategies as well as the ATDS controller are also integrated with the trajectory planning to not only increase the level of autonomy but also enhance the safety.

It is shown that by improving the trajectory, the required steering for the tractor front axle to perform the lane-change maneuver is decreased remarkably. Additionally, it is illustrated that adapting the proposed method to generate the optimal trajectory is even much more efficient than utilizing the ATDS to reduce the instability issues in highway lane-change maneuver. This confirms the remarkable improvement in energy consumption and less tire wear due to reduced steering for the tractor and neglecting the use of trailing units' steering to tackle obstacle avoidance scenarios. Furthermore, the risk of lateral instability is diminished dramatically due to considerable reduction in RWA to perform a highway lane-change maneuver.

1.6 Thesis organization

The thesis organization is as follows. In Chapter 2, an extensive literature review on the MTAHVs and the related dynamic performance issues, active control systems, autonomous driving strategies and the driver models has been conducted. Several MTAHV's models

and their validation are presented in Chapter 3. In Chapter 4, a new lateral driver model for MTAHVs using the optimal preview control method is developed. Chapter 5 includes a speed planning and control strategy for MTAHVs. A model-based predictive autonomous lateral and longitudinal MTAHV control integrated with active trailer steering is studied in Chapter 6. In Chapter 7, a model-based predictive trajectory planning for MTAHVs is devised. Finally, in Chapter 8 the conclusions are drawn.

Chapter 2. Literature review

2.1 Introduction

This chapter first sheds a light on the types of AHVs including multi-trailer ones and introduces the common configurations. Secondly, the common dynamic performance issues and the performance-based standards to evaluate the AHVs' directional performance during various maneuvers are discussed. Thirdly, the active trailer control systems for AHVs are elaborated and especially the active trailer steering system which is considered for increasing the safety of A-train double AHV in the current dissertation is reviewed and discussed. Then, the autonomous driving requirements and the studies conducted in this field for the AHVs will be reviewed. Finally, the driver models developed for MTAHVs will be surveyed.

2.2 Types of MTAHVs

A MTAHV refers to a combination of a tractor and 2 or more trailing units surpassing a length or weight limit that usually vary from one country to another. For example, in

Canada a minimum total length of 27.5 m is used [23], while a minimum gross vehicle weight of 80,000 pounds is considered in the USA in the definition of MTAHV [24]. Figure 2.1 shows the constituent units of AHV [25]. Although most countries use conventional heavy vehicle combinations with a maximum length of 18.75 m and a weight of 40 tons, some countries have laws permitting longer combination vehicles. For example, Sweden and Finland allow LCVs with lengths and weights of up to 25.25 m and 60 tons respectively [26].

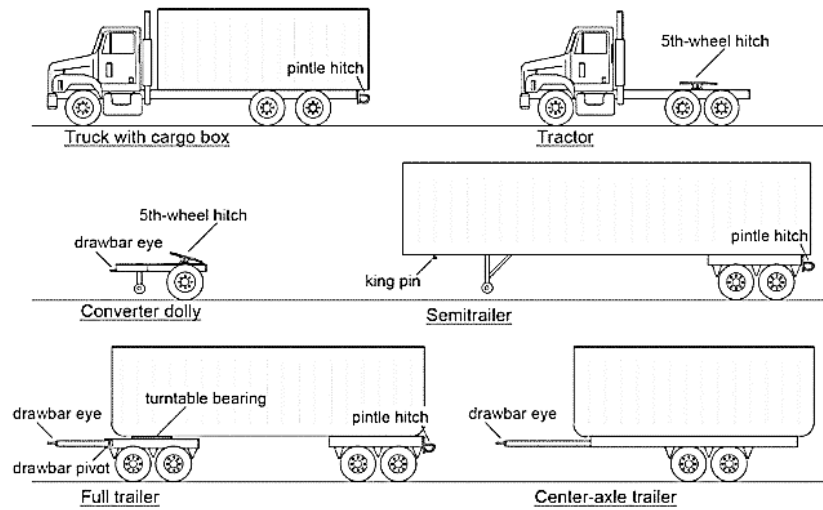


Figure 2.1. Different types of vehicle units and couplings used in AHVs [25]

In the US and Canada, there are various types of LCVs, including the Turnpike double, which can be as long as 41 m and as heavy as 67.5 tons [27]. Figure 2.2 demonstrates these common types in North America. In Brazil and Australia, the Rocky mountain doubles can weigh up to 74 t and 85.7 t, respectively [28]. Australia even allows longer vehicles called road trains, which can be up to 53.5 m in length and a maximum weight of 125.5 tons, but are only permitted to operate in remote areas [29]. Long combination vehicles have been in use in Canada for about 50 years, and since 2016, nine out of thirteen provinces and

territories in Canada have permitted LCVs to operate on a highway network that is approximately 17000 km long [27].




LCV configuration	Diagram of a typically-configured LCV	Axle configuration
Turnpike double		3-S2-3, 3-S2-4 (shown), 3-S2-5, others
Rocky Mountain double		3-S2-2 (shown), others
Triple trailer combination		2-S1-2-2 (shown), 3-S1-2-2, others

Figure 2.2. Three common LCV configurations in North America [27].

Multi-trailer combinations with more than one trailer are often named vehicle trains. They are referred to as A-, B-, or C-trains relying on the type of coupling between trailers [25].

Figure 2.3 illustrates the three configurations.

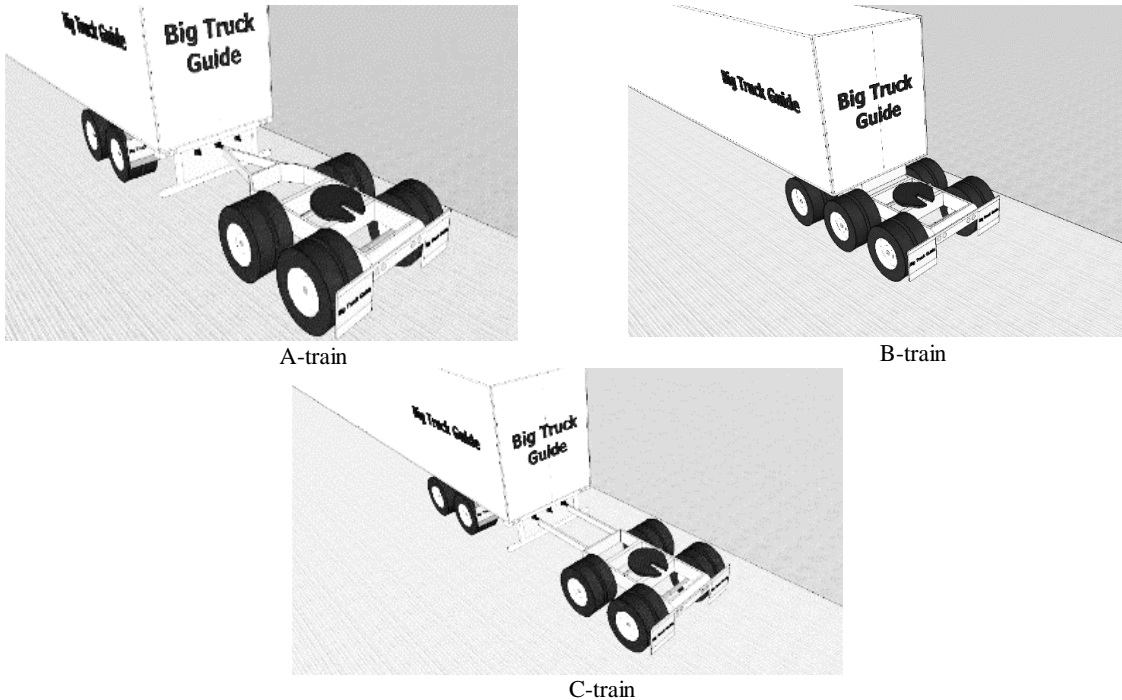


Figure 2.3. different ways that two trailers are hooked to one another in North America [30].

2.3 Dynamic performance of AHVs

Since the 1980s, researchers have been investigating the performance of AHVs in various studies [30][31][32]. The first Performance-Based Standards (PBS) was introduced in Canada [30], and in 1999 the Australian National Road Transport Commission (ANRTC) launched a project [33] leading to an Australian version of the PBS [34], which can be used to evaluate the dynamic performance of heavy vehicles with multiple axles, including MTAHVs. In the Australian PBS, the standards are classified into four groups based on the road classes, ranging from level one, which represents general access routes, to level four, which covers remote area operations. The primary objective of developing these standards was to design and produce AHVs that are optimized and innovative while ensuring acceptably safe dynamic performance. Each defined performance standard has a numerical criterion dedicated to a performance measure, which is used to assess vehicle performance through a specific maneuver. The use of PBS is expected to improve the delivery of goods and services while meeting safety requirements, benefiting all roadway users and maintaining road infrastructures properly [25].

The performance issues of AHVs are divided into various groups based on various factors, such as vehicle speed, direction of forces and moments, and road infrastructure conditions [35]. Kati, et al. [36], have redefined some of the common performance characteristics and added new performance features, including stopping distance, lateral clearance time, downhill holding capability, high-speed steady state off-tracking, and deceleration capability in a turn. Understanding these performance metrics is crucial for comprehending the effect of active control systems, trajectory planning and automated driving strategies

on LCVs' dynamic performance. Table 2.1 provides a list of common performance measures associated with dynamic issues regulated in PBS standards.

Table 2.1. Longitudinal and directional performance issues of AHVs

	Longitudinal	Directional
Low-speed	Startability Gradeability Acceleration capability	Swept path Frontal swing Tail swing Steer-tire friction demand
High-speed	Overtaking Straight-Line Off-tracking (SLO) Ride quality Stopping distance Down-grade holding capability Gradeability	Static rollover threshold (SRT) Lateral transfer ratio (LTR) Rearward amplification Transient off-tracking (TO) Steady-state off-tracking Yaw damping (rear most trailer) Handling quality

2.3.1 Directional performance measures

Directional performance measures for MTAHVs refer to a set of criteria used to evaluate the dynamic performance of MTAHVs in terms of their ability to safely navigate various types of turns and maneuvers, while minimizing risks to other road users and infrastructure. These standards and measures are critical for ensuring the safe operation of MTAHVs, which are large and complex vehicles that pose unique challenges to drivers and operators. As shown in Table 2.1, some examples of directional performance measures for MTAHVs include swept path width, off-tracking, and rollover stability, among others. These

standards and measures are used to evaluate the design and operation of MTAHVs, and to identify areas for improvement in order to enhance their safety and performance on the road especially when they are equipped with some control systems. Some of the frequently used measures for low-speed and high-speed maneuvers are explained below.

2.3.1.1 Low-speed performance measures

Swept path width (SPW) is a measurement of the maximum distance between the vehicle's innermost and outermost points projected onto the ground plane during a low-speed turn of 90 degrees. A wider swept path width indicates that the last trailing unit of the vehicle will have a greater off-tracking, which increases the risk of collisions with parked vehicles, pedestrians, road furniture, and curbs. A diagram of this performance measure is shown in Figure 2.4.

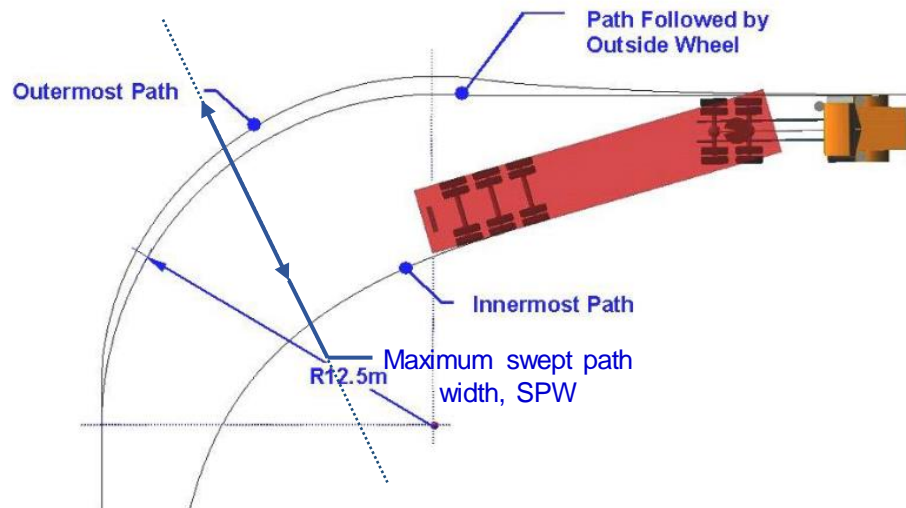


Figure 2.4. Maximum swept path width performance measure schematic representation [35].

The two low-speed performance measures related to LCVs are the frontal and tail swings. The frontal swing is usually measured as the maximum sideways displacement between

the outer front corner of the vehicle and the outside point of the front end of the second unit. On the other hand, the tail swing is defined as the farthest distance between the path of the outer rear corner of the last towed unit and the entry and exit path tangents. This displacement is caused by the overhang at the rear of the last unit being towed. Figure 2.5 displays these performance metrics. The test methods and conditions used for the low-speed SPW performance measure are also applied here.

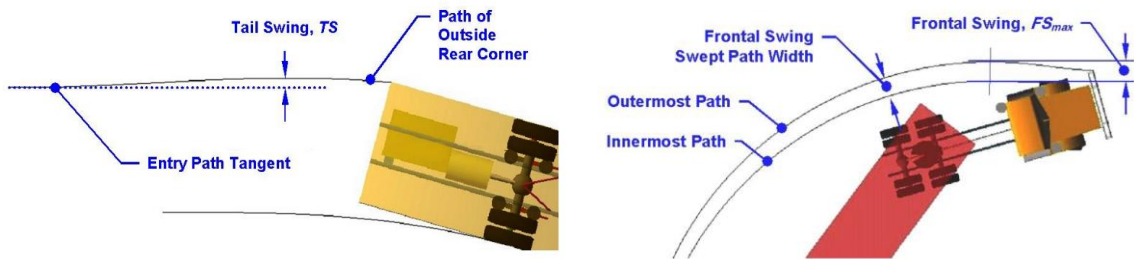


Figure 2.5. Frontal swing performance metric perspective illustration (right image), tail swing performance measure illustration (left image) [35].

The other low-speed performance metric is steer-tire friction demand, and it is determined by the maximum amount of friction needed to create the necessary side force and keep the vehicle on the intended path while making a sharp turn at low speeds. This demand should not exceed a certain proportion of the maximum tire/road friction limit (e.g., 80% in the Australian PBS) to avoid ploughing. This is typically experienced by the leading vehicle unit with tridem-axle drive systems, which can cause reduced steering response or understeering due to the high friction demand [37]. However, this can be mitigated by adjusting the vertical load on the steer-tires and drive-tires. Like the low-speed SPW test method, this metric is measured by performing a 90-degree turn maneuver.

2.3.1.2 High-speed performance measures

Additionally, there are the high-speed directional performance concerns, which are more difficult to manage from a safety perspective than the performance measures mentioned earlier. The most significant safety issue for LCVs is their roll stability dynamic problem, which can result in accidents that cause severe injuries or fatalities. Heavy vehicle rollover incidents are more frequent and can be more dangerous than those involving light vehicles [21]. Roll instability is an even greater safety concern for LCVs than for heavy trucks because the driver of the tractor may be isolated from the roll motion of the towed units due to the cab's suspension and couplings between adjacent units. Furthermore, LCVs are much longer than regular heavy rigid trucks and can obstruct entire highway lanes if a rollover occurs, potentially causing a serious crash that traps more traffic.

The Static Rollover Threshold (SRT) is a fundamental measure of roll stability that is determined by the lateral acceleration of the vehicle's center of gravity (CG) during a steady turn without rolling over, measured in g's. Generally, the higher the SRT is for a heavy vehicle, the more roll-stable it is considered to be. The SRT test can be conducted using either a tilt table or a high-speed circular turn with a constant radius of at least 100 meters, over a specific time period until the vehicle rolls over. For LCVs, which are longer, the initial speed should be maintained until the vehicle reaches a steady-turn condition, and then the speed should be gradually increased until a rollover occurs. Although the SRT is used to evaluate the roll stability of LCVs in near-static conditions, it does not account for the lateral acceleration response of AHVs during sudden movements. Therefore, an AHV may experience a rollover at a lateral acceleration that is significantly different from the SRT when executing a dynamic maneuver such as high-speed lane-change (HSLC) [38].

Calculating the SRT for an LCV is different from a single-unit heavy vehicle because the lateral acceleration of each unit should be considered since they have different values. According to the National Transport Commission of Australia [34], the resultant lateral acceleration of a LCV that consists of N roll-coupled units can be determined by

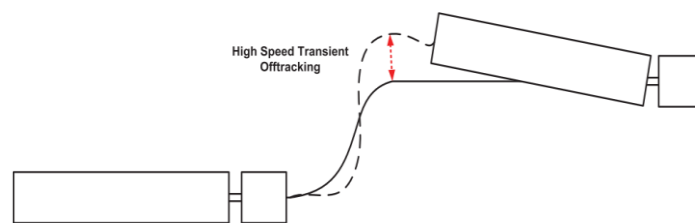
$$AY_{rcu} = \frac{\sum_{n=1}^N m_n h_n AY_n}{\sum_{n=1}^N m_n h_n} \quad (2.1)$$

where m_n represents the n^{th} sprung mass, h_n the height of the n^{th} sprung mass CG, and AY_n the lateral acceleration of at each vehicle unit's CG.

The next important high-speed dynamic performance measure for MTAHVs is Rearward Amplification (RWA), which is defined as the ratio of the maximum motion variable (e.g. yaw rate or lateral acceleration) of the rearmost roll-coupled towed unit to that of the hauling unit during a high-speed obstacle-avoidance maneuver with a single-cycle sinewave lateral acceleration (SCSLA) steering input at a specific road friction level. The RWA measures, in terms of lateral acceleration and yaw rate, are usually similar. However, in certain special cases involving reduced tire/road friction conditions, use of self-steered trailer axles, and difficulty in mounting acceleration sensors at the very CG of vehicle units, the RWA results for both variables may be significantly different [39]. Hence, the appropriate one should be used with caution. Moreover, the closer the RWA value is to unity, the better the directional performance of an LCV through a HSLC maneuver, and it will be less prone to rollover dynamically [40]. Zhu et al. carried out an in-depth study on methods for evaluating the high-speed dynamic stability of LCVs [41]. They found that the

RWA measures obtained from various methods were different from one another. They also identified the reasons for this difference and discussed them in detail.

In addition, LCVs display high-speed transient off-tracking (HSTO) during high-speed obstacle avoidance maneuvers. This term refers to the lateral displacement between the last axle center of the rearmost towed unit and the path of the steer axle's center of the lead unit while performing a sudden lane-change maneuver at a particular road friction level and a predetermined high speed. This measure may be either positive or negative, indicating overshoot or undershoot. The primary objective of the HSTO metric is to prevent the intrusion of the LCV's last trailers into adjacent lanes and reduce the likelihood of traffic accidents. While the RWA and HSTO are measured under similar maneuvers, the RWA represents the measure governing the lateral stability, while HSTO characterizes the capability of path-following or maneuverability. Therefore, an LCV with poor HSTO performance may have a low rollover tendency due to a low CG [25]. Figure 2.6 provides a schematic representation of HSTO.



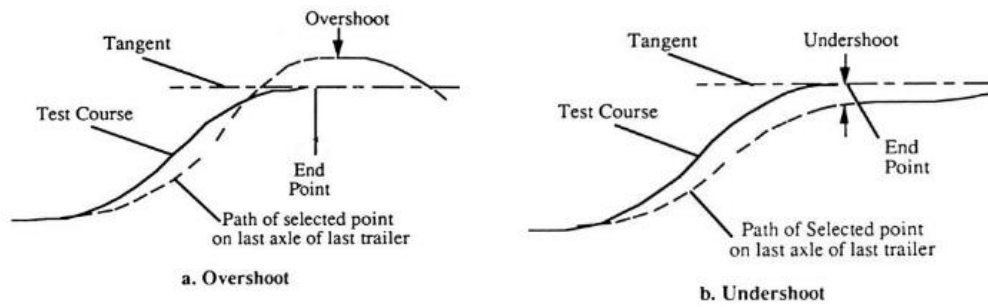


Figure 2.6. A diagram depicting the HSTO performance measure and the overshoot/undershoot conditions [11], [21].

While traversing a steady curve with a substantial radius, the rearmost trailer of an LCV produces a lateral offset between its rear axle center (RAC) and the path of the tractor front axle center (TFAC), known as high-speed steady-state off-tracking (HSSO). This is a metric for assessing steady-state path-following performance and is determined when the LCV moves on a road with a predetermined level of friction and constant high speed. Greater HSSO values can result in collisions with nearby traffic or obstacles on the road. The concept of HSSO is depicted in Figure 2.7.

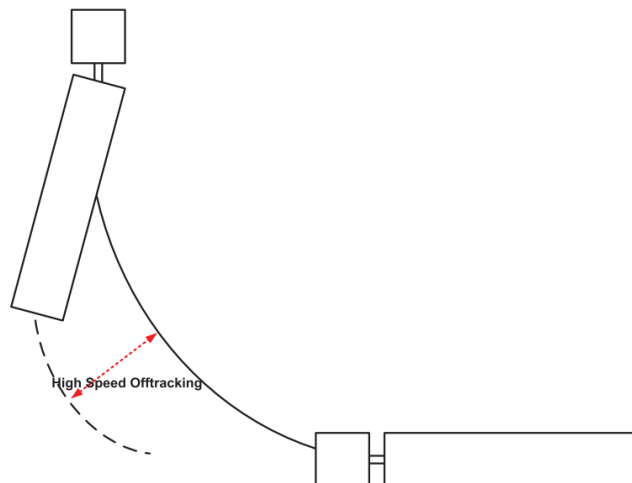


Figure 2.7. A diagram illustrating the high-speed steady-state off-tracking (HSSO) performance measure [21].

2.4 Active trailer control systems

In the trucking industry, MTAHVs are frequently used for carrying large amounts of cargo over long distances. However, these vehicles pose significant challenges to drivers due to their size, weight, and the potential for trailer sway and rollover. To address these challenges, various active trailer control systems have been developed, including electronic stability control (ESC), roll stability control (RSC), and active trailer steering (ATS). These systems are designed to improve the stability and handling of MTAHVs by utilizing sensors, control algorithms, and actuators to provide real-time control of the trailer's movements and reduce the risk of accidents, ultimately improving driver safety and ensuring efficient and reliable transportation of goods.

2.4.1 Active trailer steering for AHVs, control methods and performance improvements

In the literature, active trailer steering (ATS) has received more attention than other control systems due to its ability to enhance the dynamic performance of MTAHVs at both high and low speeds maneuvers. Cebon et al. [42] created an active trailer steering (ATS) system for a B-double LCV, where two axles of the first trailer and all three axles of the second trailer were actively steered, while a conventional tractor served as the lead unit. The developed control strategy, known as CT-AT-AT, enabled the vehicle to be steered in both forward and reverse directions. To test the controller's path-tracking performance, a standard UK roundabout [43] maneuver was carried out in the forward direction, and a teardrop maneuver was performed in reverse at low speed. The research team compared the results with a trailers' command steer strategy. The CT-AT-AT system greatly improved the performance measures of the vehicle, with 1.1 m cut-in, 0 m tail swing, and

0 m exit settling distance, compared to 2.52 m, 1.65 m, and 10 m, respectively, with the command steer strategy. The B-trailer's hitch demonstrated impressive capability by following the path of the rear door center with only 0.4 m error during the reverse teardrop maneuver. However, the manual control of the tractor front axle by the driver indicated that the tractor's hitch could not follow the path successfully.

Kharrazi et al. [44], created an ATS system for a popular fully-loaded truck-dolly-semitrailer MTAHV, commonly used in Scandinavia, to assess its high-speed lateral stability through simulations and experiments. The ATS system was evaluated in a single-lane-change (SLC) maneuver where the yaw rate RWA, lateral acceleration RWA, and TO improved significantly from 2.06 to 1.18, from 1.63 to 1.45, and from 1.02 m to 0.44 m; respectively, and the trailer swing was eliminated. Similarly, a double-lane-change (DLC) test showed significant improvements in dynamic performance metrics. To test the controller robustness, a sensitivity analysis was conducted, and results showed that the controller was not significantly affected by $\pm 20\%$ variation in MTAHV parameters such as tire cornering stiffness, CG, moment of inertia, and loading condition.

The capability of an ATS system was verified in a Nordic configuration [45], with the tractor's braking-based stability control system. The results of real-world experiments showed no adverse effects of the stability control system, and the performance measures indicated a reduction of 75% in path-following off-tracking (PFOT), a decline of 18% in acceleration RWA, and a decrease of 37% in yaw rate RWA when the weighting factors of the linear quadratic regulator (LQR) control method were properly adjusted.

The robustness of an ATS controller for a Nordic MTAHV was investigated in [46] under different driving conditions such as road friction, trailer loading, and various maneuvers.

The study showed that the controller's ability to reduce off-tracking varied more than its ability to reduce yaw rate RWA in the presence of uncertain parameters. The controller was found to be more sensitive to parameter uncertainties when the road friction was low. Moreover, the study highlighted that incorrect values for tire cornering stiffness, which is the most critical vehicle parameter, could impair the controller's performance on slippery roads. To overcome this issue, the study suggested incorporating a tyre cornering stiffness estimator into the controller.

Huang et al. developed an ATS system for an A-train double with steerable axles on all towed units [47]. They compared the dynamic performance of the actively-steered A-train with passive-steering and non-steered MTAHVs using co-simulations under both low- and high-friction road conditions. The results showed that the ATS could pass the SLC test with improved dynamic performance on both normal and icy roads, while the passive and conventional MTAHVs could not maintain directional stability on slippery roads. Additionally, on normal roads, the HSTO of the A-double with passively-steered trailers was twice worse than that of the MTAHV with non-steered trailers, indicating the disadvantage of passive steering for evasive maneuvers. In low-friction situations, the passive and conventional MTAHVs could not maintain the desired path and under-steering occurred, while the actively-steered MTAHV could do so with satisfactory off-tracking.

In another research study [48], authors developed a steering-based controller that could be used for nine different heavy vehicle combinations, including three different MTAHVs ranging from 16.5 m/40 ton to 34 m/90 ton. They used a high-speed sine-with-dwell test and a 0.4 Hz steering input frequency to analyze the results in both the frequency and time domains. The controller had two parts, a feed-forward component and a proportional

feedback component, with the former based on the linear vehicle model and the latter compensating for uncertainties, disturbances, and unmodelled dynamics. The authors claimed that the yaw oscillation was effectively dampened by the controller for all vehicle combinations, although they did not provide numerical results for this measure. Table 2.2 lists other important performance measures and the improvements achieved by their controller. According to their results, vehicle combinations with center-axle trailers had the lowest yaw damping coefficient (YDC) among all the associated AHVs, and these combinations experienced the greatest reduction in lateral acceleration due to the controller's ability to handle yaw motion and mitigate large oscillations.

Table 2.2 The improvements achieved by the controller that was created for different heavy vehicle combinations are summarized in [48].

		Yaw rate RWA			Off-tracking			Lateral acceleration RWA		
		Passive	Active	Improvement	Passive	Active	Improvement	Passive	Active	Improvement
Conventional combination vehicles	Tractor-ST	1.28	1.05	18%	0.8	0.5	38%	1.1	1.09	1%
	Truck-CAT	1.61	1.14	29%	1.4	0.6	57%	1.46	1.25	14%
	Truck-FT	2.27	1.19	48%	1.4	0.4	71%	1.77	1.29	27%
Existing longer combination vehicles	B-double	1.60	1.20	25%	1.3	0.4	69%	1.29	1.31	-2%
	Tractor-ST-CAT	2.61	1.34	49%	2.4	0.8	67%	1.80	1.55	14%
	Truck-dolly-ST	1.84	1.18	36%	1.6	0.8	50%	1.46	1.27	13%
Prospective longer combination vehicles	A-Double	2.47	1.48	40%	2.8	0.7	75%	1.72	1.36	21%
	Truck-duo CAT	3.63	1.26	65%	3.4	1.0	71%	1.79	1.42	21%
	Truck-B-double	2.26	1.32	42%	2.4	0.7	71%	1.69	1.34	21%

Ding et al. conducted a simulation for the ATS system of a B-train double, using a driver-software-in-the-loop (DSIL) [49]. The system included single-axle steered towed units and an LQR control method. The use of the ATS system resulted in significant improvements in performance measures, particularly in the low-speed 90-degree and high-speed SLC maneuvers, as specified by SAE J2179. The PFOT dropped from 4.95 m to 1.04 m, while the RWA declined from 1.128 to 0.795. Another study confirmed the capability of the LQR control method to enhance the performance of a B-train double in high-speed SLC maneuvers specified by ISO14791 and a low-speed roundabout turn with the radius of 25

m, provided that there is no remarkable external noise available [50]. The use of ATS reduced HSTO and PFOT by 87.3% and 36%, respectively.

Sadeghi et al. developed an ATS controller using two methods: gain-scheduled H_∞ synthesis and H_∞ -type static output feedback (SOFB) combined with dynamic feed-forward (DFF) [51][52]. The former controller considered vehicle speed as the scheduling variable, allowing the controller to adjust to speed changes. The latter controller had a simple architecture that was easy to implement. The results showed that both proposed controllers significantly improved the high-speed lateral stability and performance measures of MTAHVs, which was consistent with other ATS control strategies.

2.5 Autonomous driving for AHVs

There are two main goals for AHVs control within an autonomous and semi-autonomous driving [53]. To control both the longitudinal and lateral dynamics using the embedded control system with sophisticated software that are actually codes written to do the job. The control algorithms involve a higher level of control (strategy control) and a lower level of control (vehicle control). The former makes decisions based on the data received from the infrastructure and the surrounding vehicles. The later includes vehicle steering, throttle and brake control.

2.5.1 Lateral motion and stability control

Lateral control of AHVs is to drive the vehicle close to the center of the desired lane, which includes not only straight road sections, but also curved paths, and roundabout ways (lane-keeping maneuver). Under such complicated operating conditions, rollover is a common accident that AHVs may experience during lane changes or cornering maneuvers, which

often causes harsh results, e.g., considerable financial costs and fatalities. This is usually because of higher CG of heavy vehicles compared with passenger cars. Hence, effective control strategies like active suspension control, active steering and active braking should be employed to increase the roll stability.

Path following is a vital issue for autonomous driving. The path following control for AGVs involves maneuvering the vehicle autonomously through the steering control. This aims to help the vehicle follow the desirable path defined by the navigation system via sensors. There are different strategies for the lateral control of AHVs during path following. Some researchers proposed the use of an active trailer steering system to enhance the path following and stability control of AGVs.

For example, in a study a model predictive controller was utilized to make a tractor/semi-trailer follow a path and yaw angle predicted for the trailer while minimizing the side slip angle for different vehicle conditions [54]. The designed controller efficiently improved the lateral stability and off-tracking of the trailer through numerical simulations for an evasive maneuver. However, no results were presented to confirm the applicability of the suggested method for low-speed driving scenarios. Further, no information was provided relating to the driver model utilized. The design doesn't involve an autonomous driving control strategy. In another study [55], a LQR-based active trailer steering controller was designed to improve tractor-semitrailer lateral stability at high speeds and the maneuverability at low speeds. The researchers used a 3-DOF linear model and a simulated annealing particle swarm optimization algorithm based on the TruckSim-Simulink environment and the results were promising.

A lateral-longitudinal control method for a backward motion was proposed to avoid jackknifing during automated steering for a car-trailer [56]. The jackknifing was prevented by employing an anti-windup mechanism in that the articulation angle was controlled not to exceed the limit. Reference [57] reported a research work in which a control strategy was adopted to make both tractor and semitrailer of an AHV follow different paths at different vehicle speeds and in the presence of external disturbances. They used a nonlinear kinematics-based controller for low speed performance improvement, while it was not appropriate for high speeds because of tire side-slip characteristics. Hence, they combined both low and high-speed controllers using a speed-dependent gain in mid-speed range. The simulation results proved an improvement in maneuverability at low speeds and an enhancement of stability at high speeds.

In another research work [58], a new lane-keeping controller was introduced to keep an AHV position (lateral and angular) aligned with the lane, as well as maintaining its stability in critical situations. An optimal control technique and a fuzzy supervisory strategy were utilized to adapt the controller to various driving behaviors of drivers. The system was basically a human driven AHV that reacted appropriately in a case that the AHV deviated from the desired path. Different testing maneuvers were used to show the effectiveness of the controllers designed.

A controller design was proposed to deal with the path following issue for articulated robotic vehicles that had been equipped with a number of off-axle hitched trailers [59]. The controller was highly scalable nonlinear cascade-like that did not require setting the shortest distance to an ideal path. Instead, it used a segment-platooning reference path

(introduced by the researchers) to ensure asymptotic path following. Empirical results showed the small sensitivity of the designed controller to parameter uncertainties.

In another research study [60], a new sliding mode control (SMC) strategy was introduced to do trajectory tracking for articulated vehicles. The designed controller targeted better tracking capability while minimizing the tracking error and preventing the chattering phenomenon. The SMC was derived based on a nonlinear kinematic model of the articulated vehicle, and the stability of the control strategy was tested using the Lyapunov's stability method. Finally, the investigators evaluated their controller performance in various paths scenarios using a small-scale model.

As for the rollover prevention in heavy vehicles, reference [61] documented a combined active anti-roll bar (AARB) and active braking controller. Reference [62] introduced a linear quadratic static output feedback control strategy using both AARB and an electronic stability program to handle the rollover issue more efficiently.

In [63], a MPC-based control strategy was designed to improve the roll stability in a path following maneuver. While the brake and steering interconnected in the upper layer controller, the simulation results demonstrated that this multilayer control structure guarantees the path tracking with small error. Researchers introduced an AARB including four electronic servo-valve hydraulic actuator to actively control a heavy vehicle by solving a LQ optimization problem where the front steering considered to be an uncertain disturbance [64]. The simulation results in the frequency and time domains confirmed a remarkable improvement in terms of rollover stability.

A novel roll stability control strategy for heavy vehicles, termed dynamic game theory-based path following active anti-roll (AAR) with interactive shared control strategy was proposed in [65]. It was indeed a cooperative path-following and roll-stability controller that had two players, i.e. AARB and AS, determined via a closed-loop feedback Nash equilibrium theory. Simulations based on various driving scenarios were conducted to investigate the effectiveness of the method.

2.5.2 Longitudinal motion control

Longitudinal dynamics control of AHVs mainly refers to regulating vehicle speed in order to retain enough space between vehicles. For implementing a successful longitudinal control four types of data are needed: speed and acceleration of the host vehicle, speed and acceleration of the preceding vehicle, the distance from the leading vehicle and, in the case of platooning, speed and acceleration of the first vehicle.

Attempts have been made for longitudinal motion control for SUVs. In [66], the driving behavior considering the driver capability envelope was analyzed during braking a car in a turn through a closed-loop simulation. This approach can be inferred as an automated braking scheme for a car, but it did not consider throttling. In another research, the driver's steering and speed control performance was investigated for a SUV while negotiating a curved path [67]. It was assumed that the vehicle should reach a predefined speed at the circular part of the road. Indeed, the proposed method was not autonomous and the speed was not adjusted based on road curvatures and driving strategies.

A convex optimization-based speed planning strategy for a heavy truck was studied considering both the acceleration and deceleration demand for a path with varying curvatures [68]. A two-level control strategy for longitudinal motion control of a truck was

proposed [69]. The authors used the engine and brake system states for the speed control. The model introduced a reference speed to follow and speed was not planned based on road curvatures. A clothoid-based speed profiler and control using a receding horizon fashion was introduced for a SUV during a low-speed S-curve path negotiation, but the vehicle performance envelope and the high-speed transient maneuver functionality of the designed controller were disregarded [70]. Unfortunately, there is no published autonomous speed controller in the literature dedicated to MTAHVs considering their unique dynamics.

2.6 Driver models for MTAHVs

Driver models play significant roles in any autonomous driving strategy design. A myriad number of driver models for single-unit vehicles for use in closed-loop tests have been introduced so far; some of which have been well validated and examined in different studies either theoretically using simulation methods or experimentally through road tests [10], [71]–[74]. However, a MTAHV dramatically differs from a passenger car in terms of path-following capabilities as well as directional performance because of remarkable differences in the vehicles' dimensions, weights and articulation points [21][25]. As a result, the introduced driver models for single-unit vehicles will not operate efficiently for MTAHVs, and specialized driver models for these large vehicles are required.

Among the research conducted pertaining to study of articulated heavy vehicle dynamics performance, almost none consider the impact of trailing units on the path-following or lateral stability tests. In reality, the lateral position of the trailers with respect to the target path as well as their lateral acceleration will impact the driver's decision-making process for giving the demanded steer input.

Ding and He studied the impact of motion cues coming from either tractor or trailer, and they developed a driver model for a tractor-semitrailer considering these motion cues [75]. They concluded that considering all the units' motion cues will improve the directional performance of the vehicle. Despite noticeable merits of considering the impact of trailing units' motions on designing driver models for MTAHVs, they have been remarkably ignored in the literature. For instance, He et.al. made use of a driver model that utilizes the tractor's steering demand based on the difference in heading angle of the tractor with respect to a desired point on the target path over a constant preview distance in a B-train double MTAHV directional performance optimization study [76].

Brown et al. used the TruckSim software with a built-in driver model by MacAdam for analyzing a B-train double AHV driver's driving skill through closed-loop dynamic simulation [22]. It is noteworthy to mention that the built-in driver model in TruckSim was designed for single-unit vehicles and doesn't consider the trailing units' impact on the towing unit steering demand. Ni et al. also employed the TruckSim built-in driver model for comparing the different test maneuvers' results as for the rearward amplification of an A-train double AHV [77].

Zhu et al. implemented the idea of employing the trailing units' motions for the design of the driver model for a B-train double AHV using a sliding mode controller [78]. They defined a sliding surface as the combination of all units' lateral deviations from target path plus the deviation rates, and then calculated the steering input so that the sliding surface becomes zero. To investigate the capabilities of their introduced driver model, only an evasive single-lane-change (SLC) path-following maneuver through a closed-loop simulation was executed. While their model demonstrates advantages for a high-speed SLC

maneuver over other driver models introduced in the literature, they didn't verify it under low-speed path-following maneuvers with sharp turns. Since they have utilized an inertial coordinate system that produces remarkable accumulated error over driving scenarios with high yaw motions [79], it is inferred that the driver model may not be applicable for low-speed path-following maneuvers with sharp turns.

Chapter 3. MTAHV modelling and validation

3.1 Introduction

Vehicle dynamic models are essential for the design, development, and control of MTAHVs. These vehicles are complex in configuration, and their dynamic behavior is affected by multiple factors, such as the number of trailers, the length of the trailers, the type of coupling mechanism between tractor and trailer, and the load distribution.

Vehicle dynamic models are crucial for understanding the dynamic behavior of MTAHVs, predicting their responses to various inputs, and designing control systems that ensure safe and efficient operations. By developing vehicle models of MTAHVs, engineers can simulate the vehicle's behavior under different operating conditions and optimize control strategies to improve safety, maneuverability, and stability.

In order to design and analyze driver models, active trailer steering system and automated driving strategy for MTAHVs, two vehicle models were developed in this study. First, a five DOF linear yaw-plane model was derived for the A-train double to design the driver model and the speed planner/controller. Then, a six DOF non-linear yaw plane model was built to develop ATS and trajectory planning for the A-train double. The highly nonlinear A-train double model with a high fidelity in TruckSim was utilized to verify the capabilities of designed control strategies via co-simulation using MATLAB/TruckSim, in different MTAHV maneuvers and driving scenarios.

3.2 Fundamental linear yaw-plane model

Figure 3.1 demonstrates a five degrees of freedom (DOF) linear yaw-plane model of an A-train double LCV. The motions considered include the tractor's lateral and yaw motions, as well as the trailers' and convertor dolly's yaw motions. As illustrated in the figure, the vehicle system is laterally telescoped into the axle centers and one wheel represents all the wheels on each axle. This model is the single-track representation of the vehicle combination. By means of the body-fixed coordinate system of each vehicle unit, with Newton's laws of dynamics, the governing equations of motions for tractor, first trailer, convertor dolly and second trailer are derived [80], and represented by equations 3.1 to 3.4, respectively.

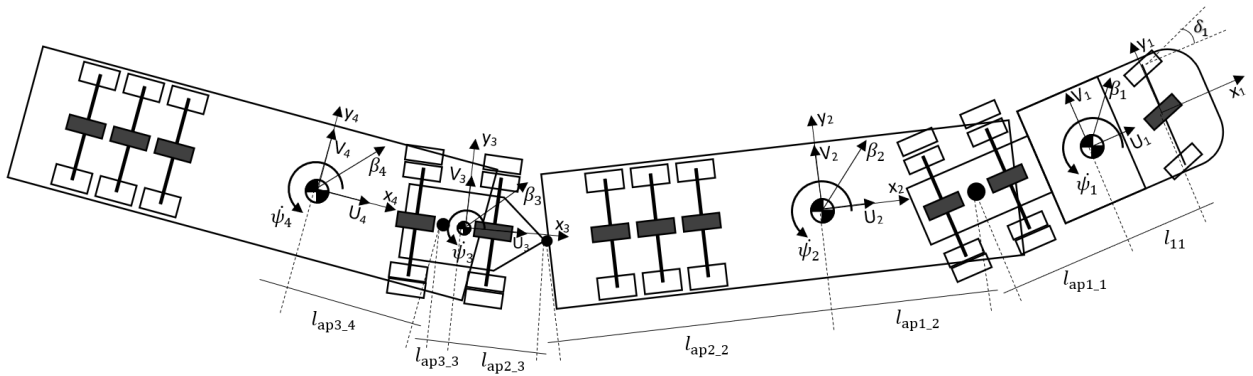


Figure 3.1. A schematic representation of the A-train double.

Following assumptions are made to achieve the linearized equations of motions: 1) the longitudinal speed of the vehicle is constant during the maneuver and all the units share the same forward-speed; 2) the linear tire model is used; 3) roll motion and pitch motion are ignored. 4) side-slip angles of all units are small; 5) the leading unit steering angle is small; and 6) products of variables are neglected.

$$\begin{aligned}
m_1 u_1 (\dot{\beta}_1 + \dot{\psi}_1) &= Y_{\beta_1} \beta_1 + Y_{\dot{\psi}_1} \dot{\psi}_1 + Y_{\delta_1} \delta_1 + F_{y1} \\
I_1 \ddot{\psi}_1 &= N_{\beta_1} \beta_1 + N_{\dot{\psi}_1} \dot{\psi}_1 - l_{12} F_{y1} + N_{\delta_1} \delta_1
\end{aligned} \tag{3.1}$$

$$\begin{aligned}
m_2 u_2 (\dot{\beta}_2 + \dot{\psi}_2) &= Y_{\beta_2} \beta_2 + Y_{\dot{\psi}_2} \dot{\psi}_2 - F_{y1} + F_{y2} \\
I_2 \ddot{\psi}_2 &= N_{\beta_2} \beta_2 + N_{\dot{\psi}_2} \dot{\psi}_2 - l_{21} F_{y1} - l_{22} F_{y2}
\end{aligned} \tag{3.2}$$

$$\begin{aligned}
m_3 u_3 (\dot{\beta}_3 + \dot{\psi}_3) &= Y_{\beta_3} \beta_3 + Y_{\dot{\psi}_3} \dot{\psi}_3 - F_{y2} + F_{y3} \\
I_3 \ddot{\psi}_3 &= N_{\beta_3} \beta_3 + N_{\dot{\psi}_3} \dot{\psi}_3 - l_{31} F_{y2} - l_{32} F_{y3}
\end{aligned} \tag{3.3}$$

$$\begin{aligned}
m_4 u_4 (\dot{\beta}_4 + \dot{\psi}_4) &= Y_{\beta_4} \beta_4 + Y_{\dot{\psi}_4} \dot{\psi}_4 - F_{y3} \\
I_4 \ddot{\psi}_4 &= N_{\beta_4} \beta_4 + N_{\dot{\psi}_4} \dot{\psi}_4 - l_{41} F_{y3}
\end{aligned} \tag{3.4}$$

As mentioned earlier it is presumed that $u_1 = u_2 = u_3 = u_4 = u$. The mathematical expressions of Y_{δ_1} , N_{δ_1} , Y_{β_i} , $Y_{\dot{\psi}_i}$, N_{β_i} , $N_{\dot{\psi}_i}$ and also the definition of other used parameters have been represented in Appendix A.1. The coupling forces F_{y1} , F_{y2} and F_{y3} can be eliminated utilizing the following kinematic constraints equations at the fifth wheels.

$$\begin{aligned}
\dot{\beta}_1 - \frac{l_{ap1.1}}{u} \ddot{\psi}_1 - \dot{\beta}_2 - \frac{l_{ap1.2}}{u} \ddot{\psi}_2 + \dot{\psi}_1 - \dot{\psi}_2 &= 0 \\
\dot{\beta}_2 - \frac{l_{ap2.1}}{u} \ddot{\psi}_2 - \dot{\beta}_3 - \frac{l_{ap2.2}}{u} \ddot{\psi}_3 + \dot{\psi}_2 - \dot{\psi}_3 &= 0 \\
\dot{\beta}_3 - \frac{l_{ap3.1}}{u} \ddot{\psi}_3 - \dot{\beta}_4 - \frac{l_{ap3.2}}{u} \ddot{\psi}_4 + \dot{\psi}_3 - \dot{\psi}_4 &= 0
\end{aligned} \tag{3.5}$$

where, the term $l_{api.j}$ is defined in the appendix A.1. Combining equations (3.1) to (3.5), 8 independent equations governing the lateral dynamics of the A-train double are attained.

These equations are rewritten in the state-space form expressed as

$$\begin{aligned}\dot{\mathbf{x}}_b &= \mathbf{A}_b \mathbf{x}_b + \mathbf{B}_b \mathbf{u} \\ \mathbf{y} &= \mathbf{C}_b \mathbf{x}_b\end{aligned}\tag{3.6}$$

where $\mathbf{A}_b = \mathbf{J}^{-1}\mathbf{K}$ and $\mathbf{B}_b = \mathbf{J}^{-1}\mathbf{L}$, matrices $\mathbf{A}_b, \mathbf{B}_b, \mathbf{C}_b, \mathbf{J}, \mathbf{K}$ and \mathbf{L} are the state space matrices given in Appendix A.2. \mathbf{x}_b represents the state variable vector defined as

$$\mathbf{x}_b = [\beta_1 \ \psi_1 \ \beta_2 \ \psi_2 \ \beta_3 \ \psi_3 \ \beta_4 \ \psi_4]'\tag{3.7}$$

and the control variable \mathbf{u} is defined as

$$\mathbf{u} = [\delta_1]\tag{3.8}$$

where δ_1 is the tractor front wheel steer angle.

3.2.1 Linear vehicle model extension

The fundamental linear model developed in the previous section includes eight states. However, in order to design the driver model proposed in the Chapter 4, the lateral displacement and yaw angle states for all the vehicle units are also required. Hence, the state-space matrices given in Equation (3.7) should be reformulated.

Considering the small yaw angles assumption, the lateral position of tractor front axle center and trailers' CGs in the inertial coordinate system are achieved by solving the following equation set,

$$\begin{aligned}
\dot{Y}_1 &= u\psi_1 + (v_1 + l_{11}\psi_1) \\
\dot{Y}_2 &= u\psi_2 + v_2 \\
\dot{Y}_3 &= u\psi_3 + v_3 \\
\dot{Y}_4 &= u\psi_4 + v_4
\end{aligned} \tag{3.9}$$

Equation 3.9 is an approximate representation of the associated states under the condition of small heading angles in the global coordinate system. However, if we assume that at current simulation time step, the inertial coordinate system coincides with each unit's body-fixed coordinate system [81], then, Y_i ($i=1,2,3,4$) represents the predicted lateral coordinate of the units over their previewed positions, P_i ($i = 1,2,3,4$), with respect to their own body-fixed coordinate system. These lateral coordinates are shown by $y_{i_loc}(t + T_p)$ ($i = 1, 2,3,4$). This approach will be explained more later on in this chapter.

The yaw rate of each vehicle unit is determined by

$$\frac{d\psi_i}{dt} = \dot{\psi}_i \quad i=1,2,3,4 \tag{3.10}$$

Combining equations (3.6), (3.9) and (3.10) leads to the augmented state-space formulation as

$$\begin{aligned}
\dot{\mathbf{x}}_d &= \mathbf{A}_d \mathbf{x}_d + \mathbf{B}_d \mathbf{u} \\
\mathbf{y} &= \mathbf{C}_d \mathbf{x}_d
\end{aligned} \tag{3.11}$$

where matrices \mathbf{A}_d , \mathbf{B}_d and \mathbf{C}_d are given in Appendix A.3. \mathbf{x}_d represents the augmented state vector specified as

$$\mathbf{x}_d = [Y_1 \psi_1 v_1 \dot{\psi}_1 Y_2 \psi_2 v_2 \dot{\psi}_2 Y_3 \psi_3 v_3 \dot{\psi}_3 Y_4 \psi_4 v_4 \dot{\psi}_4]'$$
 (3.12)

The input variable remains the same as defined in equation (3.8), i.e. δ_1 , which is the tractor front wheel steer angle.

Regarding the global lateral position of each unit CG, it is presumed that the current values of associated states, i.e. Y_i and ψ_i ($i = 1, 2, 3, 4$) are zero, and they are treated as the initial state values. It means that the inertial coordinate system coincides each unit's body-fixed coordinate system frequently during the simulation. Besides, using current values of the other states i.e. v_i and $\dot{\psi}_i$ ($i = 1, 2, 3, 4$) generated by TruckSim real-time closed-loop simulation as the initial states values assures that the solution for state-space equations over the preview time will provide the predicted values of all the sixteen states with respect to vehicle units' local coordinate systems. Figure 3.2 illustrates this approach just for the tractor which is extended to the trailing units as well.

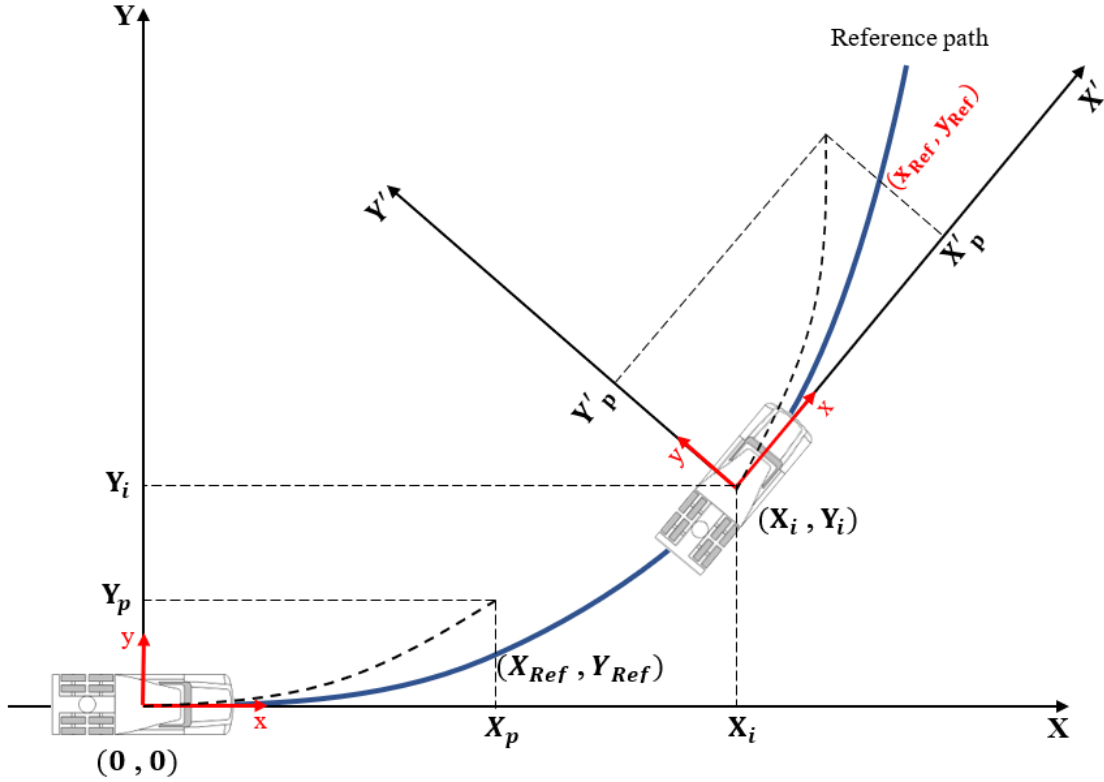


Figure 3.2. Global and body-fixed coordinates schematics depicted for the tractor.

3.2.2 Non-linear yaw-plane model

In order to design the active trailer and dolly steering (ATDS) control system in Chapter 6, a non-linear vehicle model is generated. In addition to the five motions considered in the 5-DOF linear yaw-plane vehicle model, this model considers the longitudinal motion of the vehicle. The resulting vehicle model is a 6-DOF non-linear yaw-plane model. Moreover, the vehicle lateral position and orientation deviations with respect to the reference path are taken into account in this vehicle model.

This 6-DOF vehicle model shares the equation (3.1) to (3.5). Hence, the states v_i and ψ_i are still present. However, instead of the lateral displacement and yaw angle states in the first vehicle model extension, some new states including the yaw error, lateral position error, longitudinal velocity and longitudinal acceleration are introduced. In order to

redefine the equation (3.7) and generate the new state-space model some equations are utilized as follows.

First, using a time lag τ , the longitudinal vehicle dynamics is approximated by equation (3.13) [82].

$$a_x = \frac{1}{\tau s + 1} a_{x_des} \quad (3.13)$$

Simplifying this equation and rewriting that in time domain yields equation (3.14).

$$\dot{a}_x = \frac{1}{\tau} (a_{x_des} - a_x) \quad (3.14)$$

This equation represents a first-order dynamic system, where the desired acceleration a_{x_des} is the input and the actual acceleration a_x is the state. The time constant τ determines how quickly the state responds to any changes in the input. A smaller τ means that the vehicle will respond more quickly to changes in the desired acceleration, while a larger τ means that the vehicle will respond more slowly. The time constant is typically determined by the physical characteristics of the vehicle, such as its mass, engine power, and transmission. For heavy vehicles such as trucks and buses, the time constant is typically larger than for passenger cars, due to their greater weight and lower acceleration. A typical value for the time constant for heavy vehicles might be in the range of 1 to 3 seconds, although this can vary widely depending on factors such as the vehicle's weight, engine power, and transmission.

Furthermore, the longitudinal component of the absolute acceleration of the CG of a vehicle is formulated as shown in equation (3.15) [83].

$$\dot{V}_x = v_1 \psi_1 + a_x \quad (3.15)$$

where v_i is the lateral velocity and $\dot{\psi}_1$ is the yaw rate of the tractor, respectively. Having this equation, required formula for including the longitudinal velocity as a state is also achieved.

Besides, the lateral position deviation rate of the vehicle units' CGs with respect to the reference path \dot{e}_{1i} is given using the equation (3.16) [82].

$$\dot{e}_{1i} = v_i + V_x(\psi_i - \psi_{i_des}) = v_i + V_x e_{2i} \quad (3.16)$$

where, ψ_i and ψ_{i_des} , $i=1,2,3,4$, are the vehicle units' yaw angles and the reference points' yaw angles corresponding to the vehicle units' CGs, and $e_{2i} = \psi_i - \psi_{i_des}$ denote the yaw angle deviation of the vehicle unit with respect to the target point on the reference path, which can be determined by

$$\dot{e}_{2i} = \dot{\psi}_i - \dot{\psi}_{i_des} \quad (3.17)$$

The desired yaw rate $\dot{\psi}_{i_des}$ is determined by the vehicle units' longitudinal speed and the reference path curvature κ_i corresponding to the current tractor's TFAC and the trailing units' CG.

$$\psi_{i_des} = V_{x_i} \cdot \kappa_i \quad (3.18)$$

The continuous-time matrix representation for the 6-DOF based model is given in equation (3.19). It is noteworthy to mention that since there are some products of states (equation 3.22) in the equations as it is seen in equations 3-15 and 3-16, the final dynamics model is considered non-linear.

$$\begin{aligned} \dot{\mathbf{x}} &= \mathbf{A}_t(\mathbf{x})\mathbf{x} + \mathbf{B}_t(\mathbf{x})\mathbf{u} + \mathbf{B}_s(\mathbf{x})\mathbf{u}_s + \mathbf{F}_s(\mathbf{x})\mathbf{d} \\ \mathbf{y} &= \mathbf{C}_t\mathbf{x} \end{aligned} \quad (3.19)$$

where, \mathbf{d} is the measured disturbance and represents the road curvature κ_i which is continuously updated during the simulation based upon the reference path geometry. \mathbf{u} is a vector of the desired longitudinal acceleration and the tractor front axle steering δ_1 denoted by

$$\mathbf{u} = [a_{x_des} \delta_1]' \quad (3.20)$$

In equation (3.19), \mathbf{u}_s is the steering input for the trailing units' axles given in equation (3.21). Note that in order to improve stability and maneuverability, an active trailer and dolly steering system is introduced, which will be discussed later on in Chapter 6.

$$\mathbf{u}_s = [\delta_{tr1_1} \delta_{tr1_2} \delta_{tr1_3} \delta_{dolly_1} \delta_{dolly_2} \delta_{tr2_1} \delta_{tr2_2} \delta_{tr2_3}]' \quad (3.21)$$

Matrices $\mathbf{A}_t(\mathbf{x})$, $\mathbf{B}_t(\mathbf{x})$, $\mathbf{B}_s(\mathbf{x})$, $\mathbf{F}_s(\mathbf{x})$ and \mathbf{C}_t are provided in Appendix A.4. The state vector involves 18 states, which is specified by

$$\mathbf{x} = [v_1 \psi_1 V_x a_x e_{11} e_{21} v_2 \psi_2 e_{12} e_{22} v_3 \psi_3 e_{13} e_{23} v_4 \psi_4 e_{14} e_{24}]' \quad (3.22)$$

3.2.3 TruckSim model

TruckSim is a vehicle simulation software developed by Mechanical Simulation Corporation. It is designed to simulate the behavior of heavy-duty commercial vehicles such as trucks, buses, and trailers, and is widely used in the automotive industry for vehicle development, testing, and validation. TruckSim generates vehicle dynamics models by using a combination of analytical and experimental data. The TruckSim software is created using a symbolic multi-body program called VehicleSim Lisp, which generates equations of motion for 3D multi-body vehicle systems.

Figure 3.3 shows a digital twin of the A-train double LCV modeled in TruckSim and used as the main vehicle model in all the control design strategies in the current dissertation. The configuration of this vehicle is described as S_SS+SSS+dSS+SSS, where S represents a solid axle, an underline () separates axle groups, and a plus sign (+) denotes a fifth wheel connecting two vehicle units. Besides, d indicates the dolly. This means that the A-train double consists of a three-solid-axle tractor with one front axle and two rear axles. It also consists of two semitrailers each having three solid axles as well as a dolly with two solid axles.

To create the equations of motion for the MTAHV, VS Lisp takes input in the form of geometric terms, such as the body DOF, point locations, and force vector directions. VS Lisp then generates a computer source code (C or Fortran) to solve the equations of motion. The TruckSim software package consists of three relevant elements: the VS browser, the TruckSim databases, and the VS solver [84].



Figure 3.3. Open-loop steering input for linear model verification through high-speed lane-change maneuver.

The VS browser is the primary interface to TruckSim, providing a graphical user interface that allows users to define the vehicle geometry, suspension characteristics, tire properties, and other parameters. Users can also specify the driving conditions, such as road profile, speed, and steering input. The TruckSim databases are used to select vehicle configuration templates (e.g. S_SS+SSS+SSS) and define system parameters, tire/road interactions, test maneuvers, etc. The VS solver is used to solve the equations of motion of the vehicle model and execute dynamic simulations. The VS browser can also be used to allow other applications, such as design optimization in MATLAB, and access to the TruckSim databases via an interface.

TruckSim also includes a range of advanced features that enable users to simulate complex maneuvers, such as braking, cornering, and rollover. The software uses a range of mathematical models to simulate the behavior of the vehicle under different driving conditions, taking into account factors such as tire slip, suspension compliance, and vehicle mass distribution.

Overall, TruckSim is a powerful tool for generating vehicle dynamics models that accurately simulate the behavior of heavy-duty commercial vehicles, and can help automotive control engineers to design and test vehicles and controllers more efficiently and effectively via co-simulations and if required through real-time simulations tests.

3.3 5-DOF-based linear vehicle model verification

The derived 5-DOF linear model is the basis for the other vehicle models generated in the previous section. Furthermore, the main linearization assumptions expressed in the previous sections are considered to generate the linear vehicle model. Hence, verifying the fundamental model under high-speed and low-speed driving maneuvers will assure the extended models' reliability and effectiveness.

Since some of the assumptions to linearize the vehicle model, such as small side-slip angles and small articulation angles, may not be valid for many of driving scenarios, especially in sharp turn negotiations with lower vehicle speeds, it is expected that the linear model may not be in good agreement with the respective TruckSim model. Hence, control strategies designed for the urban driving scenarios should not utilize the linearized vehicle model. However, using the proposed modelling and simulation method to be introduced, the linear model can work effectively in low-speed driving and perform well for the control design purposes in the current research, i.e. driver model, speed planner, ATDS controller and trajectory planning strategy for a wide range of driving situations.

In [54], [55], [85], researchers used optimization methods to find the optimal parameters of the linear tractor/semi-trailer model under a large number of steering inputs and vehicle speeds. The cost function of the optimization problem was a combination of yaw rate and side-slip angle deviations with respect to those of the corresponding TruckSim vehicle

model under similar driving inputs. By means of this method, the optimal tires' cornering stiffness as well as the lateral acceleration and the vehicle speed values are stored off-line. Then, in numerical simulations, by means of an on-line look-up table, the appropriate values of tire cornering stiffness are chosen based on the current vehicle speed and lateral acceleration to match the non-linear vehicle performance. Their strategy showed very good linear model reliability through a number of co-simulations and empirical tests for complex steering input and various vehicle speeds.

This method was also employed in the current research for an A-train double AHV. The cost function is formulated using the Mean Absolute Error (MAE) method and the cost function is formulated as

$$F = \frac{\sum_{i=1}^M \sum_{n=1}^N \left\{ \text{abs} \left(\beta_{i_{TS}}(n) - \beta_{i_{LM}}(n) \right) + \text{abs} \left(\psi_{i_{TS}}(n) - \psi_{i_{LM}}(n) \right) \right\}}{M \cdot N} \quad (3.23)$$

where M is the number vehicle units, N is the amount of available simulation data, β is side-slip angle and ψ is the yaw rate, TS and LM stand for TruckSim and Linear Models, respectively. In this optimization problem, the cornering stiffnesses of the linear tire model of the linear vehicle model are considered as the variables. With given step steering angle inputs at various vehicle speeds, the optimization problem is solved using the Particle Swarm Optimization (PSO) search algorithm. The optimal tire cornering stiffness values and associated data are stored to generate a look-up table. In the simulation of the A-train double, the tire cornering stiffness values are continuously updated using the look-up table to improve the fidelity of the linear model.

The 5-DOF-based linear model was verified under the open-loop high-speed single-lane change and low-speed sharp turn maneuvers by means of comparing the achieved simulation results with those derived from the corresponding TruckSim model. In fact, the steering input was given to both the linear vehicle model and the TruckSim model. Then, the significant outputs, such as yaw rate and side-slip angle, were analyzed to investigate the vehicle models' discrepancies.

3.3.1 Vehicle model verification under high-speed maneuver

For implementing the linear model verification under high-speed driving maneuver, the vehicle speed and the steering input applied to both the linear model and the TruckSim model are the same. The steering amplitude, frequency and the vehicle speed are 0.025 rad, 0.4 Hz and 90 km/h, respectively. Figure 3.4 illustrates the steering input curve applied for the maneuver simulation. This steering input represents the time-history of a vehicle front wheel steering angle over a single lane-change maneuver.

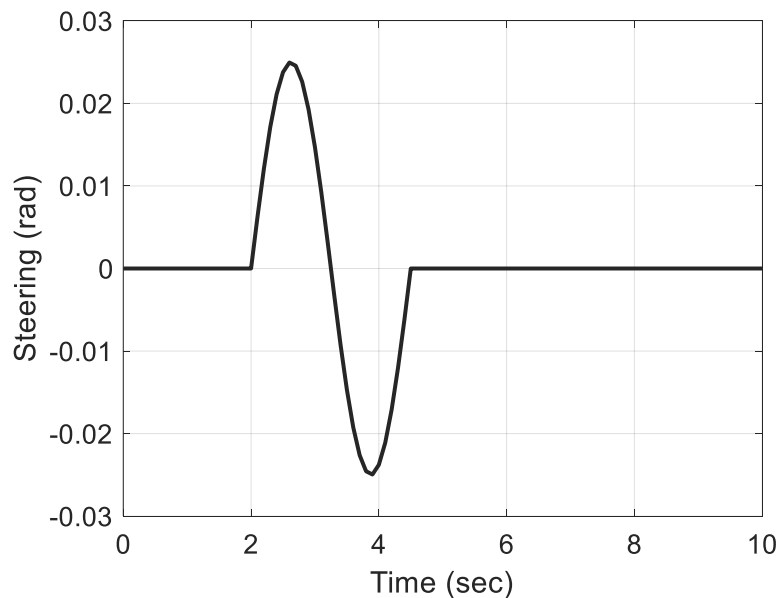
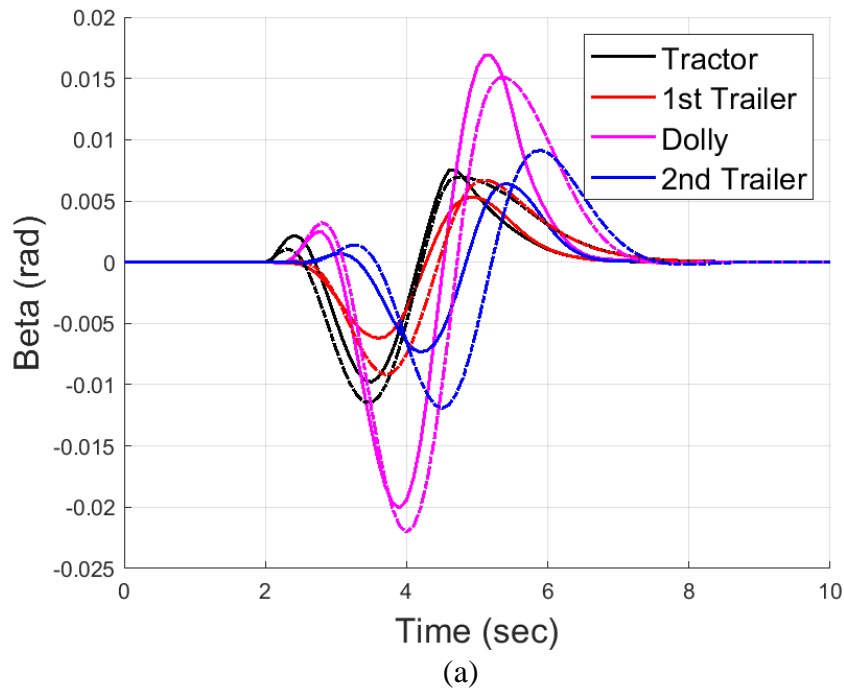


Figure 3.4. Open-loop steering input for linear model verification through high-speed lane-change maneuver.

Figure 3.5 demonstrates the selected simulation results, i.e. yaw rate, side-slip angle, and lateral acceleration. The graphs include TruckSim high-fidelity vehicle model response (solid line) versus the linear dynamics model response (dashed lines) when the nominal tire cornering stiffness values are exploited. As seen, the difference between two sets of results is large and the linear model cannot effectively represent the non-linear vehicle model performance in this driving scenario. Hence, any model-based control design strategy would be unreliable and impractical.



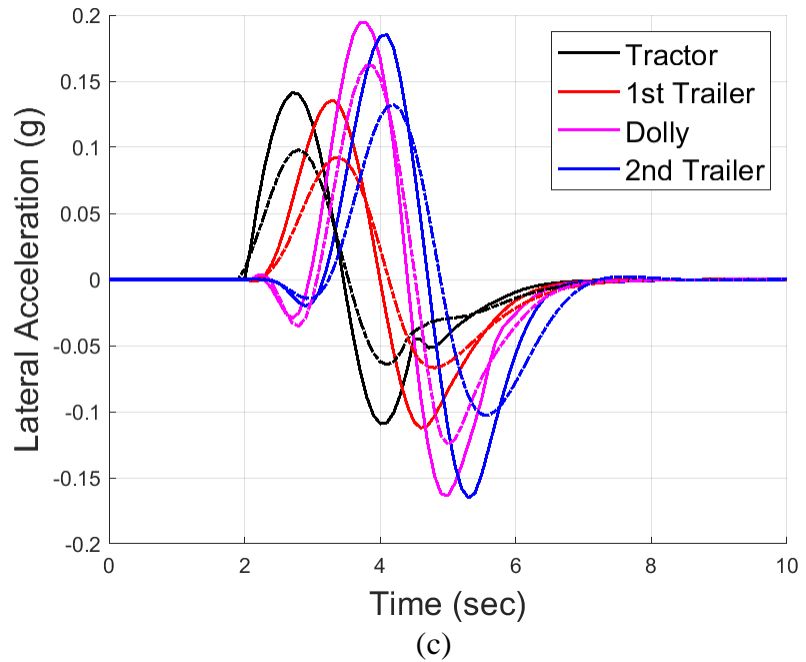
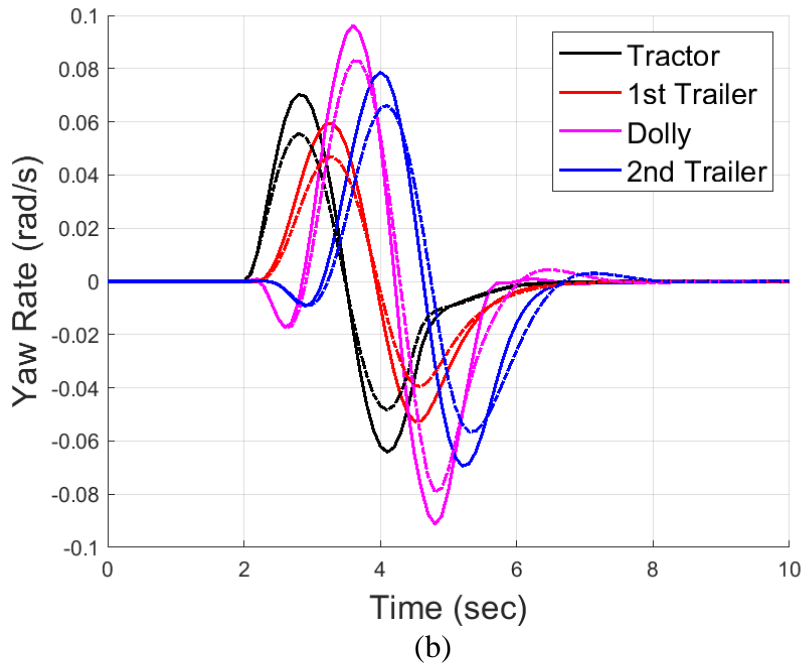
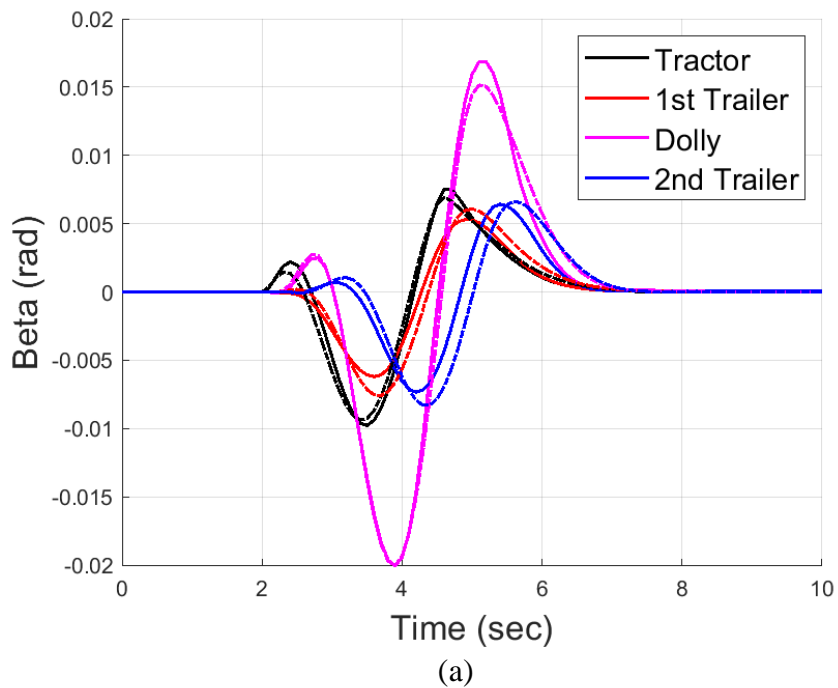


Figure 3.5. Simulation results achieved under high-speed lane-change maneuver for linear vehicle model with nominal tires cornering stiffness values (dashed lines) and the TruckSim model (solid lines): (a) side-slip angle, (b) yaw rate, (c) lateral acceleration.

Figure 3.6 illustrates simulation results in terms of yaw rate, side-slip angle, and lateral acceleration of the linear vehicle model with optimized tire cornering stiffness values. For

the purpose of comparison, the simulation results of the TruckSim model are also plotted in Figure 3.6. Compared with the simulation results of the linear vehicle model with nominal tire cornering stiffness values shown in Figure 3.5, the simulation results of the linear vehicle model with optimal tire cornering stiffness values shown in Figure 3.6 are much closer to those of the TruckSim model. Thus, the optimization method enhances the linear model's accuracy dramatically. The linear vehicle model with the optimal tire cornering stiffness values can well represent the lateral dynamics of the MTAHVs under high-speed lane change maneuvers.



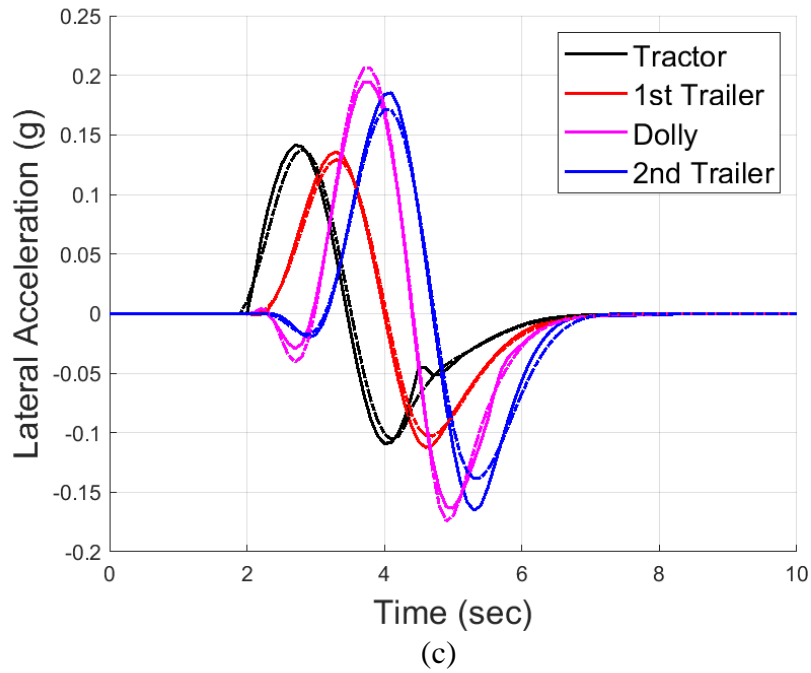
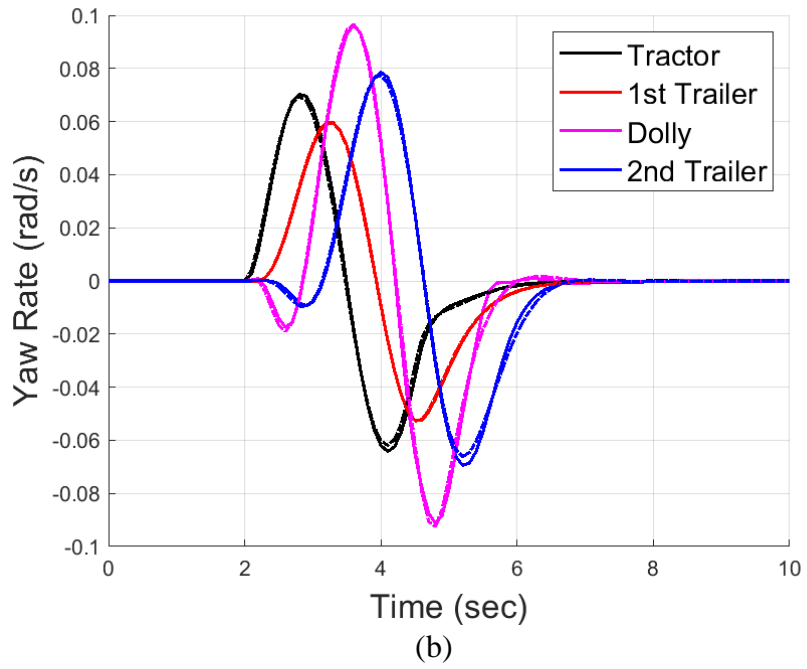


Figure 3.6. Simulation results achieved under high-speed lane-change maneuver for the linear vehicle model with optimal tire cornering stiffness values (dashed lines) and the TruckSim model (solid lines): (a) side-slip angle, (b) yaw rate, (c) lateral acceleration.

3.3.2 Vehicle model verification under low-speed maneuver

The same approach was employed to verify the linear model under the low-speed maneuvers with sharp turns. To this end, an open-loop single cycle sinewave steering input with the amplitude of 0.5 rad and the frequency of 0.04 Hz was applied. The vehicle speed during the maneuvers was kept at 10 km/h. Figure 3.7 shows this steering input.

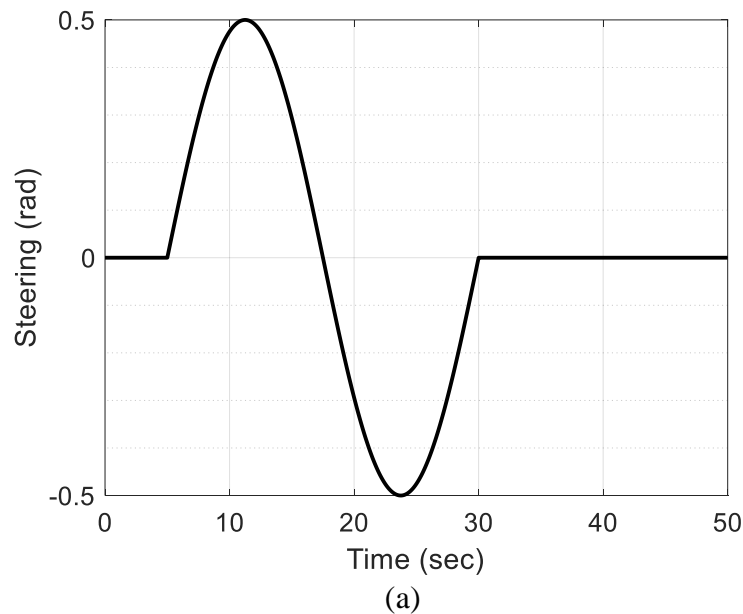
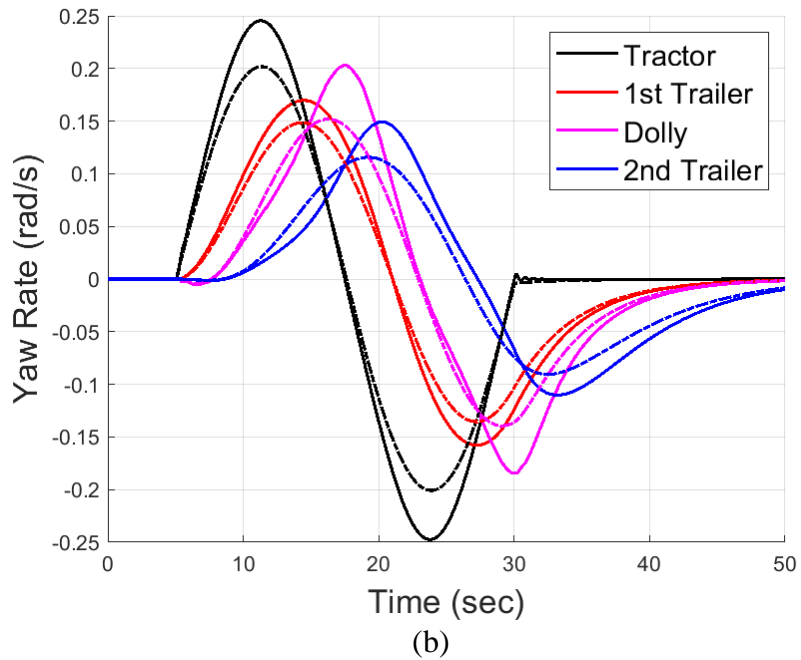
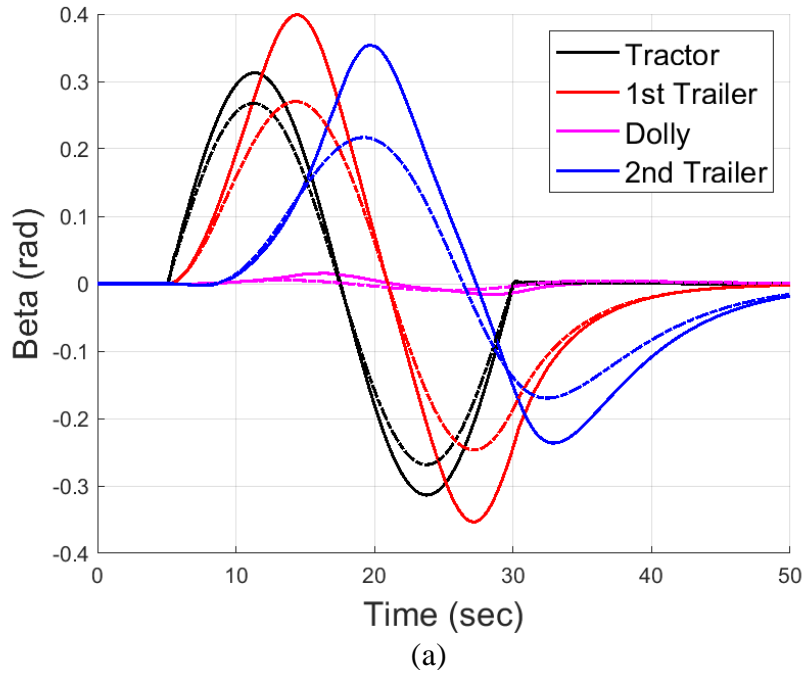


Figure 3.7. Open-loop steering input for linear model verification under a low-speed maneuver.

The simulation results for both the TruckSim model and the linear vehicle model with the nominal cornering stiffness values are illustrated in Figure 3.8. Similar to the high-speed situation, the difference between the simulation results of the two models is considerable. Figure 3.9 shows the simulation results for the TruckSim model and the linear vehicle model with the optimal tire cornering stiffness values. In contrast with the results seen in Figure 3.8, the results shown in Figure 3.9 indicate that the linear vehicle model with the optimal tire cornering stiffness values achieves good agreement with the TruckSim model.

Thus, it can be concluded that the linear vehicle model with the optimal tire cornering stiffness values can also well represents the dynamic behavior of the MTAHV under low-speed maneuver with aggressive steering inputs.



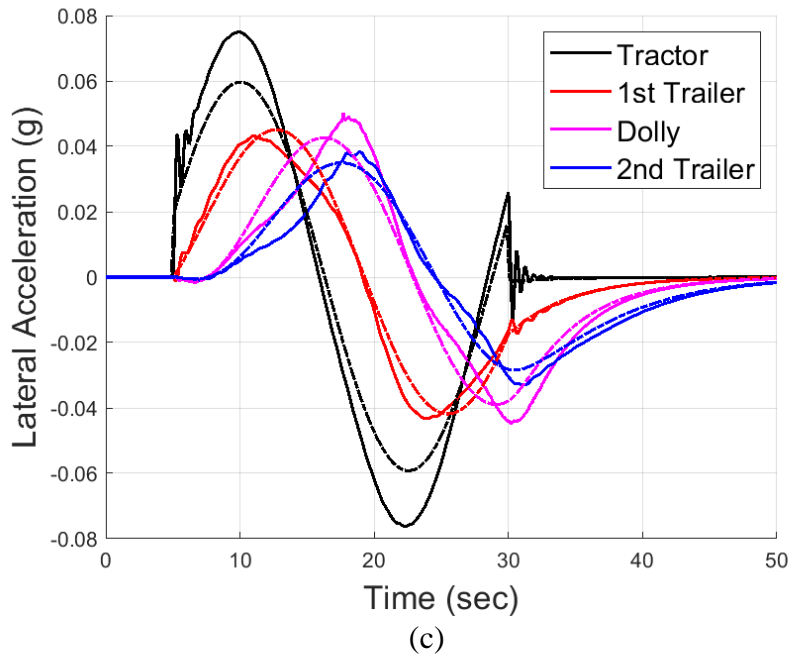
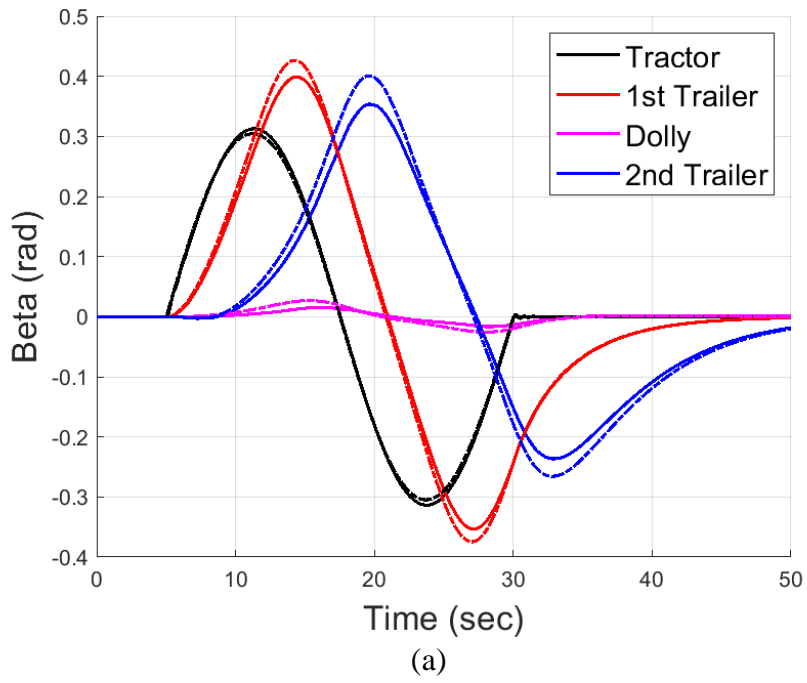


Figure 3.8. Simulation results achieved under low-speed maneuver for the linear vehicle model with the nominal tire cornering stiffness values (dashed lines) and the TruckSim (solid lines): (a) side-slip angle, (b) yaw rate, (c) lateral acceleration.



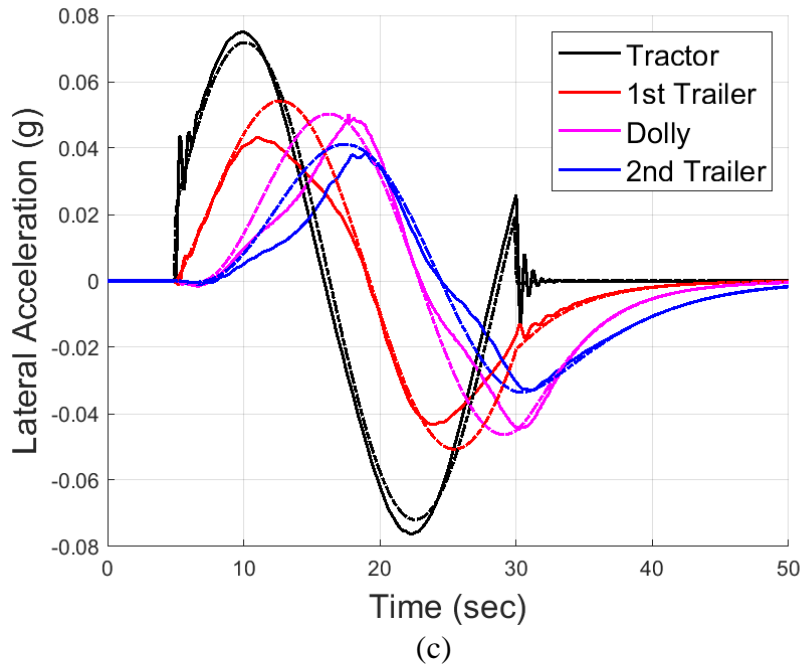
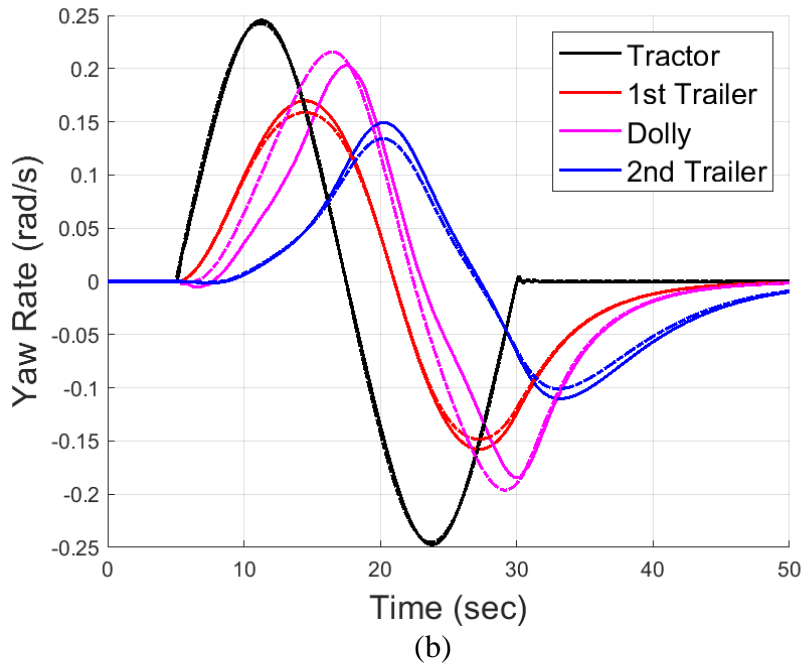


Figure 3.9. Simulation results achieved under low-speed maneuver for the linear vehicle model with the optimal tire cornering stiffness values (dashed lines) and the TruckSim results (solid lines): (a) side-slip angle, (b) yaw rate, (c) lateral acceleration.

3.4 Summary

The study developed a fundamental linear vehicle dynamics model for the A-train double LCV, followed by two linear and non-linear extensions of the fundamental model. Each model is used for specific control strategies with particular requirements. However, the linearization assumptions are valid only for some high-speed driving scenarios with small side-slip angles and steering input. Therefore, an optimization method was used to amend the linear model by minimizing a cost function consisting of yaw-rates and side-slip angles of vehicle units. This approach enabled finding the optimal cornering stiffness of tires for each specific maneuver with determined steering input and vehicle speed, resulting in a linear model that operates similarly to the non-linear TruckSim model.

The study utilized an adequate amount of data and an online look-up table to select the appropriate values of cornering stiffness in real-time for all other steering and speed conditions. This approach proved effective in various controller verifications through different tests. The fundamental vehicle model was verified for low-speed and high-speed driving scenarios and showed significant similarity to the non-linear TruckSim model.

Chapter 4. Driver model development

4.1 Introduction

Decades have passed since a real vehicle was represented by a dynamic model using differential equations, and vehicle system dynamics was understood fundamentally. Around the mid-1960s, it was already conceived that a vehicle and the driver must be dealt with as an integral system since they are essential elements of the system [86]. With the development of active vehicle safety systems, driver models become increasingly important. Modelling of driver behaviors is a huge challenge, and a lot of uncertainties exist under various operating conditions. A driver may react differently under the same driving scenario. Extensive studies have been conducted to explore human drivers' behaviors and driving skills. An effective driver model is critical to simulate drivers' performance precisely. Various driver models have been developed considering different factors, e.g., drivers' experiences and driving skills, drivers' driving behaviors in terms of aggressiveness, vehicle traveling on highways or on urban roads, etc. [87].

Vehicle test maneuvers may be conducted in two ways, i.e., open-loop and closed-loop. For open-loop tests, the input variable's time trajectory, which is usually the front axle steering, is predefined and the test can be repeated using some experimental robots. Albeit, for closed-loop tests, e.g., a target path should be followed with the minimum lateral deviation, the human reaction plays an important role [71]. Human drivers generally make closed-loop tests quite unrepeatable, because the handling tests are usually performed in harsh driving scenarios.

An effective means to analyze the vehicle/human driver interaction during a closed-loop test is using computer simulation. This can be performed even in a vehicle design stage to foresee the quality of performance via a vast number of different maneuvers and to make sure that the design expectations are met [88]. This approach reduces safety issues and costs for road tests with real vehicles and human drivers in near-to-crash driving scenarios.

A myriad number of driver models for single-unit vehicles in order to use in closed-loop simulations have been introduced so far, some of which have been yet well validated and examined in different studies either theoretically using simulation methods or experimentally through the road tests [10], [71]–[74]. However, a MTAHV dramatically differs from a passenger car dynamically in terms of path-following and lateral stability because of remarkable differences in dimensions, weights and configurations [21], [25]. Thus, driver models for single-unit vehicles may not be suitable for MTAHVs and dedicated driver models need to be developed for these large vehicles.

Among the research conducted pertaining AHV dynamics performance, almost none considers the impact of trailing units on the path-following and lateral stability capabilities of the driver model over various driving tests. While in reality, the lateral position of trailers with respect to the target path as well as their lateral acceleration will impact the driver's decision-making process for a given steer input. A driver-tractor/semi-trailer model considering various driver skills was introduced in [89], [90]. The proposed model makes use of a multi-loop structure comprising the tractor lateral deviation, the lead unit's and semi-trailer's lateral acceleration, articulation angle rates of the vehicle combination, and roll angle of the trailer's sprung mass in order to calculate the steering demand. However, the main focus of that study was to examine the reaction of the vehicle to the driver's

behavior and study vehicle combination design criteria from driver points of view. Hence, the maneuverability and lateral stability capabilities and improvements of their devised driver model through various driving scenarios of AHVs was not investigated. For instance, as an outcome of the research, it is concluded that the adaptability of the AHV to the driver can be remarkably improved through variations in the suspension, tire, dimensions and weights and so forth. In [91], a driver model for tractor/semi-trailer was proposed, in which the feedback of the vehicle units' instantaneous states considering a time delay is employed to calculate the optimal steering angle. To do so, a cost function involving the feedback gains was defined and a sensitivity analysis was performed. However, the driver model lacked the differentiation between the perceived motion cues coming from the towing and towed units. In the driver model design for AHVs, Ding and He studied the impact of motion cues coming from either tractor or trailer, and compared these cases with the one in which both vehicle units' motion cues are considered [75]. They concluded that considering all the units' motion cues will improve the directional performance of the vehicle. Despite noticeable merits of considering the impact of trailing units' motions on designing driver models for MTAHVs, they have been ignored in the literature. For instance, He et al. made use of a driver model that utilizes the tractor's steering demand based on the difference in heading angle of the tractor with respect to a desired point on the target path over a constant preview distance [76]. Brown et al. analyzed a MTAHV driver's driving skill through closed-loop dynamic simulation based on the built-in driver in TruckSim [22]. It is noteworthy to mention that the built-in driver model in TruckSim is basically designed for single-unit vehicles and it doesn't consider the trailing units' impact on the towing unit steering demand. Zhituo et al. also employed the built-in driver model

for comparing the different test maneuvers' results as for the rearward amplification of an A-train double AHV [77].

Zhu et al. implemented the idea of employing the trailing units' motion cues in the design of the driver model for a B-train double using a sliding mode controller [78]. They defined a sliding surface as a combination of all units' lateral deviations from target path plus the deviation rates, and then calculated the steering input so that the sliding surface becomes zero. To investigate the capabilities of the driver model, only an evasive single-lane-change (SLC) path-following maneuver through a closed-loop simulation was executed. While, their model demonstrates advantages for a high-speed SLC maneuver over other driver models introduced in the literature, they didn't verify their driver model for other test maneuvers comprising low and high-speed maneuvers. By means of numerical simulations, it was confirmed that this driver model is not applicable for tight cornering operations in urban areas, since the kinematic model for representing the target path is generated only considering highway operations [79].

This research proposes a driver model that takes the dynamics of the MTAHV into account and uses optimal preview control strategy to find the optimized tractor front axle steering input. The advantages of this driver model are as follows: 1) considering the motion cues of all the vehicle units, and simulating the drivers' driving behavior more precisely; 2) tackling more driving test scenarios, including high-speed and low-speed; 3) using optimal preview control strategy, which is mathematically simple to apply; and 4) being applicable for autonomous and semi-autonomous MTAHVs path-following and motion planning operations. Compared with previous driver models, this driver model may simulate the

human driver more accurately in low-speed vehicle path-following maneuvers with sharp turns.

4.2 Preview/predictive driver models

Earlier driver models, which were referred to as the transfer function driver models, considered only compensatory action. Using combined pursuit/compensatory approach will mimic the preview/prediction driver behavior better [71]. These driver models look ahead of the car over an adjustable preview distance, which is often proportional to vehicle forward speed. That is, for higher speed, the preview distance is longer, and vice versa. The driver is also considered to have the ability to predict the future dynamics states of the car over the preview time. These driver models usually apply inverse control actions, and superior control quality can thus be achieved compared against the transfer function driver models.

Among the preview/predictive driver models, the MacAdam driver model is one of the most reputed and verified ones [71], and is founded upon optimal preview control for linear systems [92]. The improved lateral preview driver model introduced in this chapter is closely correlated with Macadam driver model. Hence, this model will be explained herein in detail.

Given the state space representation of equations of motion for the vehicle model generated in Chapter 3, the quadratic cost function represented in equation (4.1) needs to be minimized to find the optimal control variables, which in the case of vehicle lateral preview driver model, is the tractor front axle steering demand.

$$J \triangleq \frac{1}{T} \int_t^{t+T} \{[f(\eta) - y(\eta)]^2 W(\eta - t)\} d\eta \quad (4.1)$$

Where $f(\eta)$ is the lateral position of the vehicle units' previewed points on the reference path, $y(\eta)$ is the predicted lateral position of the vehicle units over the preview time, and $W(\eta - t)$ is the weighting factor over the preview interval. The weighting factors for the current study are set to unity, but for the sake of future development of the driver model and completeness, they are included in equation (4.1). Given the vehicle dynamic model by equation (3.11) and solving the state-space equations, the solution over the preview time T can be rewritten as [93]

$$\mathbf{x}(t + T) = e^{\mathbf{A}_d(t+T)} \mathbf{x}(t) + \int_t^{t+T} e^{\mathbf{A}_d(t+T-\tau)} \mathbf{B}_d \mathbf{u}(\tau) d\tau \quad (4.2)$$

where

$$e^{\mathbf{A}_d(t+T)} = I + \sum_{n=1}^{\infty} \frac{\mathbf{A}_d^n \cdot T^n}{n!} = \mathbf{\Phi}(T|t) \quad (4.3)$$

and

$$\int_t^{t+T} \mathbf{\Phi}(t + T - \tau) \mathbf{B}_d \mathbf{u}(\tau) d\tau = \left[I + \sum_{n=1}^{\infty} \frac{\mathbf{A}_d^n \cdot T^n}{(n + 1)!} \right] \mathbf{B}_d T \mathbf{u}(t) = \mathbf{K}(T|t) \mathbf{u}(t) \quad (4.4)$$

The output can be calculated as

$$\mathbf{y}(t + T) = \mathbf{C}_d \mathbf{x}(t + T) \quad (4.5)$$

Substituting this output into the cost function defined by equation (4.1) and then calculating the derivative of the cost function with respect to the input variable and setting the equation equal to zero, the optimal value of the tractor's front axle steering angle, $\delta_{1_{opt}}$, will be obtained as is demonstrated in the next part. Note that by defining the proper matrix C_d the error term $f(\eta) - y(\eta)$ can be adjusted to consider all the vehicle units' deviations from the reference path so as to find the optimal steering angle.

4.3 Lateral preview driver model methodology

Lateral control of MTAHVs needs to keep the vehicle following the center line of a target path, which involves a wide range of maneuvers, such as straight road drives, curved path negotiations and roundabout turns, by providing the appropriate steering demand [94]. Besides, a few of studies using lateral preview driver models for AHVs only consider the leading unit's motion cue for steering control, which is neither based on actual drivers' driving behaviors nor effective for real-world steering control operations [1], [20], [95]. In addition, the MTAHV drivers' driving behaviors in high-speed and low-speed operations would be quite different. For instance, in high-speed situations when the driver has to react fast to avoid an obstacle, they would rather care about the lateral stability of the vehicle; in low-speed curved path negotiations, they will pay more attention to follow a predefined path accurately. Obviously, vehicle forward speed is an important factor to be considered in the design of driver models, especially for the MTAHV driver models.

Considering the aforementioned factors, to the best of the knowledge of the author, no comprehensive lateral driver model has been designed for MTAHVs. The proposed driver model comprises two modes: 1) low-speed path following mode, and 2) high-speed lateral

stability mode. The low-speed path following mode aims to keep all the vehicle units following the target path with the minimum lateral deviation; whereas the high-speed lateral stability mode tries to keep the leading unit following the desired path, while the trailing units follow the tractor front axle center (TFAC) trajectory in order to make the RWA approach 1.0. Figure 4.1 schematically depicts the proposed driver model in terms of the lateral path deviations. Moreover, Figure 4.2 shows the flowchart of the proposed driver model in a simplified manner.

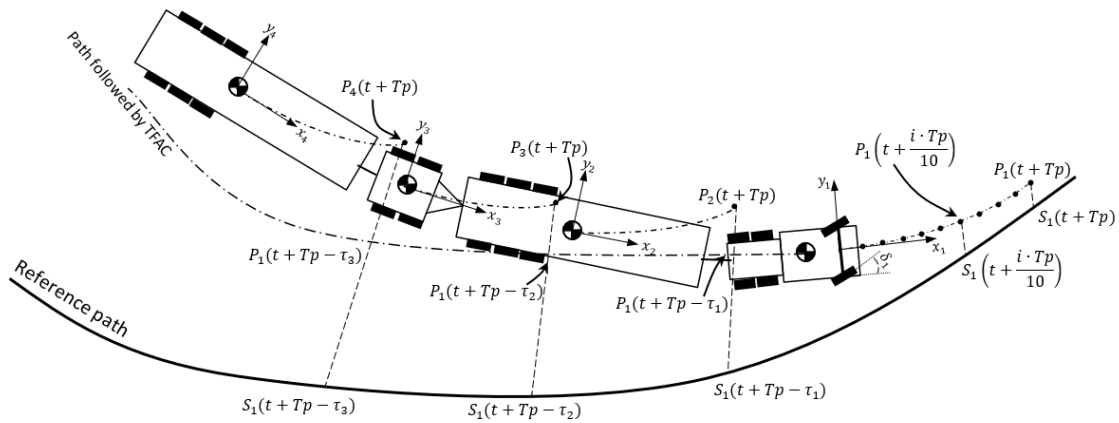


Figure 4.1 Schematic representation of preview driver model for A-train double MTAHV

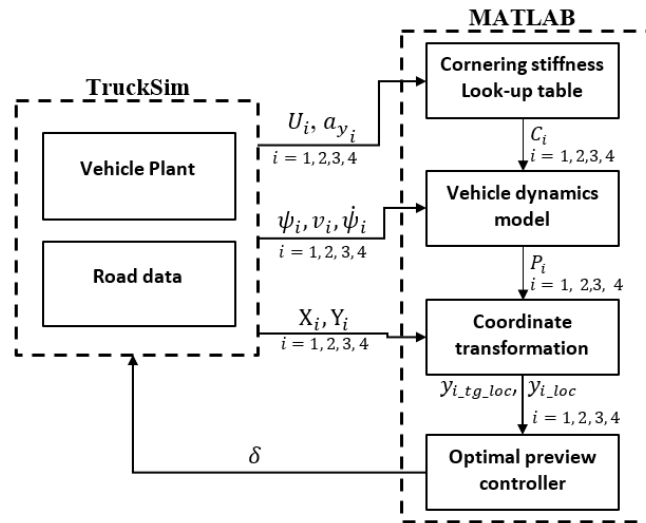


Figure 4.2 Simple representation of the flowchart of the proposed lateral preview driver model

4.3.1 Low-speed path-following mode (First mode):

The first mode, i.e., low-speed path-following, is designed for low-speed driving scenarios.

The total deviations of all the vehicle units from the reference path e_{pf} is defined as

$$e_{pf} = e_1 + k_1 e_{2_pf} + k_2 e_{3_pf} + k_3 e_{4_pf} \quad (4.6)$$

where $0 \leq k_i \leq 1$, $i=1,2,3$ is the weighting factor that indicates how much attention the "driver" is giving to the motion cues of the towed units when controlling the steering. Also

$$e_1 = \sum_{i=1}^n \left(y_{1_tg_loc} \left(t + \frac{iT_p}{n} \right) - y_{1_loc} \left(t + \frac{iT_p}{n} \right) \right) \quad (4.7)$$

where e_1 denotes the accumulated error for n preview points ahead of the TFAC with respect to desired reference path. $y_{1_loc} \left(t + \frac{iT_p}{n} \right)$ is the predicted lateral coordinate of the i^{th} point over the preview window ahead of the TFAC, i.e. $P_1 \left(t + \frac{iT_p}{n} \right)$, with respect to the body-fixed frame of the tractor. $y_{1_tg_loc} \left(t + \frac{iT_p}{n} \right)$ represents the desired lateral coordinate of the i^{th} target point on the reference path, i.e. $S_1 \left(t + \frac{iT_p}{n} \right)$ corresponds to the aforementioned i^{th} preview point in front of the TFAC. These lateral coordinates are also given in the trailing units body-fixed coordinate system.

Three following errors for the trailing units are calculated based on one preview point ahead of each unit's CG and the delayed tractor's target point on the reference path considering each towed unit's speed.

$$e_{2_pf} = y_{1_tg_loc}(t + T_p - \tau_1) - y_{2_loc}(t + T_p) \quad (4.8)$$

$$e_{3_pf} = y_{1_tg_loc}(t + T_p - \tau_2) - y_{3_loc}(t + T_p) \quad (4.9)$$

$$e_{4_pf} = y_{1_tg_loc}(t + T_p - \tau_3) - y_{4_loc}(t + T_p) \quad (4.10)$$

where $y_{j_loc}(t + T_p), j = 2,3,4$, are the predicted lateral coordinates of the three trailing units' preview points, $P_j(t + T_p), j = 2,3,4$, over the preview time T_p measured in their own body-fixed frames, $y_{1_tg_loc}(t + T_p - \tau_j), j = 1,2,3$, represents the lateral coordinates of the target points (*i. e.*, $S_1(t + T_p - \tau_j), j = 1,2,3$) on the reference path defined in each of the body-fixed lateral coordinate of the towed units. These target points are generated using the tractor's last target point $S_1(t + T_p)$ and the delay factors of each trailing unit $\tau_j, j = 1,2,3$.

Indeed, τ_1, τ_2 and τ_3 are respectively the times needed for the first, second and third trailing units' CGs to reach the tractor's current target point on the reference path over the preview time. These time delays are determined by

$$\tau_1 = \frac{l_{11} + l_{ap1_1} + l_{ap1_2}}{U_2} \quad (4.11)$$

$$\tau_2 = \frac{l_{11} + l_{ap1_1} + l_{ap1_2} + l_{ap2_2} + l_{ap2_3}}{U_3} \quad (4.12)$$

$$\tau_3 = \frac{l_{11} + l_{ap1_1} + l_{ap1_2} + l_{ap2_2} + l_{ap2_3} + l_{ap3_3} + l_{ap3_4}}{U_4} \quad (4.13)$$

Note that the term l_{api_j} is defined in Appendix A.1.

It is assumed that 10 preview points ahead of the TFAC are considered. Substituting the previously defined errors determined by equations (4.6) to (4.10) into equation (4.1) and solving for the optimal steering input in order to minimize the cost function, the optimal steering δ_{1_opt} is formulated by

$$\delta_{1_opt} = \frac{Q_1 - \left(\mathbf{C}_d(1, :) \sum_{i=1}^{10} \Phi \left(\frac{i \cdot T_p}{10} \middle| t \right) + W_1 \Phi(T_p | t) \right) \cdot \mathbf{x}(t)}{\left(\mathbf{C}_d(1, :) \sum_{i=1}^{10} \mathbf{K} \left(\frac{i \cdot T_p}{10} \middle| t \right) + W_1 \mathbf{K}(T_p | t) \right)} \quad (4.14)$$

where,

$$Q_1 = \sum_{i=1}^{10} y_{1_tg_loc} \left(t + \frac{i \cdot T_p}{10} \right) + k_1 \cdot y_{2_tg_loc}(t + T_p) + k_2 \cdot y_{3_tg_loc}(t + T_p) + k_3 \cdot y_{4_tg_loc}(t + T_p) \quad (4.15)$$

$$W_1 = k_1 \cdot \mathbf{C}_d(5, :) + k_2 \cdot \mathbf{C}_d(9, :) + k_3 \cdot \mathbf{C}_d(13, :) \quad (4.16)$$

Figure 4.3 illustrates the geometrical method used to determine the lateral position of target points on the desired path with respect to the body-fixed coordinate systems of the vehicle units. Having the global coordinates of the target path constituent points; for instance, the GPS data is used, i.e. a set of predefined global coordinates representing the reference path, a curve is fitted in MATLAB, and the target path function $f(X)$ is generated. Utilizing the

global coordinates of the TFAC and trailing units' CGs as well as the $f(X)$, the minimum distances and the corresponding points on the target path are mathematically calculated at each time step using a MATLAB code. The nearest point to the TFAC on the target path which is a perpendicular projection of the TFAC on path is denoted by S_0 and the respective target path yaw angle is represented by θ . The simplest way to calculate the nearest points to the TFAC preview points is drawing a perpendicular line from the corresponding preview point to the target path, i.e. $S_1'(t + T_p)$, as shown in Figure 4.3. This strategy might be correct for the smooth reference paths, such as HSLC maneuver. However, as it is evident from the figure, for sharp turns it is not an accurate way and the estimated point is further away from the real position of the TFAC at its current speed. Assuming the last position of the TFAC over the preview time is $P_1(t + T_p)$, estimated longitudinal positions of the TFAC on the body-fixed x axis over the preview times is $P_1'(t + T_p) = u_1 T_p$. For other points in the preview time window, i.e. $t + \frac{i \cdot T_p}{10}$, the longitudinal positions can be estimated by $P_1' \left(t + \frac{i \cdot T_p}{10} \right) = u_1 \frac{i \cdot T_p}{10}$ $i = 1 \sim 9$. Considering the difference between the tractor heading and the corresponding path point direction, i.e. ψ_{rel} , the new points $P_1'' \left(t + \frac{i \cdot T_p}{10} \right)$ is generated. The global coordinates of the $P_1'' \left(t + \frac{i \cdot T_p}{10} \right)$ are calculated by

$$\begin{aligned}
 X_{P_1'' \left(t + \frac{i \cdot T_p}{10} \right)} &= X_{TFAC} + u_1 \cdot \frac{i \cdot T_p}{10} \cdot \cos \psi_{rel} \cdot \cos \theta \quad i = 1, 2, \dots, 10 \\
 Y_{P_1'' \left(t + \frac{i \cdot T_p}{10} \right)} &= Y_{TFAC} + u_1 \cdot \frac{i \cdot T_p}{10} \cdot \cos \psi_{rel} \cdot \sin \theta \quad i = 1, 2, \dots, 10
 \end{aligned} \tag{4.17}$$

where u_1 is the tractor longitudinal velocity, T_p is the preview time, X_{TFAC} and Y_{TFAC} are global coordinates of the tractor front axle center and $\psi_{rel} = \theta - \psi$ is the relative yaw angle of the tractor relative to the reference path. Having the $X_{P_i''(t+\frac{i.T_p}{n})}$, $Y_{P_i''(t+\frac{i.T_p}{n})}$ and $f(X)$, similar to finding point S_0 , $S_1(t + \frac{i.T_p}{10})$, that represents the nearest points on the reference path to the point $P_i''(t + \frac{i.T_p}{10})$, is estimated using the MATLAB code. Then, the respective global coordinates i.e. $X_{S_1(t+\frac{i.T_p}{10})}$ and $Y_{S_1(t+\frac{i.T_p}{10})}$, can be determined.

Finally, the lateral position of point $S_1(t + \frac{i.T_p}{10})$ in the tractor's body-fixed coordinate system is determined by

$$y_{1_tg_loc}\left(t + \frac{i.T_p}{10}\right) = \left(Y_{S_1(t+\frac{i.T_p}{10})} - Y_{TFAC}\right) \cdot \cos\psi - \left(X_{S_1(t+\frac{i.T_p}{10})} - X_{TFAC}\right) \cdot \sin\psi \quad (4.18)$$

Similarly, for the trailing units, $y_{2_tg_loc}(t + T_p)$, $y_{3_tg_loc}(t + T_p)$ and $y_{4_tg_loc}(t + T_p)$ can be calculated. Given the tractor's last target point $S_1(t + T_p)$, the time delays τ_i determined by equations (4.11) to (4.13), and the reference path function $f(x)$, the corresponding target points of the trailing units, $S_1(t + T_p - \tau_i)$, $i = 1,2,3$, can be identified. Note that these target points are to be followed by the trailing units' CGs.

$$e_{2_{ls}} = y_{P_1}(t + T_p - \tau_1) - y_{2_{loc}}(t + T_p) \quad (4.21)$$

$$e_{3_{ls}} = y_{P_1}(t + T_p - \tau_2) - y_{3_{loc}}(t + T_p) \quad (4.22)$$

$$e_{4_{ls}} = y_{P_1}(t + T_p - \tau_3) - y_{4_{loc}}(t + T_p) \quad (4.23)$$

Albeit, the second terms on the right side of equations (4.21) to (4.23), i.e., $y_{j_{loc}}(t + T_p), j = 2,3,4$ are calculated similarly to those for the first mode. However, the first terms on the right side of these equations, i.e. $y_{P_1(t+T_p-\tau_j)}, j = 1,2,3$, are the lateral coordinates of the trailing units' target points on the TFAC trajectory, which are defined in the respective trailing unit's body-fixed frame. Hence, to shed a light on how these terms are calculated, it should be pointed out that if the predicted local positions of trailers and dolly over their preview time is situated in front of the TFAC, the corresponding point on the predicted TFAC trajectory is utilized to calculate the errors. This case may happen only at very high vehicle speeds because the predicted trailing units' CG positions are velocity-dependent. Thus, the preview distances may be longer than the distances between the TFAC and the trailing units' CGs. Figure 4.4 shows the geometrical method used to map the delayed TFAC last predicted position, i.e. $P_1(t + T_p - \tau_1)$, into the first trailer's body-fixed coordinate system in order to calculate the local lateral position error relative to the first trailer's predicted CG position, that is, $P_2(t + T_p)$. This approach is then repeated for the dolly and the second trailer using the relative yaw angles between each two adjacent unit to calculate the respective errors. But for the purpose of simplicity, only geometrical illustration of the first error is depicted in Figure 4.4.

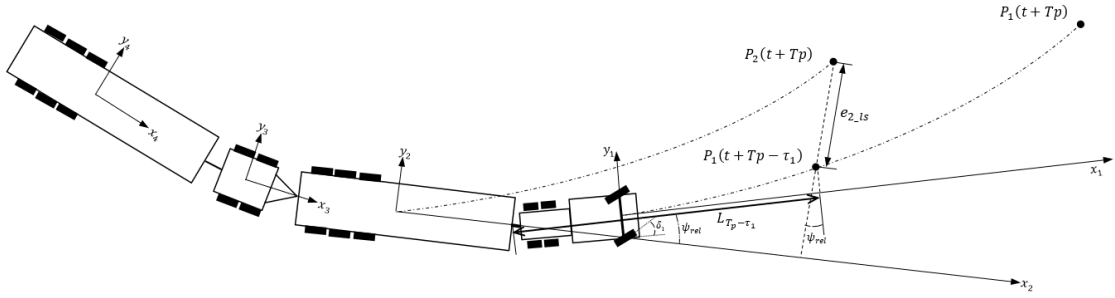


Figure 4.4 Geometrical method used to calculate the 1st trailer deviation from the tractor delayed preview path described in the 1st trailer body-fixed coordinate system

Similarly, τ_1 , τ_2 and τ_3 are respectively the times required for the first, second and third trailing units' CGs to reach to the current position of the TFAC. They are defined by equations (4.11) to (4.13).

On the other hand, if the predicted points of the trailing units are located behind the TFAC, i.e. when vehicle forward speed is not too high and as a result $\tau_i > T_p$, the trajectory of the TFAC in global coordinate system needs to be stored in the memory. Using the stored data, the coordinates of the TFAC at time $(\tau_i - T_p)$ is calculated. Then the global coordinates of trailing units' CGs are applied to calculate the delayed position of the buffered TFAC in the trailing units' body-fixed coordinate systems. The target points for each trailing unit is thus determined by

$$\begin{aligned}
 y_{P_1(t+T_p-\tau_i)} = & (Y_{TFAC}(\tau_i - T_p) - Y_{j_CG}) \cos \psi_j \\
 & - (X_{TFAC}(\tau_i - T_p) - X_{j_CG}) \sin \psi_j
 \end{aligned} \tag{4.24}$$

where, X_{j_CG} and Y_{j_CG} , $j = 2,3,4$ are the global coordinates of trailing units' CGs, and $y_{P_1(t+T_p-\tau_i)}$ represents the lateral coordinates of the target points on the TFAC trajectory

in each towed unit's body-fixed frame. Given $y_{P_1(t+T_p-\tau_i)}$ determined by equation (4.24), the terms of $e_{j_{ls}}$, $j=2,3,4$, on the left side of equations (4.21) to (4.23) can be calculated.

Substituting equation (4.19) into equation (4.1), and solving for $\delta_{1_{opt}}$, the optimal steering is calculated by

$$\delta_{1_{opt}} = \frac{Q_2 - \left(\mathbf{C}_d(1, :). \sum_{i=1}^{10} \Phi \left(\frac{i \cdot T_p}{10} \middle| t \right) + W_1 \cdot \Phi(T_p | t) - P \right) \cdot \mathbf{x}(t)}{\left(\mathbf{C}_d(1, :). \sum_{i=1}^{10} \mathbf{K} \left(\frac{i \cdot T_p}{10} \middle| t \right) + W_1 \cdot \mathbf{K}(T_p | t) + R \right)} \quad (4.25)$$

where:

$$\begin{aligned} Q_2 = \sum_{i=1}^{10} y_{1_{tg_loc}} \left(t + \frac{i \cdot T_p}{10} \right) &+ k_1 \cdot L_{T_p - \tau_1} \sin \psi_{rel_{1,2}} + k_2 \cdot L_{T_p - \tau_2} \sin \psi_{rel_{1,3}} \\ &+ k_3 \cdot L_{T_p - \tau_3} \sin \psi_{rel_{1,4}} + k_2 \cdot L_2 \sin \psi_{rel_{2,3}} \\ &+ k_3 \cdot L_2 \sin \psi_{rel_{2,4}} + k_3 \cdot L_3 \sin \psi_{rel_{3,4}} \end{aligned} \quad (4.26)$$

$$\begin{aligned} P = \mathbf{C}_d(1, :). (k_1 \cdot \Phi(T_p - \tau_1 | t) \cos \psi_{rel_{1,2}} &+ k_2 \cdot \Phi(T_p - \tau_2 | t) \cos \psi_{rel_{1,3}} \\ &+ k_3 \cdot \Phi(T_p - \tau_3 | t) \cos \psi_{rel_{1,4}}) \end{aligned} \quad (4.27)$$

$$\begin{aligned} R = \mathbf{C}_d(1, :). (k_1 \cdot \mathbf{K}(T_p - \tau_1 | t) \cos \psi_{rel_{1,2}} &+ k_2 \cdot \mathbf{K}(T_p - \tau_2 | t) \cos \psi_{rel_{1,3}} \\ &+ k_3 \cdot \mathbf{K}(T_p - \tau_3 | t) \cos \psi_{rel_{1,4}}) \end{aligned} \quad (4.28)$$

$$W_1 = k_1 \cdot \mathbf{C}_d(5, :) + k_2 \cdot \mathbf{C}_d(9, :) + k_3 \cdot \mathbf{C}_d(13, :) \quad (4.29)$$

where $\psi_{rel_{i,j}}$ is the relative yaw angle between i^{th} and j^{th} units, $L_{T_p - \tau_i}$ is the preview distance from the first articulation point over the $T_p - \tau_i$ preview times, L_2 and L_3 are the distance between first articulation point to second articulation point and second articulation point to third articulation point, respectively. It is important to note that the actual steering angle applied to the vehicle model, δ'_{1_opt} , should consider the time delay, τ_d , due to the neuromuscular delay caused by the human driver [96]. This delay is applied using a Simulink delay block during the closed-loop simulations. Figure 4.5 illustrates the flowchart of the detailed algorithm used for the lateral preview driver model.

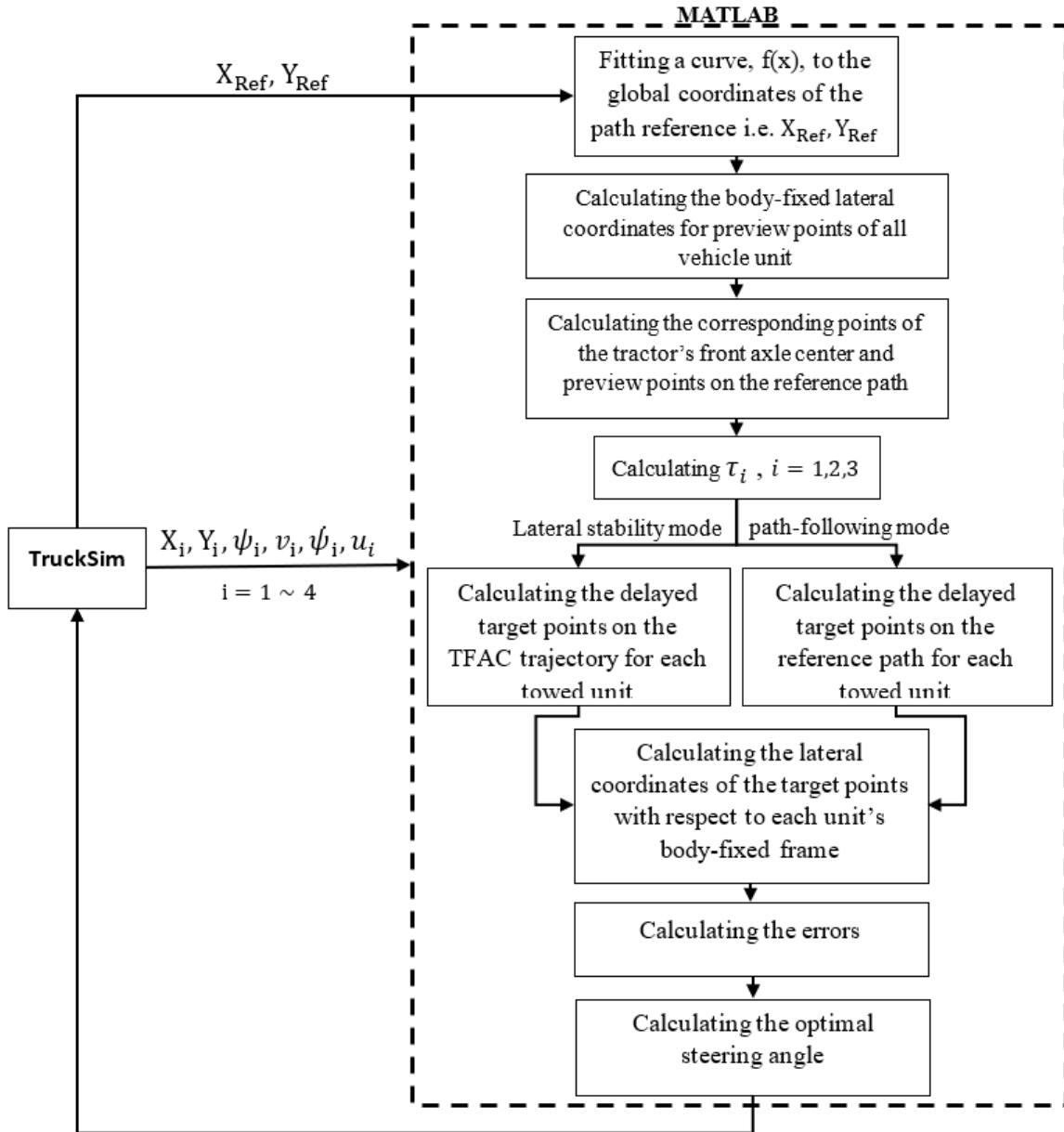


Figure 4.5 Flowchart of the algorithm used for the lateral preview driver model.

4.4 Driver model validation

In this section a number of justifications will be provided to demonstrate the validity of the proposed driver model which makes use of a linear yaw-plane vehicle model. In Chapter 3, it is proved that using the optimization method to find the optimal tires' cornering

stiffness values, the linear model operates well with the current time step in terms of similar dynamics response with various steering inputs. However, someone might doubt if the linear vehicle model will perform well for low-speed sharp turn negotiations over the prediction horizon. Indeed, using a predictive driver model, the only restriction in applying the linear model is that the preview time shouldn't be too long, otherwise the linear model will not precisely predict the states of the vehicle units over the preview time. Based on the biased directional performance regions for MTAHV [22] for a transport delay ranges from 0.1 to 0.2 seconds, which is valid for a driver with acceptable driving skills, the preview time between 0.8 to 1.8 seconds can assure both the path-tracking and stability goals under high-speed evasive maneuvers. Generally, a preview time between 0.5 and 2.0 seconds is used by human drivers with different driving skills [71]. For the proposed driver model, the value of 1 second was applied as the preview time. Generally, under low-speed sharp turn maneuvers, which challenge the vehicle model linearization assumptions due to considerable articulation angles and tractor front wheel steering angles. Based upon the performance-based standard (PBS) [34], this maneuver should be executed at very low vehicle speed on a 90-degree turn with a circular arc of 12.5 meters radius, and it makes the use of the linear model unreliable. However, even in that scenario, the preview distance corresponding to the one-second preview time is 1.38 meters. It is equal to approximately 6 degrees of yaw motion over the preview time, which is quite small to assure the correctness of the linearization assumption, thereby using linearized equations of motions over the preview time, provided the linear dynamics model performs well at the current time step. It is noteworthy that the approach of using linear expression of nonlinear dynamics equations considering the current states of the vehicle as well as body-fixed

coordinate system to estimate the states over the limited preview distance is similar to partially linearizing a nonlinear system under various operating conditions.

In order to validate the proposed lateral preview driver model, firstly the MacAdam driver model [97] and the unified lateral preview driver model [98] were replicated precisely. Then, their simulation results for a number of driving scenarios were compared with the proposed driver model's results to show the improvements achieved. It is noteworthy once again that the MacAdam driver model is designed for single-unit vehicles. Thus, the motions of the trailing units are not taken into account for optimal steering calculation. Furthermore, the unified lateral preview driver model which considers the motion cues from all the vehicle units, is not appropriate for dealing with all the driving scenarios that will be shown later.

The first driving maneuver simulated is a SLC maneuver. Figure 4.6 shows the target path geometry and the lateral displacements of all the vehicle units for the unified lateral preview driver model and the proposed driver model.

As it seems unrealistic to assume that the driver receives the same motion cues from the trailers and dolly as they receive from the tractor due to the trailing units' isolation from the tractor via the articulation joints and cab suspension; consequently, the weighting factors equal to 1 would be infeasible; hence $k_1 = 0.6$, $k_2 = 0.1$ and $k_3 = 0.3$ were selected in all the driving maneuvers. Other factors were chosen as $T_p = 1$ s, $\tau_d = 0.1$ s, $U = 88$ km/h. The high vehicle speed entails using the second mode of the unified driver model, i.e. high-speed mode. The closed-loop SLC maneuver geometry was defined using the kinematic equation recommended by ISO 14791 [99], which is given by

$$Y = \frac{a_y}{(2\pi f)^2} \left[2\pi f \frac{X}{U} - \sin\left(2\pi f \frac{X}{U}\right) \right] \quad (4.30)$$

where f is the frequency in Hertz, U is the tractor forward speed and a_y is the tractor peak lateral acceleration. This study selects the testing maneuvering parameter values: $f = 0.35$ Hz, $U = 88$ km/h and $a_y = 0.25$ g, the maximum lateral displacement $Y=3.184$ m.

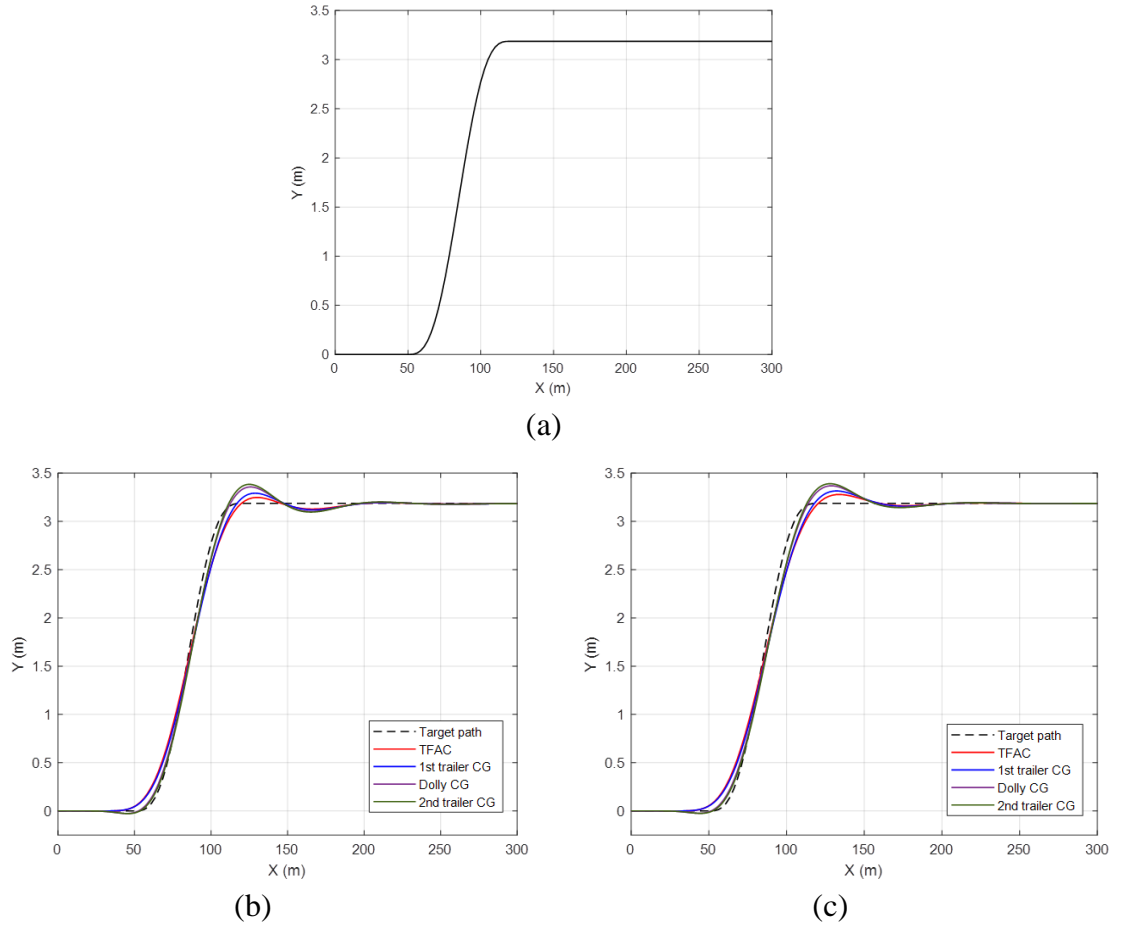


Figure 4.6. High-speed lane change maneuver: (a) target path geometry, (b) lateral position of vehicle units using the unified lateral preview driver model, (c) lateral position of vehicle units using the proposed driver model.

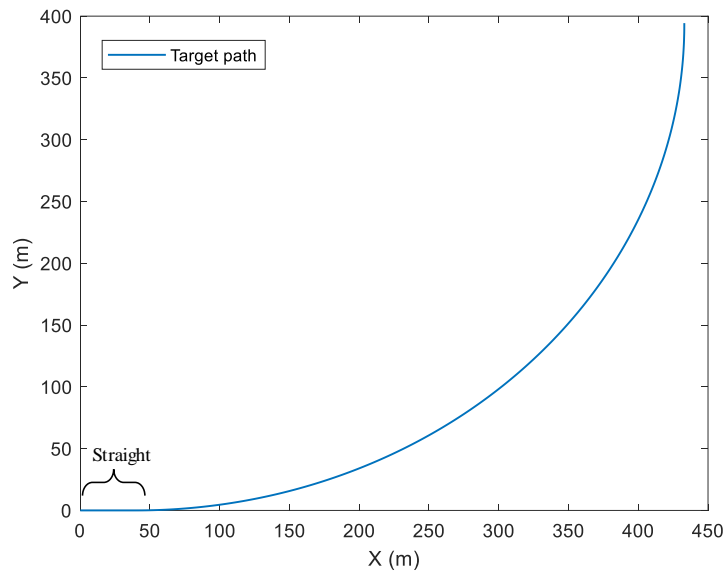
From Figures 4.6 (b) and (c), it is inferred that the transient off-tracking achieved from the unified lateral preview and the proposed driver models are quite similar under the high-speed single-lane change maneuver. Thus, the proposed driver model can be trusted for

testing other maneuvers. However, it can also be seen that the oscillations for the unified driver model are a little bit severe. It is necessary to mention that the main purpose of this study is not to discuss the merits of using all the vehicles motion cues in optimal steering calculation over the MacAdam driver model as well as the advantages of employing two driver model modes for low and high-speed driving for a single-lane change maneuver, because they are already well approved in [78] and [89]. Instead, it is intended to prove that the proposed driver model has much more flexibility and accuracy over the unified driver model and MacAdam driver model, by which more challenging MTAHV driving scenarios like high-speed turn or roundabout turn are not possible to be simulated. To the best knowledge of the author, there is no study in the literature in that regard.

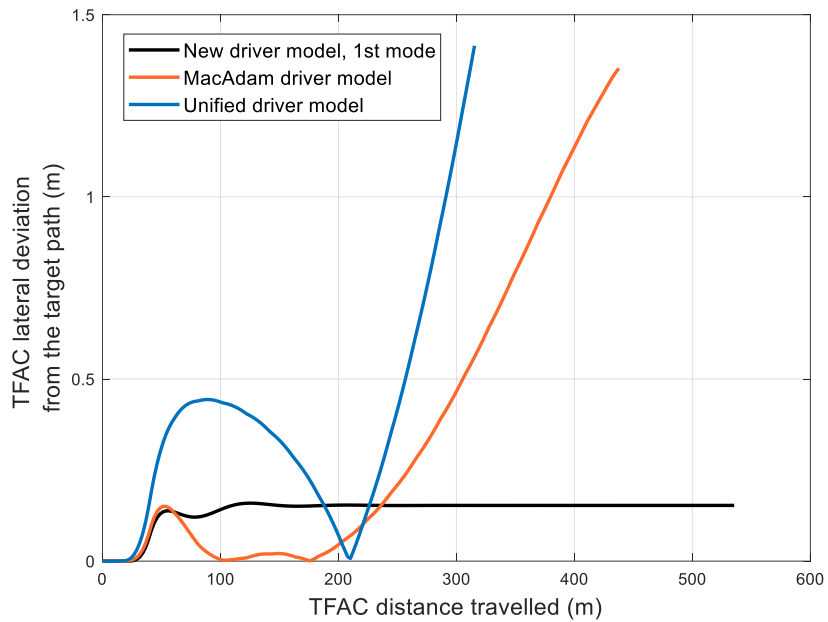
The second testing maneuver simulated is a high-speed turn (HST). Figure 4.7 (a) shows the geometry of the target path, which is derived from [100]. The testing course begins with a straight part followed by a circular course, and then a straight line. Similar to the HSLC maneuver, the vehicle speed is 88 km/h. Since the speed is high, the second mode of the proposed driver model, i.e. the high-speed mode, was initially applied to demonstrate the pros of the proposed driver model over the other two driver models. However, to show the capabilities of the lateral stability mode, the path-following mode is also employed and the results are discussed.

As shown in Figure 4.7 (b), MacAdam driver model and the unified driver model couldn't finish the testing maneuver successfully. The reason is the formulation used for calculating the deviation error over the global coordinate system is suitable only for small cornering angles [79]. That is why after tracing the curvilinear path, the lateral deviation of vehicle units from the target path starts introducing some accumulated error. Consequently, the

calculated steering value becomes very large, the vehicle dynamics model gets unstable, and finally the TruckSim simulation crashes. Figure 4.7 (b) demonstrates the absolute values of the TFAC lateral deviation from the target path for all the driver models. It is evident that MacAdam driver model can travel the path longer than the unified driver model, since the former only uses the tractor lateral position error in order to calculate the optimal steering, While the latter utilizes all the units' errors, and hence the accumulated error due to the increasing cornering angle would be higher, and the software crash happens faster.



(a)

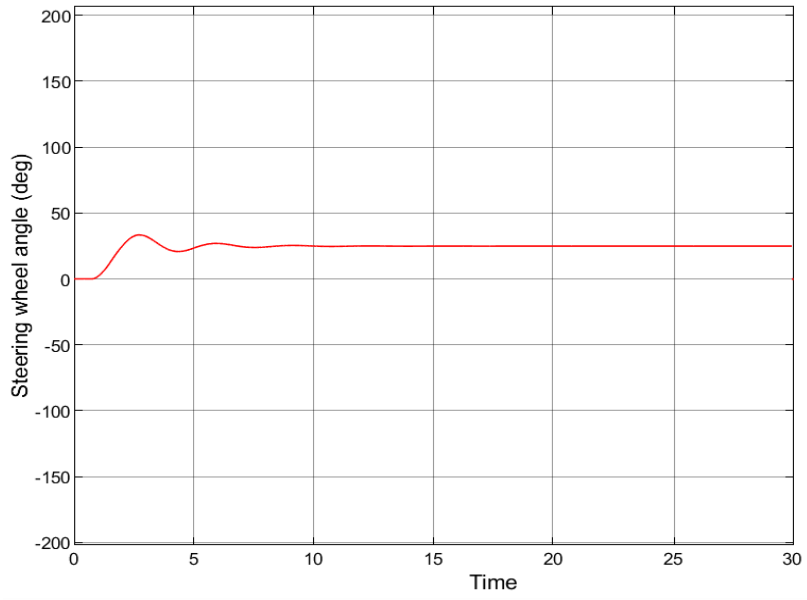


(b)

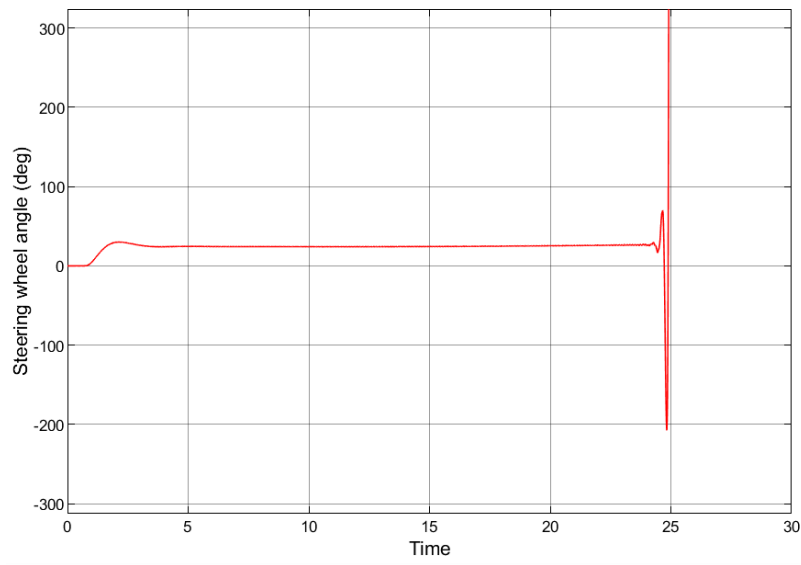
Figure 4.7. High-speed turn: (a) target path geometry, (b) absolute values of the TFAC lateral deviation from the target path based on different driver models.

For the proposed driver model, the high-speed off-tracking is less than 0.23 m, which is considerably smaller than the acceptable value of 0.8 m recommended by the PBS [34]. For the other two driver models, the respective measures are divergent.

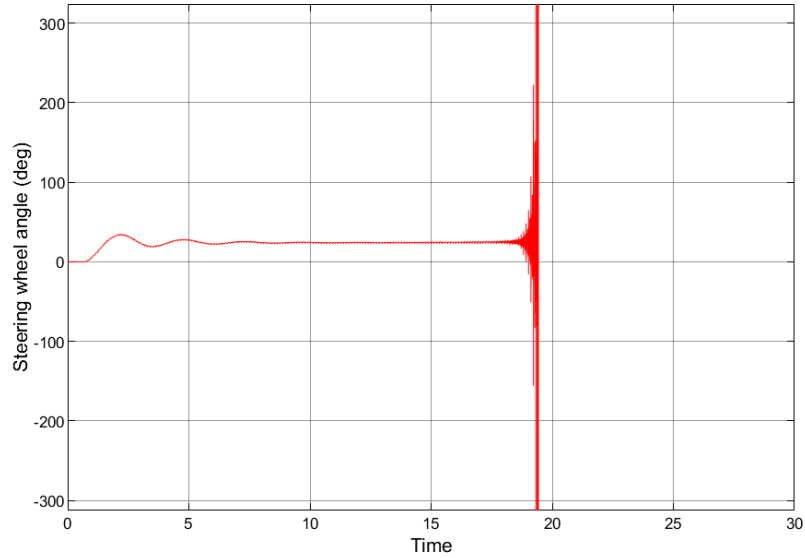
Figure 4.8 exhibits the time histories of steering wheel angles during the HST maneuver. The proposed driver model enters the circular part of the path, and then follows the final straight section without any issue. The other two driver models cannot successfully follow the path, and as noted before due to remarkable deviation error accumulated over the circular course because of the large yaw motions. The steering angles for the two driver models suddenly increase dramatically, thereby leading to the failure of the testing maneuver.



(a)



(b)



(c)

Figure 4.8. Steering wheel angle time history: (a) proposed driver model, (b) MacAdam driver model, (c) unified driver model.

Figure 4.9 illustrates the lateral acceleration and lateral distance of the TFAC and the reference path from the 2nd trailer rear axle center (RAC) for both the lateral stability and path-following modes of the proposed driver model. Figure 4.9 (a) indicates that using the first mode causes a larger transient off-tracking once the vehicle leaves the straight lane and arrives the curvilinear part of the road compared with that shown in Figure 4.9(b), in which the second mode has been utilized. The oscillations for the former are also more violent than those for the latter. From Figures 4.9 (c) and 4.9 (d), it is perceived that the lateral acceleration of tractor and second trailer CGs using the lateral stability mode are lower than those of generated by the path-following mode. Improvements are achieved for the second mode by compromising the lateral deviation of the TFAC, which is larger than that for the first mode, while still in the acceptable range. However, in the case of the second mode, the second trailer lateral deviation from the target path is reduced with respect to the first mode.

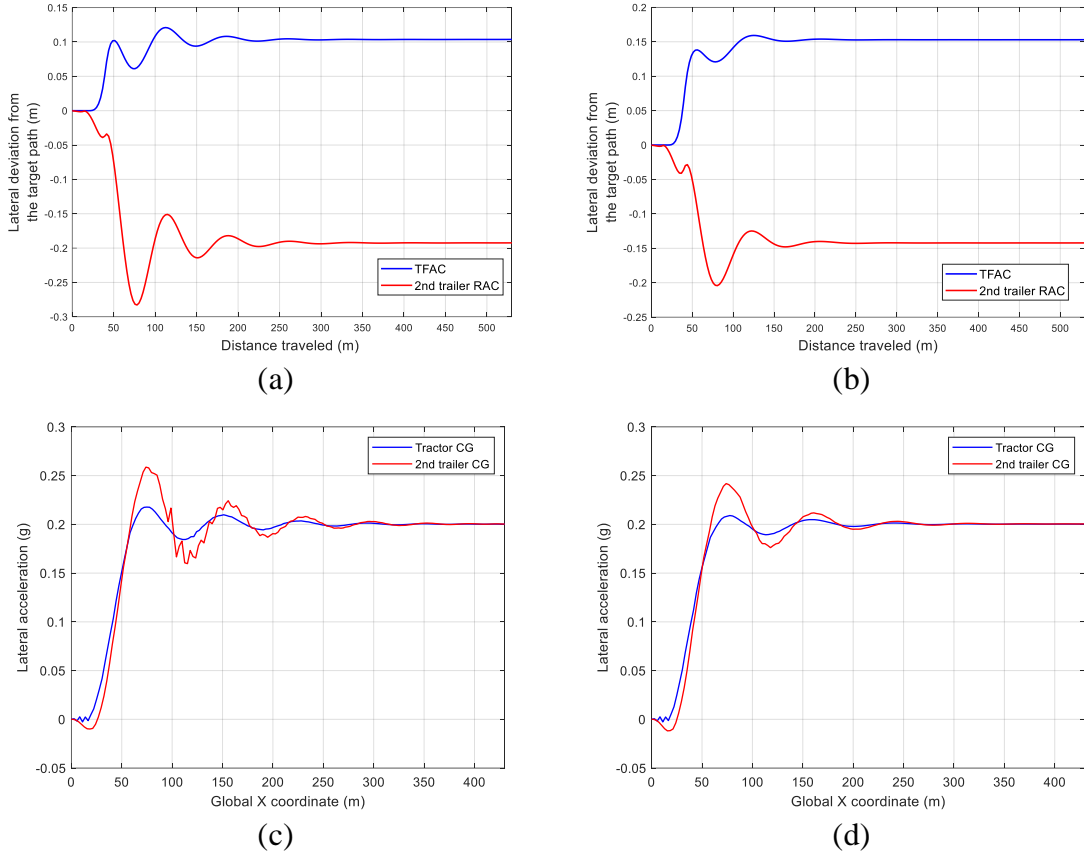
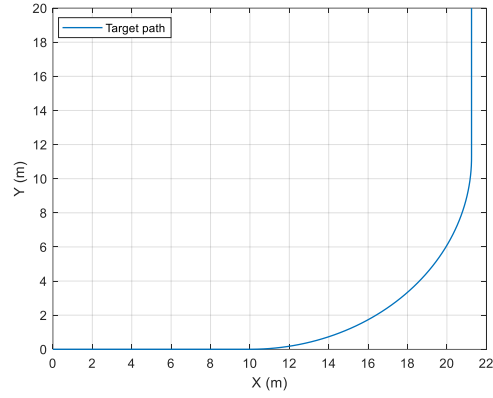
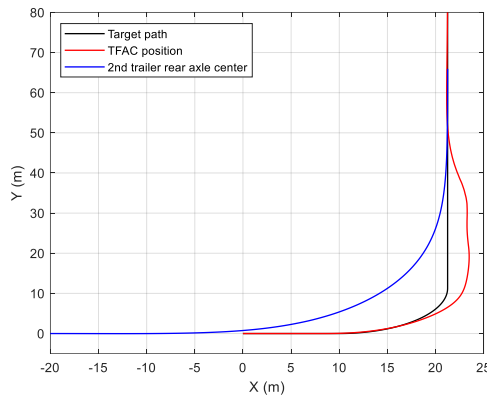


Figure 4.9. Comparison of the simulation results of the two modes the proposed driver model under the high-speed turn maneuver: (a) lateral displacement for path-following mode, (b) lateral displacement for lateral stability mode, (c) lateral acceleration for path-following mode, (d) lateral acceleration for lateral stability mode.

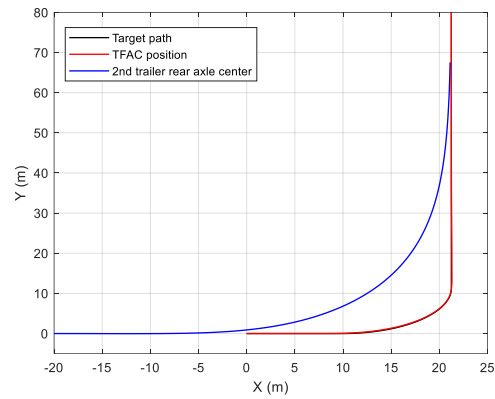
The next two maneuvers executed are low-speed ones. As these two maneuvers are performed at low vehicle speeds, the first mode of the proposed driver model, i.e. the low-speed mode, is applied. The first driving scenario, which was simulated based on the Australia PBS [34], is low-speed 90° turn. The forward speed for this maneuver is 10 km/h. Figure 4.10 shows the paths of the TFAC and the second trailer RAC by employing the proposed driver model through the curve negotiation. Unfortunately, there is no result produced for the other two driver models, since due to the sharp corner and rapid path angle change, the simulation was not successfully implemented. This happens due to the remarkable path-following errors accumulated for these two lateral preview driver models.



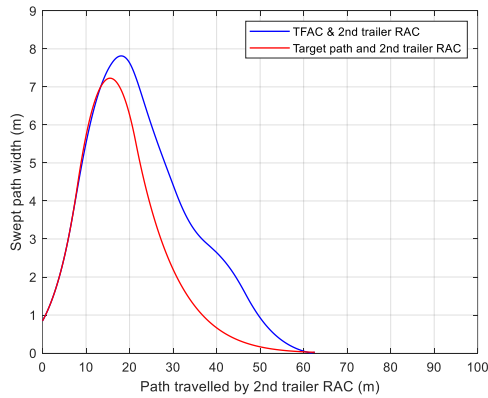
(a)



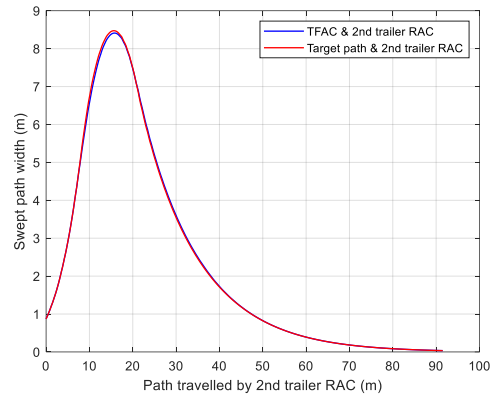
(b)



(c)



(d)

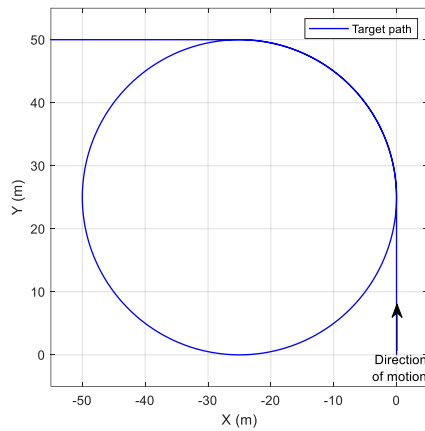


(e)

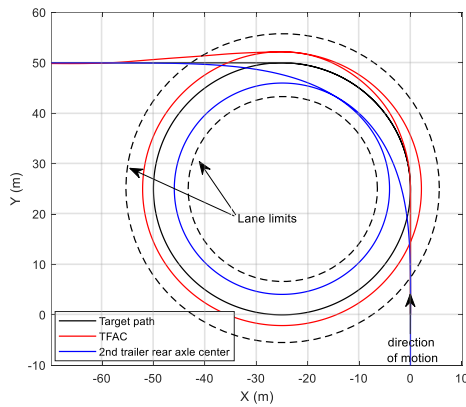
Figure 4.10. Simulation results of the proposed driver model under the low-speed 90° turn maneuver: (a) target path, (b) TFAC and 2nd trailer RAC positions with $k_1 = 0.6$, $k_2 = 0.1$ and $k_3 = 0.3$, (c) TFAC and 2nd trailer RAC positions with $k_1 = k_2 = k_3 = 0$, (d) swept path width of TFAC and 2nd trailer RAC positions with $k_1 = 0.6$, $k_2 = 0.1$ and $k_3 = 0.3$, (e) swept path width of TFAC and 2nd trailer RAC positions with $k_1 = k_2 = k_3 = 0$.

Figure 4.10 (b) illustrates the paths followed by the first and last unit, while the impacts of all the trailing units are considered for the purpose of steering calculation. In contrast, Figure 4.10 (c) shows the respective result while only the tractor motion cue is considered. Obviously, the former is much more similar to reality, in which the driver tries to a full use of the road width in order to reduce the trailer cut-in as much as possible. This approach is highly advantageous for the purpose of MTAHV autonomous driving, in which the more the decision-making process for steering is similar to human drivers' behaviors, the more successfully and reliably the path-following task would be carried out. Figure 4.10 (d) shows the swept path width between the TFAC and the 2nd trailer RAC as well as the swept path width between the target path and the 2nd trailer RAC. Figure 4.10 (e) shows the corresponding results for the case where the driver model considers only the motion cues of the tractor. A comparison of the results shown in Figure 4.10 (d) and 4.10 (e) discloses the fact that considering the motion cues results in a significant improvement in path-following performance under the low speed 90° turning maneuver.

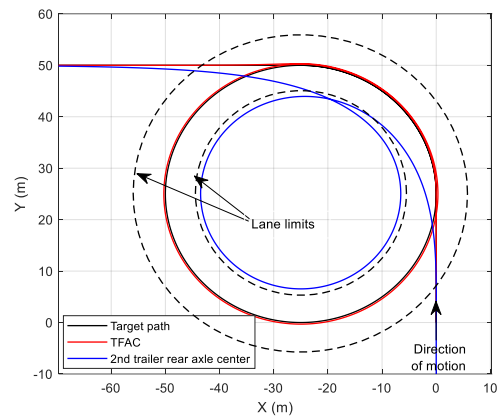
The last maneuver simulated in this study is a 360° roundabout turn [49]. Similar to the LST maneuver the forward speed is set to 10 km/h. Figure 4.11 illustrates the target path and the lateral off-tracking as well as the swept path by the tractor and the 2nd trailer. As shown in Figure 4.11 (c), without considering all the trailing units' motion cues, the 2nd trailer's rear end will cut the road curb, which is shown by the inner dashed line. On the other hand, as seen in Figure 4.11 (b), considering the motions cues of all the trailing units leads to the improvement of the path-following performance with the trajectories of the TFAC and the second trailer's RAC located within the boundary lines denoted by the inner and outer black dashed circular lines.



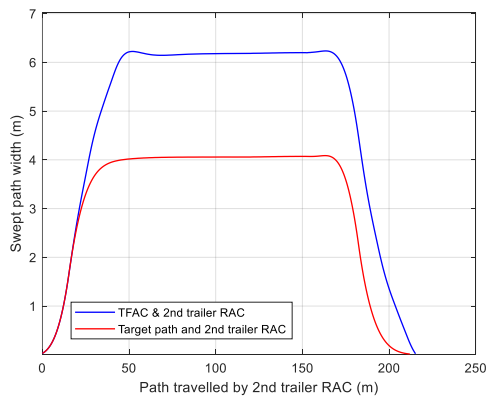
(a)



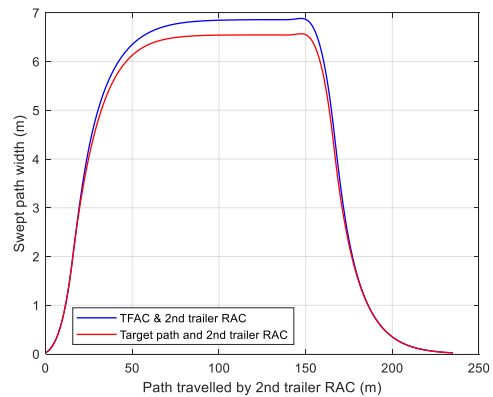
(b)



(c)



(d)



(e)

Figure 4.11. Simulation results under the low-speed 360° roundabout turn: (a) target path, (b) TFAC and 2nd trailer RAC trajectories with $k_1 = 0.6$, $k_2 = 0.1$ and $k_3 = 0.3$, (c) TFAC and 2nd trailer RAC trajectories with $k_1 = k_2 = k_3 = 0$, (d) swept path width between TFAC and 2nd trailer RAC trajectories with $k_1 = 0.6$, $k_2 = 0.1$ and $k_3 = 0.3$, (e) swept path width between TFAC and 2nd trailer RAC trajectories with $k_1 = k_2 = k_3 = 0$.

Figures 4.11 (d) and 4.11 (e) show the swept path width by the 2nd trailer RAC and TFAC and the 2nd trailer RAC and target path for the proposed driver model with and without considering the motion cues of all the trailer units, respectively. It is observed that considering all the units' motion cues results in reducing the maximum swept path by 0.8 m, and the lateral offset between the 2nd trailer RAC and target path also reduces from 6.5 m to 4 m. This approach is very common in driving MTAHVs and tractor-semitrailers while negotiating a 90° or roundabout turn by the drivers. Modifying the weighting factors can determine the level of trade-off between the tractor path-following and rearmost trailer cut-in.

4.5 Summary

In this chapter a lateral preview driver model for closed-loop dynamic simulation of an A-train double MTAHV was introduced. A linear 5 DOF yaw-plane vehicle model was generated for the driver model design. A non-linear TruckSim model was also employed as the dynamic model for the simulations. As introduced in Chapter 3, with an optimization method for fine tuning the tire cornering stiffness, the linear and non-linear vehicle models achieve good agreement. Then, an optimal preview control method was utilized in order to find the optimal value for tractor front axle steering during the simulations. Four body-fixed coordinate systems were considered instead of only using a global coordinate system to calculate the position errors for all the vehicle units separately.

The proposed driver model was verified for a high-speed SLC maneuver by the unified lateral preview driver model, which was designed for a B-train double. However, that driver model has many limits and restrictions for some more dynamically challenging

driving scenarios, such as high- and low-speed 360° roundabout and 90° turns. The proposed driver model also considers two modes, including lateral stability mode and path-following mode. The former is more effective under the driving maneuvers at high vehicle speeds, while the latter is more useful for the purpose of path-following under low-speed maneuvers. Besides, the proposed driver model takes into account the motion cues of all the vehicle units separately for optimal steering calculation by using some weighting factors for their lateral errors with the target path. This approach makes this driver model more realistic and considerably similar to human driver steering behavior. This advantage and also the flexibility of the proposed driver model for negotiating complex target paths with different vehicle speeds makes it more suitable for MTAHV autonomous and semi-autonomous lane-keeping. In Chapters 5 and 7, the proposed driver model will be used for vehicle automated path-following control.

Chapter 5. A longitudinal speed control strategy for MTAHVs

5.1 Introduction

It is reported that globally, road vehicle accidents claim the lives of roughly 1.25 million individuals each year [1]. To address this safety issue, active vehicle safety systems have been introduced in the market [8]. Nevertheless, these systems do not typically account for the influence of human driver mistakes, which are responsible for the more than 90% of road accidents [4]. One possible solution to this issue is to remove human factors from the control loop by implementing autonomous driving [10].

However, the vast majority of research activities dedicated to autonomous driving have been focused on single-unit vehicles (SUVs), e.g., cars [94]. Due to their environmental and economic advantages, MTAHVs are increasingly used worldwide [6-8]. Notwithstanding the pros, MTAHVs exhibit low lateral stability and poor maneuverability due to high center of gravity (CG), big sizes and multi-unit structures [76]. Moreover, in highway operations, MTAHVs represent a 7.5 times higher risk than SUVs [13]. However, few attempts have been made to study predictive safety systems (PSSs) for MTAHVs. In recent years, some studies have focused on autonomous driving of construction trucks [16], articulated construction vehicles [14]–[16], and automated reverse parking for articulated vehicle [15]. However, these studies only consider low-speed motion planning and path tracking while ignoring high-speed features of MTAHVs, e.g. rollover, jack-knifing and trailer sway.

The main goals of designing autonomous vehicles are to increase vehicle safety and improve transportation efficiency. Multi-trailer articulated heavy vehicles (MTAHVs)

have poor directional performance during high-speed evasive maneuvers, with trailing units experiencing larger lateral motions than leading units. An indicator used to measure the amplified lateral motion of the rearmost trailer is Rearward Amplification (RWA), with an ideal value of 1.0 [20]. High RWA values imply a high level of safe risk in highway operations. MTAHVs with B- and C-train configurations usually have an RWA measure of about 1.5, while an A-train double has an RWA of 2.0 [21], indicating an even worse situation. Therefore, designing autonomous MTAHVs without considering their high-speed lateral stability features may not be acceptable.

Attempts have been made for longitudinal motion control for SUVs. In a study [66], the driving behavior considering the driver capability envelope was analyzed during braking a car in a turn through a closed-loop simulation. This approach can be inferred as an automated braking scheme for a car, but it did not consider throttling. In another research [67], the driver's steering and speed control performance was investigated for a SUV while negotiating a curved path. It was assumed that the vehicle should reach a predefined speed at the circular part of the road. Indeed, the proposed methodology was not autonomous and the speed was not adjusted based on road curvatures and driving strategies.

A convex optimization-based speed planning strategy for a heavy truck was studied considering both the acceleration and deceleration demand for a path with varying curvatures [68]. A two-level control strategy for longitudinal motion control of a truck was proposed [69]. The authors used the powertrain and brake system states for the speed control. The model introduced a reference speed to follow and speed was not planned based on road curvatures. A clothoid-based speed profiler and control using a receding horizon fashion was introduced for a SUV during a low-speed S-curve path negotiation, but the

vehicle performance envelope and high-speed transient maneuvers functionality of the designed controller were disregarded [70]. Unfortunately, there is no published autonomous speed controller in the literature dedicated to MTAHVs considering their unique dynamics features.

This chapter proposes a speed profiler and control strategy considering curvature of the target path and all the vehicle units' states. The proposed controller works using two anticipatory and compensatory lateral acceleration control approaches via adjusting acceleration/deceleration to form a speed profile in order to reach the safe maximum speed and minimum trip time.

5.2 Longitudinal Motion Control Methodology

A driver gathers the visual cues from the surroundings and combines the gained information with the knowledge that he/she has about the dynamics of the vehicle to make decisions based on all the data collected. Those decisions are then compiled into predictive and corrective reactions by choosing appropriate steering and throttling/braking to follow a path safely.

The lateral driver model proposed in Chapter 4 demonstrated reliable performance for different driving maneuvers and various vehicle speeds considering all vehicle units' motion cues and can be used as the lateral control strategy during a MTAHV automated driving. To design an autonomous/semi-autonomous MTAHV, longitudinal dynamics control shouldn't be ignored. To control the acceleration of an A-train double described earlier by applying the appropriate brake force or throttling and as a result to adjust the vehicle speed in order to successfully trace the course, a fuzzy logic control strategy is

employed. The governing equations of motion and the linearization assumptions made for the longitudinal speed control strategy are the same as what were introduced in Section 4.1. Indeed, the longitudinal dynamics equations have been neglected; however, the vehicle units' velocities are variables and the state-space matrices are updated with the speed values for MTAHV's units generated by the nonlinear TruckSim model during closed-loop simulation at each time step.

In regular highway driving scenarios, adjusting forward speed is not so crucial. This issue becomes vital during obstacle avoidance scenarios or curve negotiations. Upon approaching a curve or confronting a transient lane-change maneuver, the driver needs to decide well in advance as the strategy will be used for manipulating the steering-wheel and throttle/brake pedals. Drivers usually consider the preview curvature of the road over a preview distance relative to the current speed of the vehicle. Over a curved path negotiation, the vehicle's lateral acceleration is correlated with the forward speed; a high forward speed will lead to a high lateral acceleration, which may trigger a rollover. Thus, drivers try to adjust vehicle forward speed considering road curvature over the preview distance. Actually, the precision and efficiency of vehicle speed adjustment is based on the driver's experience and knowledge about the handling characteristics and throttle/brake response delay of the vehicle.

However, even skilled drivers may make a mistake when estimating the braking demand for a curved path negotiation due to some natural disturbances such as poor visibility and harsh weather conditions. Hence, a compensatory approach is also necessary to mitigate the inappropriate vehicle state estimation over the preview distance. This is done using a supplementary compensation braking/throttling once the vehicle is on the previewed spot

of the curve and the driver has the realistic estimation of the lateral acceleration. Thus, applying the brake force by a reasonable value may assure that the lateral acceleration does not exceed the safe one.

To properly mimic the predictive and corrective reactions of the driver, the acceleration controller comprises two approaches, i.e., anticipatory and compensatory, respectively. As for the anticipatory approach, 10 preview points are considered in front of the Tractor's CG. The preview distances are tractor's velocity-dependent and they are evenly distributed over the 5-second prediction time, i.e. 0.5 second time gap between two adjacent points. The reason for choosing 10 preview points is that if just one point in front of the tractor is selected, for high vehicle speeds the preview distance would be long, and the controller will probably ignore any path curvature alteration between the current position of the vehicle and the preview point due to either a sudden change in planned motion or an obstacle avoidance maneuver. Considering 10 points assures that at any simulation time step, a wide range of preview distance is observed, and based on the previewed states of the vehicle best speed control policy will be adopted. This will be explained in detail.

Based on the global x and y coordinates of the target path, a curve is fitted on the path ahead of the tractor's CG and then the curvature of the road for each preview point is separately estimated. Figure 5.1 represents a schematic diagram including the so-called anticipatory acceleration control approach. Having the current states of the tractor comprising longitudinal velocity V_{x0} , longitudinal acceleration a_{x0} , current station of the tractor's CG on the path S_0 and considering the current states' values as their initial values at each simulation time step and also assuming the longitudinal acceleration is constant

over the preview distance, the anticipated states over the preview time T_p can be estimated using the kinematic equations specified by

$$\begin{aligned} V_{x_i} &= a_{x_0} \cdot T_{p_i} + V_{x_0} \\ S_i &= \frac{1}{2} \cdot a_{x_0} \cdot (T_{p_i})^2 + V_{x_0} \cdot T_{p_i} + S_0 \end{aligned} \quad (5.1)$$

where i ($i = 1, 2, \dots, 10$) represents the i^{th} preview point on the target path. V_{x_i} is the predicted velocity and S_i is the previewed station of the tractor's CG on the i^{th} point of the trajectory. As mentioned earlier using curve fitting on the target path coordinates in front of the tractor's CG, curvature for each preview point, k_{p_i} , is estimated. It is important to mention that since only the road coordinates in front of the tractor are used for anticipatory speed control strategy, the path global coordinates ahead of the tractor's CG are mapped to its body-fixed coordinate system (x, y) to find the fitted curve $y = f(x)$. Note that curve-fitting function in MATLAB is used for that purpose. Equations (5.2) are used to transform the global coordinates to the local coordinate system of the tractor.

$$\begin{aligned} x &= (Y - Y_0) \sin \psi + (X - X_0) \cos \psi \\ y &= (Y - Y_0) \cos \psi - (X - X_0) \sin \psi \end{aligned} \quad (5.2)$$

where (X_0, Y_0) are the global coordinate of the tractor's CG at each simulation time step. Having the previewed stations S_i calculated by equations (5.1) and the equation of trajectory $y = f(x)$, which is recursively calculated in MATLAB at each time step, the local coordinates of the preview points x_{S_i} are estimated solving equation (5.3).

$$S_i = \int_{S_0}^{x_{S_i}} \sqrt{1 + (\dot{f}(x))^2} dx \quad (5.3)$$

It is assumed that at each time step the origin of tractor's body-fixed coordinate is on the S_0 , hence in the above equation, we have $S_0 = 0$. Then the attained longitudinal local coordinates are used to calculate the curvatures by

$$k_{p_i} = \frac{|\ddot{y}(x_{S_i})|}{\left[1 + (\dot{y}(x_{S_i}))^2\right]^{\frac{3}{2}}} \quad (5.4)$$

As noted earlier, since the preview distances are velocity-dependent, when the vehicle speed is high even the closest preview point may be rather far from the tractor's CG for the controlling purposes. Thus, the anticipatory approach may introduce some errors to the current demanding acceleration/deceleration, and when MTAHV reaches to the previewed position on the path, the speed and consequent lateral acceleration will be different from what expected.

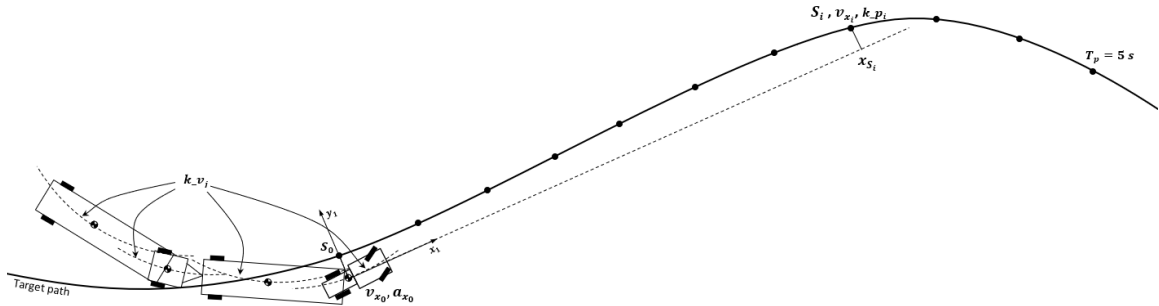


Figure 5.1. Schematic diagram representing the anticipatory and compensatory control points for MTAHV speed planning.

Hence, a corrective approach should also be deemed for the acceleration controller design. The corrective reaction of the driver is modelled using the same kinematic equations for the predictive approach; however, in this case, the lateral accelerations of all the MTAHV units' CGs as well as the estimated instantaneous curvatures of the paths followed by towing and trailing units' CGs are employed to calculate the demand

acceleration/deceleration. As discussed in Section 4.1, while tracing a curved course due to considering all the vehicle units' motion cues, the tractor doesn't exactly follow the target path and there is some deviation error between TFAC and the corresponding point on the path to reduce the lateral position errors for the trailing units. Besides, the MTAHVs are usually very long and even if the tractor traces the trajectory closely, the trailing units will experience considerable deviations from the target path due to the articulation points as well as the high-speed steady-state and transient off-tracking or the low-speed path-following off-tracking, especially when negotiating sharp turns. Consequently, the instantaneous curvatures, k_{vj} , traced by MTAHV trailing units are different from the corresponding road curvatures at the current time. Hence, the estimated instantaneous curvatures, which are illustrated in Figure 5.1, should be calculated by

$$k_{vj} = \frac{a_{yj}}{V_{xj}^2} \quad (5.5)$$

where j ($j = 1,2,3,4$) denotes the vehicle unit's number beginning from the tractor up to the second trailer, respectively, a_{yj} and V_{xj} represent the values of the lateral accelerations and longitudinal velocities for all the units' CGs.

The main strategy for acceleration/deceleration automated control in this chapter is to drive the MTAHV as speedily and safely as possible, while following a trajectory with variable road curvatures. To reach this goal, it is presumed that the maximum lateral acceleration of the vehicle should be kept below a safe threshold during carrying out a wide range of maneuvers and negotiating various road curvatures. As there is a direct relation between the lateral acceleration and longitudinal velocity, i.e. $a_{yi} = V_{xi}^2 \cdot k_i$, accomplishing this objective ensures the highest speed while having a safe ride.

The static rollover threshold, which is usually measured by lateral acceleration in gravitational unit, is a valuable measure to investigate the rollover stability. The mentioned variable can be as low as 0.25 g in some harsh driving scenarios and load conditions for an AHV. Drivers can often drive their vehicles with a lateral acceleration around 0.2 g [21]. Besides, as the linear vehicle dynamics model of MTAHV is utilized for the purpose of steering and speed control, the maximum lateral acceleration of all the vehicle units should be less than 0.35 g to prevent non-linear dynamics excitation [76]. A typical A-train double usually exhibits a maximum rearward amplification of 2.0 [21]. Hence, a maximum lateral acceleration of 0.2 g was considered as the safe lateral acceleration, $a_{y_{safe}}$, for all road segments with curvatures greater than zero.

The performance of a MTAHV can be approximately evaluated by a graph named “g-g” diagram [101]. The maximum lateral acceleration and longitudinal acceleration/deceleration synthesize a curve, which envelopes the g-g diagram and is called the performance envelope of the vehicle. The capability envelope’s shape relies on a number of factors comprising vehicle speed, driver’s driving skill, tire/road friction condition and so forth. But, in the current study, a theoretical operating envelope is applied and it is assumed that the autonomous speed controller should react similar to a skilled driver’s capabilities. Adopted from [66], the capability envelope during acceleration/deceleration is described by.

$$\left(\frac{|a_x|}{a_{x_{max_dec}}}\right)^2 + \left(\frac{|a_y|}{a_{y_{safe}}}\right)^2 \leq 1 \quad (5.6)$$

Figure 5.2 illustrates the exaggerated graphical representation of the capability envelope in this study (the grey area). Under a forward acceleration operation, the grip between road

surface and tire is an effective factor similar to the braking process, and the engine power would also be a limiting factor. That is why the limit for the forward acceleration a_{acc_max} , is different from that of for the braking, i.e. a_{dec_max} . The maximum longitudinal acceleration/deceleration are defined based on the TruckSim built-in model for engine capability and road friction condition.

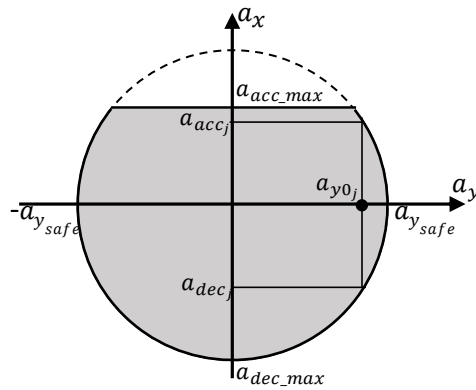


Figure 5.2. MTAHV performance envelope diagram.

Figure 5.3 shows the flowchart for the acceleration/deceleration demand calculation. The final value a_{x_ctrl} is then used as the input for the fuzzy controller to estimate the required brake pedal force or throttle, which will then be sent to the TruckSim MTAHV model via SIMULINK S-function as the speed control signal.

Based on the performance envelope demonstrated in Figure 5.2, if the lateral acceleration of the MTAHV reaches the measure of a_{y_safe} , the capable deceleration would be zero. Hence, to ensure that there always exists a reserved amount of braking capability for the vehicle when reaches the previewed station of the road, the desired lateral acceleration a_{y_max} is deemed to be a bit less than the measure of a_{y_safe} for anticipatory acceleration

calculation approach. In the current study, the following values are assigned: $a_{y_{max}} = 0.18$ g, $a_{acc_max} = 0.06$ g and $a_{dcc_max} = -0.6$ g.

5.3 Fuzzy controller

Conventional vehicle dynamic controllers are designed using a vehicle model considering the respective interrelations between inputs and outputs. However, a fuzzy controller doesn't solely use the mentioned model or precise plant parameters. Instead, it relies on the mapping of the inputs to the outputs via membership functions and fuzzy rules [102].

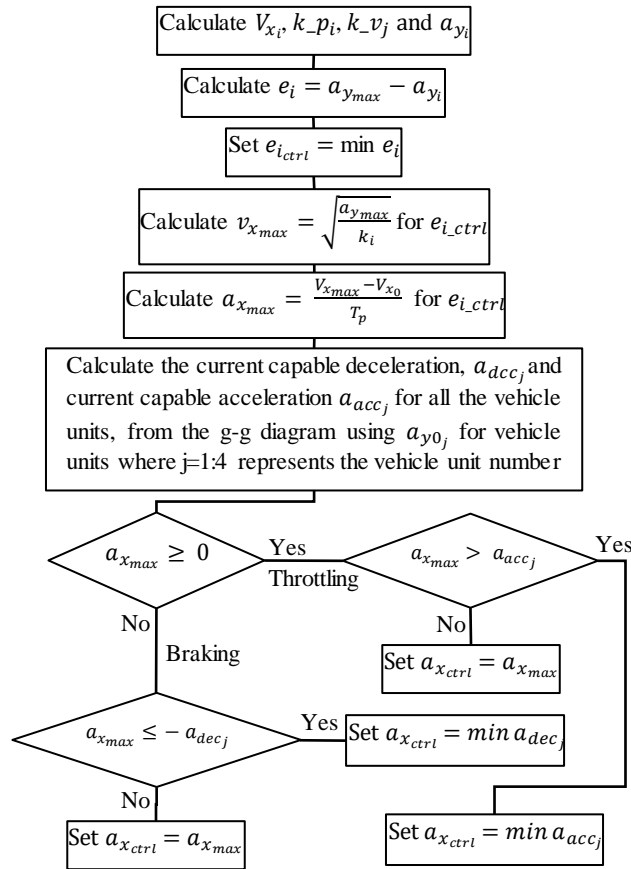
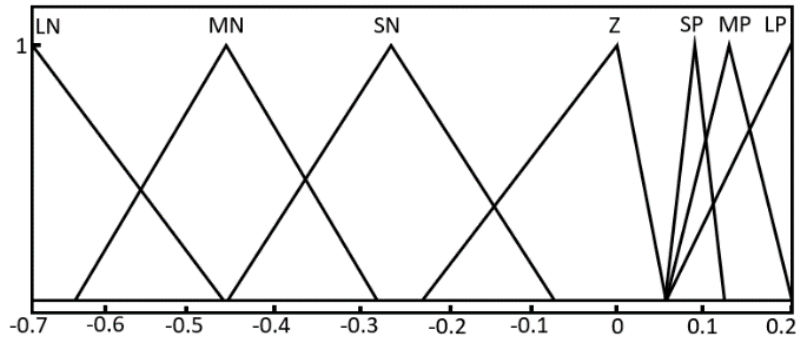


Figure 5.3. Speed planning and control strategy flowchart.

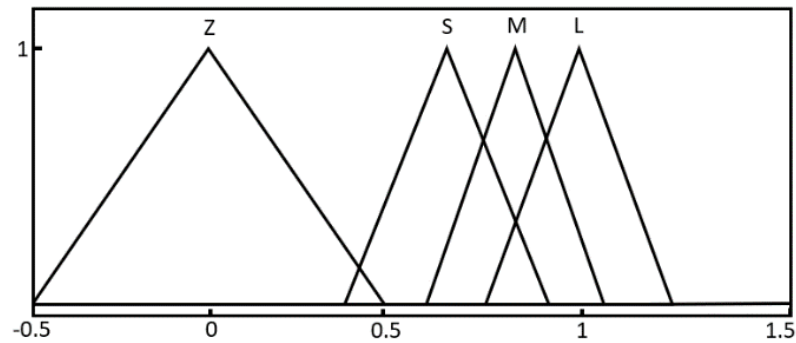
Fuzzy systems don't necessitate using linear plant model and provide a model-free estimation of a non-linear plant. The precision and validity of control outputs highly depend

upon choosing correct membership functions and fuzzy rules among numerous options that are defined based on the experience and knowledge of the designers [103].

The driver model introduced in Chapter 4 takes the advantage of a linear vehicle dynamics model. However, during the vehicle acceleration control process, the velocity may change remarkably, a non-linearity will thus be introduced to the state-space matrices. To tackle this issue, at every time step, the state-space matrices, which are coded in MATLAB, are updated by new vehicle's velocity provided by TruckSim. The fuzzy input and output membership functions are demonstrated in Figure 5.4.



(a)



(b)

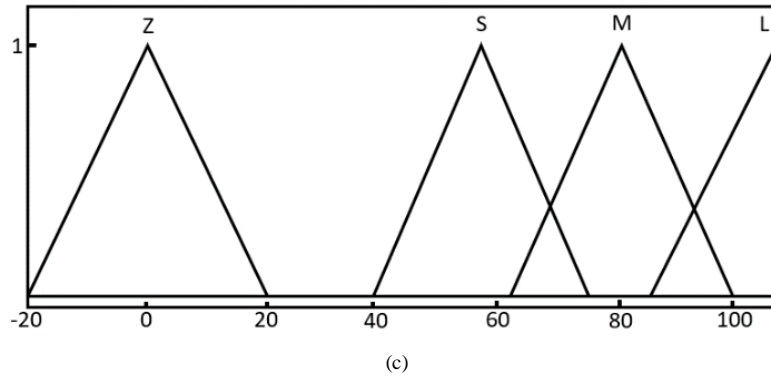


Figure 5.4. Membership functions: (a) acceleration demand as input variable, (b) throttle as first output, (c) pedal brake force as second output.

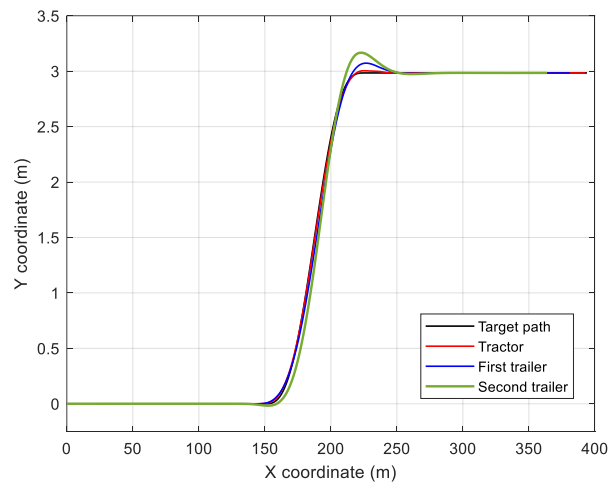
5.4 Simulation results and discussion

To evaluate the performance of the proposed speed controller, co-simulations using MATLAB/SIMULINK and TruckSim were conducted. The controller was coded in MATLAB and a VS S-function block in SIMULINK was utilized to receive the states from TruckSim and send the control signals, including the brake force and engine throttle to TruckSim.

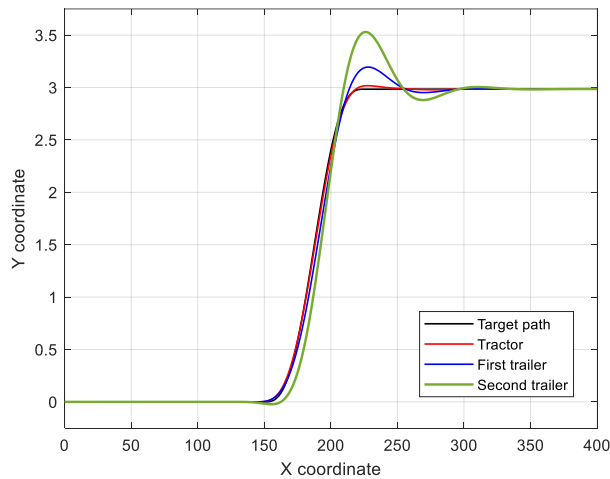
Two driving scenarios, i.e. high-speed lane change (HSLC) and a 180-degree curve negotiation were simulated to verify the controller. In the first scenario, the MTAHV is moving with an initial speed of 108 km/h. Then it performs a single-lane-change maneuver with the maximum lateral displacement of 2.984 m. To effectively evaluate the controller performance, simulations for the SLC maneuver with and without the controller were carried out, and the results were compared. The achieved results are shown in the following graphs.

Form Figure 5.5, it is inferred that using the speed controller, the transient off-tracking has been remarkably reduced for all the trailing units. The high decline is seen for the dolly

and the second trailer. This result is achieved because the speed controller considers the lateral acceleration of all the trailing units and the tractor. This interesting result proves that the proposed speed controller can operate as a reactive safety system (RSS) for autonomous MTAHV in some high-speed transient maneuvers, thereby taking advantage of the anticipatory/compensatory lateral acceleration control approach and compromising the speed.



(a)

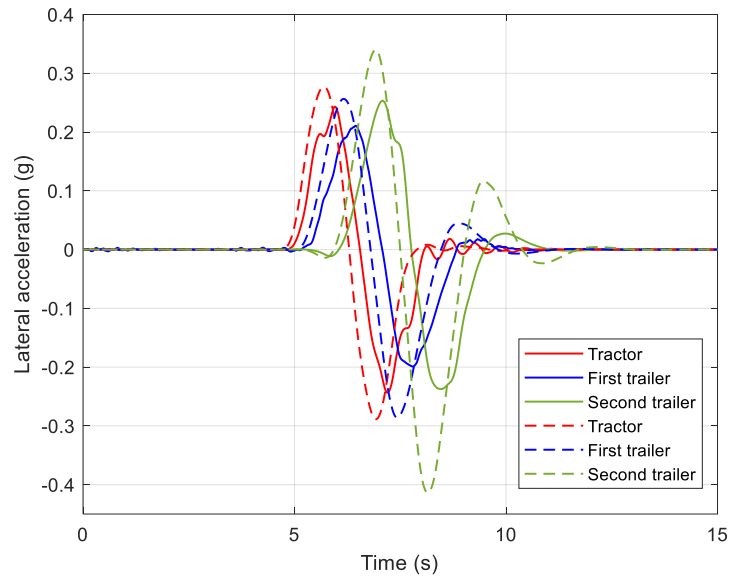


(b)

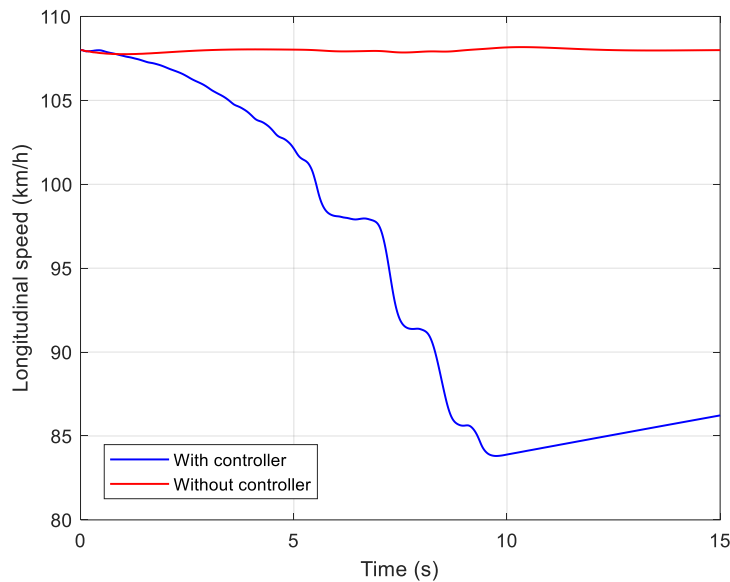
Figure 5.5. Lateral displacement for HSLC maneuver: (a) with controller, (b) without controller.

Figure 5.6(a) shows the time-histories of the lateral accelerations for all the MTAHV units. It is observed that the designed controller performs quite well to keep the maximum lateral acceleration below the specified bound value, i.e. 0.24 g. Among the trailing units, the second trailer has the highest lateral acceleration, which is exactly the same as the predefined bound value for the controller design. In comparison, when the controller is deactivated, the second trailer's maximum peak lateral acceleration is 0.42 g, increasing by 75% of the counterpart with the controller activated. Another interesting point to be mentioned is that when the speed controller is off, the rearward amplification is 1.5, while if the controller is activated, the rearward amplification is 1.0, which assures a stable obstacle avoidance maneuver.

Figure 5.6 (b) illustrates the time-histories of longitudinal speed over the simulated maneuver. When the controller is off, it is found that the speed remains approximately constant during the maneuver, as seen in the figure. When the vehicle starts the SLC maneuver, the speed is decreased as required by the controller in order to prevent the lateral acceleration going beyond the specified bound. Once all the vehicle units pass the curvilinear path and enter the straight part of the prescribed path, the speed begins increasing again.



(a)

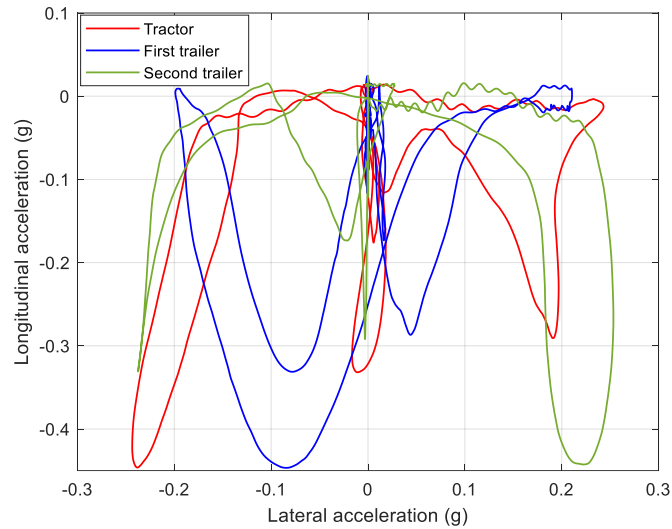


(b)

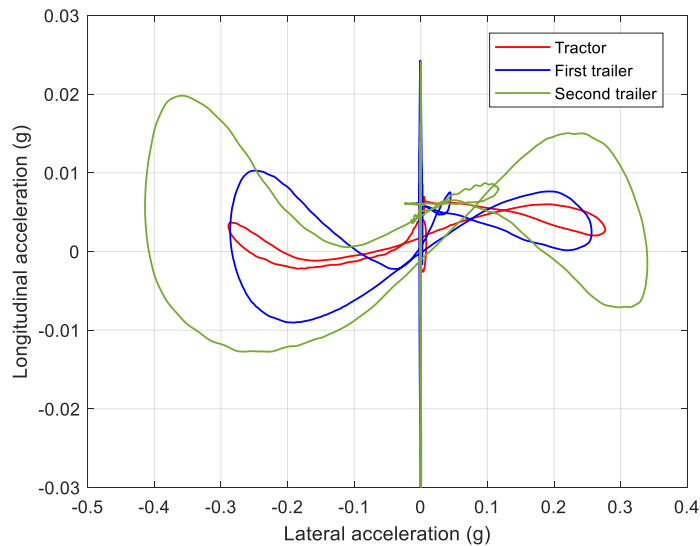
Figure 5.6. A-train double HSLC maneuver results: (a) lateral acceleration with controller (solid line) and without controller (dashed line), (b) Longitudinal speed.

Figure 5.7 (a) and (b) show the g - g diagrams for situations, in which the speed controller is activated and deactivated, respectively. When the controller is on, the vehicle performance envelope is implemented more efficiently, like how a skilled driver tries to drive safely while exploiting the maximum capabilities of the vehicle as much as possible.

However, when the controller is off, the vehicle capability is not implemented appropriately, and there is a risk of rollover because of an RWA value of more than 1.5, very similar to a novice driver performance during an urgent situation.



(a)



(b)

Figure 5.7. Longitudinal and lateral accelerations shown in the g-g diagrams for HSLC maneuver: (a) with controller, (b) without controller.

The next driving scenario is a rather sharp curve negotiation with an initial speed of 100 km/h [66]. Figure 5.8 shows the curvature of the path with respect to the road station. The

road involves five segments, including two straight part with zero curvature, a circular bend which has a constant curvature, and two clothoids which have linearly varying curvatures and connect the bend to the straight path smoothly.

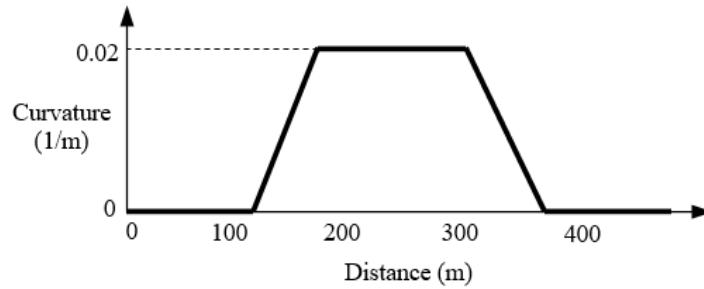
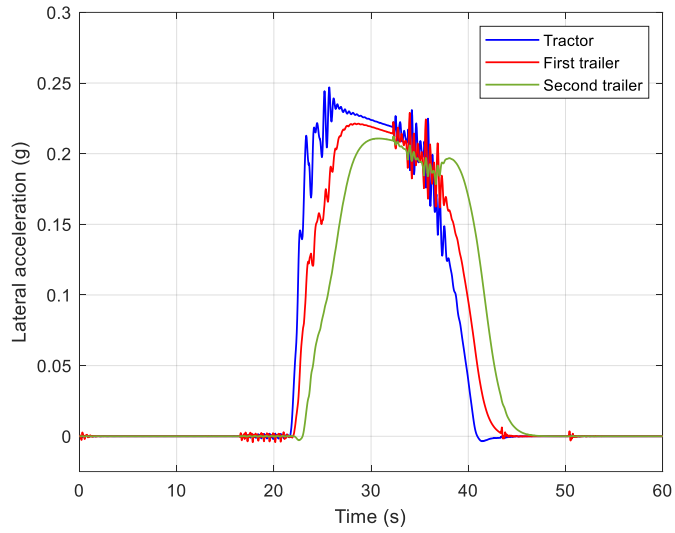


Figure 5.8. The target path curvature diagram for a U-turn negotiation maneuver

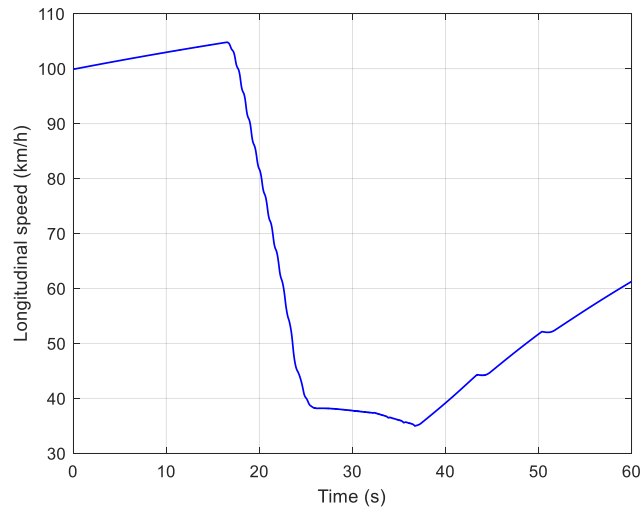
Simulation results are displayed in Figure 5.9. From Figure 5.9 (a), it is well understood that the speed controller successfully kept the maximum lateral acceleration below the specified bound value. Note that in this case, the tractor experiences the maximum lateral acceleration among all the vehicle units of the A-train double. The trailing units also show the similar lateral acceleration during negotiating the bend segment of the road. It is really promising for the A-train double that can almost achieve and remain the desired lateral acceleration, while having a high velocity and enters a rather sharp turn for such a long vehicle with three articulation points.

Figure 5.9 (b) shows the speed change graph for reaching the previously mentioned valuable goal. Speed value initially goes up because the vehicle moves on the straight part of the path. Then the controller begins reducing the speed while arriving the clothoid at a forward speed up to 40 km/h, where the road has the highest curvature. This velocity remains around 40 km/h during passing the circular course. Upon exiting the bend and arriving the second clothoid, speed gradually increases based on the engine power limits

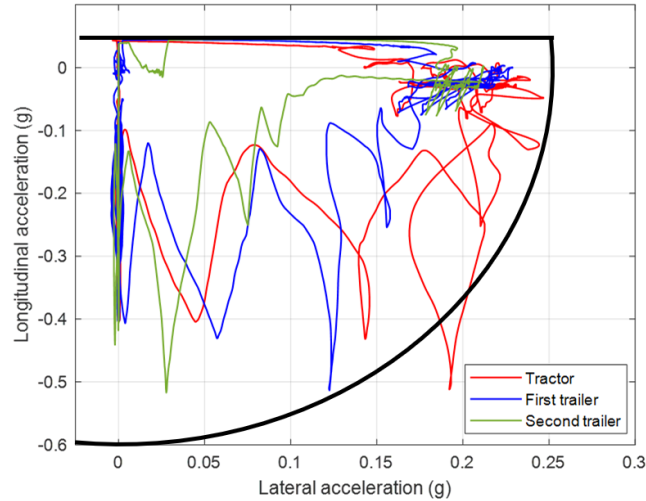
and feasible MTAHV acceleration. The graph achieved from a 60 seconds simulation shows a selected speed control process.



(a)



(b)



(c)

Figure 5.9. U-turn negotiation results: (a) lateral acceleration, (b) longitudinal velocity, and (c) g-g diagram.

The g-g diagram for the mentioned driving scenario is shown in Figure 5.9 (c). The maneuver is performed either on straight line sections, or turning to the left; thus, the curves of all the vehicle units in terms of the relationship between the lateral and longitudinal accelerations are almost enclosed in one quarter of graph. The thick black lines show the limits of the vehicle performance envelope. First of all, it is seen that the controller has kept the lateral and longitudinal acceleration between the thresholds, i.e. 0.06 g for longitudinal acceleration, and 0.18 g for the lateral acceleration. Furthermore, similar to the HSLC maneuver, in this case the controller has exploited almost all the feasible acceleration/deceleration taking into account the predefined constraints very similar to a professional human driver, who tries to keep the MTAHV dynamics operating close to the performance limits. This will increase the vehicle speed and minimize the trip time, especially during long journeys.

5.5 Summary

Findings acquired through this chapter are summarized as follows. A new autonomous speed planner/controller was proposed for an A-train double MTAHV considering realistic operation and decision-making process of a skilled human driver for driving over different roads with various curvatures. The main objective of the autonomous speed controller is to maintain the lateral vehicle acceleration within the maximum safe range when negotiating curvilinear paths which assures the highest capable vehicle speed as well. The acceleration/deceleration autonomous control strategy uses a compensatory approach in collaboration with the anticipatory strategy to tackle the vehicle inaccurate states prediction over the preview horizon which may even happen for a skilled driver due to some unforeseen conditions, such as poor visibility. The compensatory approach utilizes all the vehicle units' lateral accelerations to plan the best speed control scenario to decline the lateral instability occurrence due to inappropriate vehicle throttling or braking effort while following a curved path. The vehicle performance envelope is also utilized to make sure that at every moment there is always some reserved braking capability for the MTAHV while the vehicle performance capabilities are exploited efficiently. Since the proposed automated controller uses both previewed and real-time MTAHV states and the main goal is to limit the lateral acceleration within a desirable range by adjusting the vehicle speed, it can operate as a reactive safety system (RSS) to improve the lateral stability. Additionally, this MTAHV speed control strategy may reduce the trip time and increase the safety for long journeys.

Chapter 6. Model-based predictive autonomous driving control strategies for MTAHVs with active trailer and dolly steering

6.1 Introduction

The majority of research efforts in autonomous driving have been focused on single-unit vehicles (SUVs), such as cars. In highway operations, heavy goods vehicles pose a risk 7.5 times greater than that of passenger cars [13]. However, there has been far less emphasis on investigating PSSs for articulated vehicles [105], particularly for MTAHVs. In recent years, a few studies have tackled autonomous driving for articulated construction vehicles [10], and articulated vehicles equipped with automated reverse parking [11]. These autonomous systems were designed considering only low-speed motion planning and trajectory tracking using kinematic control, while neglecting high-speed dynamic behaviors of MTAHVs, such as rollover, jack-knifing, and trailer sway.

The primary objectives of developing autonomous driving systems for road vehicles are to increase operational safety and improve transportation efficiency. MTAHVs are becoming more prevalent on highways. Compared to a single-trailer articulated heavy vehicle (AHV), the use of an MTAHV with an A-train double structure can reduce mileage traveled, decrease fuel consumption and greenhouse gas emissions, and lessen tire-road wear dramatically [76]. However, due to their multi-unit structures, large sizes, and high centers of gravity, MTAHVs have poor low-speed maneuverability and low high-speed lateral stability. MTAHVs typically experience exaggerated lateral/yaw movements of trailing

vehicle units when making high-speed evasive maneuvers. This phenomenon is called rearward amplification [20]. The rearmost trailer tends to experience higher lateral acceleration than the tractor, and it may be the first unit to rollover. However, when the driver realizes that a rollover is about to happen, it is too late to control the vehicle [21]. Human drivers mainly control MTAHVs based on the motion cues of leading vehicle units, since the perceived motion cues from trailing vehicle units are very weak due to the filtering function of the tractor cabin suspension and articulation joints [22]. Driving an MTAHV requires drivers to have rigorous training, skills, and experience. The development of autonomous driving technologies is crucial for improving the safety of MTAHVs.

In [106], a model predictive controller was used for the motion planning and trajectory tracking of an autonomous tractor/semitrailer, in which a SUV model was used and the trailer's dynamics was disregarded. In [105], a predictive model was generated for path planning and trajectory following for a tractor/semitrailer. However, the autonomous driving control for a small-scaled tractor/semitrailer prototype was based on the kinematic model of the vehicle and a vision-based system. To date, little attention has been paid to automated driving of MTAHVs considering the dynamics of the leading unit and trailing units to improve the maneuverability and lateral stability simultaneously.

This chapter proposes and designs an innovative autonomous driving control strategy considering the unique dynamic features of MTAHVs. To this end, a MTAHV with the configuration of A-train double is selected as the subject vehicle; a 5-DOF yaw-plane model is generated to represent the MTAHV [84]; the yaw-plane MTAHV model and a nonlinear model predictive control (NLMPC) technique are used to design the autonomous

driving controller. In addition to the design of autonomous driving controller, to further enhance the safety of the self-driving MTAHV, an active trailer safety system, i.e., active trailer and dolly steering [20], is incorporated. The NLMPC-based autonomous driving control strategy is devised for trajectory tracking for the MTAHV under various operating conditions. The autonomous driving controller is focused on the direction and speed control of the tractor, while the active trailer and dolly steering (ATDS) controller is dedicated to lateral motion control of trailing vehicle units. By means of a coordinated control approach [76], the autonomous driving and the ATDS controller are integrated.

6.2 Autonomous driving and active trailer and dolly steering control

method

Various control strategies have been proposed for active safety systems of AHVs, e.g., linear quadratic regulator (LQR) [22],[25],[107],[108], sliding mode control (SMC) [109], PID[110] and fuzzy-logic control[111]. The LQR technique makes use of a linear time-invariant plant model to control the system. Fuzzy logic control strategy doesn't necessitate using linear plant model. However, the precision and validity of control outputs highly depend upon choosing correct membership functions and fuzzy rules among numerous unclear options. As a result, the performance of a fuzzy logic controller considerably relies on the designer's expertise [103]. However, the optimization mechanism of the MPC technique and its feedback correction feature as well as the capability of controlling a time-varying plant model ensures good control performance and a remarkable imprecision reduction resulting from model reductions and simplifying assumptions.

6.2.1 Model predictive control method

Autonomous driving relies on future event control, which is a key feature of the MPC technique. Basically, MPC method uses an optimization strategy to find the optimal control inputs by discretizing the prediction model over a finite prediction horizon and minimizing the objective function by employing a specific number of control actions through the prediction horizon. However, only the first control input is applied to control the plant at every time step. Thus, new values of the state variables are calculated for the next step. The process repeats to find subsequent control action and state values.

The MPC controller is given by a general formulation as follows [112]:

$$\min_{\mathbf{u}} \sum_{k=0}^{N_p-1} J_k(\mathbf{x}_p(k), \mathbf{u}_p(k), \mathbf{x}_p^{\text{ref}}(k)) + J_k(x_p(N_p), x_p^{\text{ref}}(N_p)) \quad (6.1)$$

$$\text{s. t. : } \mathbf{x}_p(k+1) = f(\mathbf{x}_p(k), \mathbf{u}_p(k)), k = 0, \dots, N_p - 1 \quad (6.2)$$

$$G(\mathbf{x}_p(k), \mathbf{u}_p(k)) \leq \mathbf{g}_b, k = 0, \dots, N_p - 1 \quad (6.3)$$

$$G(\mathbf{x}_{N_p}) \leq \mathbf{g}_p \quad (6.4)$$

$$\mathbf{x}_0 = \mathbf{x}_p(0) \quad (6.5)$$

where J_k is the cost function, which should be minimized for calculating the optimal manipulated input $\mathbf{u}_p(k)$. $\mathbf{x}_p^{\text{ref}}(k)$ is the reference state values at prediction instant k . Function G involves the constraints for the states and inputs with the \mathbf{g}_b and \mathbf{g}_p as the bounding limits. To solve the equation (6.3), there are several toolboxes available to do the job. The MATLAB MPC toolbox was employed in the current study.

6.2.2 Non-linear model predictive control design

As explained before in section 3.2.2, so as to design an integrated lateral and longitudinal vehicle control as well as the active steering for the trailing units of the A-train double, a

simple kinematic longitudinal model which approximates the longitudinal dynamics combined with the lateral dynamics model was employed. Furthermore, the lateral displacement and yaw angle deviations of all the vehicle units with respect to the reference path are considered as the states. These new added states to the fundamental linear vehicle model are interrelated. As a result, the final representative equations of motions are non-linear. The conventional state-space representation of the non-linear vehicle model is given by equation (3.19).

The plant measurements, prediction model, control goals, and the actuator/plant limitations are utilized to formulate the control problem. The prediction vehicle model has a fundamental role in determining the controller's performance and is represented by the following differential equations:

$$\dot{\mathbf{x}}_p(t) = f(\mathbf{x}_p(t), \mathbf{u}_p(t), \mathbf{d}(t)) \quad \mathbf{x}_p(0) = \mathbf{x}_0 \quad (6.6)$$

where $\mathbf{x}_p(t)$ and $\mathbf{u}_p(t)$ are the plant's states and inputs, respectively. The states and inputs are defined in Chapter 3. The discretized representation of the prediction plant model is:

$$\mathbf{x}_p(k+1) = f(\mathbf{x}_p(k), \mathbf{u}_p(k), \mathbf{d}(k)) \quad (6.7)$$

$$\mathbf{u}_p(k) = \mathbf{u}_p(k-1) + \Delta \mathbf{u}_p(k) \quad (6.8)$$

$$\mathbf{y}_p(k) = \mathbf{C} \mathbf{x}_p(k) \quad (6.9)$$

where $\mathbf{y}_p(k)$ denotes the output variable vector. The plant input $\mathbf{u}_p(k)$ consists of two parts; $\mathbf{u}(k)$ including the tractor's longitudinal acceleration a_{x_des} and the tractor's first axle steering δ_1 , as well as $\mathbf{u}_s(k)$ which consists of the trailing units' axles steering δ_2 to δ_9 . The vector \mathbf{d} is the measured disturbance and consists of $\kappa_i(k)$ ($k = 0, 1, \dots, N_p$ and $i = 1 \sim 4$)

which represents the corresponding curvature of the reference path corresponding to the all vehicle units' control points over the prediction horizon.

The state variables vector is specified as

$$\mathbf{x}_p = [v_1 \ \psi_1 \ V_x \ a_x \ e_{11} \ e_{21} \ v_2 \ \psi_2 \ e_{12} \ e_{22} \ v_3 \ \psi_3 \ e_{13} \ e_{23} \ v_4 \ \psi_4 \ e_{14} \ e_{24}] \quad (6.10)$$

where v_i and ψ_i , $i = 1,2,3,4$ are the vehicle units' lateral velocity and yaw rate, respectively, V_x is the tractor's longitudinal speed and a_x is the tractor's longitudinal acceleration. At each time step these state variables as well as the current vehicle units' global coordinates and yaw angles generated by the high-fidelity TruckSim nonlinear vehicle model are delivered to MATLAB. Next, the nearest points of vehicle units' coordinates on the target path are found and then e_{i1} and e_{i2} , $i = 1,2,3,4$ which are the vehicle units' lateral deviation and relative yaw angle with respect to the target trajectory are calculated. Figure 6.2 and Figure 6.3 illustrate e_{i1} and e_{i2} and required information for calculating them.

Furthermore, the NLMPC requires an optimization function including a cost function and a few constraints. The process involves solving an open-loop optimal control problem using the current state of the virtual vehicle plant, which is represented by a 3-D TruckSim model, at a specific sampling time. The goal of this online optimization problem is to minimize the differences between predicted outputs and reference states by calculating the optimal control input over a short time window, while considering related constraints. The resulting optimal control input is then applied to the virtual plant for the following sampling interval. This procedure is repeated at each time step, using the new state of the vehicle system to solve a new optimal control problem with a shifted time window. This approach, known as "receding horizon implementation," transforms the NLMPC algorithm into a

feedback controller. The NLMPC controller design is formulated as a constrained optimization problem with the following cost function subject to the specified constraints.

A more specific cost function utilized in this dissertation is represented by

$$\begin{aligned} \min_{\Delta U(k|k), \dots, \Delta U(k+H_c-1|k)} & \sum_{i=1}^{H_p} \|\mathbf{r}(k+i|k) - \mathbf{y}_p(k+i|k)\|_{\mathbf{Q}}^2 \\ & + \sum_{i=0}^{H_c-1} \|\Delta \mathbf{u}_p(k+i|k)\|_{\mathbf{R}}^2 + \sum_{i=0}^{H_c-1} \|\mathbf{u}_p(k+i|k)\|_{\mathbf{S}}^2 \end{aligned} \quad (6.11)$$

Subject to:

$$\mathbf{x}_p(k+1+i|k) = \mathbf{f}(\mathbf{x}_p(k+i|k), \mathbf{u}_p(k+i|k)), i = 0, \dots, H_p - 1 \quad (6.12)$$

$$\mathbf{u}_p(k+i|k) = \mathbf{u}_p(k-1+i|k) + \Delta \mathbf{u}_p(k+i|k), i = 0, \dots, H_p - 1 \quad (6.13)$$

$$\mathbf{y}_p(k+i|k) = \mathbf{C} \mathbf{x}_p(k+i|k), i = 0, \dots, H_p \quad (6.14)$$

$$\mathbf{u}_{p,\min}(k+i|k) \leq \mathbf{u}_p(k+i|k) \leq \mathbf{u}_{p,\max}(k+i|k), i = 0, \dots, H_c - 1 \quad (6.15)$$

$$\Delta \mathbf{u}_{p,\min}(k+i|k) \leq \Delta \mathbf{u}_p(k+i|k) \leq \Delta \mathbf{u}_{p,\max}(k+i|k), i = 0, \dots, H_c - 1 \quad (6.16)$$

$$\Delta \mathbf{u}_p(k+i|k) = \mathbf{0}, i = H_c, \dots, H_p - 1 \quad (6.17)$$

where H_p and H_c are the prediction horizon and control horizon, respectively. \mathbf{Q} , \mathbf{R} and \mathbf{S} are the weighting matrices with proper size. Note that $H_p > H_c$.

For the current model predictive controller, the prediction horizon is $H_p = 10$, the control horizon is $H_c = 2$ and the time step is 0.1 s. The front axle wheels steering angle and tractor longitudinal acceleration constraints are set to $|\delta_1| \leq 1.13$ rad and $-0.6 \text{ g} \leq a_{x_{des}} \leq +0.06 \text{ g}$ respectively, which are determined based on the TruckSim vehicle model capabilities on a road with a friction coefficient of 0.85. The steering angle constraint for all the other steered axles is limited to $|\delta_i| \leq 0.785$ rad.

Figure 6.1 shows the architecture of the proposed integrated autonomous driving and active safety and maneuverability control system. The non-linear vehicle model and the NLMPC

are both modelled using MATLAB code. The nonlinear high-fidelity TruckSim vehicle model is used as the virtual plant of the A-train double in order to generate state variables required. The autonomous driving and ATDS shown in the figure are to be introduced in Sections 6.2.2 and 6.2.3, respectively.

The designed MPC consists of two controlling goals. The first goal is to keep the leading unit following the target path and tracking the target speed by manipulating tractor's front axle steering, as well as engine throttling or braking. The second goal is to enhance the vehicle safety and maneuverability by manipulating the trailing units' axles steering under the low- and high-speed maneuvers.

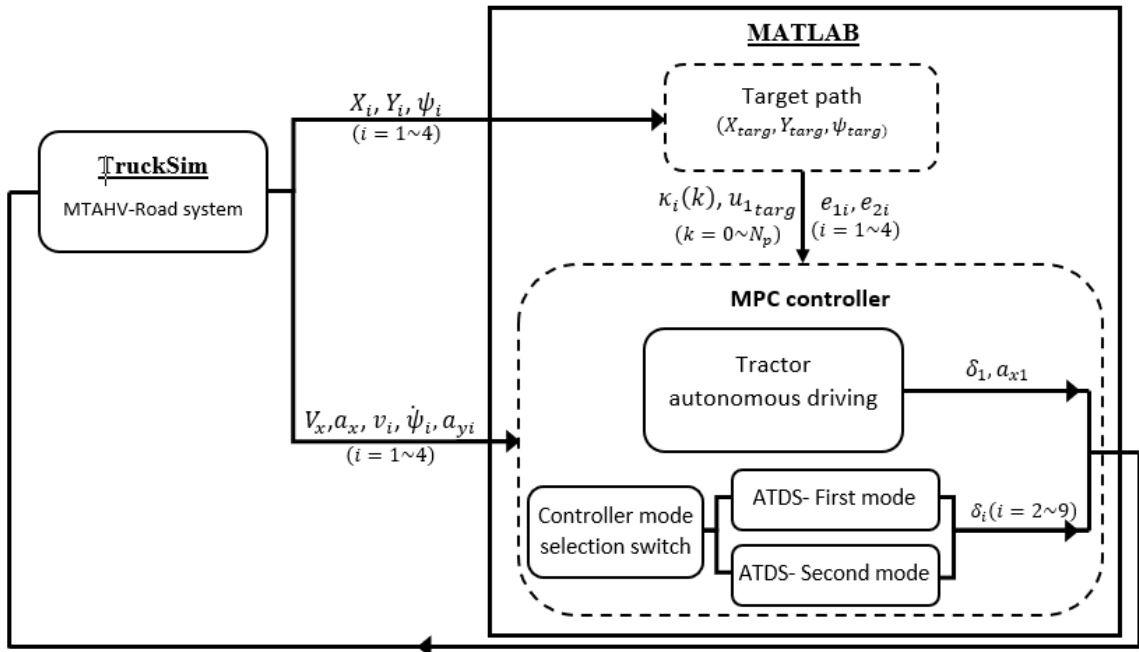


Figure 6.1. Architecture of integrated autonomous driving and active safety/maneuverability control system.

6.2.3 Autonomous driving control

A path following control is a manipulated operation, in which the vehicle tracks the centerline of a reference road while maintaining the vehicle longitudinal speed within a preset range [94]. No matter how the speed demand is determined, the autonomous driving strategy should successfully manipulate the acceleration and tractor front axle steering in order to reduce the deviation of the tractor's heading, lateral displacement and speed with respect to the target path and demand speed. If the above goals cannot be met simultaneously, they should be balanced by the MPC controller. Figure 6.1 illustrates the autonomous driving, as a part of the MPC control, in which the required tractor's longitudinal acceleration and front axle steering are regulated using the measured and predicted vehicle states, as well as the curvature of the road as the measured disturbance. Then, the calculated control variables are sent to the TruckSim to make the virtual vehicle effectively follow the target path and speed.

6.2.4 Active Trailer and Dolly Steering

To fully consider the unique dynamic features of MTAHVs, the active trailer and dolly steering (ATDS) control is designed with two operating modes: 1) low-speed path-following as shown in Figure 6.2, and 2) high-speed lateral stability as shown in Figure 6.3. The first mode is defined as low-speed path-following mode with the intention of improving the maneuverability of the MTAHV while negotiating curved paths at low speeds. In this mode, the tractor's front axle center (TFAC) and all the towed units' rear ends are supposed to follow the target path. Executing this mode, the axles will be steered appropriately, and the path will be followed by all the vehicle units with minimum tracking

errors, including lateral deviation and relative yaw angle of unit's controlling points with respect to the target path.

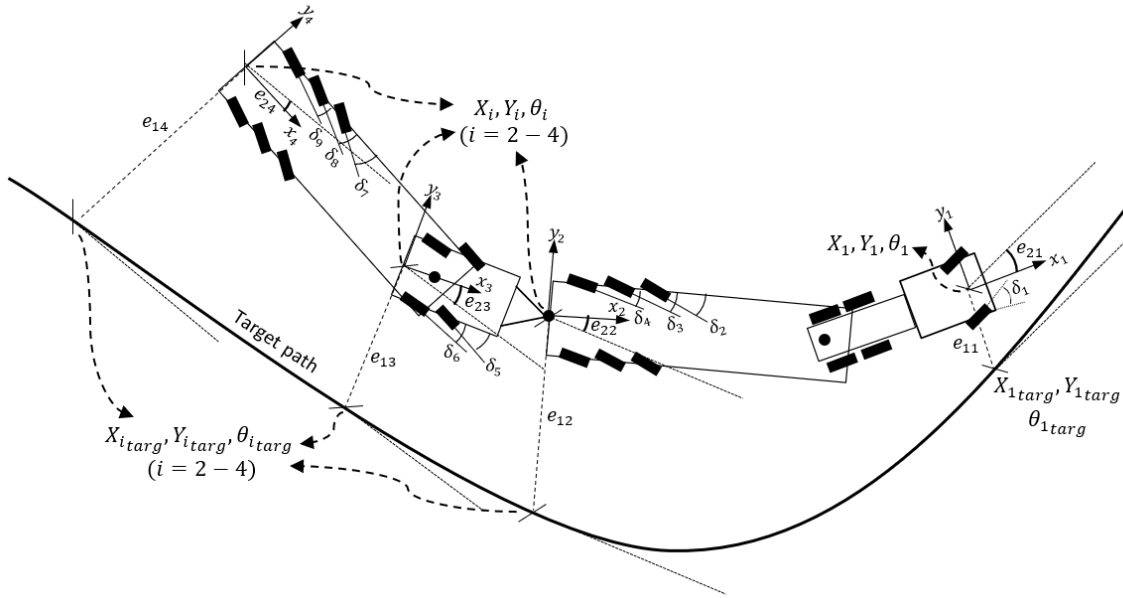


Figure 6.2. Schematic representation of the low-speed path-following mode (first mode).

The second mode is the high-speed lateral stability mode, which places emphasis on improving the lateral stability of towed units under evasive maneuvers at high speeds, e.g., single-lane change (SLC) maneuvers in highway operations.

In this mode, the first trailer's and dolly's rear ends will follow the trajectory generated by the first fifth-wheel, and the second trailer's rear end will track the trajectory made by the second fifth-wheel. Thus, the global position of each articulation point is buffered, then a curve is fitted to the buffered points to find the corresponding curvature of each articulation joint on the relative trajectory. The measured data are used to calculate the plant outputs, which are lateral deviation and relative yaw angle of the controlling points with respect to the desired trajectory. The outputs will be used in the ATDS-based controller to find the appropriate steering angles of the trailers' and dolly's axles. It is expected that

compromising the maneuverability in this case may lead to less lateral acceleration for the trailing units while negotiating a path at high speeds. As a result, the lateral stability of the trailers may be enhanced [98]. Figure 6.1 illustrates both of the modes of ATDS controller as a part of the integrated MPC control.

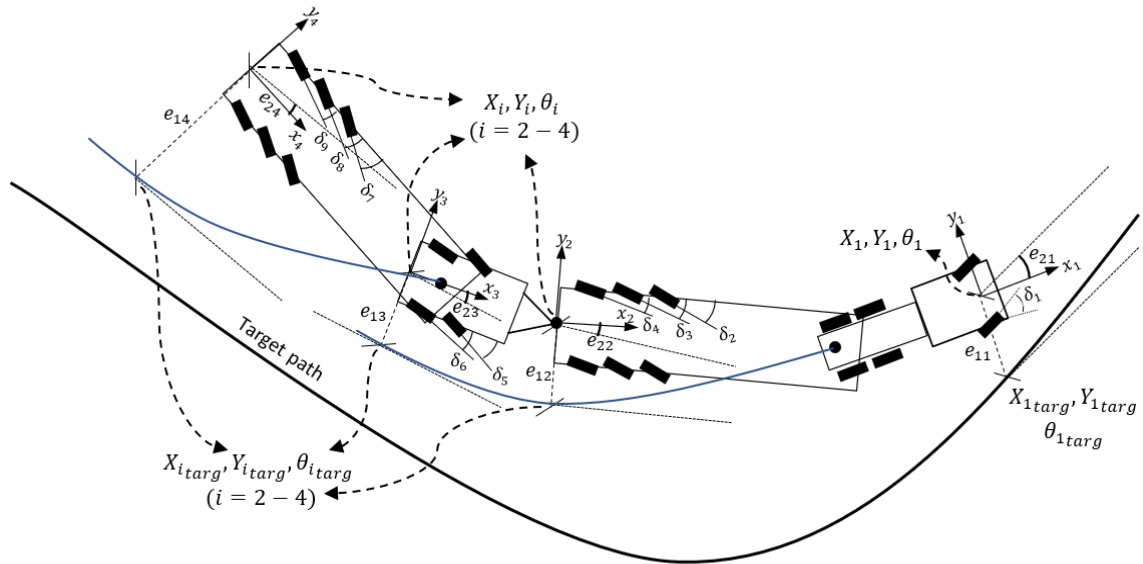


Figure 6.3. Schematic representation of the high-speed lateral stability mode (second mode).

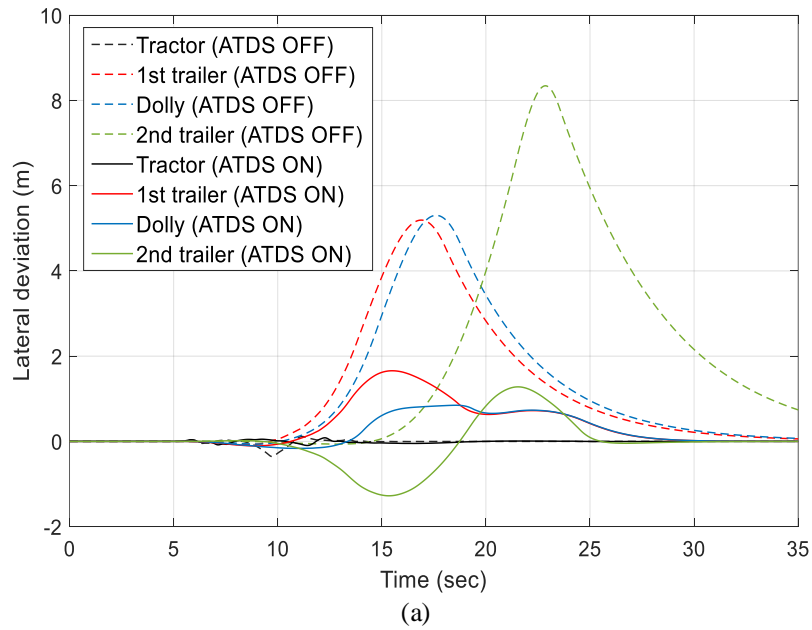
6.3 Simulation results

The performance of the proposed autonomous driving and the ATDS was evaluated via co-simulations using SIMULINK/MATLAB and TruckSim. MATLAB was utilized to code the controller, and the S-function block in SIMULINK was employed to receive the ‘measured’ states from the virtual plant, i.e., the TruckSim model, and to send the control signals to the virtual plant.

Three driving scenarios, including low-speed 90° turn, low-speed roundabout turn and high-speed lane change (HSLC), were simulated to examine the controller capabilities. In

the first driving scenario, the MTAHV negotiates a sharp turn with the radius of 11.25 m, in which the initial speed is 18 km/h and the target speed is set to 10.8 km/h.

Figure 6.4 (a) shows the lateral deviation from the target path when the ATDS is either OFF or ON. When the ATDS is inactive, the lateral deviations for all the towed units are considerably high. For instance, the second trailer deviates from the target path by more than 8.0 meters, while when it is active (i.e., the first mode), the lateral deviation plummets to around 1.0 meter. Figure 6.4 (b) illustrates the longitudinal speed control during the maneuver, which is well kept around the target value. The required steering angles for the trailing units' axles over the maneuver are illustrated in Figure 6.4 (c).



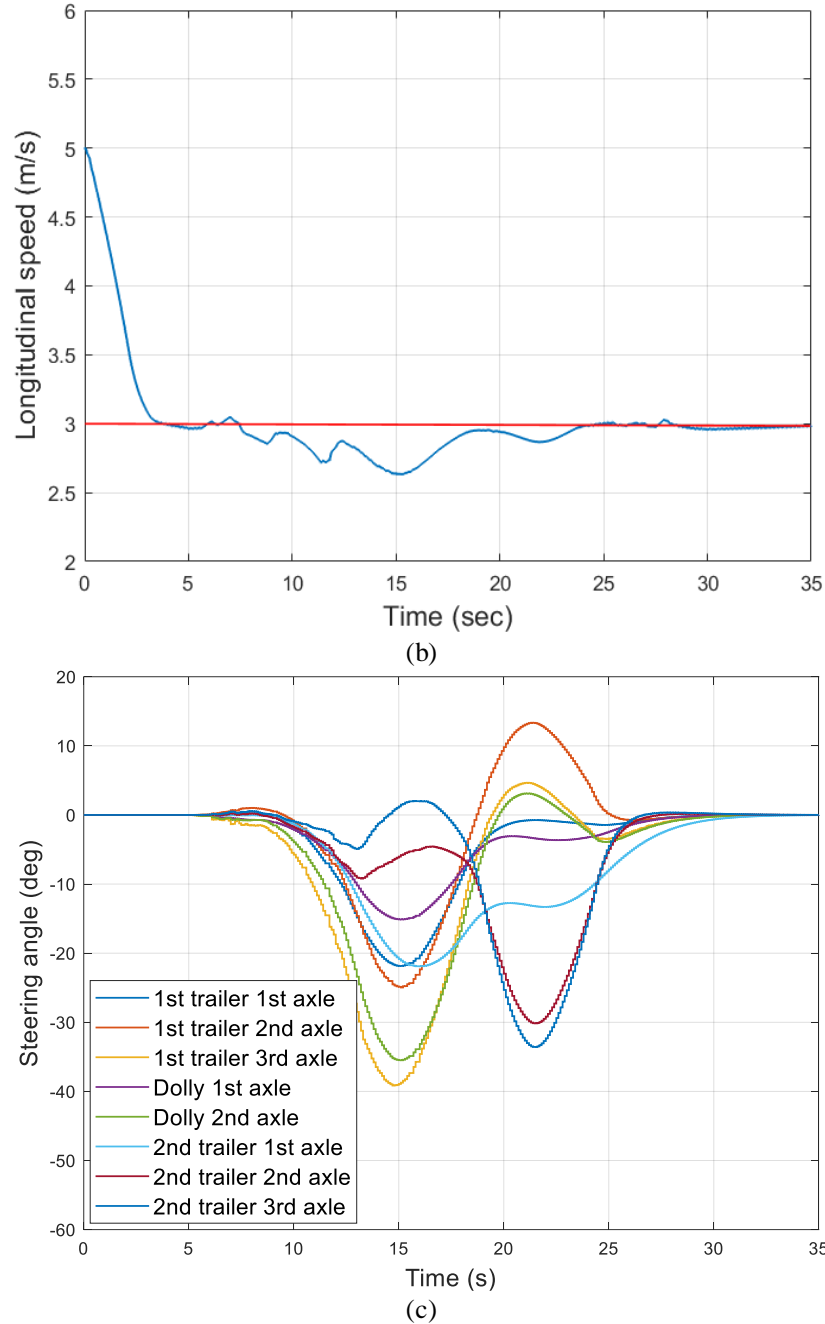


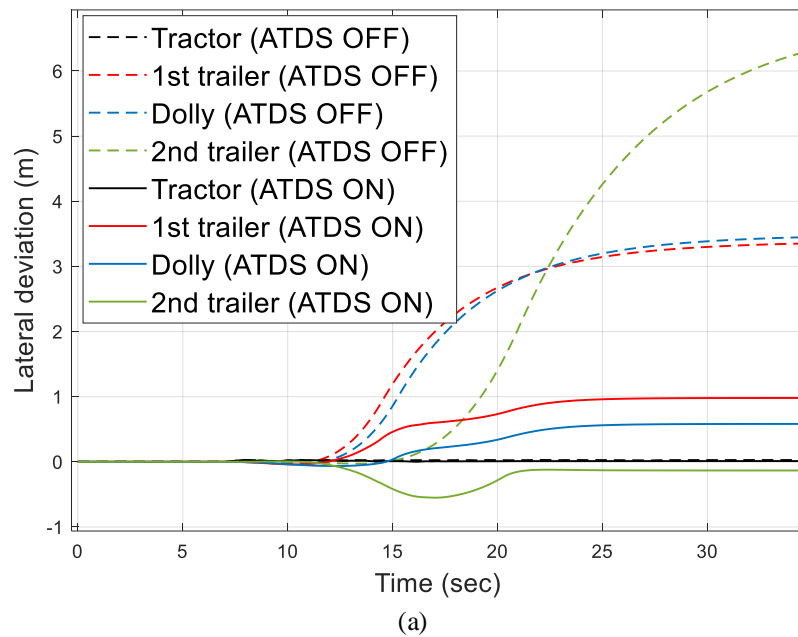
Figure 6.4. A-train double low-speed 90° turn maneuver results: (a) time history of the vehicle units' rear end lateral deviation from the target path, (b) vehicle's longitudinal speed time history versus the target speed, (c) required steering angles for the trailing units' axles when the ATDS is active.

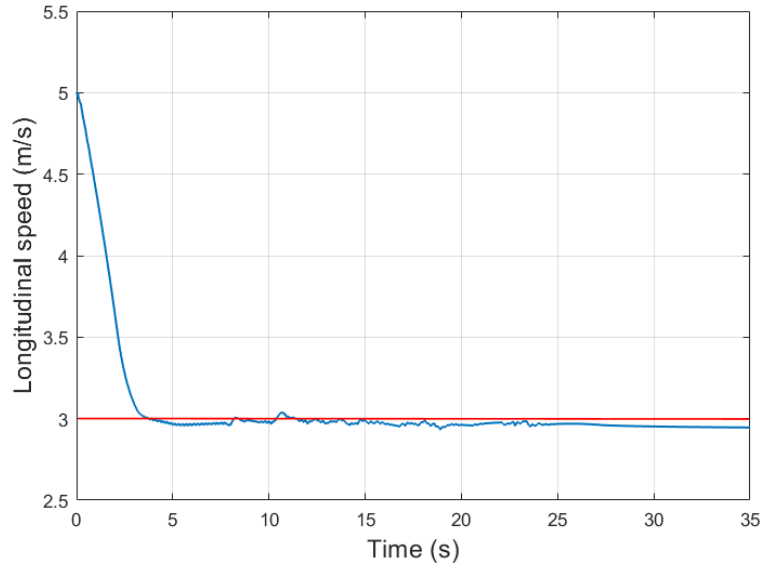
The next simulation test is a roundabout turn with 25 meters radius of the circular course.

The initial and target speeds are the same as for the 90°-turn maneuver. Figure 6.5 (a) indicates the lateral deviation from the target path for all the vehicle units when the ATDS

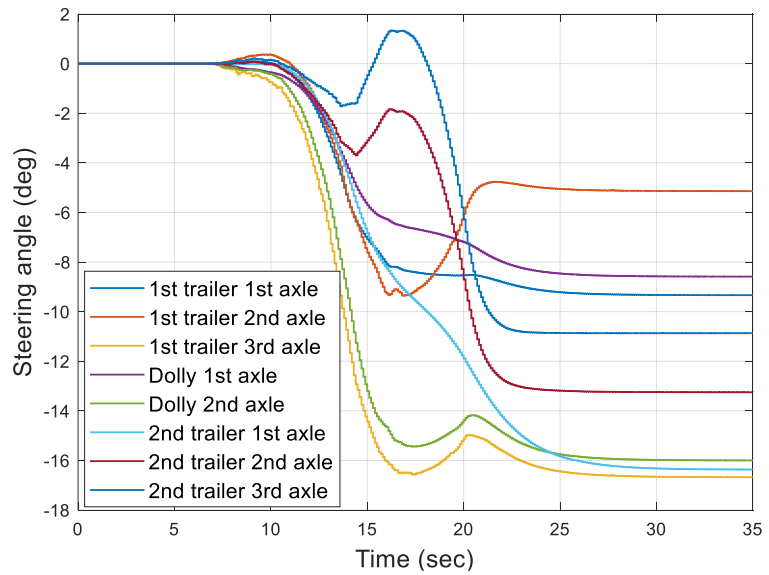
is either active and inactive. Similar to the results achieved under the 90° turn maneuver, when the ATDS is ON, the lateral deviations for the trailing units reach constant values (which are much smaller than their counterparts if the ATDS is OFF) less than 10 seconds after the towed units enter the circular part of the road.

However, in the case of the second trailer if the ATDS is OFF, even after more than 20 seconds, the deviation is still increasing and goes beyond 6 meters at the end of simulation. Figure 6.5 (b) and Figure 6.5 (c) display the time histories for the tractor’s speed and the demand steering angles for the trailing units’ axles throughout the course negotiation, respectively.



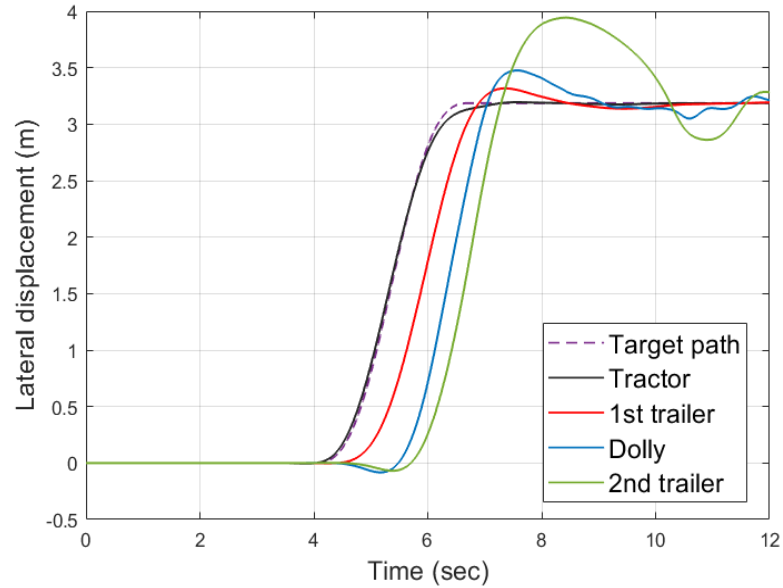


(b)

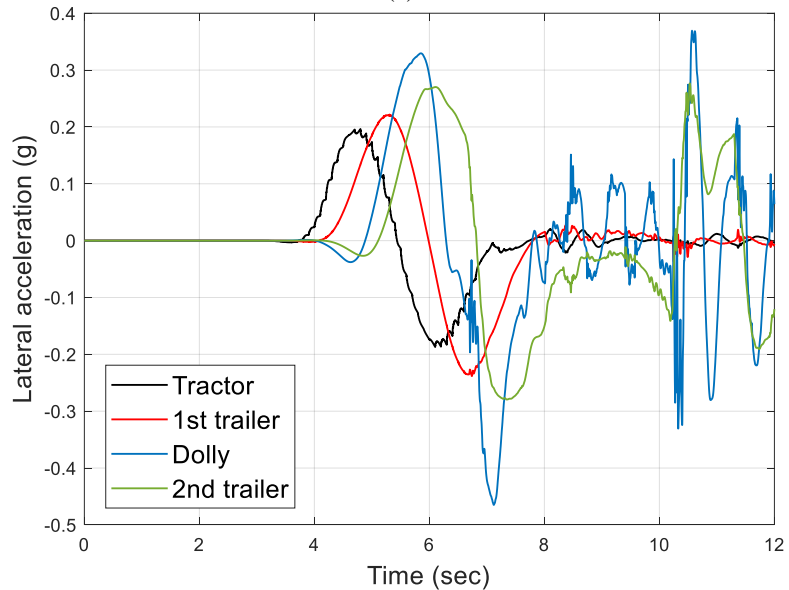


(c)

Figure 6.5. A-train double low-speed 360° turn maneuver results: (a) time history of the vehicle units' rear end lateral deviation from the target path; (b) vehicle's longitudinal speed time history versus the target speed; (c) required steering angles for the trailing units' axles when the ATDS is active.



(a)

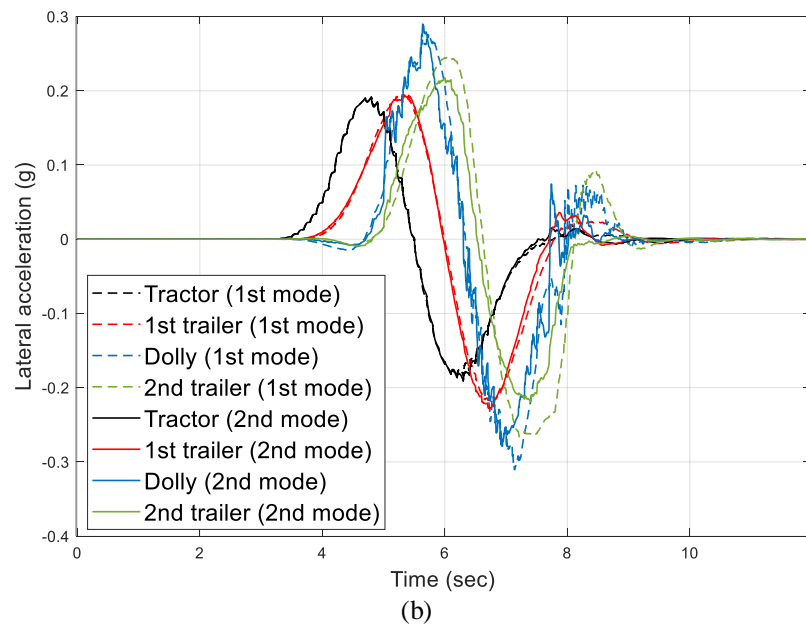
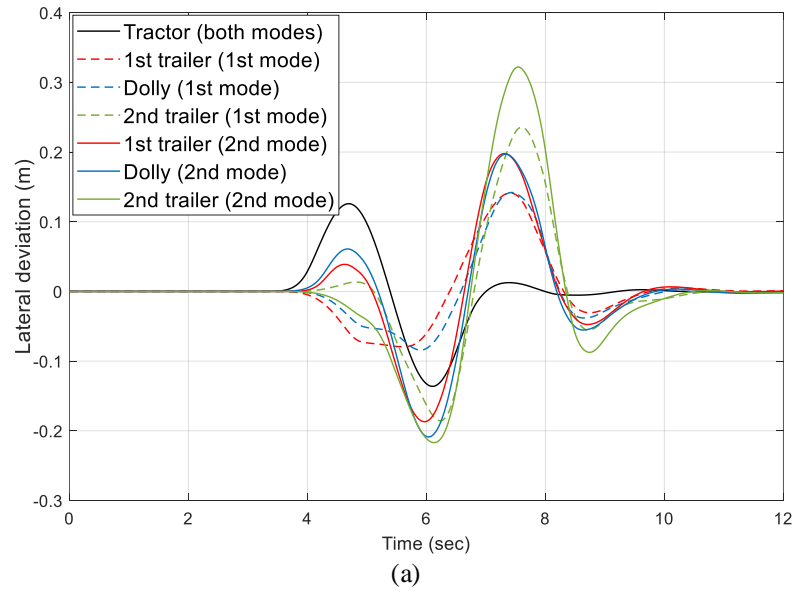


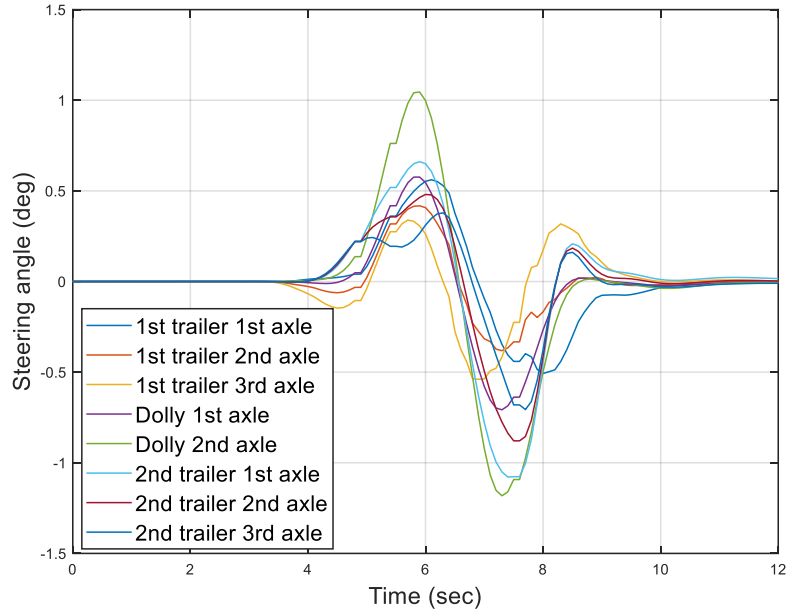
(b)

Figure 6.6. A-train double HSLC maneuver results when ATDS is inactive: (a) vehicle units' rear end lateral deviation from the target path, (b) vehicle units' CG lateral acceleration.

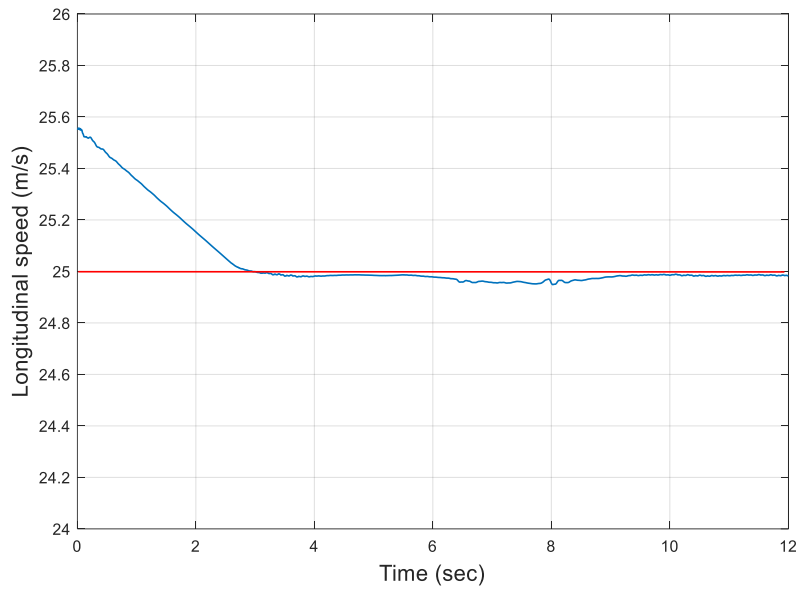
The final driving scenario is a high-speed obstacle avoidance maneuver with the maximum lateral displacement of 3.2 m. The initial speed is 95 km/h and it is supposed that the speed to be maintained around 90 km/h during the closed-loop simulation. Figure 6.6 exhibits the lateral deviation of the vehicle units and the resultant lateral acceleration while going

through the maneuver and the ATDS is inactive. It is inferred that, without the active safety control, the second trailer is laterally unstable and rollover is highly possible. However, the tractor follows the predefined path perfectly.





(c)



(d)

Figure 6.7. A-train double HSLC maneuver results when ATDS is active and the controller is set to operate in either the first mode or the second mode: (a) vehicle units' rear end lateral deviation from the target path, (b) vehicle units' CG lateral acceleration, (c) required steering angles for the trailing units' axles, (d) vehicle's longitudinal speed time history versus the target speed.

On the other hand, when the ATDS controller is active, the vehicle is stable. In order to effectively evaluate the performance of the controller modes, two simulations for the SLC maneuver with either of the first or the second mode were carried out and the results were

compared. Figure 6.7(a) indicates that, as expected, the lateral deviation of all the trailing units from the target path when the second mode of the ATDS is employed, is higher than that of the first mode. This is due to the fact that the second mode intends to keep the towed units following the trajectory of the coupling points, instead of the target path. Hence, the transient off-tracking is higher when the second mode is applied. However, Figure 6.7(b) shows that the peak lateral acceleration of the second trailer is about 0.2g when the second mode is utilized, while the first mode is active, the lateral acceleration of the second trailer is around 0.27 g. The rearward amplification is about 1.4 under the first mode, and declines to 1.1 under the second mode. Figure 6.7(c) and (d) show the required steering angles for the towed units' axles and the time history of the tractor's speed throughout the lane-change test maneuver.

6.4 Summary

A new integrated active trailers safety and autonomous driving control for MTAHVs was proposed. This control strategy distinguishes itself from the others in that it considers the trailing units states in addition to the tractor's state to find the optimal manipulated variables to track the target trajectory with the minimum error. Besides, both the automated driving and safety enhancement strategy are integrated in one control scheme, i.e. NLMPC. Furthermore, the proposed ATDS consists of a low-speed and a high-speed mode to fully take into account the unique dynamics feature of the MTAHVs. Adding some other autonomous driving features for MTAHVs to the current control strategy, e.g., longitudinal speed controller [113] and motion planning, makes the autonomous driving control scheme more effective and reliable.

Chapter 7. Model-predictive-based motion planning for highway operations of autonomous MTAHVs

7.1 Introduction

MTAHVs are an essential part of the logistics industry, and their efficient operation is crucial for the transportation of goods. However, the complexity of these vehicles, with multiple trailers and heavy payloads, poses significant challenges for their motion planning. This chapter will explore the motion planning for MTAHVs to generate smooth and safe reference trajectories.

Motion planning for MTAHVs involves finding a collision-free trajectory for the vehicle to follow while taking into account various factors, such as vehicle kinematics, dynamics, and environmental constraints. The motion planning problem is particularly challenging for multi-trailer vehicles, as their complex dynamics requires the consideration of multiple degrees of freedom, such as the relative motion between the trailers and the tractor.

The motion planning techniques used for MTAHVs, including optimization-based methods, and model predictive control (MPC) will be discussed in this chapter. The advantages and limitations of these techniques, along with their practical applications, will be explored. Furthermore, the importance of using the Frenet frame for motion planning in nonholonomic vehicle systems will be highlighted. The Frenet frame provides a natural way to describe the motion of a vehicle along a path, accounting for nonholonomic constraints, such as the need to maintain a constant velocity or heading. This chapter will demonstrate the effectiveness of the Frenet frame approach in generating smooth and safe reference trajectories for MTAHVs.

In general, an automated driving strategy for a MTAHV in the current study is divided into three categories. Global motion planning, considering the road geometry data e.g. by accessing the GPS several hundred meters ahead of the vehicle in order to manipulate the vehicle speed to maintain the vehicle within the safe driving condition well in advance. The speed planning control strategy proposed in Chapter 5 aims to accomplish this goal. Next, local path planning that intends to look ahead within a closer distance to accurately plan the vehicle motion so as to avoid obstacles and adjust the vehicle speed based upon the surrounding traffic. This is the target of the current chapter for the MTAHVs automated driving purposes. Last but not least, is the path-following approach. The lateral driver model proposed in Chapter 3 is the control strategy customized for MTAHV path following intent.

Motion planning for nonholonomic vehicles involves determining the optimal path and speed profile for the vehicle to follow, while taking into account the nonholonomic constraints that limit the vehicle's motion. Two commonly used reference frames for motion planning are the Cartesian and Frenet frames, each with its own set of pros and cons.

The Cartesian frame is a rectangular coordinate system that is fixed in space and defined by three orthogonal axes. It is convenient for describing the position and orientation of the vehicle, as well as the location of obstacles in the environment. However, the Cartesian frame can be limiting for nonholonomic vehicles, as it does not explicitly account for the constraints on the vehicle's motion, such as the inability to move laterally without turning.

The Frenet frame, on the other hand, is a curvilinear coordinate system that is defined by the path of the vehicle. For a curved path on a level plane, the Frenet frame includes two

orthogonal axes: the tangent vector, which points in the direction of the vehicle's motion, and the normal vector, which is perpendicular to the tangent vector and points towards the center of curvature of the path. The Frenet frame is advantageous for nonholonomic vehicles motion planning, because it allows for explicit consideration of the vehicle's constraints, such as the minimum turning radius. It also allows for a natural representation of the path and trajectory of the vehicle, making it easier to plan and execute maneuvers. Indeed, as illustrated in Figure 7.1, by utilizing the Frenet frame, the coordinate system becomes uncurled, and this enables the independent optimization of path planning along the lengthwise and crosswise directions.

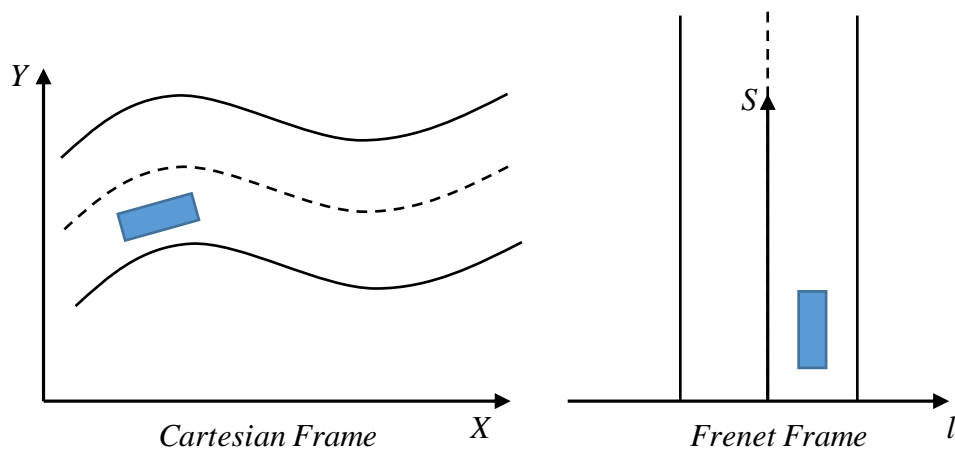


Figure 7.1. The difference between vehicle coordinate representation in Cartesian frame versus Frenet frame, regenerated from [114].

7.2 Frenet-Serret coordinate system

Assume that \vec{r}_t is a curved path in a three-dimensional Euclidean space which represents a particle's position vector as a time function. In addition, the particle's velocity and acceleration are given by $\dot{\vec{r}}_t$ and $\ddot{\vec{r}}_t$ vectors. The Frenet frame is a frame that traverses this path and the Frenet-Serret formulas interpret the curve's geometric properties. In general,

the dynamic Frenet coordinate system in a 3D space is made by \mathbf{T} , \mathbf{N} and \mathbf{B} , i.e. the tangent, normal and binormal unit vectors respectively, which are formulated as follows [115].

$$\mathbf{T} = \frac{\frac{d\vec{r}}{ds}}{\left\| \frac{d\vec{r}}{ds} \right\|} \quad \mathbf{N} = \frac{\frac{d\mathbf{T}}{ds}}{\left\| \frac{d\mathbf{T}}{ds} \right\|} \quad \mathbf{B} = \mathbf{T} \times \mathbf{N} \quad (7.1)$$

where $s(t)$ is the curve length traced by the particle and is given by:

$$s(t) = \int_0^t \left\| \dot{\vec{r}}(\sigma) \right\| d\sigma \quad (7.2)$$

The Frenet-Serret formulas are demonstrated by the matrix below

$$\begin{bmatrix} \mathbf{T}' \\ \mathbf{N}' \\ \mathbf{B}' \end{bmatrix} = \begin{bmatrix} 0 & \kappa & 0 \\ -\kappa & 0 & \tau \\ 0 & -\tau & 0 \end{bmatrix} \begin{bmatrix} \mathbf{T} \\ \mathbf{N} \\ \mathbf{B} \end{bmatrix} \quad (7.3)$$

where $(\cdot)' = \frac{\partial}{\partial s}(\cdot)$, and κ and τ are the curvature and torsion of the curve, respectively.

In the case of vehicle trajectory planning, it is presumed that the vehicle is driven on a 2-D plane, hence the torsion is considered as zero. Thus, any point on the generated trajectory \vec{P} is defined by the tangential vector \vec{t}_r and the normal vector \vec{n}_r through the moving frame on the reference path. Figure 7.2 shows the schematic representation of generating the trajectory in the Frenet coordinate system. Based on the parameters shown on the graph [116], the trajectory \vec{P} is given in the new frame by

$$\vec{P}(s(t), l(t)) = \vec{R}(s(t)) + l(t)\vec{n}_r(s(t)) \quad (7.4)$$

where, $\vec{R}(s(t))$, $s(t)$ and $l(t)$ are the root point on the reference line, the length of the arc travelled and the perpendicular offset of the trajectory \vec{P} from the Frenet reference \vec{R} root point, respectively.

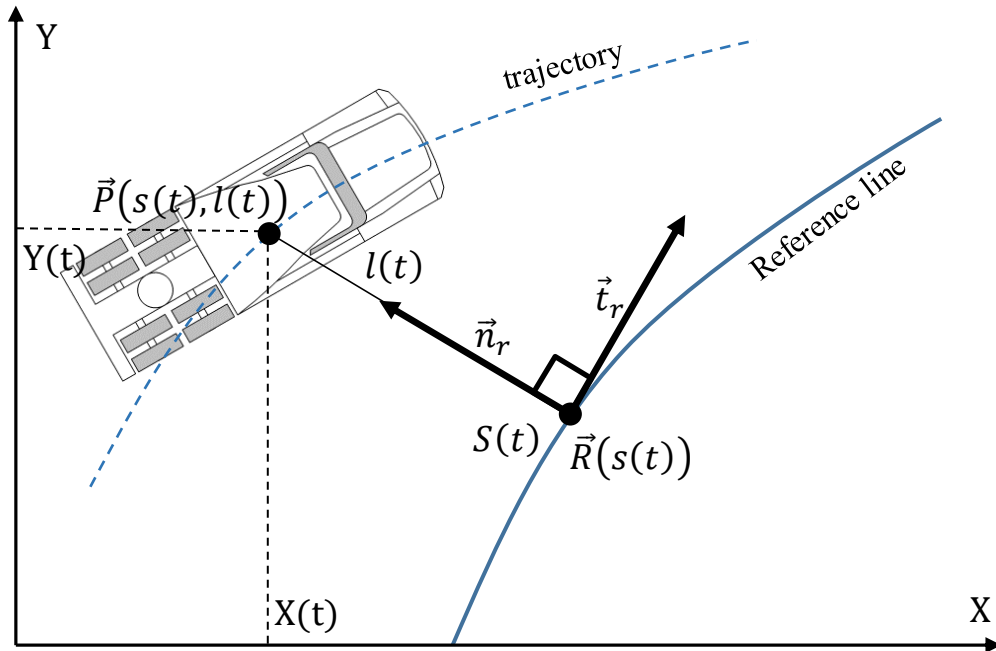


Figure 7.2 The Frenet frame representation of a sample point on the trajectory

7.3 Coordinates transformation between Frenet and Cartesian frames

In reality, the GPS generates the sensed data in the Cartesian coordinate system. Furthermore, the roads' and highway's coordinates are also available in the Cartesian frame. In order to drive automatically on the highway, the Cartesian coordinates of the highway centerline are required and considered as the waypoints of the reference path, which constitutes the S axis of the Frenet coordinate system. Hence, the current position of the vehicle and any trajectory represented in the Frenet frame is generated concerning this reference line. Having the current global coordinate of the vehicle and the global coordinates of the reference path, and also using some simple mathematical methods such as the one presented in [115], it is possible to fit a curve to the available waypoints of the reference path W_i , and create the S axis for the Frenet frame and also transform the current vehicle position in the Cartesian frame $P(X(t), Y(t))$ to the vehicle position in the Frenet

frame $P(s(t), l(t))$. Equations (7.5) and (7.6) show how the position of the vehicle in the Frenet frame is formulated.

$$s_p = \sum_{i=1}^{R-1} s_i + \Delta s \quad (7.5)$$

$$l_p = d \cdot \cos \psi \quad (7.6)$$

where, $\Delta s = d \cdot \sin \psi$ and d is the Euclidean distance between the point P and the nearest waypoint on the reference path. Figure 7.3 illustrates the way that the S axis is created using the reference path waypoints W_i , and also how the point P is transformed to the Frenet frame having the global coordinates of the waypoints and the vehicle current position.

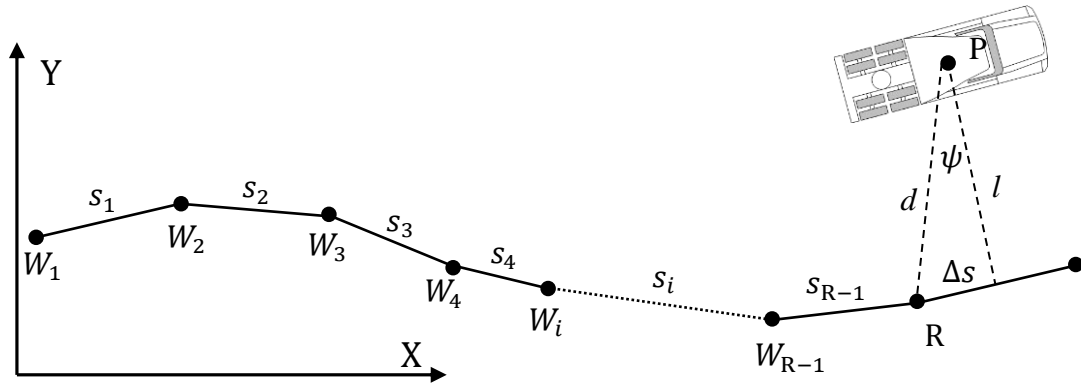


Figure 7.3. Vehicle position transformation from the Cartesian frame to the Frenet frame.

Additionally, it will be demonstrated that there are certain situations where obtaining global coordinates is essential after the trajectory has been created in the Frenet frame. Thus, the transformation from the Frenet frame to the Cartesian frame is required at times. As a result, it is mandatory to come up with the transform functions that interprets the Frenet frame to the Cartesian coordinate.

The Frenet states for a particle in Frenet frame are given by a vector of form $[s, \dot{s}, \ddot{s}, l, l', l'']$, where s is the arc length, and l is the perpendicular deviation from the reference path as noted before. \dot{s} and \ddot{s} are the time derivatives of s , while l' and l'' are the derivatives relative to the arc length i.e. s . The particle's global states in the Cartesian frame are also given by $[X, Y, \theta, \kappa, v, a]$, where X and Y are the global coordinates. θ is the heading angle in radian and κ is the relevant curvature. Besides, v and a are the speed and the acceleration, respectively.

First, assume that given the trajectory data in the Frenet frame, it is required to generate the trajectory states in the Cartesian frame. Having $\vec{R}(s(t))$, $s(t)$ and $l(t)$, the global coordinates of trajectory $\vec{P}(s, l)$ at moment t are determined by

$$\begin{aligned} X_P &= X_R + l \cos\left(\theta_R + \frac{\pi}{2}\right) \\ Y_P &= Y_R + l \sin\left(\theta_R + \frac{\pi}{2}\right) \end{aligned} \quad (7.7)$$

where, θ_R is the heading angle, and X_R and Y_R are the global coordinates of the reference path $\vec{R}(s(t))$ at moment t .

The following equations also hold for the trajectory $\vec{P}(s, l)$ [116].

$$\begin{aligned} l' &= [1 - \kappa_R l] \tan \Delta\theta \\ l'' &= -[\kappa'_R l + \kappa_R l'] \tan \Delta\theta + \frac{1 - \kappa_R l}{\cos^2 \Delta\theta} \left[\kappa_P \frac{1 - \kappa_R l}{\cos \Delta\theta} - \kappa_R \right] \end{aligned} \quad (7.8)$$

where, $\Delta\theta = \theta_P - \theta_R$, θ_P is the heading angle of trajectory \vec{P} , κ_R is the reference path curvature, θ_P and κ_P are determined by solving equations (7.8). Additionally, the trajectory's velocity and acceleration are calculated by

$$v_P = \dot{s} \frac{1 - \kappa_R l}{\cos \Delta\theta} \quad (7.9)$$

$$a_P := \dot{v}_P = \dot{s} \frac{1 - \kappa_R l}{\cos \Delta\theta} + \frac{\dot{s}^2}{\cos \Delta\theta} [[1 - \kappa_R l] \tan \Delta\theta \Delta\theta' - [\kappa_R' l + \kappa_R l']]$$

Hence, having the Frenet states of trajectory \vec{P} its global states will also be attained. It is important to mention that for a trajectory \vec{P} with continuous curvature κ_P , the reference path \vec{R} requires to have a continuous change of curvature κ_R' . The same formula is used to transform the trajectory from the Cartesian frame to the Frenet frame. This is done using the MATLAB coding and some available tools in the MATLAB Navigation Toolbox.

7.4 Local trajectory generation for highway scenario

When using automated self-driving vehicles, the driver is not required to actively participate in driving, and instead becomes a passive passenger or occupant. However, if the lateral and longitudinal acceleration and acceleration rate due to autonomous driving strategy are not within the acceptable range, this can result in motion sickness for occupants, which occurs due to a conflict between what is visually perceived as movement and the sense of movement in the vestibular system [117]. Indeed, jerk which is the derivative of acceleration with respect to time is a significant parameter in determining the motion smoothness and comfort level for the passengers and driver. According to [118][119], the lateral and longitudinal jerk for a vehicle shouldn't exceed 0.2g/s to maintain the occupant's comfort.

Polynomials can be very useful and efficient for trajectory generation in automated vehicle driving. If the generated polynomial trajectory optimizes the jerk, it would be desirable for motion planning purposes. Through formulating the trajectory using polynomials, usually a cost function and a number of constraints are considered which can generate the optimal

trajectory as required. The generated trajectories which are time-varying and are defined in a 2-D space normally satisfy several lateral and longitudinal motion constraints. Selecting the polynomial orders is a crucial part of the trajectory generation process. The accuracy and computational cost of the trajectory generated by this method is highly dependent on the order of the polynomial [120]. Quintic polynomials are known as jerk optimal trajectories between two points P_1 and P_2 represented by $[s_1, \dot{s}_1, \ddot{s}_1, l_1, l'_1, l''_1]$ and $[s_2, \dot{s}_2, \ddot{s}_2, l_2, l'_2, l''_2]$ states in the Frenet frame, respectively [121]. Actually, the quintic polynomials as the planned trajectory can minimize the cost function defined by

$$J_m := \int_{t_1}^{t_2} \ddot{f}^2(\tau) d\tau \quad (7.10)$$

where \ddot{f} is the motion jerk between two points P_1 and P_2 , and f must be a continuous function between P_1 and P_2 points. Otherwise, the optimization problem couldn't be solved due to infinite parameter appearance in the equation. It is important to mention that f itself consists of two parts namely lateral and longitudinal trajectory functions which represent the trajectories for lateral and longitudinal motions, separately.

$$J_m := \int_{t_1}^{t_2} \ddot{f}_{lateral}^2(\tau) d\tau + \int_{t_1}^{t_2} \ddot{f}_{longitudinal}^2(\tau) d\tau = C_{lateral} + C_{longitudinal} \quad (7.11)$$

The solution for the minimization problem of each cost function in equation (7.11) is a quintic polynomial trajectory. The quintic polynomial has the form of

$$f(t) = a_0 + a_1 t + a_2 t^2 + a_3 t^3 + a_4 t^4 + a_5 t^5 \quad (7.12)$$

To find the polynomial parameters a_0 to a_5 , the Frenet states of the desired start and end points of the various automated trajectory planning scenarios, are taken into account and the resultant equations are solved for the polynomial parameters. To do so, the first and second derivatives of the equation are calculated by

$$\begin{aligned}
f(t) &= a_0 + a_1t + a_2t^2 + a_3t^3 + a_4t^4 + a_5t^5 \\
\dot{f}(t) &= a_1 + 2a_2t + 3a_3t^2 + 4a_4t^3 + 5a_5t^4 \\
\ddot{f}(t) &= 2a_2 + 6a_3t + 12a_4t^2 + 20a_5t^3
\end{aligned} \tag{7.13}$$

Having these equations as well as the initial and terminal states of the trajectories in the Frenet frame, six equations for each lateral and longitudinal polynomial are attained. Solving the equations for the coefficients, the f will be reformulated in a parametric form based upon the initial and terminal states of the trajectory. Taking the third derivative of the f function, the parametric form of the optimization problem cost function 7.11 is concluded.

However, in order to find the fastest optimal trajectory between two initial and end points, a new cost function is added to equation (7.11). This cost function represents the time duration required for traversing the trajectory, i.e. T , where $T = t_2 - t_1$. Furthermore, it is expected that the vehicle follows the reference path as close as possible. Hence, another cost function C_{offset} is introduced into equation (7.11) so as to penalize large deviations from the reference line. This cost function is specified by

$$C_{offset} = \int_{t_1}^{t_2} f_{lateral}^2(\tau) d\tau \tag{7.14}$$

In some automated driving situations, it is intended that the vehicle speed is kept close to a desired speed. Hence, another cost function is appended to the original cost function defined by equation (7.11) to reach this goal while the trajectory smoothness is guaranteed. This cost function is defined by

$$C_v = \left(v_{target} - f_{longitudinal}(t_2) \right)^2 \tag{7.15}$$

The new cost function is formulated using the aforementioned factors as demonstrated in equation (7.16). It can be proved that the new cost is also a quintic polynomial [116].

$$C_t = k_m J_m + k_t T + k_o C_{offset} + k_v C_v \quad (7.16)$$

where k_m , k_t , k_o and k_v are positive constants. By minimizing the total cost function formulated in equation (7.16), a jerk optimal trajectory which satisfies all the required constraints is achieved. The MATLAB script and Navigation toolbox were utilized to generate the trajectories for various previously-mentioned typical highway driving behaviors namely lane-change, Cruise control and adaptive cruise control [122].

7.4.1 Cruise control behavior

In a situation in which there is no other vehicle on the highway in an immediate distance ahead of the current ego vehicle position, i.e. when there is no possibility of collision within the intended preview time window τ , the ego vehicle can drive while keeping the speed near to the highway speed limit. Hence, one of the final trajectory constraints, that is, the endpoint Frenet longitudinal velocity state is defined as the highway speed limit denoted by $\dot{s}_{limit} = \text{speed limit}$. The endpoint of the generated trajectory can be at any distance ahead of the vehicle provided other constraints are met. Hence, the longitudinal position s_1 is not constrained. It is logically assumed that the lateral speed, lateral and longitudinal accelerations at the trajectory end are zero. The lateral distance of the trajectory endpoint $l_{predict}$ is defined as the lateral distance of center of the predicted lane with respect to the reference path at which the vehicle predicted position would hold within the preview time τ . Consequently, the final Frenet states for generating the cruise control behavior trajectory are determined by

$$states_{finalCruiseCtrl} = P_{FCC} = [\forall s \dot{s}_{limit} 0 l_{predict} 0 0] \quad (7.17)$$

Having the initial Frenet states of the tractor T_{init} and the final states the optimal cruise control quintic polynomial trajectory is generated as explained before. Figure 7.4 shows the schematic trajectory generated for the cruise control.

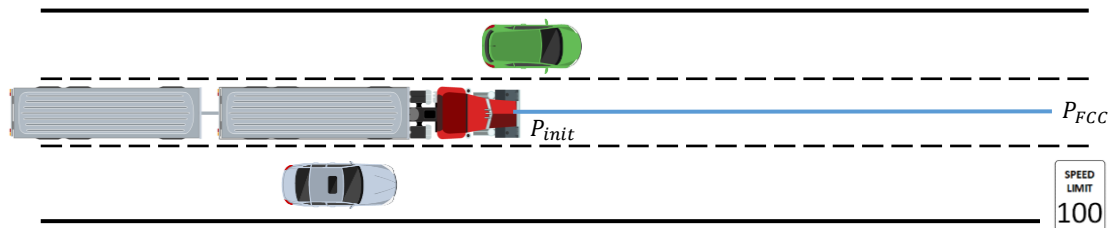


Figure 7.4. The trajectory generated for cruise control.

7.4.2 Lane-change behavior

If the current lane is occupied by another vehicle ahead of the tractor and there is a possibility of collision based upon the current vehicle speed and the preceding traffic, the ego vehicle should reduce the speed and try to maintain the speed close to the preceding vehicle's speed within a safe distance to avoid any accident. An alternative option is to change lane, and the ego vehicle moves to a vacant adjacent lane if there is no chance of colliding. The former is termed vehicle-following behavior, which will be explained, while the latter is known as lane-change behavior. The lane-change approach has priority over the vehicle-following, because in this way the speed is assumed to be kept within the legal speed limit of the highway and no braking activity is required. Hence, the vehicle will travel at a high average speed with less fuel consumption, tire and brake pad wear during a long journey.

Similar to the cruise control behavior, in lane-change trajectory generation the endpoint is not constrained and it can be at any distance in front of the vehicle. However, the final speed is set to the current vehicle's speed, and the acceleration is considered zero. In order to determine the lateral deviation from the reference path for the trajectory end state, the current vehicle lane and the available adjacent lanes are detected. Then, the centers of the neighboring lanes are set as the lateral displacement of the Frenet states for trajectory generation. The lateral acceleration trajectory state at the final point is also reasonably presumed to be zero. The Frenet states for the lane-change trajectory at the endpoints are considered as indicated in equation 7.18. It is required to mention that the available adjoining lanes can be either one or two.

$$states_{finalLaneChange} = P_{FLC} = [\forall s \dot{s}_{current} \ 0 \ l_{adjacent} \ 0 \ 0] \quad (7.18)$$

Similarly, the quintic polynomials for lane-change trajectories can be achieved by using the initial and final Frenet states, i.e. T_{init} and T_{FLC} , respectively. Figure 7.5 illustrates the trajectories required for a lane-change behavior.

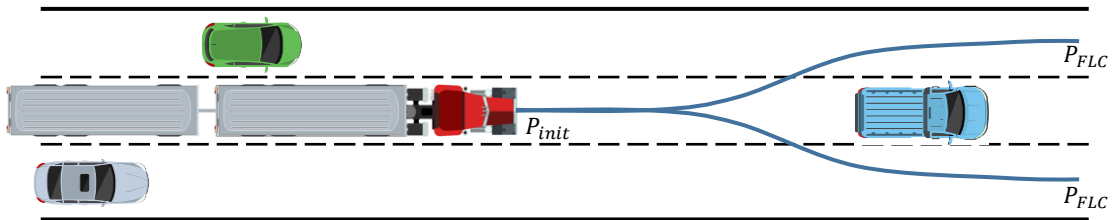


Figure 7.5. The trajectory generated for lane-change.

7.4.3 Vehicle-following behavior

As mentioned before, in some cases the ego vehicle can neither maintain the current speed nor change lane due to surrounding traffic. Hence, it needs to adapt its speed to the

preceding vehicle. For the preview time window τ , the preceding vehicle position is estimated based upon the current lateral and longitudinal speed and the expected lane is identified. Hence, the nearest preceding vehicle is recognized and its states are estimated as well. The terminal longitudinal position state for the vehicle-following trajectory generation is calculated based upon the lead vehicle's preview speed and an velocity-dependent safety gap determined by [123]

$$\begin{aligned} States_{finalVehicleFollowing} = P_{FVF} &= s_{lead} - safety\ gap \\ &= s_{lead} - (t_{safe}(\dot{s}_{ego} - \dot{s}_{lead}) + d_{safe}) \end{aligned} \quad (7.19)$$

where s_{lead} and \dot{s}_{lead} are the position and the speed of the preceding vehicle, respectively. \dot{s}_{ego} is the ego vehicle current speed. d_{safe} is a constant safety distance gap required between the ego vehicle and the preceding vehicle. t_{safe} is a constant time gap which adjusts the total required gap between vehicles based on their relative speed. The Frenet terminal speed state is considered the same as the preceding vehicle's speed. The longitudinal final acceleration is considered zero. The lateral position state is assumed to be the same as the preceding vehicle lateral position with respect to the reference path. The lateral speed Frenet state for end trajectory point is also equal to the lateral velocity of the preceding vehicle, while the lateral acceleration state for the final point is set to zero. The final terminal states for vehicle-following is represented by

$$states_{finalVehicleFollowing} = P_{FVF} = [s_{FVF} \ \dot{s}_{lead} \ 0 \ l_{lead} \ \dot{l}_{lead} \ 0] \quad (7.20)$$

The quintic trajectory representing the vehicle-following behavior is then calculated by using T_{init} and T_{FLC} . Figure 7.6 shows the vehicle-following schematic illustration when the two other aforementioned behaviors are not feasible.

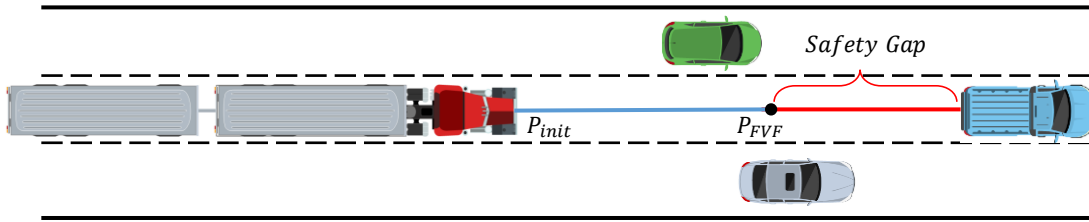


Figure 7.6. The trajectory generation for adaptive cruise control behavior.

7.5 Trajectory evaluation

At each timestep, the aforementioned trajectories are generated simultaneously. If there are two adjacent lanes beside the ego vehicle, the total number of generated trajectories would be four, otherwise it will be three. The priority is always given to the cruise control behavior in which the vehicle will move with the highest speed indicated by the road sign. The other maneuvers may lead to more constraints, which in turn cause more tire and brake pads wear, higher road surface wear, greater safety risks due to lane-change or braking activity, especially in the case of MTAHVs and high-speed operations.

The next priority is given to the lane-change maneuvers, since the vehicle still moves on the road with the assumption of keeping the current speed and no braking action involvement, which remains a high transportation efficiency as a significant autonomous driving goal for MTAHVs. However, as there is always a safety risk for MTAHVs lane-change maneuver especially with high driving speeds. Thus, some safety measures, e.g., advanced trailer safety systems, are considered in the current study. In case that both left and right lane-change maneuvers are possible, the priority is given to the left lane-change, unless otherwise there is a collision probability.

The final priority goes to the vehicle-following behavior, in which the acceleration/deceleration is utilized by applying the brake or throttle, and the ego vehicle speed is determined by the preceding vehicle considering the safety distance. As explained before, this autonomous strategy is not of interest unless other trajectory generation strategies don't meet the collision avoiding requirements simultaneously.

7.6 Collision checking

Once the trajectory with the highest priority is planned, it should be checked for the probability of collision with other road participants. To detect any possible collision between the ego vehicle and the surrounding vehicles, it is necessary to first encapsulate the ego vehicle and other dynamic/static obstacle vehicles on the road with an estimated shape. Next, the future motion of surrounding dynamic obstacles over the prediction horizon should be approximately calculated. Finally, the generated trajectories for the ego vehicle and the dynamic obstacles should be verified to find any overlap, which represents the probable accident.

Several methods have been introduced in the literature to approximate vehicle shape. In [124], the authors proposed disk approximation, by which the vehicle shape can be estimated using either of three, six or ten discs as shown in Figure 7.7(a). In [125], Darms et al. recommended that either a box model or a point model approximation, as seen in Figure 7.7(b), could be enough for urban driving scenario applications.

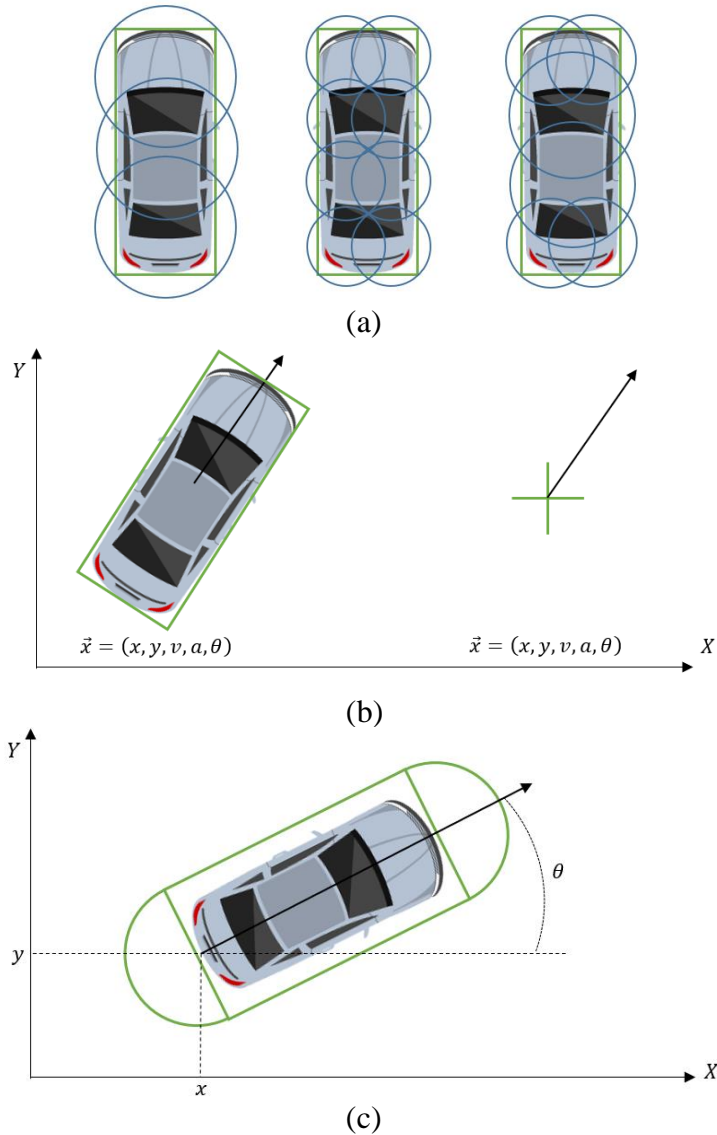


Figure 7.7. The vehicle shape approximation methods for collision checking: (a) multiple discs approximation, (b) box or point approximation, and (c) proposed approximation method.

For the current study, a combined approach is employed to model the vehicles' shapes like what is considered in [122]. Indeed, the vehicle is assumed to be enclosed in a capsule shape which includes three states, x , y and θ , denoting the longitudinal and lateral position of the vehicle, as well as its heading direction. For the sake of added safety, each vehicle is surrounded by a shape, which is bigger than the vehicle dimensions, and the objective is

to reserve a safety gap between the various vehicle sides. Figure 7.7(c) shows this approach.

As noted before, an object tracking strategy is also required to track the obstacles' motions and estimate their states within the prediction horizon. Many studies have been conducted to tackle this issue and generate the position, velocity and acceleration of the moving objects as the main variables demanded for surrounding traffic motion prediction. For instance, using linear dynamics models and Kalman filter, the object tracking and prediction over the limited preview time window for the surrounding traffic was implemented [126], [127]. In [128], Dellaert et al. used a similar approach for detecting and tracking utilizing laser scanner. Moreover, they used extended Kalman filter to formulate a non-linear state estimation model. To tackle the limitations of Kalman filter estimation method, which takes advantage of a single vehicle model and cannot handle the driving scenarios with considerable dynamic changes, the interacting multiple model (IMM) filter was deployed in another study [129]. The IMM implements a soft decision, utilizes several parallel models simultaneously, and generates a weighted combined state estimate. In fact, this method applies various models for different driving situations involving remarkable acceleration, speed change, and other highly dynamic modes. In [130], Lin et al. proposed a simple yet effective prediction method for moving obstacles using a simplified driver model and the sideslip and yaw angles states data gained from the surrounding vehicles via v2v information interaction. There are some other approaches for obstacle motion prediction, such as in [131][132]. However, as the main goal for the current study is not surrounding traffic detection and motion prediction, it is assumed that their estimated position, heading angle, velocity and acceleration information are available.

Thus, a simple predefined trajectory approach for each obstacle vehicle on the road over the prediction horizon is adopted.

Given the coordinates and heading angles of the obstacle vehicles at each preview timestep, a capsule shape is drawn repeatedly throughout the predefined trajectory for the preview time window. The analogous approach is exploited to draw the ego vehicle's representative capsule shapes for the prediction horizon over the trajectory generated based upon the aforementioned methods in previous sections. Figure 7.8 illustrates a graphical representation of this approach for three moving obstacle vehicles and the ego LCV, each of which has different speed. After creating all the capsule trajectories, any intersection between the ego vehicle future trajectory and the obstacles' trajectories is analyzed. If there exists any overlap, as seen in Figure 7.8, between the left lane-change trajectory and the left obstacle vehicle predicted trajectory, it is considered that the vehicles might collide. Thus, this trajectory is rejected, and next trajectory is evaluated. The acceptable trajectory, which is the collision-free one, is shown with green color. Collision checking is computationally expensive and usually postponed to the final steps after initial trajectory evaluation. Furthermore, once the collision-free trajectory is found, it is marked as the optimal trajectory, and the collision checking process for the rest of trajectories in the list is prevented unless otherwise a new collision is detected for the prevailing optimal trajectory.

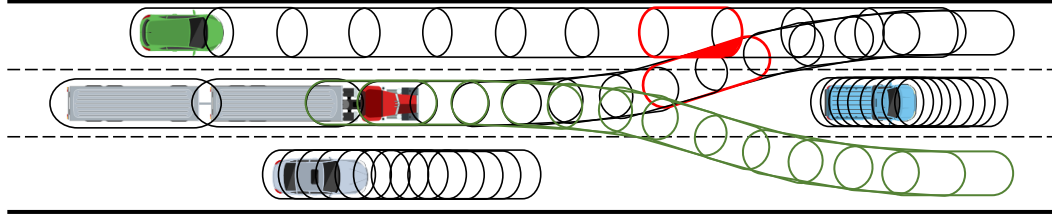


Figure 7.8. Collision checking process schematic representation.

It is worthwhile to mention that in the case of MTAHVs, the hypothetical capsule shapes trajectory for the trailing units over the prediction horizon should also be considered to make sure no collision will occur between the towed units and surrounding obstacle vehicles. Obviously, in some cases the trajectory of the tractor might not have any intersection with the trajectories of the surrounding vehicles. However, the trailing units might still collide with the surrounding vehicles. Having the optimal trajectory calculated from the previous section, the tractor's steering input for the prediction time window is calculated so that the TFAC follows the trajectory with negligible error. Then the predicted steering vector is used as the input to the vehicle state-space dynamics equation to predict the position and heading angles of the trailing units over the prediction horizon. These data will then be used to generate the trajectories for the towed units. This approach is executed using the model predictive control path-following methodology. Consider the continuous-time state-space representation of the governing equations of motion for the MTAHV expressed by

$$\begin{aligned}\dot{\mathbf{x}} &= \mathbf{A}_d \mathbf{x}(t) + \mathbf{B}_d \mathbf{u}(t) \\ \mathbf{y} &= \mathbf{C}_d \mathbf{x}(t)\end{aligned}\tag{7.21}$$

where state variables are specified by

$$\mathbf{x}(t) = [Y_1 \psi_1 v_1 \psi_1 Y_2 \psi_2 v_2 \psi_2 Y_3 \psi_3 v_3 \psi_3 Y_4 \psi_4 v_4 \psi_4]' \quad (7.22)$$

The input variable $u(t)$ is δ , which is the tractor's front wheel steering angle. Matrices \mathbf{A}_d , \mathbf{B}_d and \mathbf{C}_d are given in the appendix A.3. Using a zero-order hold method, the \mathbf{A}' and \mathbf{B}' matrices are redefined and the discrete-time state-space model is described by equation (7.23). This will simplify the control design and facilitate the implementation of the model.

$$\begin{aligned} \mathbf{x}(k+1) &= \mathbf{A}'\mathbf{x}(k) + \mathbf{B}'\mathbf{u}(k) \\ \mathbf{y}(k) &= \mathbf{C}'\mathbf{x}(k) \end{aligned} \quad (7.23)$$

Equations (7.23) will generate the predicted states and outputs of the system for one timestep ahead. In order to predict them for n_p timesteps (the prediction horizon) ahead of the current time, equation (7.24) holds.

$$\mathbf{x}_{k+n_p|k} = \mathbf{E}_x \mathbf{x}_k + \mathbf{F}_x \mathbf{u}_{k+n_p-1|k} \quad (7.24)$$

where,

$$\mathbf{E}_x = \begin{bmatrix} \mathbf{A}' \\ \mathbf{A}'^2 \\ \vdots \\ \mathbf{A}'^{n_p} \end{bmatrix} \quad \text{and} \quad \mathbf{F}_x = \begin{bmatrix} \mathbf{B}' & 0 & \dots & 0 \\ \mathbf{A}'\mathbf{B}' & \mathbf{B}' & \dots & 0 \\ \vdots & \vdots & \ddots & 0 \\ \mathbf{A}'^{n_p-1}\mathbf{B}' & \mathbf{A}'^{n_p-2}\mathbf{B}' & \dots & \mathbf{B}' \end{bmatrix} \quad (7.25)$$

The outputs for the prediction window are also given by

$$\mathbf{y}_{k+n_p|k} = \mathbf{C}\mathbf{x}_{k+n_p|k} = \mathbf{C}(\mathbf{E}_x \mathbf{x}_k + \mathbf{F}_x \mathbf{u}_{k+n_p-1|k}) = \mathbf{G}_x \mathbf{x}_k + \mathbf{H}_x \mathbf{u}_{k+n_p-1|k} \quad (7.26)$$

where

$$\mathbf{G}_x = \begin{bmatrix} \mathbf{C}' \mathbf{A}' \\ \mathbf{C}' \mathbf{A}'^2 \\ \vdots \\ \mathbf{C}' \mathbf{A}'^{n_p} \end{bmatrix} \quad \text{and} \quad \mathbf{H}_x = \begin{bmatrix} \mathbf{C}' \mathbf{B}' & 0 & \cdots & 0 \\ \mathbf{C}' \mathbf{A}' \mathbf{B}' & \mathbf{C}' \mathbf{B}' & \cdots & 0 \\ \vdots & \vdots & \ddots & 0 \\ \mathbf{C}' \mathbf{A}'^{n_p-1} \mathbf{B}' & \mathbf{C}' \mathbf{A}'^{n_p-2} \mathbf{B}' & \cdots & \mathbf{C}' \mathbf{B}' \end{bmatrix} \quad (7.27)$$

Having the global coordinates of the TFAC at each time and using the optimal trajectory determined by the global coordinates as the reference path, the trajectory is also represented in the body-fixed coordinate system of the tractor, i.e. $y_{ref_{k+i|k}}$. Then, by using the predicted lateral position of the TFAC over the prediction horizon with respect to the tractor's body-fixed-coordinate system $Y_{1_{k+i|k}}$, a cost function is formulated as

$$J = \sum_{i=1}^{n_p} \|y_{ref_{k+i|k}} - Y_{1_{k+i|k}}\|^2 + \sum_{i=1}^{n_p} \|u_{k+i-1|k}\|^2 + \sum_{i=1}^{n_p} \|\Delta u_{k+i-1|k}\|^2 \quad (7.28)$$

Utilizing the Fmincon function in MATLAB and minimizing the cost function subject to the following constraints in inequalities (7.29) when the steering angle is considered as the manipulated variable, the $\delta_{k+i-1|k}$ over the prediction horizon will be attained.

$$\begin{aligned} \delta_{min} &\leq \mathbf{u}_{k+i-1|k} \leq \delta_{max} \\ \Delta \delta_{min} &\leq \Delta \mathbf{u}_{k+i-1|k} \leq \Delta \delta_{max} \end{aligned} \quad (7.29)$$

Having the steering angle values for the prediction horizon, and using the second equation of equation set (7.23), the lateral displacements and heading angles of the trailing units in the preview time window can be calculated. As a result, utilizing this information, the capsule shape trajectories of the towed units are generated for subsequent collision checking purposes.

If the prioritized trajectory is found collision-free, that trajectory will be chosen for the path-following purpose using the developed lateral driver model in Chapter 4. Otherwise,

the next trajectory with the highest priority is selected. This process will continue until a collision-free trajectory is found. Otherwise, the vehicle goes through the last autonomous driving behavior, i.e. the adaptive cruise control in order to adjust the vehicle speed with respect to the nearest preceding obstacle vehicle on the highway. Since all the trajectories are continually generated and evaluated, once a collision-free trajectory is recognized, the controller will switch to that one to follow the path with the highest priority.

7.7 Trajectory generation methods and case studies

To implement the trajectory planning for the MTAHVs considering their unique dynamic features and utilizing the introduced ATDS in Chapter 6, six various methods/case studies are developed as shown in Table 7.1. These case studies are combined of the preview time required for the trajectory generation, the ATDS and the MPC-based optimization method employed to enhance the trajectory and increase the A-train double lateral stability.

Table 7.1. The case studies developed by combining the ATDS, optimization and preview time required for trajectory generation

Motion planning method	Preview time	ATDS	MPC trajectory optimization
Case study 1	2 seconds	No	No
Case study 2	2 seconds	Yes	No
Case study 3	2 seconds	No	Yes
Case study 4	1+2 seconds	No	No
Case study 5	1+2 seconds	Yes	No
Case study 6	1+2 seconds	No	Yes

7.8 Basic trajectory planning method (case study 1)

In the current study, the preview time for trajectory generation is set to two seconds. This value seems enough for reference trajectory generation. It is important to mention that using longer preview times is not always helpful, because the computation time will also increase and it might make the strategy less successful for real-time application. Indeed, when the computation time increases, more powerful hardware will be required. There is a trade-off among the preview time value, the required accuracy, reliability, computational and production costs. Hence, a trade-off analysis can be conducted to determine the optimal preview time. In the current study, an optimal preview time is not necessary, only a practical value is selected. For example, a two-second preview time gives a 50 m trajectory generation horizon for the situation, in which the vehicle is moving at 25 m/s. This seems reasonable to prevent any harsh lane-change or brake application maneuvers if required. On the other hand, the lateral acceleration and deceleration rates will remain within the acceptable range during the aforementioned driving scenarios provided the control strategy performs well. Figure 7.9 illustrates the schematic representation of trajectory planning and path-following simulation for an A-train double while performing a triple lane-change maneuver based upon the two-second preview time on a four-lane highway with surrounding traffic. The speed is kept constant at 90 km/h. The black curves represent the evaluated trajectories. The red curve denotes the impossible trajectory, and the green curve represents the collision-free trajectory. The grey capsules in front of the vehicles illustrate their estimated position and direction over the preview horizon. The faster the car moves on highway, the farther the capsules are spread in front of the vehicle. As shown in the

figure, the ego vehicle successfully travels without any collision, and if not necessary to change the lane, it remains moving on its current lane at the desired forward speed.

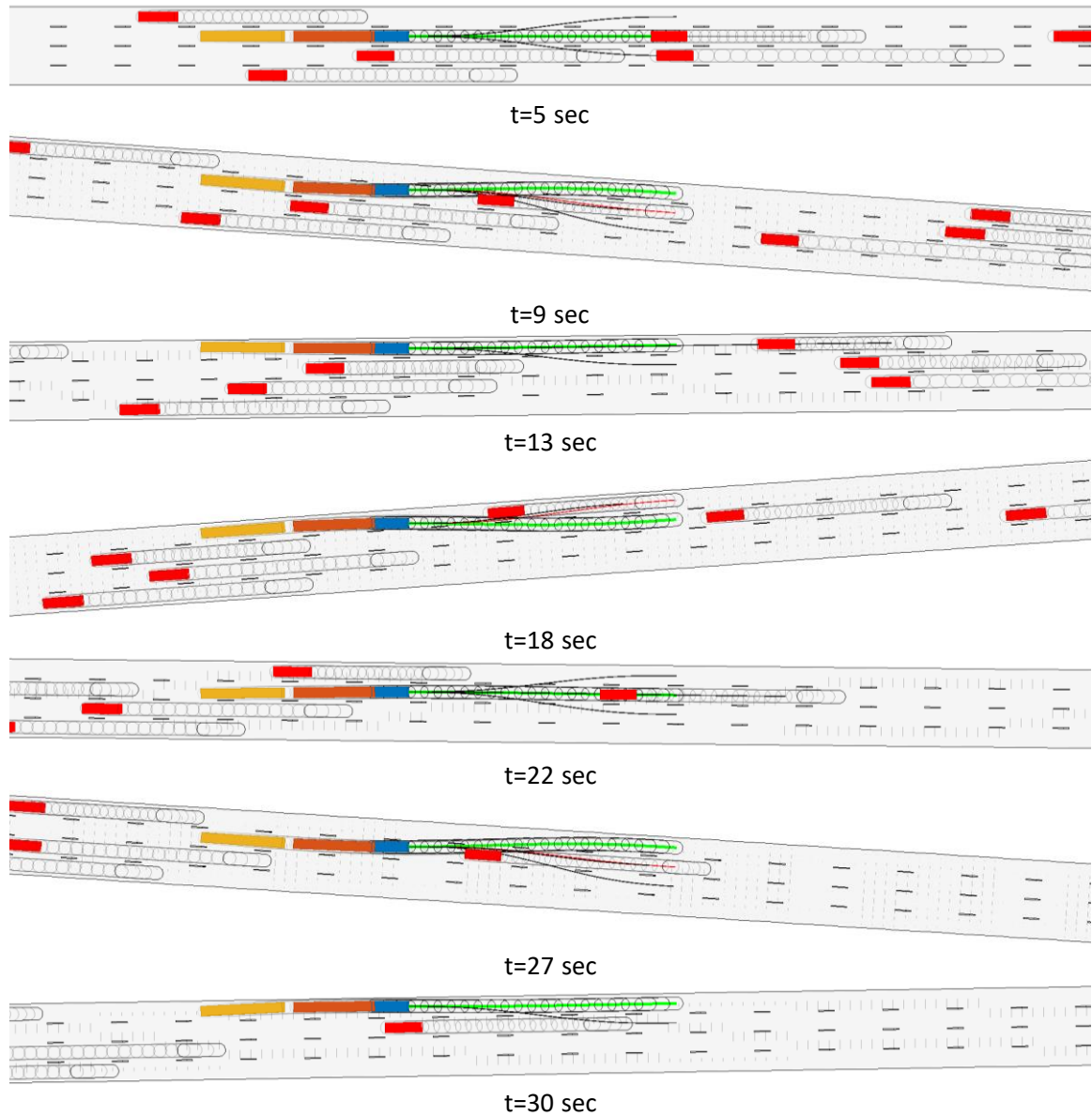
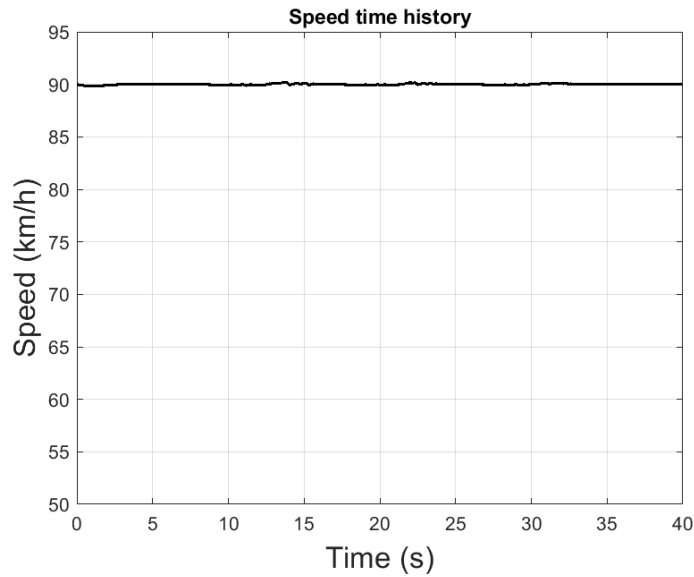


Figure 7.9. A-train double autonomous lane-change maneuver behavior on highway driving scenario with the preview time of 2 s (the red rectangles represent obstacle vehicles, the blue, orange and yellow rectangles represent the tractor, first trailer and second trailer respectively).

The ego vehicle steering input and speed over this maneuver are shown in Figure 7.10. It should be noted that to perform the lane-change maneuvers a maximum steering wheel angle of 60 degrees is required and the steering input is applied abruptly to do the job.



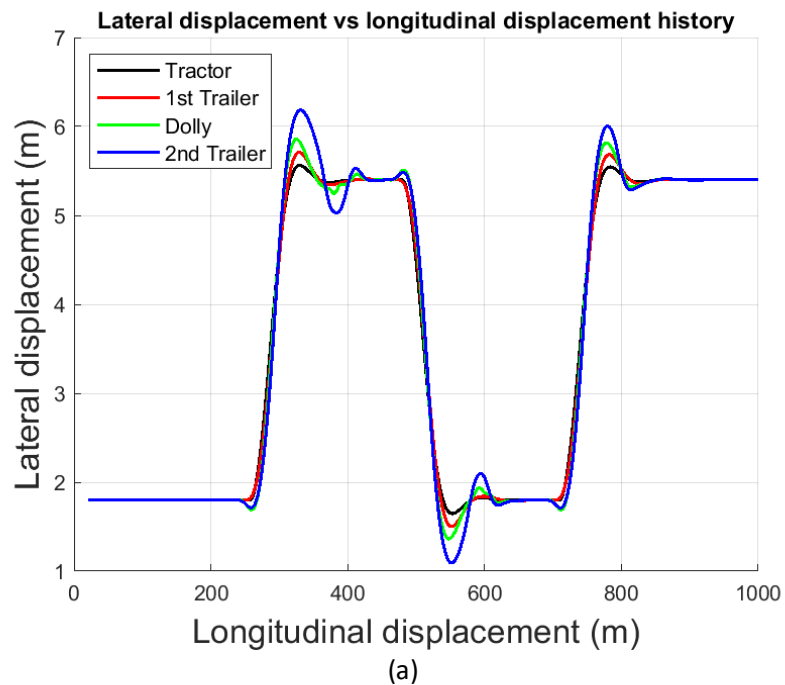
(a)

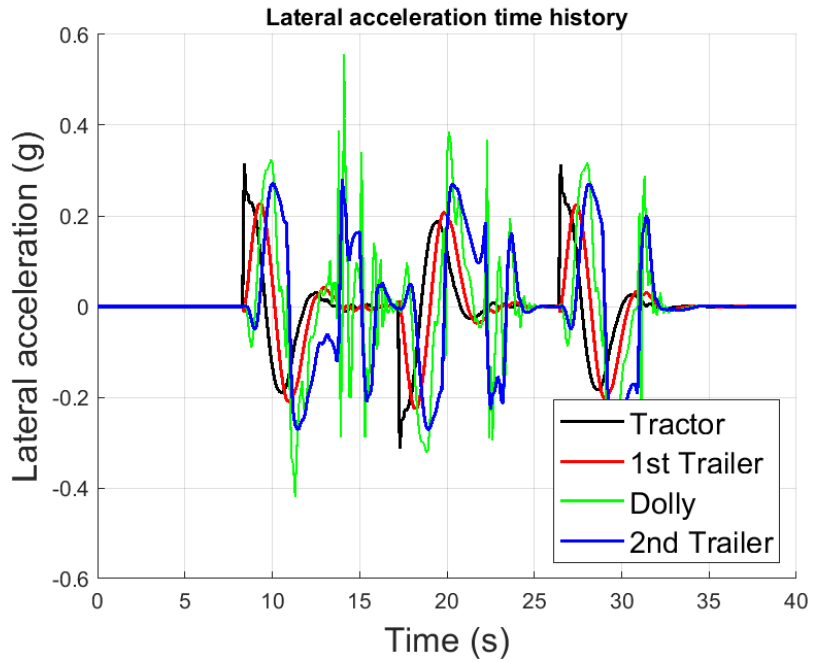


(b)

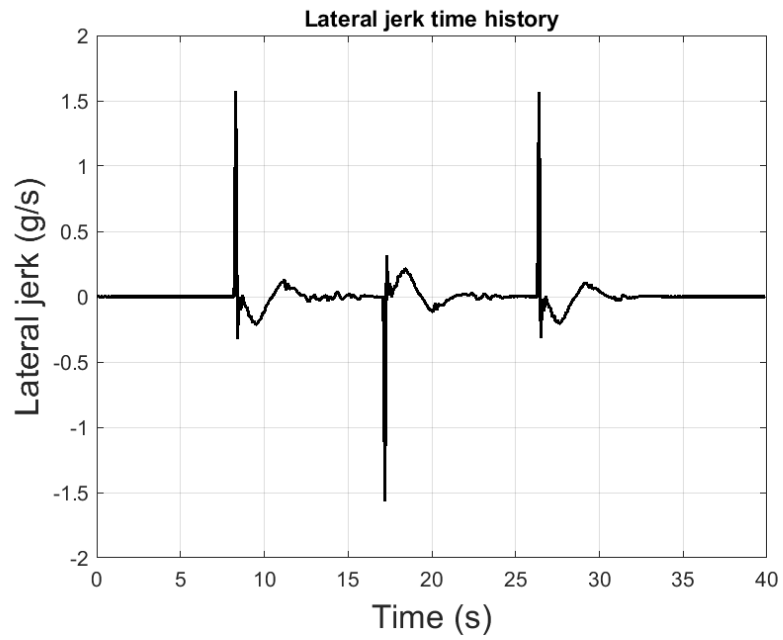
Figure 7.10 A-train double's steering inputs and forward speed over the triple lane-change maneuver with the preview time of 2 sec: (a) steering input, and (b) forward speed.

Figure 7.11 displays various vehicle states during the autonomous driving triple lane-change maneuver. Figure 7.11(a) discloses that the trailers experience significant amounts of off-tracking, which is caused by the sudden switch from the cruise control trajectory to the lane-change trajectory to avoid a collision with the preceding vehicle. This necessitates an abrupt steering action to ensure that the vehicle follows the reference path for single lane changes. Note that it is highly undesirable for MTAHVs to execute high-speed lane change maneuvers, as they are more susceptible to experience amplified lateral acceleration. As indicated by Figure 7.11(b) and (c), all the vehicle units experience substantially high lateral acceleration. Furthermore, due to the sudden lateral motion, the tractor's lateral jerk is also high, exceeding the acceptable range for ride comfort which is 0.2 g/s.





(b)



(c)

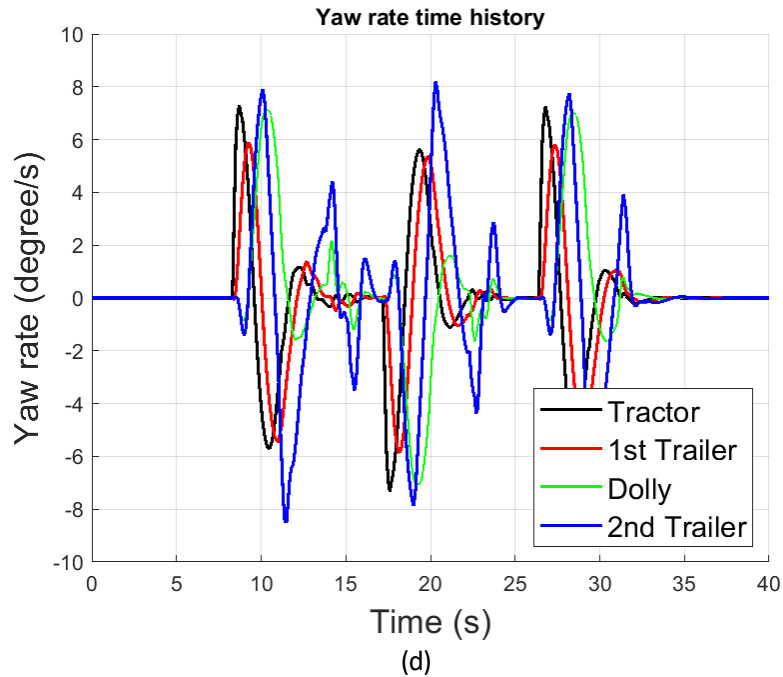
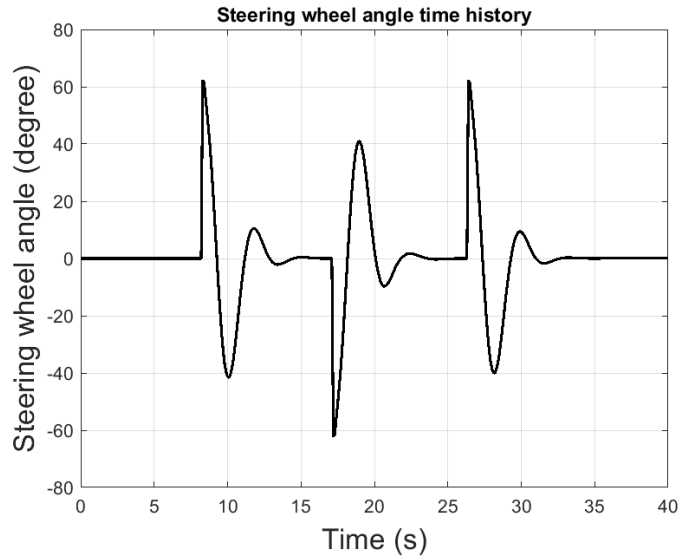


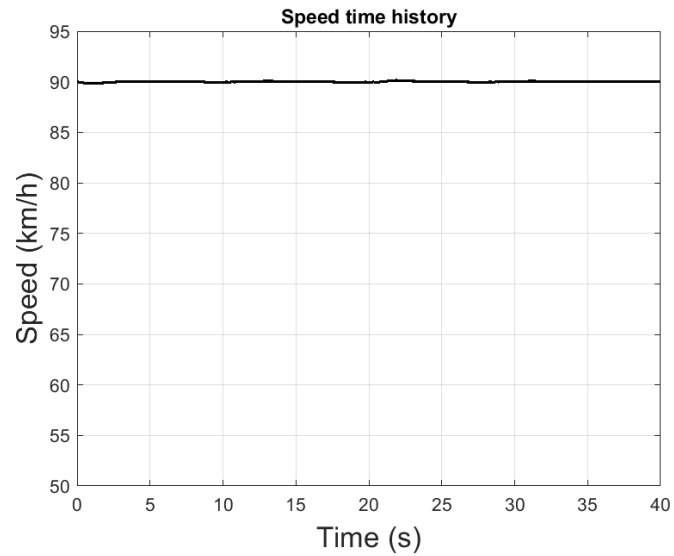
Figure 7.11 A-train double’s dynamic responses for each vehicle unit over the triple lane-change maneuver with the preview time of 2 sec: (a) lateral displacement versus longitudinal displacement, (b) time history of lateral acceleration, (c) time history of tractor’s lateral jerk, and (d) time history of yaw-rate.

7.9 Improving the vehicle lateral dynamics using ATDS controller (case study 2)

As demonstrated in Chapter 6, ATDS is an effective control technique to mitigate the lateral instability of the A-train double during evasive high-speed maneuvers. In order to enhance the trajectory-planning and path-following for the vehicle executing the maneuver introduced in Section 7.7, the active trailer steering was combined with the autonomous driving of the vehicle. Figure 7.12 (a) and (b) show the steering angle input and forward speed for the same autonomous highway driving scenario introduced in Section 7.7, when the ATDS is active. As expected, there is no remarkable difference for these two variables compared the curves shown in Figure 7.10 and 7.12, which correspond the cases with the ATDS inactivated and activated, respectively.



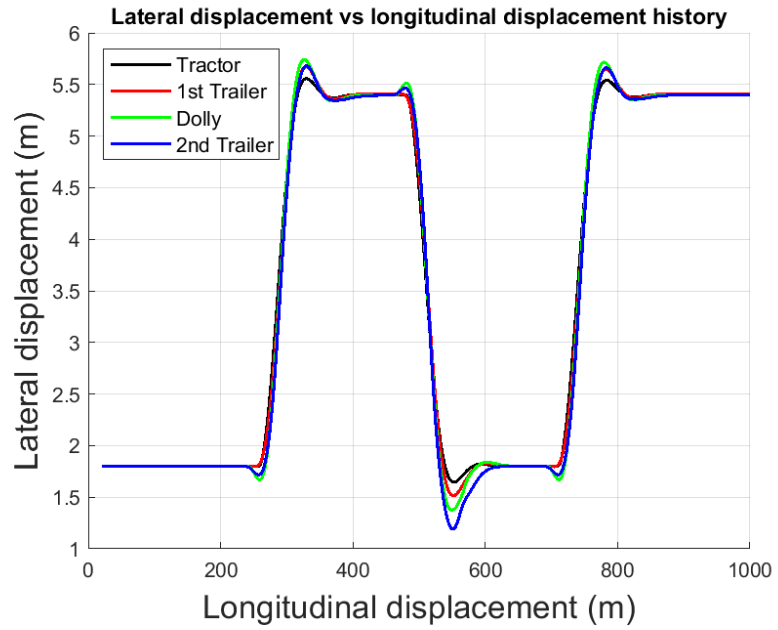
(a)



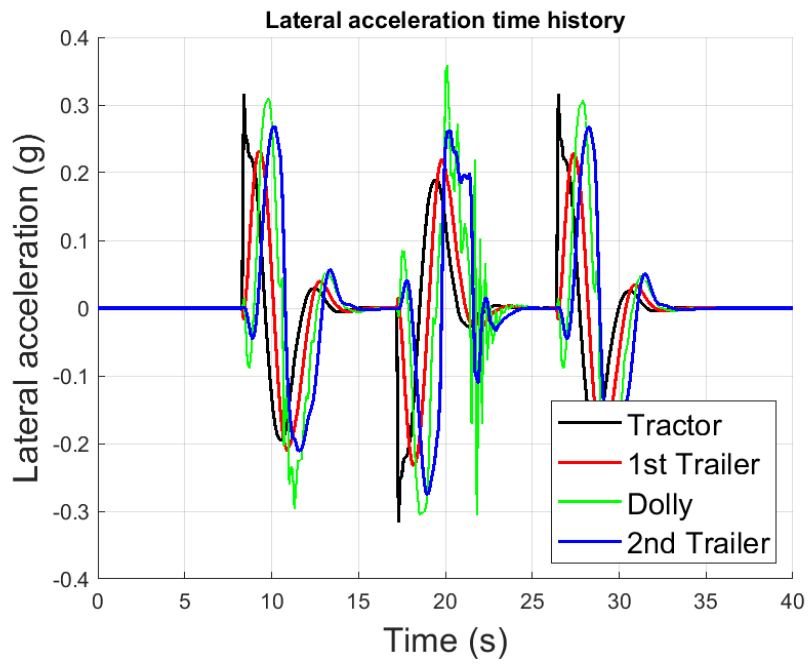
(b)

Figure 7.12 A-train double’s steering angle input and forward speed over the triple lane-change maneuver with ATDS activated and the preview time of 2 sec: (a) steering input time history, and (b) forward speed time history.

As shown in Figure 7.13(a), (b), and (d), by actively steering the trailing units’ wheels, the lateral displacement, the lateral acceleration and yaw rate values for the towed units are improved noticeably. Albeit, the tractor’s lateral jerk is still similar to previous case as illustrated in Figure 7.13(c).



(a)



(b)

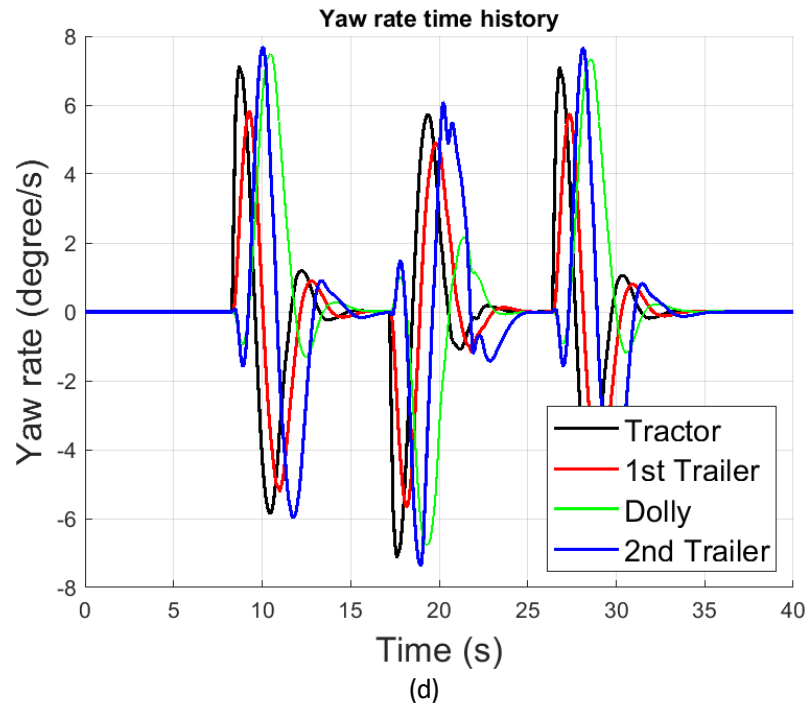
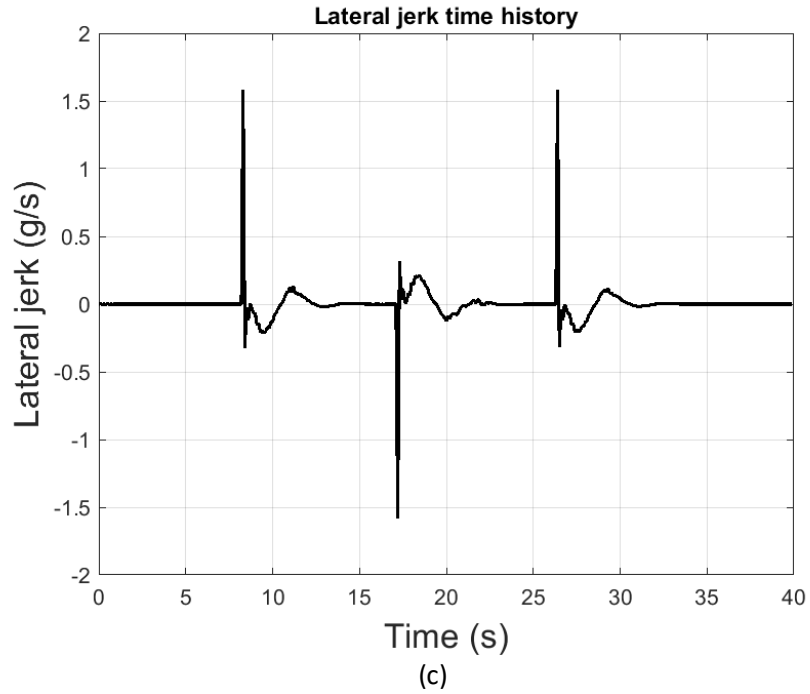


Figure 7.13. A-train double's dynamic responses of each vehicle unit over the triple single lane change maneuver with ATDS activated and the preview time of 2 sec: (a) lateral displacement versus longitudinal displacement, (b) time history of lateral acceleration, (c) time history of tractor's lateral jerk, and (d) time history of yaw-rate.

The required steering angle for each of the trailing units' axles' wheels are shown in Figure 7.14.

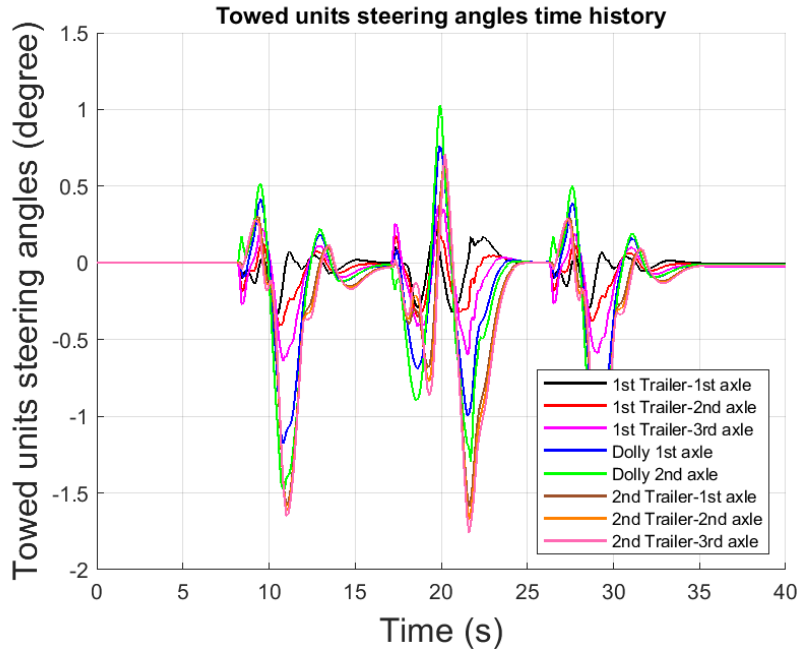


Figure 7.14. Time history of required steering angle for ATDS controller during the highway autonomous driving scenario.

7.10 Improving the basic trajectory generation considering the MTAHV unique dynamics using model-based predictive methodology (case study 3)

The trajectories generated using the Frenet frame and quintic polynomials perform well for single unit vehicles, such as passenger cars. These methods are useful when a particle tracks a trajectory. Articulated heavy vehicles and especially Multi-unit AHVs exhibit unique high-speed lateral dynamics due to large sizes and multi-unit architectures. Hence, using the quintic polynomials for trajectory generation without considering aforementioned features could degrade the trajectory planning strategy. The results achieved in Section 7.8 disclose this shortcoming of the basic trajectory planning and path-following strategy. A

model predictive-based trajectory methodology is thus employed to characterize the trajectory for the A-train double.

As shown in Figure 7.15, the solid blue curve represents the trajectory generated for a MTAHV in the Frenet frame using quintic polynomials. This trajectory doesn't take into account the lateral dynamics of the trailers. Thus, during a lane-change maneuver, the A-train double will show exaggerated lateral motions of the trailing units and the noticeable rearward amplification behavior. As a result, it is necessary to tailor the trajectory generation strategy to improve the lateral stability for MTAHV. For instance, a smoother trajectory like the dashed curve shown in Figure 7.15 might mitigate the RWA issue and also lessen the lateral jerk [117]. To optimize the basic trajectory, an analytical approach might be required.

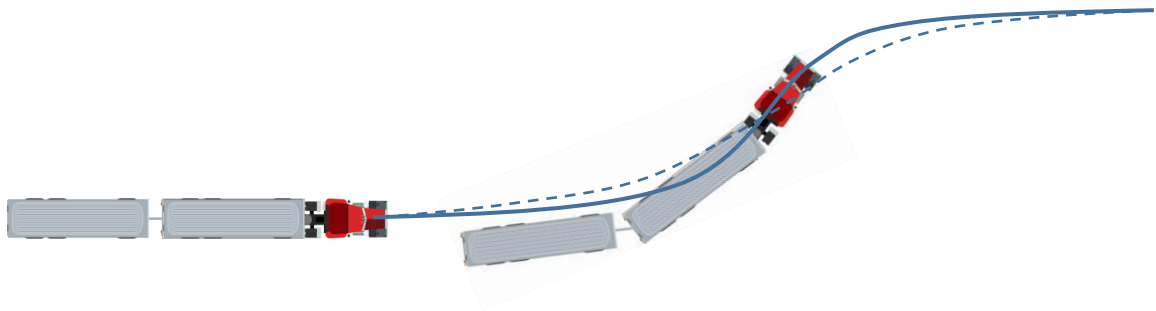


Figure 7.15. The optimized trajectory versus the initial quintic polynomial trajectory.

In Section 7.6, the model predictive-based approach was employed to generate the predicted trailing units' position and heading so as to create their collision capsule shapes over the prediction horizon. In that case, it was assumed that the cost function J defined in equation (7.28) assures the tractor to follow the quintic trajectory precisely by minimizing the lateral deviation error from the trajectory. In order to improve the high-speed lateral stability, the cost function J is modified. Two more factors are incorporated into the cost

function to reach the goal. The first factor is the tractor lateral acceleration, and the second is the second trailer lateral acceleration. The lateral acceleration of the tractor and the second trailer are calculated by

$$\begin{aligned} a_{y1} &= \dot{v}_1 + U_1 \psi_1 \\ a_{y4} &= \dot{v}_4 + U_4 \psi_4 \end{aligned} \tag{7.30}$$

where, a_{yi} , v_i , U_i and ψ_i , $i=1,4$, represent the lateral acceleration, lateral velocity, longitudinal velocity and yaw-rate of the tractor and last trailer, respectively. The modified cost function is formulated as

$$\begin{aligned} J = & \sum_{i=1}^{n_p} \left\| y_{ref_{k+i|k}} - Y_{1_{k+i|k}} \right\|^2 + \sum_{i=1}^{n_p} \left\| u_{k+i-1|k} \right\|^2 + \sum_{i=1}^{n_p} \left\| \Delta u_{k+i-1|k} \right\|^2 \\ & + \sum_{i=1}^{n_p} \left\| (\dot{v}_1 + U_1 \psi_1)_{k+i|k} \right\|^2 + \sum_{i=1}^{n_p} \left\| (\dot{v}_4 + U_4 \psi_4)_{k+i|k} \right\|^2 \end{aligned} \tag{7.31}$$

Subject to the constraints expressed in inequalities (7.29). Minimizing the cost function considering the new factors will generate the optimal steering and consequently produce the predicted states of the tractor over the prediction horizon using state-space equation (7.23), while the constraints are met. The predicted TFAC path over the preview horizon is the reference trajectory to be followed using the driver model introduced in Chapter 4. The new trajectory may lead to less lateral accelerations and improved lateral stability during lane-change maneuvers.

Figure 7.16 (a) and (b) show the steering input and the longitudinal speed under the same triple lane-change maneuver of the autonomous highway driving considering the new cost

function. As seen in Figure 7.16(a), less steering effort is required compared with the counterpart shown in Figure 7.12 for the case of non-optimal trajectory and path-following with ATDS activated.

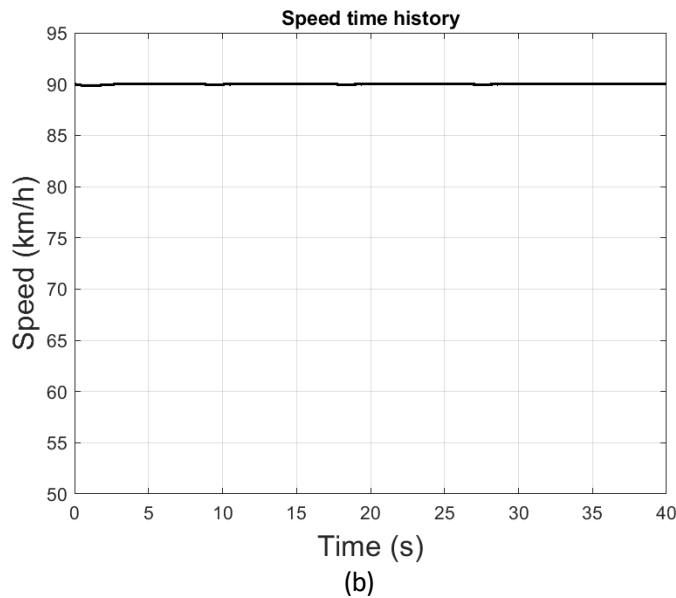
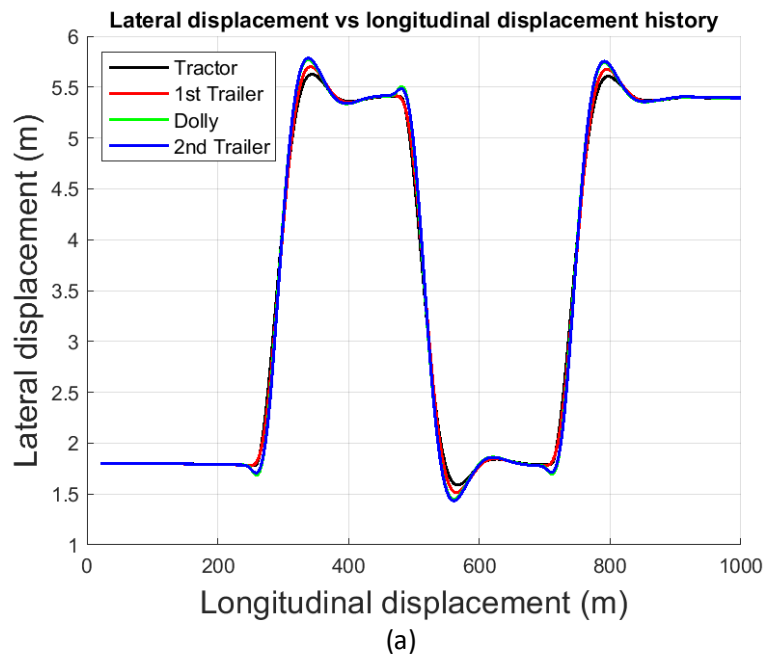
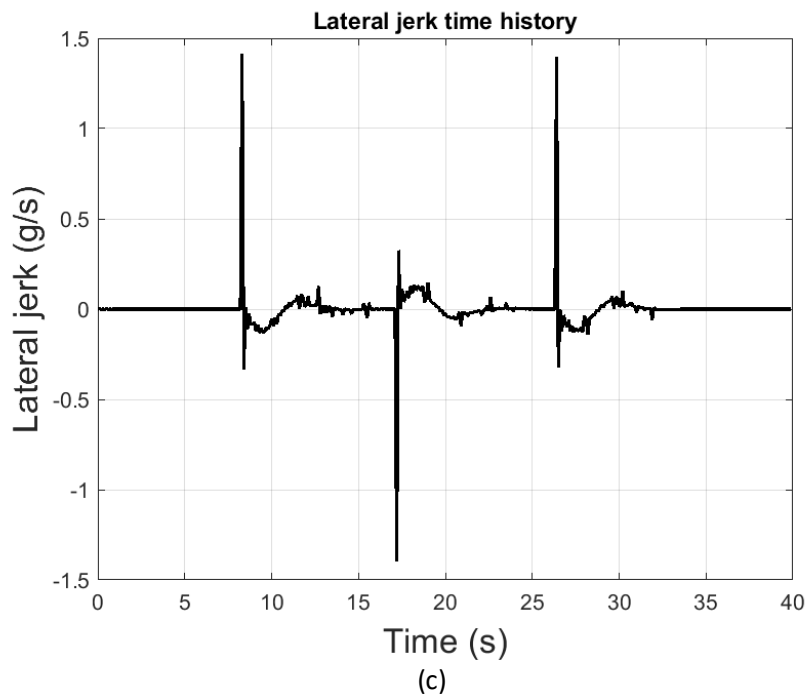
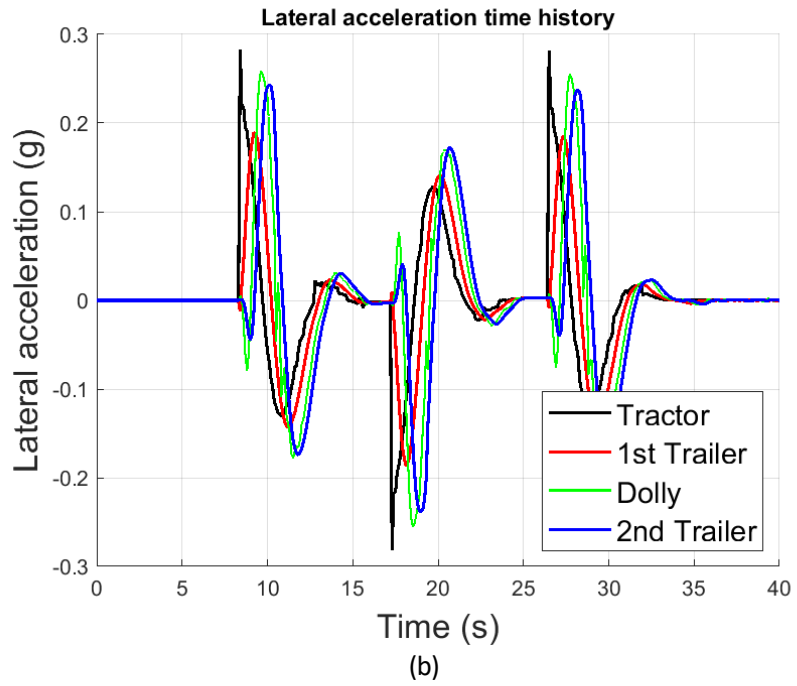


Figure 7.16. A-train double’s steering input and forward speed over the triple lane-change maneuver with the preview time of 2 sec: (a) time history of steering input, and (b) time history of longitudinal speed.

Figure 7.17 shows the ego vehicle’s dynamic responses for the improved trajectory planning. As seen in Figure 7.17(a), the transient off-tracking has reduced remarkably

compared with the counterpart of the basic trajectory planning case shown in Figure 7.11(a). Compared with the ATDS control case shown in Figure 7.13(a), although the transient off-tracking for the first and third lane-change maneuvers are larger, this metric has reduced considerably for the second lane-change. In terms of other dynamic responses, the new trajectory generation method outperforms the aforementioned two methods, i.e. ATDS and basic trajectory generation method. Figure 7.17(b) and (d) illustrate that noticeable improvements are achieved in lateral acceleration and yaw-rate for all the vehicle units. The tractor's lateral jerk is still high and beyond the acceptable ride comfort level. However, it is 12.5% less than those of the basic trajectory and the ATDS controller as expected.





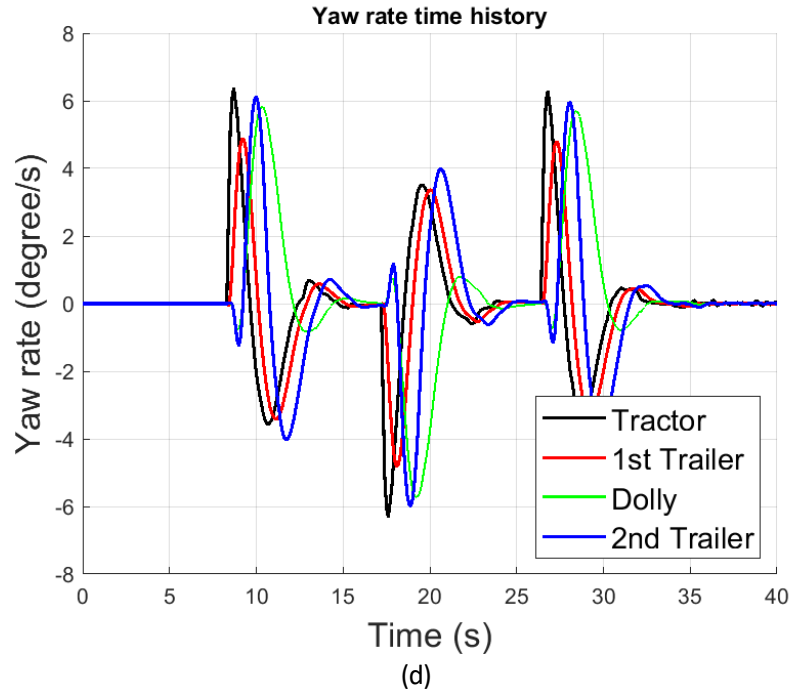


Figure 7.17. A-train double’s dynamic responses under the triple lane change maneuver for the model predictive-based trajectory optimization with the preview time of 2 sec: (a) lateral displacement versus longitudinal displacement, (b) time history of lateral acceleration, (c) time history of tractor’s lateral jerk, and (d) time history of yaw-rate time.

7.11 Trajectory generation with reduced lateral jerk (case study 4)

Although the above attempts achieved obvious improvements in path-following, and RWA dynamics of the A-train double, the large lateral jerk issue still exists. An effective approach should be incorporated into the model-based predictive trajectory strategy to tackle the problem. The potential solution is to reserve one second for tracking the final trajectory. In other words, any new trajectory needs to be generated ahead of the current TFAC position with the distance equivalent to one second preview time. This strategy is schematically illustrated in Figure 7.18. The total trajectory represented by the blue solid curve consists of two sections: 1) reversed part equivalent to a preview time of 1.0 second, and 2) newly planned part with a preview time of 2.0 seconds. Thus, the equivalent preview

time is 3.0 seconds. The 2-second part is continuously regenerated and evaluated, and the 1-second part is the final section of the previous trajectory, which has already been used as a reference path for the path-tracking aim using the lateral preview driver model developed in Chapter 4. Note that for the lateral preview driver model, 1-second preview window is needed for reliable high-speed path-following.

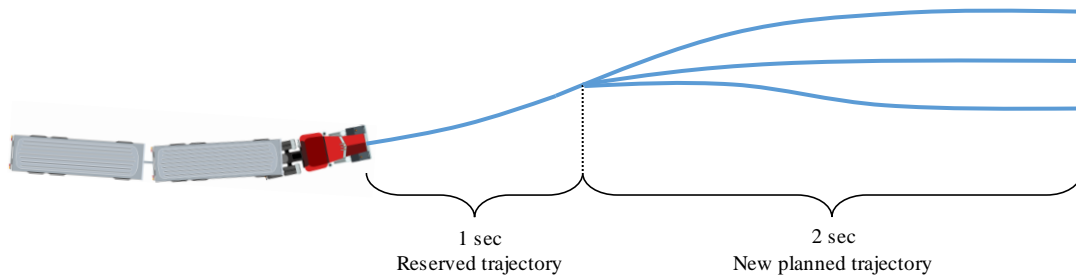
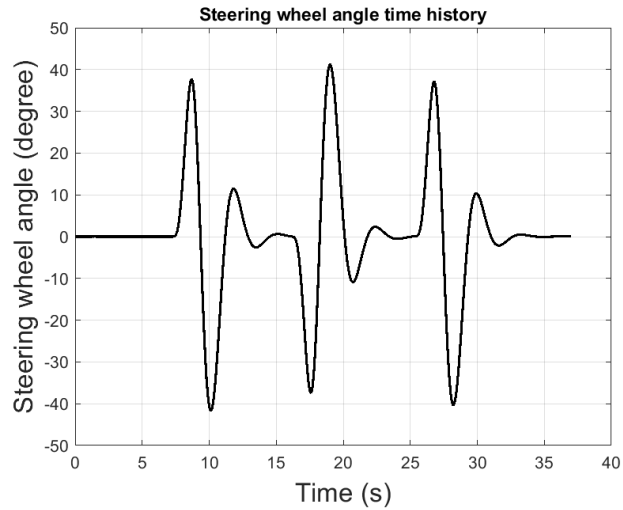


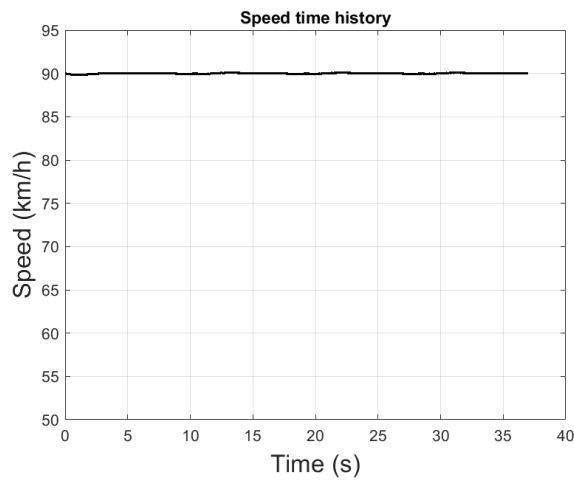
Figure 7.18. Reserved trajectory approach for reducing lateral jerk under lane-change maneuvers.

For the purpose of simplicity, hereafter, the reserved trajectory approach is denoted as 1+2 sec preview time approach. The simulation results using the 1+2 sec preview time approach are presented and discussed as follows.

To effectively identify the effect of the 1+2 sec preview time approach on mitigating the lateral jerk, the model-based predictive trajectory optimization is not included in the simulation. Figure 7.19(a) and (b) illustrate the time histories of the steering wheel angle input and the vehicle forward speed to perform the triple single lane-change maneuver. As shown in Figure 7.19, while the speed is kept around 90 km/h during the driving scenario, the steering effort for the 1+2 sec preview time approach is much less compared with its counterpart for all the above three methods with 2-sec preview time. The reduction in steering effort is about 33%, which is quite impressive.



(a)

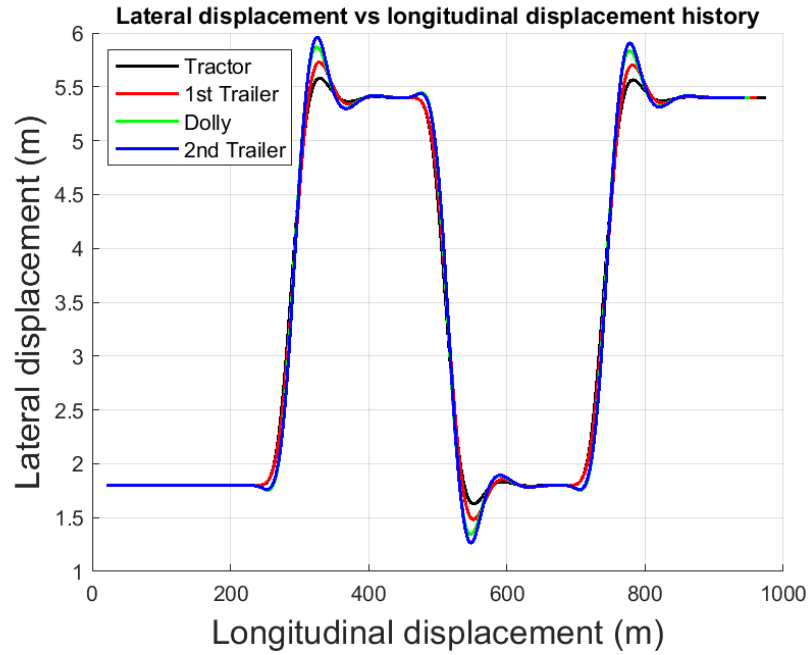


(b)

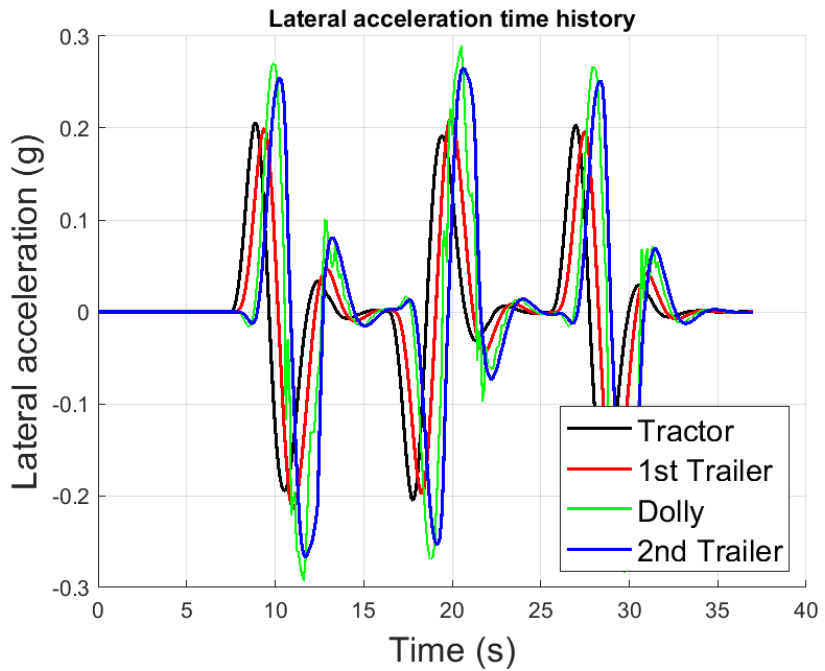
Figure 7.19. A-train double's steering input and forward speed under the triple lane-change maneuver with 1+2 sec preview time: (a) time history of steering angle input, and (b) time history of longitudinal speed.

Figure 7.20 shows the simulation results of the A-train double state using the 1+2 sec preview time approach. As shown Figure 7.20 (a) and (b), it is expected that the HSTO and lateral acceleration are still high and comparable with those based on the 2-sec preview methods without ATDS and trajectory improvement. However, as seen in Figure 7.20 (c), the tractor lateral jerk is much smaller than that based on those 2-sec preview methods. This will significantly improve the ride comfort of the driver. The yaw-rate as demonstrated

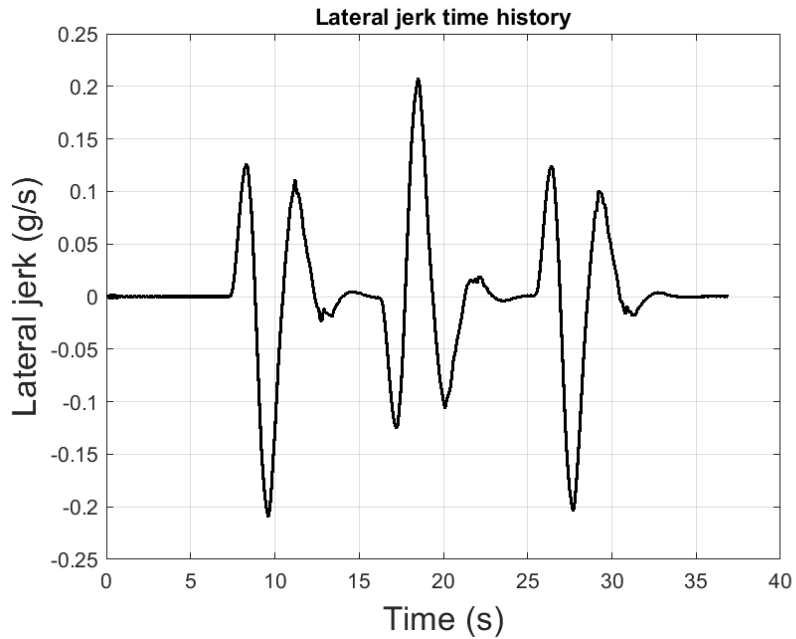
in Figure 7.20 (d) shows the time history of yaw rate of all the vehicle units, which are reduced compared with those for all the 2-sec preview cases.



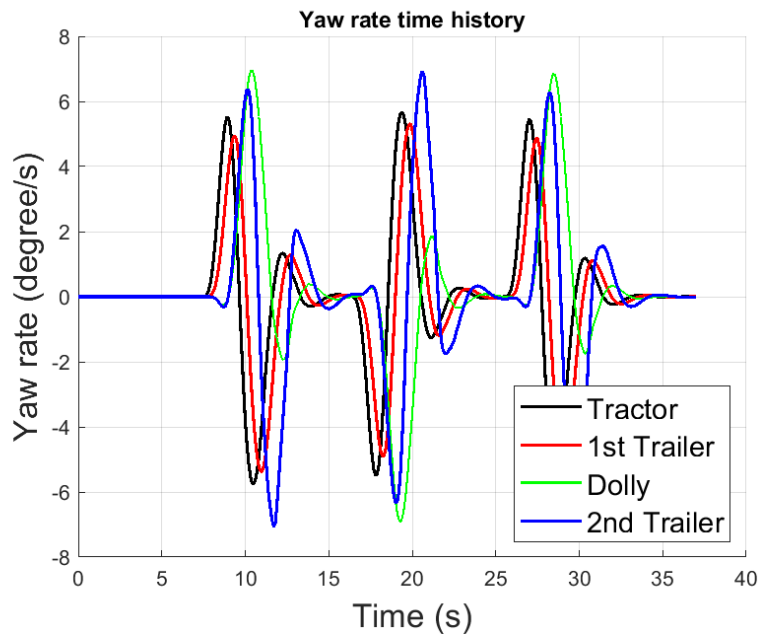
(a)



(b)



(c)



(d)

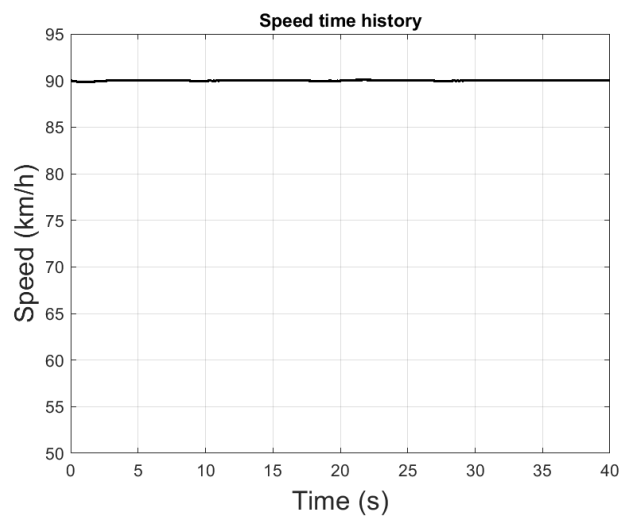
Figure 7.20. A-train double's dynamic responses under the triple lane change maneuver for the 1+2 sec preview time method: (a) lateral displacement versus longitudinal displacement, (b) time history of lateral acceleration, (c) time history of tractor's lateral jerk, (d) time history of yaw-rate.

7.11.1 Incorporating the ATDS (case study 5)

To further examine the performance of the 1+2 preview time method, the triple single lane change maneuver is simulated considering the following joint effects: 1) the 1+2 preview time method and the ATDS, and 2) the 1+2 preview time method and the optimized trajectory approach. Figure 7.21 (a) and (b) show the time history of the steering effort and vehicle forward speed over the maneuver for the first case study. The steering effort required for this case remains similar to that for the 1+2 sec preview time approach alone, while the forward speed remains constant around 90 km/h.



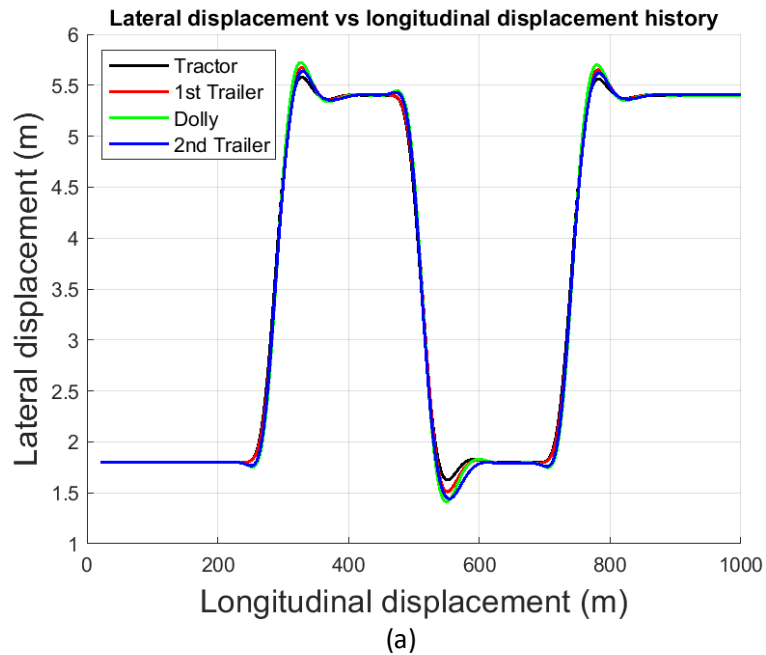
(a)

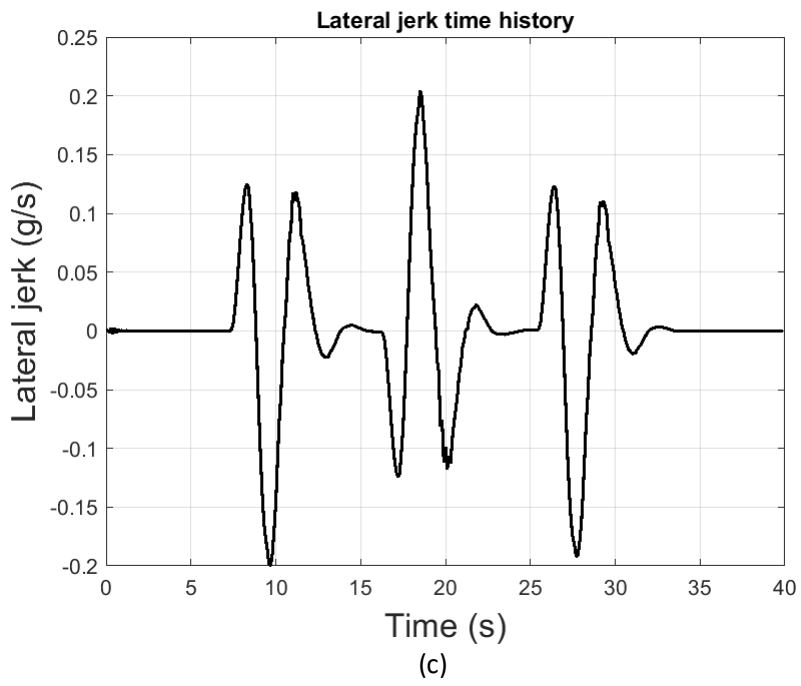
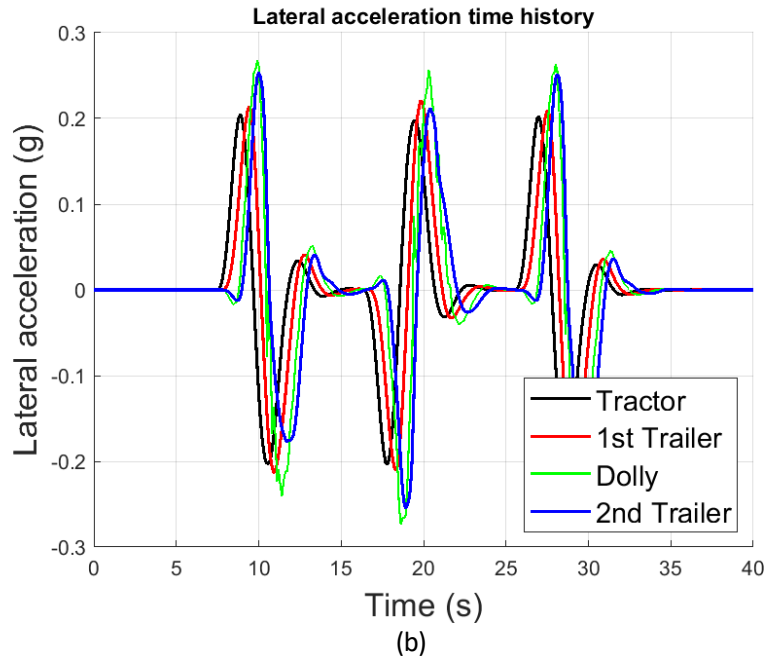


(b)

Figure 7.21. A-train double's steering angle input and forward speed under the triple single lane change maneuver for the joint effort with the 1+2 preview time and ATDA control: (a) time history of steering input, and (b) time history of forward speed.

Figure 7.22 shows the dynamic responses of the A-train double with the joint effort of the 1+2 preview time and ATDS control. Figure 7.22 (a) shows a substantial improvement in HSTO reduction due to employing the steering capabilities of the trailing units, which is mainly attributed to the contribution of the ATDA control. The lateral acceleration and lateral jerk of the tractor are comparable to those shown in Figure 7.22 (b) and (c), in which the ATDS is not active. The yaw-rate for all the trailing units are reduced significantly due to the ATDS control.





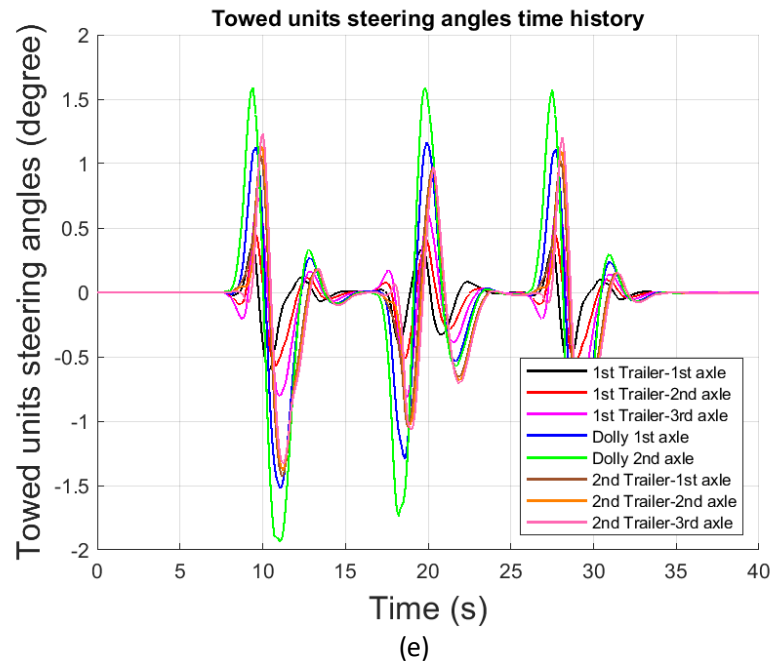
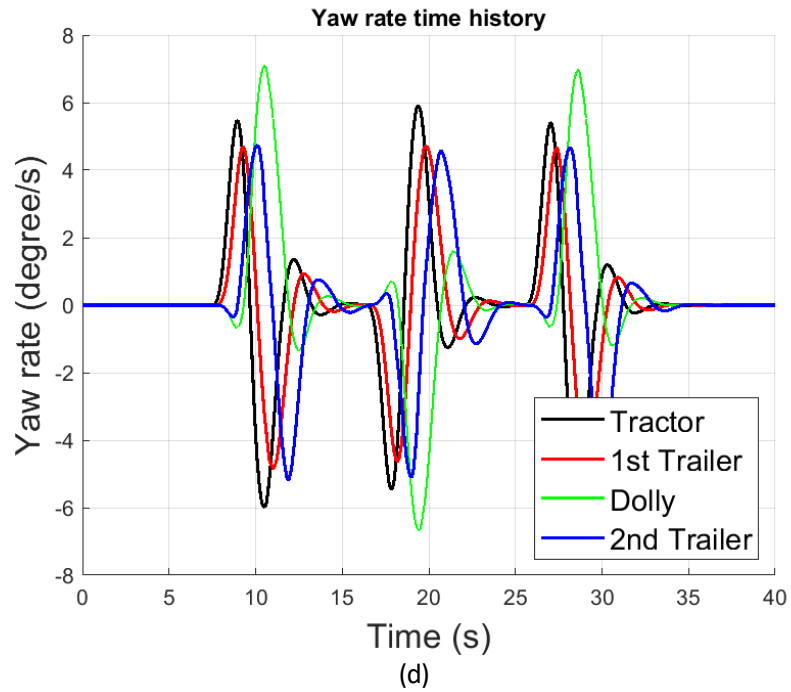


Figure 7.22. A-train double's dynamic responses under the triple single lane change maneuver for the joint effort of the 1+2 sec preview time and the ATDS control: (a) lateral displacement versus longitudinal displacement, (b) time history of lateral acceleration, (c) time history of tractor's lateral jerk, (d) time history of yaw-rate, and (e) time history of trailing units' axles steering angle.

7.11.2 Incorporating the trajectory optimization (case study 6)

In the second case study with the joint effort of the 1+2 sec preview time and optimized trajectory generation, Figure 7.23 shows the screenshots at different time instants of the simulated triple lane change maneuver. Compared with Figure 7.9, the trajectories shown in Figure 7.23 are one second longer than their counterparts. Hence, the vehicle representative capsules over the preview horizon are spread with a longer distance.

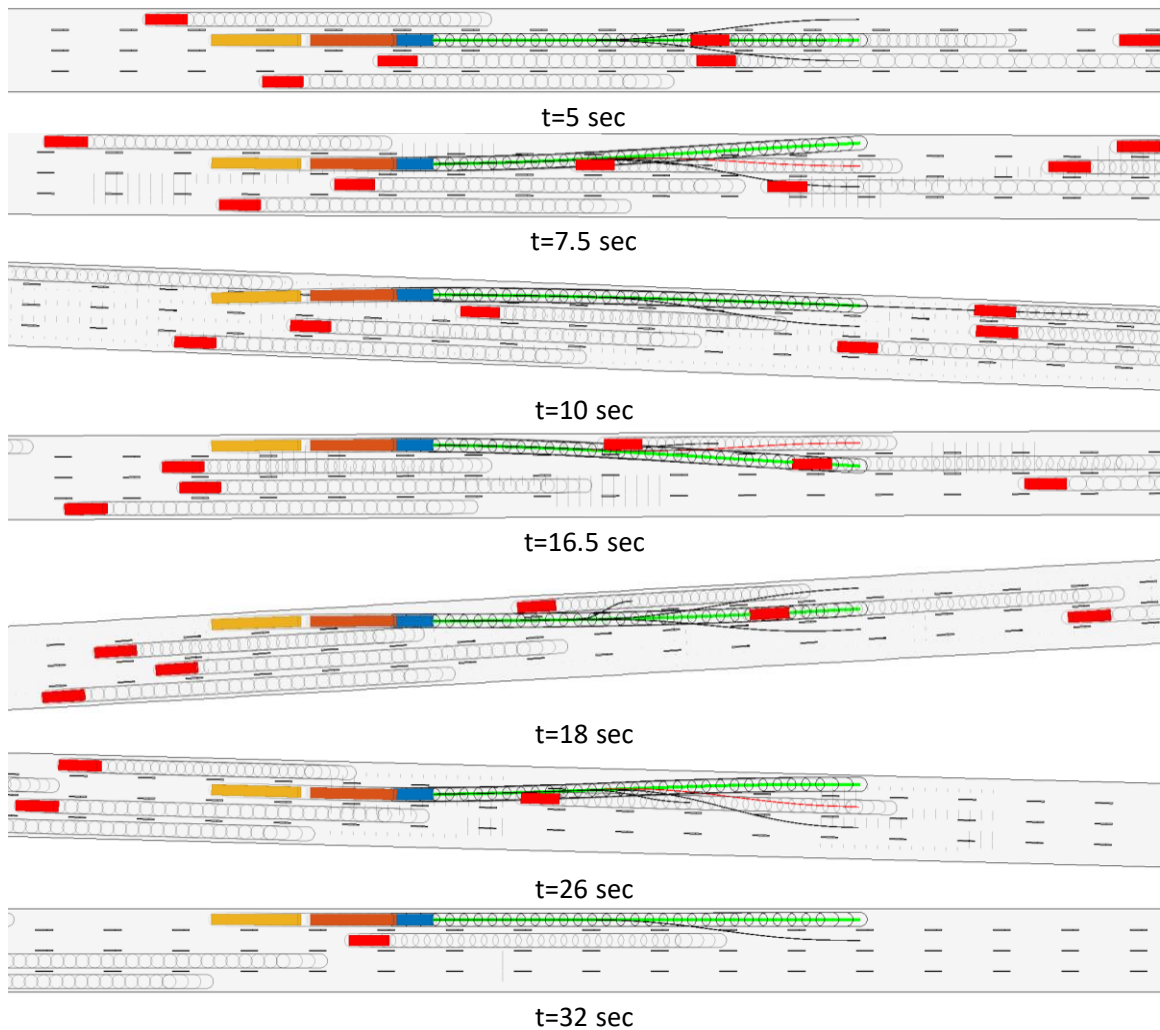
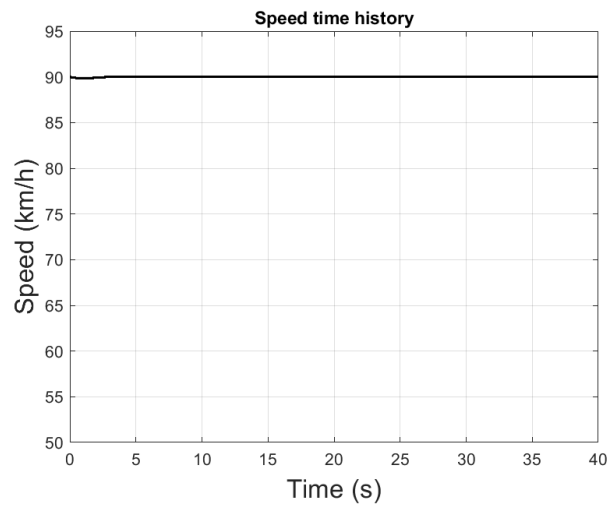


Figure 7.23. A-train double autonomously executing the triple lane-change maneuver in a highway operation with the joint effort of 1+2 sec preview time and optimized trajectory generation (red rectangles representing obstacle vehicles; blue, orange and yellow rectangles representing the tractor, first trailer and second trailer, respectively).

Figure 7.24 (a) and (b) illustrate the time history of steering angle demand and forward speed over the simulated triple single lane change maneuver. Compared with all the aforementioned methods, as shown in Figure 7.24 (a), the joint effort of the 1+2 preview time and optimized trajectory generation method results in the least steering effort with almost 60% reduction in maximum peak steering angle.



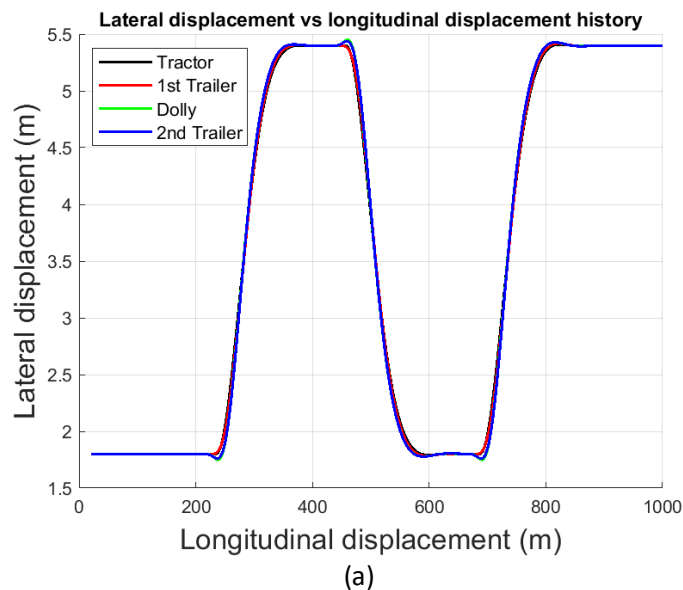
(a)

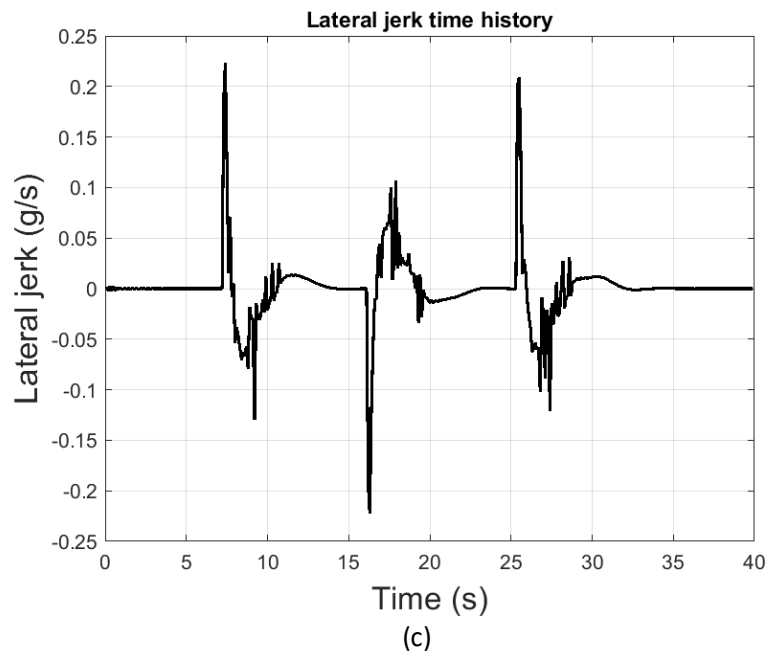
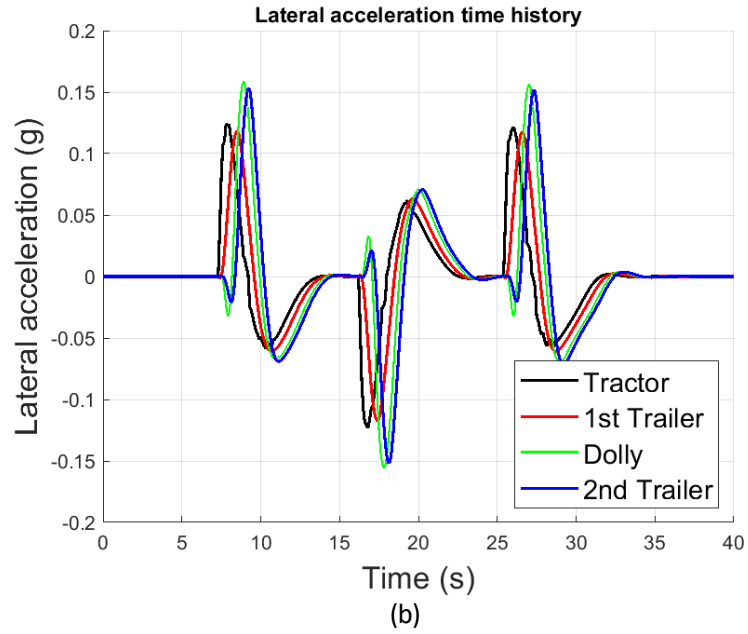


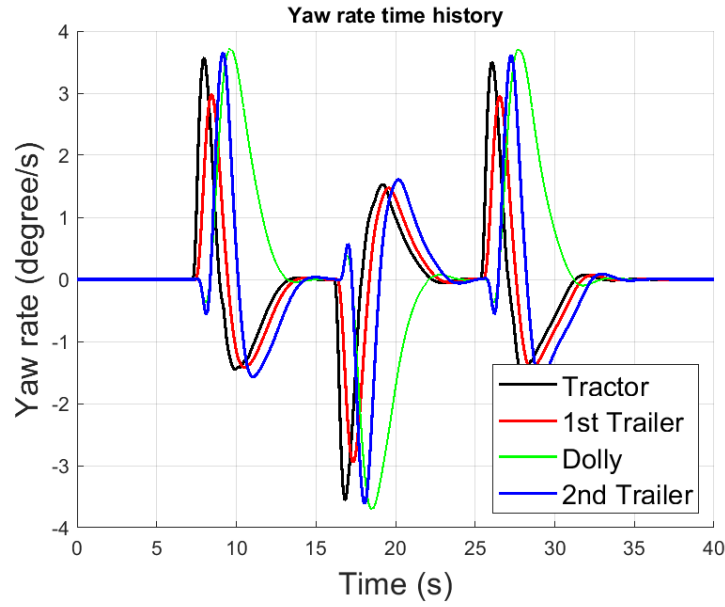
(b)

Figure 7.24. A-train double's steering angle input and forward speed under the triple single lane change maneuver with the joint effort of 1+2 preview time and optimized trajectory generation method: (a) time history of steering angle input, and (b) time history of forward speed.

Figure 7.25 (a), (b) and (d) show all the vehicle units' trajectories, time histories of lateral acceleration, and time histories of yaw rate, respectively. The HSTO is significantly reduced while the lateral jerk shown in 7.25 (c) is kept within the driver comfort range. Interestingly, the second trailer maximum lateral acceleration is kept below 0.15g, while the tractor and first trailer lateral acceleration are even lower with the values of 0.125g and 0.12g, respectively. The yaw-rates for all the vehicle units are reduced up to 50% compared with those of the above methods. All of these improvements assure a safer transportation. The jerk curve shown in Figure 7.25 (c) is a bit noisy, which may be attributed to the fact that using the optimized trajectory generation strategy, the steering inputs are regulated more frequently resulting in a less smooth steering curve as seen in Figures 7.16 (a) and 7.24 (a). However, as these jerk change rates are infinitesimal, they may not be sensed by the driver.







(d)

Figure 7.25. A-train double’s dynamic responses under the triple lane-change maneuver with the joint effort of 1+2 preview time and optimized trajectory generation method: (a) lateral displacement versus longitudinal displacement, (b) time history of lateral acceleration, (c) time history of tractor’s lateral jerk, and (d) time history of yaw-rate.

To assess the performance of each motion planning method and the effect of ATDS control, the respective performance measures of the A-train double under the simulated triple single lane change maneuver are compared. To this end, Figure 7.26 illustrates a 3D bar chart, which provides the performance measure of the vehicle for all the six combinations of trajectory generation strategies and ATDS control. As it is seen from the figure, the best performance results among all the case studies is achieved by the 1+2 second preview time with optimized trajectory. It means that by improving the trajectory and conducting a preview time enhancement strategy not only the lateral stability is increased, but also the energy consumption required for steering the tractor and the trailing units’ axles becomes considerably less. The ride comfort is also improved remarkably.

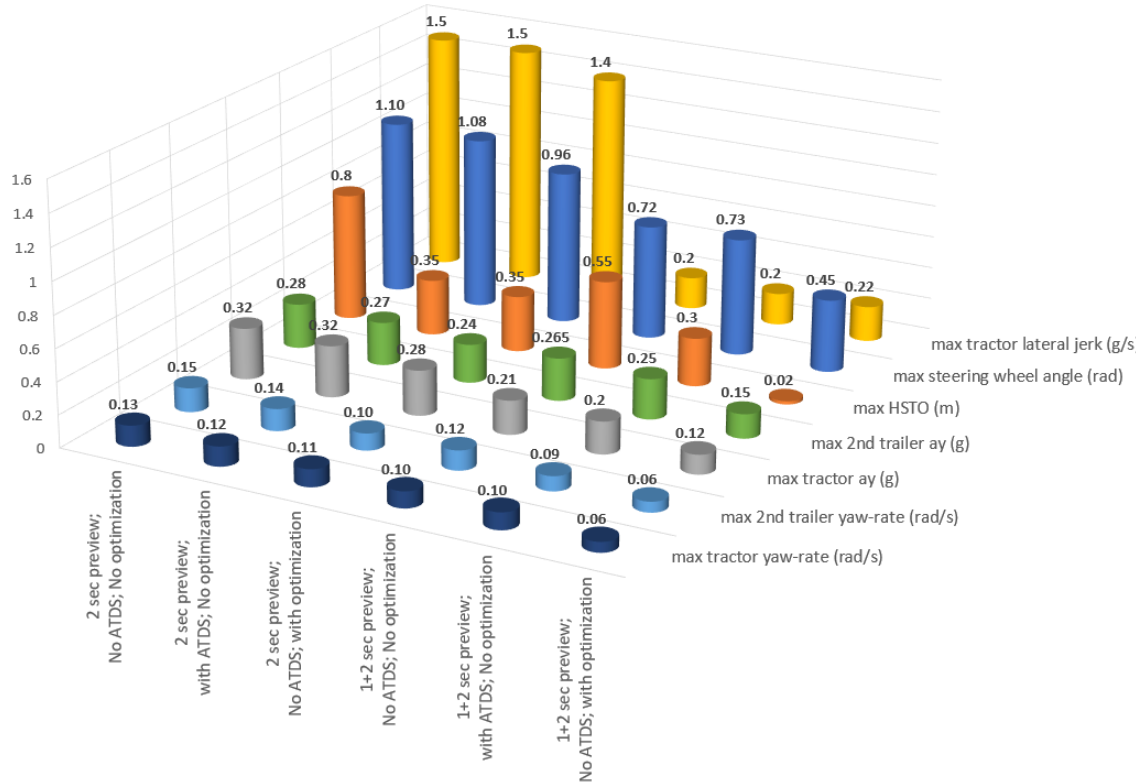
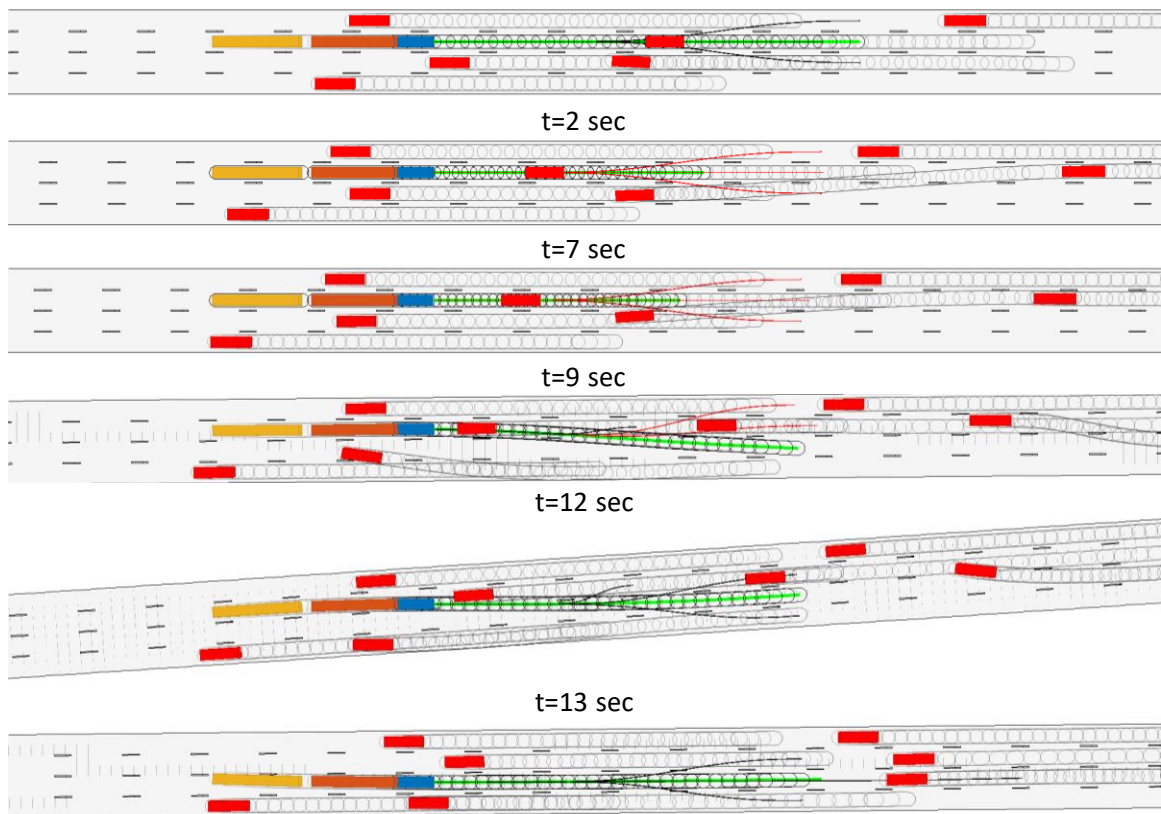


Figure 7.26. Performance measures of the A-train double under the triple lane-change maneuver for six combinations of trajectory generation strategies and ATDS safety system.

7.12 Adaptive vehicle speed control results

As mentioned in Section 7.5, the highest priority is given to cruise control and lane-change behaviors of the autonomous driving. However, if a trajectory generated for applying those behaviors are found to result in a collision of the ego vehicle with a surrounding vehicle on the highway, the last optional behavior is adaptive cruise control. This means that the A-train double needs to accommodate its speed with the preceding vehicle, and share the same highway lane. The model-based predictive control strategy used for adjusting the vehicle speed for the ATDS controller developed in Chapter 6 was utilized to regulate the vehicle speed based upon the obstacle vehicle's speed which is considered as target speed. The longitudinal vehicle dynamics developed for this goal is explained in Chapter 3. Figure

7.27 displays the screenshots taken at various time instants over the simulated autonomous driving on the highway. As shown in the figure, the ego vehicle initially moves on the second lane from the top while keeping the forward speed around 90 km/h. Then, at time instant of $t=7$ sec, a collision is detected for both the cruise control and lane-change at the constant speed of 90 km/h. Hence, the adaptive cruise control behavior of the autonomous driving controller is applied to adjust the vehicle speed. The forward speed reduction then continues for around 5 seconds until the right lane is cleared from the traffic, i.e. $t=12$ sec. Then, the lane-change behavior of the A-train double is activated, the reference trajectory generated is followed, and the ego vehicle successfully executes the lane change. Meanwhile, the vehicle gains speed to reach the road speed limit of 25m/s (90km/h) (Look at Figure 7.28 (b) for the forward speed profile). At the time instant of 29 sec, the vehicle detects an obstacle vehicle moving at a low speed. Then, a left lane-change is conducted.



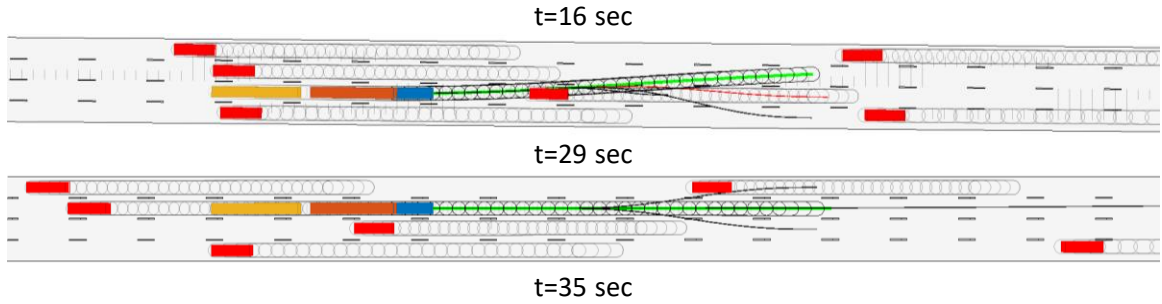


Figure 7.27. A-train double autonomous adaptive cruise control in highway driving scenario for joint effort of 1+2 preview time and optimized trajectory generation (red rectangles representing obstacle vehicles; blue, orange and yellow rectangles representing tractor, first trailer, and second trailer, respectively).

Figure 7.28 shows the automated steering input and the speed profile for the simulated maneuver presented in Figure 7.27. As shown in Figure 7.28(a), the steering effort over the maneuver is quite low during the lane changes. The low steering effort may be attributed to the optimized trajectory generation. Figure 7.28(b) illustrates the speed profile, which accommodates the situation when all cruise control and lane-change trajectories are not collision-free. The speed profile consists of three sections, i.e., constant, deceleration, and acceleration, considering the acceleration limits of the A-train double.



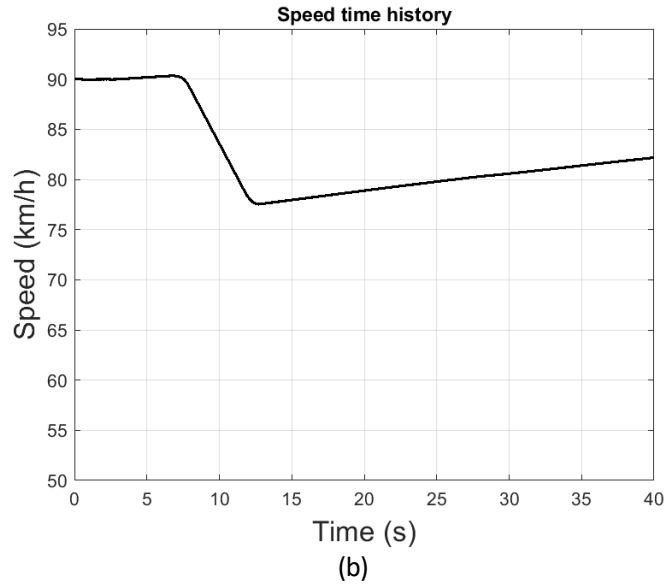
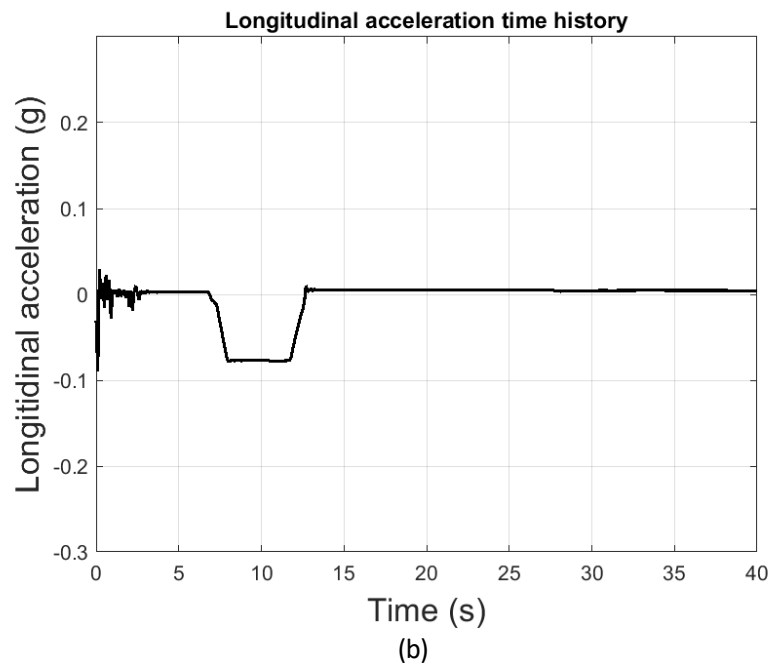
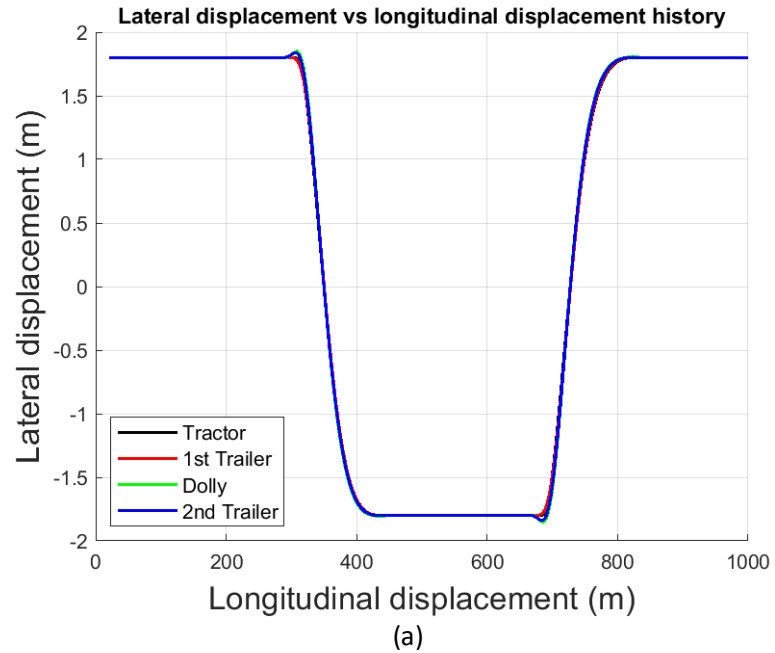


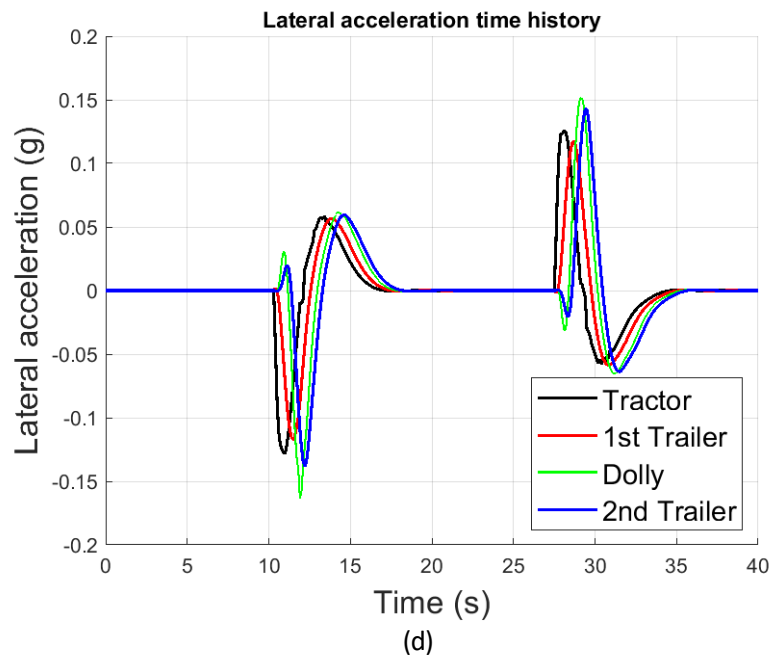
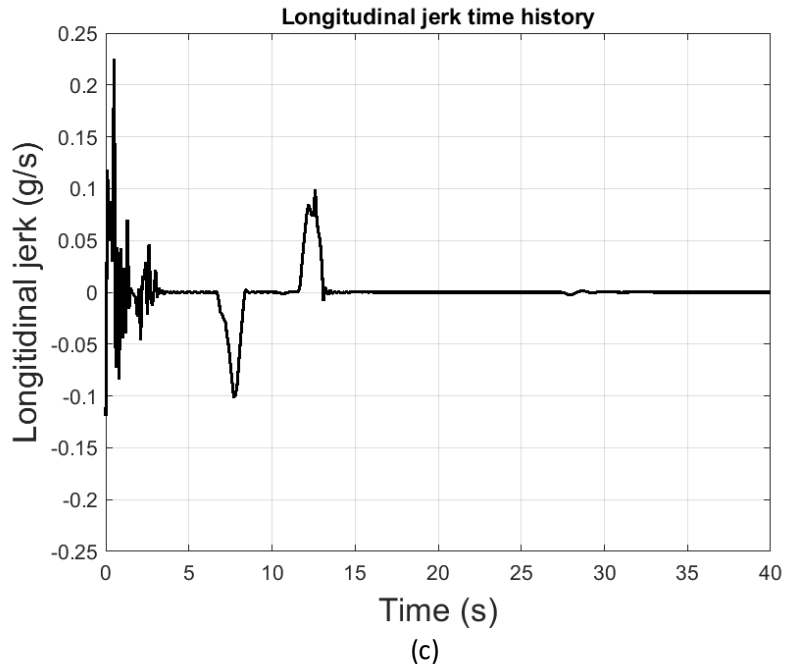
Figure 7.28. A-train double’s steering angle input and forward speed over the double lane-change maneuver for the joint effort of 1+2 preview time, optimized trajectory generation and adaptive cruise control: (a) time history of steering input, and (b) time history of forward speed.

Figure 7.29 shows the dynamic responses of the A-train double over the simulated maneuver in terms of the tracked paths for all vehicle units, time history of longitudinal acceleration of the vehicle, time history of longitudinal jerk, time history of lateral acceleration of each vehicle unit, time history of lateral jerk, and the time history of yaw rate of each vehicle unit.

As seen in Figure 7.29 (a), the HSTO measure interestingly approaches to zero. This may be attributed to the use of the effective trajectory generation method. Figure 7.29 (b) illustrates the longitudinal acceleration curve for the adaptive cruise control behavior. The maximum deceleration of 0.1g is applied in the model predictive longitudinal speed control as a constraint. Hence, the maximum deceleration is kept beneath this value. The longitudinal jerk shown in Figure 7.29 (c) is also kept within the acceptable range for the driver ride comfort. Since the optimized trajectory and the 1+2 sec preview time are utilized

in this autonomous driving scenario, the lateral acceleration, lateral jerk and yaw-rate shown in Figure 7.29 (d), (e) and (f) have the optimum values.





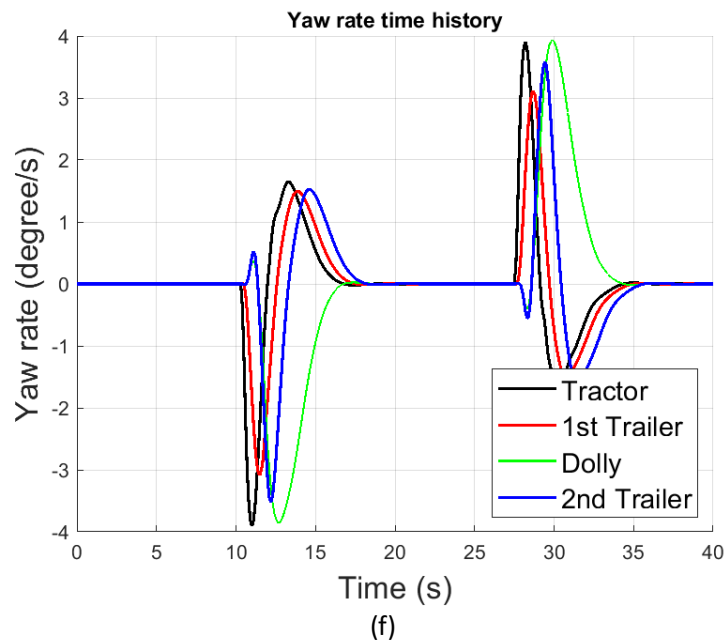
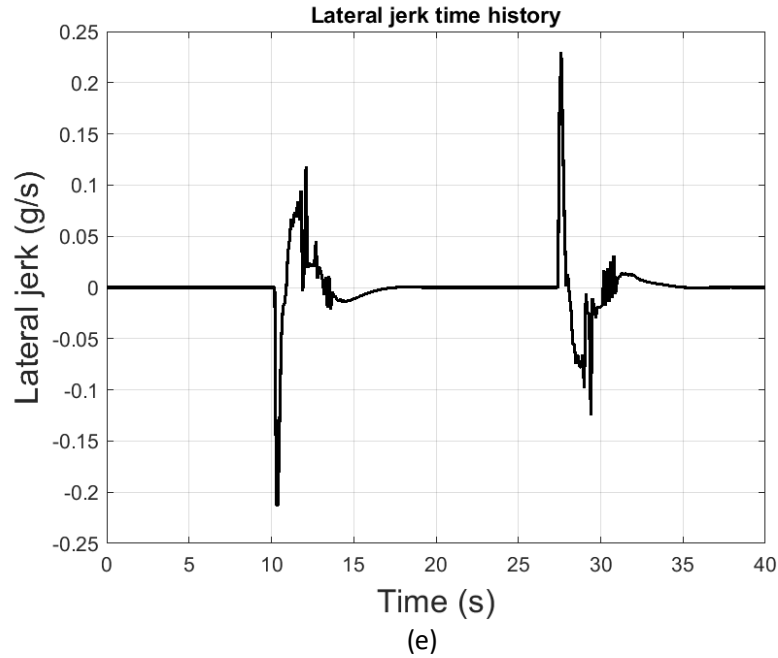


Figure 7.29. A-train double’s dynamic responses over the specified maneuver for the joint effort of 1+2 preview time, optimized trajectory generation, and adaptive cruise control: (a) lateral displacement versus longitudinal displacement, (b) time history of displacement, (c) time history of longitudinal acceleration, (d) time history of longitudinal jerk, (e) time history of lateral acceleration, (f) time history of tractor’s lateral jerk, and (g) time history of yaw -rate.

7.13 Summary

The study aimed to develop a trajectory planning strategy for A-train doubles in a highway driving scenario using the Frenet coordinate system, while considering the unique dynamics of Multi-Trailer Articulated Heavy Vehicles (MTAHVs). The motion planning stage involved regular driver behaviors such as speed maintenance, lane changing, and adaptive speed control to enable effective highway driving. Co-simulation via MATLAB and TruckSim was used to verify the trajectory planning and following with and without active trailer steering.

To address the challenges posed by the unique dynamics of MTAHVs, a model-based predictive strategy was employed to regenerate the trajectory and reduce lateral acceleration and jerk during evasive maneuvers. Simulation tests demonstrated a remarkable improvement in vehicle ride comfortability and lateral stability using the proposed approach for trajectory generation and following. These results suggest that designing a control strategy for MTAHVs without considering their unique dynamics may not be efficient enough.

Overall, the study contributes to the development of more efficient and effective control strategies for MTAHVs, which are critical for safe and reliable transportation of goods on highways.

Chapter 8. Conclusion and future work

This thesis proposes new automated driving control strategies, which are customized for a multi-trailer articulated heavy vehicle (MTAHV) with the configuration of A-train double. Additionally, an active trailer and dolly steering (ATDS) system is developed for the A-train double. Furthermore, the associated controllers are tailored for low-speed and high-speed driving scenarios, because the MTAHV exhibits unique high-speed stability and low-speed maneuverability issues. Thus, designing any control strategy should consider these directional performance features. Several closed-loop test simulations were conducted for either each controller individually or a combination of them in order to evaluate the capabilities of the individual and integrated control strategies in various driving scenarios.

8.1 Conclusion

In Chapter 3 of this dissertation, a fundamental linear vehicle dynamics model was developed for the A-train double. Then, two linear and non-linear extensions of this fundamental model were formulated. Each vehicle model is used for a specific control strategy, which has particular requirements. Since the linearization assumptions are only valid for some high-speed driving scenarios with small side-slip angles and steering input, the linear model was amended utilizing an optimization method. Indeed, through several open-loop co-simulations, a cost function consisting of yaw-rates and side-slip angles of vehicle units is minimized to find the optimal cornering stiffness of tires. As a result, for each specific maneuver with determined steering input and vehicle speed, the linear model operates very similar to the non-linear TruckSim model. Having the required data and

taking advantage of an online look-up table, the proper value of cornering stiffness is selected to mimic the non-linear vehicle model for all the other steering and speed conditions. This method demonstrates the effectiveness in various controller verifications through different tests. All in all, the fundamental vehicle model was verified over low-speed and high-speed driving scenarios and exhibited considerable similarity to the non-linear TruckSim model.

In Chapter 4, using the first extension of the linear model developed in Chapter 3, exploiting the body-fixed coordinate system of the A-train double's units and making use of the optimal preview control strategy, a comprehensive lateral preview driver model was developed. This driver model, which can be used as an autonomous steering controller for the MTAHVs, performs very well under high-speed and low-speed driving maneuvers, and operates analogously to a human driver by considering the motion cues coming from the trailing units in order to choose the optimal steering angle value for the tractor's front axle wheels. Hence, the proposed driver model distinguishes itself from other driver models used in lateral control of the MTAHVs by considering all the vehicle units' motions for highway and urban deriving scenarios.

In Chapter 5, a speed planner customized for the A-train double considering all the vehicle units' lateral acceleration in order to find the proper forward speed over a determined preview distance was developed. To estimate the lateral accelerations of the vehicle units over the preview time, the road curvature was taken into account, and the vehicle capability envelopes was exploited to determine the required deceleration to adjust forward speed. The proposed speed-planning strategy mimics the human driver longitudinal motion control behavior by utilizing both the predictive and the corrective braking/throttling

approaches to ensure the vehicle units' lateral acceleration within the maximum acceptable range. Then, based on the calculated required deceleration or acceleration, and benefiting from the fuzzy logic control methodology, the braking or throttling effort is determined. The driver model proposed in Chapter 4 is employed as the lateral preview driver model for the simulations. The co-simulations using MATLAB and TruckSim demonstrated the performance of the controller for various driving scenarios at different speeds and with various road curvatures. This longitudinal motion controller can be used as a global speed planner when the surrounding vehicles are not taken into account for speed adjustment. However, for a more accurate speed planner considering the road traffic, the methodology proposed in Chapter 7 can be utilized as a local speed planning strategy.

In Chapter 6, a model-based predictive control strategy was utilized for integrated lateral and longitudinal motion control as well as the active trailing units steering of the A-train double. In order to calculate the required steering for the towed units, the control strategy differentiates the low-speed and high-speed maneuvers. The main goal of driving the MTAHV under low-speed maneuvers is to improve the maneuverability. Hence, the vehicle units are steered in a way that they follow the reference path. However, under high-speed maneuvers, reducing the rearward amplification (RWA) is the primary objective. Thus, each trailing unit follows the trajectory generated by its preceding articulation point. Over a high-speed evasive maneuver, the co-simulation results show significant performance improvement for the high-speed mode compared against that for the low-speed mode. Furthermore, integrating the lateral vehicle control (in terms of the tractor front axle and trailing units' axles steering) into the longitudinal speed control via model-

predictive control methodology distinguishes this MTAHV autonomous driving control strategy from the others in the literature.

In Chapter 7, a trajectory planning strategy for the A-train double in a highway driving scenario utilizing the Frenet coordinate system was developed. The motion planning stage includes the regular driver behaviors for speed maintaining, lane changing and adaptive speed control to drive the MTAHV effectively on a highway. The motion-planning and track-following with and without active trailer steering were verified through co-simulation using MATLAB and TruckSim. As noted before, designing any control strategy for MTAHVs without considering their unique dynamics is reasonable. Hence, a model-based predictive strategy was employed to regenerate the trajectory so as to mitigate the lateral acceleration of the vehicle units as well as the lateral jerk under highway evasive maneuvers. The simulation tests show remarkable improvement in vehicle ride comfort and lateral stability by adopting the proposed approach for trajectory generation and path-following.

8.2 Future work

Since only the linear and simplified non-linear vehicle models are used for all the controller designs, a non-linear vehicle model with high fidelity can be employed for the controller designs. Then, a comparative analysis can be performed to justify the benefits of the non-linear vehicle models. It is worthwhile to mention that, while the non-linear models might be more accurate in the specific driving scenarios, but the computational costs might also be much higher. This could be a subject for trade-off analysis in different driving conditions.

Additionally, highway motion-planning and urban motion-planning for MTAHVs have distinct features. Highway motion-planning prioritizes high-speed driving and maintaining a safe distance from other vehicles. In contrast, urban area motion-planning needs to consider frequent lane changes and complex turning maneuvers, negotiating narrow streets, and avoiding obstacles, such as pedestrians and parked cars. Furthermore, MTAHVs have a larger turning radius, which can make them challenging to operate in urban areas autonomously. Therefore, urban area motion-planning needs to prioritize maneuverability and safety over speed and efficiency. In this dissertation, only highway automated driving is considered. The customized urban area autonomous driving for MTAHVs can be an important direction for further studies.

References

- [1] Z. Ni and Y. He, “Design and validation of a robust active trailer steering system for multi-trailer articulated heavy vehicles,” *Veh. Syst. Dyn.*, vol. 3114, 2018.
- [2] “U.S. Federal Motor Carrier Safety Administration. Large Trucks and bus crash facts 2016.” [Online]. Available: <https://cms8.fmcsa.dot.gov/safety/data-and-statistics/large-truck-and-bus-crash-facts-2016#A8>.
- [3] OECD/ITF, *Road Safety Annual Report*. 2015.
- [4] Standing Senate Committee on Transport and Communications Senate, “Driving Change-Technology and Future of Autonomous Vehicles,” no. January, 2018.
- [5] P. Nilsson, *Traffic Situation Management for Driving Automation of Articulated Heavy Road Transports From driver behaviour towards highway autopilot*. 2017.
- [6] C. Cheng and D. Cebon, “Improving roll stability of articulated heavy vehicles using active semi-trailer steering,” *Veh. Syst. Dyn.*, vol. 46, no. SUPPL.1, pp. 373–388, 2008.
- [7] *World Health Organization. GLOBAL STATUS REPORT ON ROAD SAFETY*, no. 1. 2018.
- [8] A. T. Van Zanten, “Bosch ESP systems: 5 years of experience,” *SAE Tech. Pap.*, no. 724, 2000.
- [9] S. J. Anderson, S. B. Karumanchi, K. Iagnemma, and J. M. Walker, “The Intelligent

- CoPilot,” *IEEE Intell. Transp. Syst. Mag.*, no. April 2013, pp. 45–54, 2013.
- [10] V. A. Shia *et al.*, “Semiautonomous vehicular control using driver modeling,” *IEEE Trans. Intell. Transp. Syst.*, vol. 15, no. 6, pp. 2696–2709, 2014.
- [11] A. Gray, Y. Gao, T. Lin, J. K. Hedrick, and F. Borrelli, “Stochastic predictive control for semi-autonomous vehicles with an uncertain driver model,” *IEEE Conf. Intell. Transp. Syst. Proceedings, ITSC*, no. 1239323, pp. 2329–2334, 2013.
- [12] SAE International Surface Vehicle Information Report, “Taxonomy and Definitions for Terms Related to On-Road Motor Vehicle Automated Driving Systems,” *SAE Standard J3016*, 2016. .
- [13] N. Christie, *A review of accidents and injuries to road transport drivers*. 1831.
- [14] B. J. Alshaer, T. T. Darabseh, and M. A. Alhanouti, “Path planning, modeling and simulation of an autonomous articulated heavy construction machine performing a loading cycle,” *Appl. Math. Model.*, vol. 37, no. 7, pp. 5315–5325, 2013.
- [15] A. Elhassan, “Autonomous driving system for reversing an articulated vehicle SCHOOL OF ELECTRICAL ENGINEERING,” 2015.
- [16] P. F. Lima, *Optimization-Based Motion Planning and Model Predictive Control for Autonomous Driving: With Experimental Evaluation on a Heavy-Duty Construction Truck*. 2018.
- [17] S. Taheri, “Steering Control Characteristics of Human Driver Coupled with an Articulated Commercial Vehicle,” no. January, 2014.

- [18] S. Siregar, “A New Design of Human-Machine Interaction A Leap Towards Safe Driving,” 2015.
- [19] J. Woodrooffe and L. Ash, “Economic Efficiency of Long Combination Transport Vehicles in Alberta - Final report,” 2001.
- [20] M. M. Islam, X. Ding, and Y. He, “A closed-loop dynamic simulation-based design method for articulated heavy vehicles with active trailer steering systems,” *Veh. Syst. Dyn.*, vol. 50, no. 5, pp. 675–697, 2012.
- [21] C. Winkler, “Rollover of Heavy Commercial Vehicles,” *UMTRI Res. Rev.*, vol. 31, no. 4, 2000.
- [22] J. Brown, Y. He, and H. Lang, “Quantifying drivers’ driving skills using closed-loop dynamic simulations of articulated heavy vehicles,” *Simul. Model. Pract. Theory*, vol. 99, no. March 2019, p. 102014, 2020.
- [23] Task Force on Vehicle Weights and Dimensions Policy, “Heavy Truck Weight and Dimension Limits for Interprovincial Operations in Canada.” 2019.
- [24] “Comprehensive Truck Size and Weight (CTS&W) Study,” *FHWA, U.S. Dep. Transp.*, 1995.
- [25] P. Fancher and C. Winkler, “Directional Performance Issues in Evaluation and Design of Articulated Heavy Vehicles,” *User Model. User-adapt. Interact.*, vol. 45, no. 7–8, pp. 607–647, 2007.
- [26] J. Aurell, T. Wadman, and V. Trucks, “Vehicle Combinations Based on the Modular

Concept Background and Analysis,” no. Report nr. 1/2007. 2007.

- [27] S. Wood and J. D. Regehr, “Regulations Governing the Operation of Longer Combination Vehicles in Canada,” *Can. J. Civ. Eng.*, vol. 44, no. 10, pp. 838–849, 2017.
- [28] P. Nagl, “Longer Combination Vehicles (LCV) for Asia and the Pacific Region: Some Economic Implications,” 2007.
- [29] S. Kharrazi, “Steering Based Lateral Performance Control of Long Heavy Vehicle Combinations,” Chalmers University of Technology, 2012.
- [30] R. D. Ervin and Y. Guy, “Influence of Weights and Dimensions on the Stability and Control of Heavy Trucks in Canda - Part I,” 1986.
- [31] “Vehicle Weights and Dimensions Study. Technical Steering Committee Report. Transportation association of Canada (TAC), (Via Canroad Transportation Research Corporation),” 1986.
- [32] R. D. Ervin, Fancher, G. P.S., W. T.D., C.B., and A. Wolfe, “Ad Hoc Study of Certain Safety- Related Aspects of Double-Bottom Tankers. Final Report. (Highway Safety Research Institute: Ann Arbor, MI),” pp. 78 p. UM-HSRI-78-18–1, 1978.
- [33] J. Edgar, H. Prem, and F. Calvert, “Applying Performance Standards to The Australian Heavy Vehicle Fleet,” pp. 73–96, 2002.
- [34] “Performance-Based Standards Scheme – the Standards and Vehicle Assessment Rules.” National Transport Commission (NTC); Australia, January 2020.

- [35] J. Edgar, "Development of Performance Standards for Australian Heavy Vehicles." Eighth International Symposium on Heavy Vehicle Weights and Dimensions. 14–18th March 2004. South Africa.
- [36] M. S. Kati, "Definitions of Performance Based Characteristics for Long Heavy Vehicle Combinations," 2013.
- [37] E. Amlin, P. Klawer, and D. V Hart, "Study of the aligning forces generated from a tridem drive axle group," in *Proceedings of the International Symposium on Heavy Vehicle Weights and Dimensions*, 1995, pp. 483–492.
- [38] R. Kamnik, F. Boettiger, and K. Hunt, "Roll dynamics and lateral load transfer estimation in articulated heavy freight vehicles," *Proc. Inst. Mech. Eng. Part D J. Automob. Eng.*, vol. 217, no. 11, pp. 985–997, 2003.
- [39] M. Sadeghi Kati, J. Fredriksson, L. Laine, and B. Jacobson, "Evaluation of Dynamical Behaviour of Long Heavy Vehicles Using Performance Based Characteristics," in *FISITA 2014 World Automotive Congress-2-6 June 2014, Maastricht, The Netherlands.*, 2014.
- [40] P. S. Fancher and M. Arvind, "A Vehicle Dynamics Handbook for Single-Unit and Articulated Heavy Trucks (UMTRI-87-27)," 1987.
- [41] S. Zhu, Z. Ni, A. Rahimi, and Y. He, "On dynamic stability evaluation methods for long combination vehicles," *Veh. Syst. Dyn.*, vol. 60, no. 12, pp. 3999–4034, 2022.
- [42] A. M. C. Odhams, R. L. Roebuck, and D. Cebon, "Implementation of active steering

- on a multiple trailer long combination vehicle,” in *HVTT11*, 2010, vol. 1, no. Lcv, pp. 1–13.
- [43] council directive 96/23/EC, “relating to the masses and dimensions of certain categories of motor vehicles and their trailers and amending Directive 70/156/EEC,” *MachineryDirective*., vol. 66, no. March 2000, pp. 1–27, 2010.
- [44] S. Kharrazi, M. Lidberg, R. Roebuck, J. Fredriksson, and A. Odhams, “Implementation of active steering on longer combination vehicles for enhanced lateral performance,” *Veh. Syst. Dyn.*, vol. 50, no. 12, pp. 1949–1970, 2012.
- [45] R. Roebuck, A. Odhams, K. Tagesson, C. Cheng, and D. Cebon, “Implementation of trailer steering control on a multi-unit vehicle at high speeds,” *J. Dyn. Syst. Meas. Control. Trans. ASME*, vol. 136, no. 2, pp. 1–14, 2014.
- [46] S. Kharrazi, M. Lidberg, and J. Fredriksson, “Robustness analysis of a steering-based control strategy for improved lateral performance of a truck-dolly-semitrailer,” *Int. J. Heavy Veh. Syst.*, vol. 22, no. 1, pp. 1–20, 2015.
- [47] W. Huang, A. Rahimi, L. Steinginga, J. Yu, and Y. He, “Dynamic Performance of Multi-Trailer Articulated Heavy Vehicles with Advanced Control Systems,” in *8th international conference on vibration engineering*, 2021, no. July.
- [48] S. Kharrazi, M. Lidberg, and J. Fredriksson, “A Generic Controller for Improving Lateral Performance of Heavy Vehicle Combinations,” *Proc. Inst. Mech. Eng. Part D J. Automob. Eng.*, vol. 227, no. 5, pp. 619–642, 2013.

- [49] X. Ding, S. Mikaric, and Y. He, “Design of an active trailer-steering system for multi-trailer articulated heavy vehicles using real-time simulations,” *Proc. Inst. Mech. Eng. Part D J. Automob. Eng.*, vol. 227, no. 5, pp. 643–655, 2013.
- [50] Z. W. Deng, Q. X. Zhao, Y. Q. Zhao, B. H. Wang, W. Gao, and X. X. Kong, “Active LQR Multi-Axle-Steering Method for Improving Maneuverability and Stability of Multi-Trailer Articulated Heavy Vehicles,” *Int. J. Automot. Technol.*, vol. 23, no. 4, pp. 939–955, 2021.
- [51] M. Sadeghi Kati, J. Fredriksson, B. Jacobson, and L. Laine, “Gain-scheduled H ∞ controller synthesis for actively steered longer and heavier commercial vehicles,” *Proc. Inst. Mech. Eng. Part D J. Automob. Eng.*, vol. 234, no. 7, pp. 2045–2065, 2020.
- [52] M. S. Kati, J. Fredriksson, B. Jacobson, and L. Laine, “A feedback-feed-forward steering control strategy for improving lateral dynamics stability of an A-double vehicle at high speeds,” *Veh. Syst. Dyn.*, 2021.
- [53] A. Khodayari, A. Ghaffari, S. Ameli, and J. Flahatgar, “A historical review on lateral and longitudinal control of autonomous vehicle motions,” *ICMET 2010 - 2010 Int. Conf. Mech. Electr. Technol. Proc.*, no. Icmct, pp. 421–429, 2010.
- [54] H. Guan, K. Kim, and B. Wang, “Comprehensive path and attitude control of articulated vehicles for varying vehicle conditions,” *Int. J. Heavy Veh. Syst.*, vol. 24, no. 1, 2017.
- [55] K. il Kim, H. Guan, B. Wang, R. Guo, and F. Liang, “Active steering control strategy

- for articulated vehicles,” *Front. Inf. Technol. Electron. Eng.*, vol. 17, no. 6, pp. 576–586, 2016.
- [56] H. Yuan and H. Zhu, “Anti-jackknife reverse tracking control of articulated vehicles in the presence of actuator saturation,” *Veh. Syst. Dyn.*, vol. 54, no. 10, pp. 1428–1447, 2016.
- [57] B. A. Jujnovich and D. Cebon, “Path-following steering control for articulated vehicles,” *J. Dyn. Syst. Meas. Control. Trans. ASME*, vol. 135, no. 3, pp. 1–15, 2013.
- [58] A. Goodarzi and M. Ghajar, “Integrating lane-keeping system with direct yaw moment control tasks in a novel driver assistance system,” *Proc. Inst. Mech. Eng. Part K J. Multi-body Dyn.*, vol. 229, no. 1, pp. 16–38, 2015.
- [59] M. M. Michałek, “A highly scalable path-following controller for N-trailers with off-axle hitching,” *Control Eng. Pract.*, vol. 29, pp. 61–73, 2014.
- [60] T. Nayl, G. Nikolakopoulos, T. Gustafsson, D. Kominiak, and R. Nyberg, “Design and experimental evaluation of a novel sliding mode controller for an articulated vehicle,” *Rob. Auton. Syst.*, vol. 103, pp. 213–221, 2018.
- [61] P. Gaspar, I. Szaszi, and J. Bokor, “The design of a combined control structure to prevent the rollover of heavy vehicles,” *Eur. J. Control*, vol. 10, no. 2, pp. 148–162, 2004.
- [62] S. Yim, K. Jeon, and K. Yi, “An investigation into vehicle rollover prevention by coordinated control of active anti-roll bar and electronic stability program,” *Int. J.*

Control. Autom. Syst., vol. 10, no. 2, pp. 275–287, 2012.

- [63] M. Ghazali, M. Durali, and H. Salarieh, “Path-following in model predictive rollover prevention using front steering and braking,” *Veh. Syst. Dyn.*, vol. 55, no. 1, pp. 121–148, 2017.
- [64] V. T. Vu, O. Sename, L. Dugard, and P. Gaspar, “Active anti-roll bar control using electronic servo valve hydraulic damper on single unit heavy vehicle,” *IFAC-PapersOnLine*, vol. 49, no. 11, pp. 418–425, 2016.
- [65] Y. Liu, K. Yang, X. He, and X. Ji, “Active steering and anti-roll shared control for enhancing roll stability in path following of autonomous heavy vehicle,” *SAE Tech. Pap.*, vol. 2019-April, no. April, pp. 1–10, 2019.
- [66] Y. Hisaoka, M. Yamamoto, and A. Okada, “Closed-loop analysis of vehicle behavior during braking in a turn,” *JSAE Rev.*, vol. 20, no. 4, pp. 537–542, 1999.
- [67] A. R. Savkoor and S. Ausejo, “Analysis of driver’s steering and speed control strategies in curve negotiation,” *Veh. Syst. Dyn.*, vol. 33, no. SUPPL., pp. 94–109, 2000.
- [68] R. Hasan, “Convex Optimization-based Design of a Speed Planner for Autonomous Heavy Duty Vehicles,” 2019.
- [69] X. Y. Lu and J. K. Hedrick, “Heavy-duty vehicle modelling and longitudinal control,” *Veh. Syst. Dyn.*, vol. 43, no. 9, pp. 653–669, 2005.
- [70] P. F. Lima, M. Trincavelli, J. Martensson, and B. Wahlberg, “Clothoid-Based Speed

- Profiler and Control for Autonomous Driving,” *IEEE Conf. Intell. Transp. Syst. Proceedings, ITSC*, vol. 2015-Octob, pp. 2194–2199, 2015.
- [71] A. Y. Ungoren and H. Peng, “An adaptive lateral preview driver model,” *Veh. Syst. Dyn.*, vol. 43, no. 4, pp. 245–259, 2005.
- [72] C. MacAdam, “Development of a Driver Model for Near/At-Limit Vehicle Handling,” *Transp. Res.*, no. 2, 2001.
- [73] P. Bolia, T. Weiskircher, and S. Müller, “Driver steering model for closed-loop steering function analysis,” *Veh. Syst. Dyn.*, vol. 52, no. SUPPL. 1, pp. 16–30, 2014.
- [74] K. Driggs-Campbell, V. Govindarajan, and R. Bajcsy, “Integrating Intuitive Driver Models in Autonomous Planning for Interactive Maneuvers,” *IEEE Trans. Intell. Transp. Syst.*, vol. 18, no. 12, pp. 3461–3472, 2017.
- [75] X. Ding and Y. He, “Numerical Simulation and Analysis of Closed-Loop Driver/Articulated Vehicle Dynamic Systems,” *SAE Int. J. Commer. Veh.*, vol. 5, no. 1, pp. 111–118, 2012.
- [76] Y. He, M. M. Islam, S. Zhu, and T. Hu, “A design synthesis framework for directional performance optimization of multi-trailer articulated heavy vehicles with trailer lateral dynamic control systems,” *Proc. Inst. Mech. Eng. Part D J. Automob. Eng.*, vol. 231, no. 8, pp. 1096–1125, 2017.
- [77] Z. Ni, S. Zhu, and Y. He, “A comparison of test manoeuvres for determining rearward amplification of articulated heavy vehicles,” vol. 27, no. 4, pp. 405–421,

2020.

- [78] S. Zhu and Y. He, “A Unified Lateral Preview Driver Model for Road Vehicles,” *IEEE Trans. Intell. Transp. Syst.*, pp. 1–11, 2019.
- [79] C. Cheng, R. Roebuck, A. Odhams, and D. Cebon, “High-speed optimal steering of a tractor-semitrailer,” *Veh. Syst. Dyn.*, vol. 49, no. 4, pp. 561–593, 2011.
- [80] j R. Ellis, “vehicle-dynamics.” .
- [81] “Road vehicles–vehicle dynamics and road-holding ability–vocabulary.,” *International Organization for Standardization: Geneva, Switzerland, ISO 8855:2011(E)*, p. 3, 2011.
- [82] R. Rajamani, *Vehicle Dynamics and Control*. 2016.
- [83] J. Y. Wong, *Theory of Ground Vehicles*. 2001.
- [84] M. M. Islam, Y. He, S. Zhu, and Q. Wang, “A comparative study of multi-trailer articulated heavy-vehicle models,” *Proc. Inst. Mech. Eng. Part D J. Automob. Eng.*, vol. 229, no. 9, pp. 1200–1228, 2015.
- [85] Y. Li, Q. Shi, and D. Qiu, “Parameter Identification of Tractor-Semitrailer Model under Steering and Braking,” *Math. Probl. Eng.*, vol. 2019, 2019.
- [86] N. Rashevsky, *Neglected Factors in Highway Safety*. University of Michigan Mental Health Research Institute, Grant GM-12032-01, 1966.
- [87] M. Plöchl and J. Edelmann, *Driver models in automobile dynamics application*, no.

March 2015. Taylor, Publisher, 2007.

- [88] R. S. Sharp, D. Casanova, and P. Symonds, “A Mathematical Model for Driver Steering Control , with Design , Tuning and Performance Results A Mathematical Model for Driver Steering Control , with Design , Tuning and P,” no. April 2014, pp. 37–41, 2010.
- [89] X. Yang, S. Rakheja, and I. Stiharu, “Adapting an articulated vehicle to its drivers,” *J. Mech. Des. Trans. ASME*, vol. 123, no. 1, pp. 132–140, 2001.
- [90] X. Yang, S. Rakheja, and I. Stiharu, “Structure of driver model for articulated vehicles,” *Int. J. Heavy Veh. Syst.*, vol. 9(1), pp. 27–51, 2002.
- [91] Z. Liu, “Characterisation of optimal human driver model and stability of a tractor-semitrailer vehicle system with time delay,” *Mech. Syst. Signal Process.*, vol. 21, no. 5, pp. 2080–2098, 2007.
- [92] C. C. MacAdam, “An optimal preview control for linear systems,” *J. Dyn. Syst. Meas. Control. Trans. ASME*, vol. 102, no. 3, pp. 188–190, 1980.
- [93] Ogata, *Modern control systems*, vol. 39, no. 12. 2002.
- [94] A. Rahimi and Y. He, “A Review of Essential Technologies for Autonomous and Semi-autonomous Articulated Heavy Vehicles,” 2020.
- [95] F. M. Barbosa, L. B. Marcos, M. M. da Silva, M. H. Terra, and V. Grassi, “Robust path-following control for articulated heavy-duty vehicles,” *Control Eng. Pract.*, vol. 85, no. January, pp. 246–256, 2019.

- [96] C. C. Macadam, “MacAdam human driver,” vol. 40, no. 734, pp. 101–134, 2003.
- [97] C. C. MacAdam, “Application of an Optimal Preview Control for Simulation of Closed-Loop Automobile Driving,” *IEEE Trans. Syst. Man Cybern.*, vol. 11, no. 6, pp. 393–399, 1981.
- [98] S. Zhu and Y. He, “A Unified Lateral Preview Driver Model for Road Vehicles,” *IEEE Trans. Intell. Transp. Syst.*, pp. 1–11, 2019.
- [99] “Road Vehicles – Heavy Commercial Vehicle Combinations and Articulated Buses – Lateral Stability Test Methods,” *International Organization for Standardization, Geneva. (2000) ISO-14791: 2000(E)*,.
- [100] B. Jujnovich and D. Cebon, “COMPARATIVE PERFORMANCE OF SEMI-TRAILER STEERING SYSTEMS.”
- [101] R. S. Rice, “MEASURING CAR-DRIVER INTERACTION WITH THE g-g DIAGRAM,” in *SAE Paper 730018*, 1973.
- [102] H. M. Kim, J. Dickerson, and B. Kosko, “Fuzzy throttle and brake control for platoons of smart cars,” *Fuzzy Sets Syst.*, vol. 84, no. 3, pp. 209–234, 1996.
- [103] A. Sala and P. Albertos, “Fuzzy Logic Controllers: Advantages and Drawbacks,” *Anales*, vol. III, no. September, pp. 833–844, 1998.
- [104] I. Noy, “Automated driving: Proceed with caution,” in *Canadian Association of Road Safety Professionals Conference*, 2007.
- [105] N. And En, A. G. Martín, K. Hoogendijk, L. Niklasson, F. Sandblom, and F. S.

Seholm, “Predictive Control for Autonomous Articulated Vehicles,” 2017.

- [106] R. Oliveira, “Planning and Motion Control in Autonomous Heavy-Duty Vehicles,” 2014.
- [107] Y. He and M. Manjurul Islam, “An automated design method for active trailer steering systems of articulated heavy vehicles,” *J. Mech. Des. Trans. ASME*, vol. 134, no. 4, 2012.
- [108] K. Rangavajhula and H. S. J. Tsao, “Active trailer steering control of an articulated system with a tractor and three full trailers for tractor-track following,” *Int. J. Heavy Veh. Syst.*, vol. 14, no. 3, pp. 271–293, 2007.
- [109] S. Zhu, Y. He, and J. Ren, “On robust controllers for active steering systems of articulated heavy vehicles,” *Int. J. Heavy Veh. Syst.*, vol. 26, no. 1, pp. 1–30, 2019.
- [110] A. M. C. Odhams, R. L. Roebuck, D. Cebon, and C. B. Winkler, “Dynamic safety of active trailer steering systems,” *Proc. Inst. Mech. Eng. Part K J. Multi-body Dyn.*, vol. 222, no. 4, pp. 367–380, 2008.
- [111] X. Ding, Y. He, J. Ren, and T. Sun, “A comparative study of control algorithms for active trailer steering systems of articulated heavy vehicles,” *Proc. Am. Control Conf.*, pp. 3617–3622, 2012.
- [112] N. Chowdhri, L. Ferranti, F. S. Iribarren, and B. Shyrokau, “Integrated nonlinear model predictive control for automated driving,” *Control Eng. Pract.*, vol. 106, no. October 2020, p. 104654, 2021.

- [113] A. Rahimi, W. Huang, and Y. He, “A Longitudinal Speed Controller for Autonomous Multi-Trailer Articulated Heavy Vehicles A Longitudinal Speed Controller for Automomous Multi-Trailer Articulated Heavy Vehicles,” no. June, 2021.
- [114] Y. Sun, D. Ren, S. Lian, M. Fan, and X. Teng, “An Efficient Generation Method based on Dynamic Curvature of the Reference Curve for Robust Trajectory Planning,” *arXiv:2012.14617*, 2020.
- [115] J. Fickenscher, S. Schmidt, F. Hannig, M. E. Bouzouraa, and J. Teich, “Path planning for highly automated driving on embedded GPUs,” *J. Low Power Electron. Appl.*, vol. 8, no. 4, pp. 1–15, 2018.
- [116] M. Werling, J. Ziegler, S. Kammel, and S. Thrun, “Optimal trajectory generation for dynamic street scenarios in a frenét frame,” *Proc. - IEEE Int. Conf. Robot. Autom.*, no. March, pp. 987–993, 2010.
- [117] M. Elbanhawi, M. Simic, and R. Jazar, “In the Passenger Seat: Investigating Ride Comfort Measures in Autonomous Cars,” *IEEE Intell. Transp. Syst. Mag.*, vol. 7, no. 3, pp. 4–17, 2015.
- [118] S. Moon and K. Yi, “Human driving data-based design of a vehicle adaptive cruise control algorithm,” *Veh. Syst. Dyn.*, vol. 46, no. 8, pp. 661–690, 2008.
- [119] I. Bae *et al.*, “Self-Driving like a Human driver instead of a Robocar: Personalized comfortable driving experience for autonomous vehicles,” no. NeurIPS, 2020.

- [120] B. Peng, D. Yu, H. Zhou, X. Xiao, and C. Xie, “A Motion Planning Method for Automated Vehicles in Dynamic Traffic Scenarios,” *Symmetry (Basel)*, vol. 14, no. 2, 2022.
- [121] A. Takahashi, T. Hongo, Y. Ninomiya, and G. Sugimoto, “Local path planning and motion control for AGV in positioning,” in *The Autonomous Mobile Robots and Its Applications. IROS’89*, 1989, pp. 392–397.
- [122] “MathWorks, (2021). Navigation Toolbox: User’s Guide (R2016b). Retrieved September 2021 from www.mathworks.com/help/pdf_doc/nav/nav_ug.pdf,” 2021.
- [123] S. Yin, C. Yang, I. Kawsar, H. Du, and Y. Pan, “Longitudinal Predictive Control for Vehicle-Following Collision Avoidance in Autonomous Driving Considering Distance and Acceleration Compensation,” 2022.
- [124] J. Ziegler and C. Stiller, “Fast collision checking for intelligent vehicle motion planning,” *IEEE Intell. Veh. Symp. Proc.*, pp. 518–522, 2010.
- [125] M. Darms, P. Rybski, and C. Urmson, “An adaptive model switching approach for a multisensor tracking system used for autonomous driving in an urban environment,” *VDI Berichte*, no. 2009, pp. 521–530, 2008.
- [126] H. Cramer, U. Scheunert, and G. Wanielik, “Object Detection Using Generalized Feature Models,” pp. 2–10, 2003.
- [127] C. Stiller, J. Hipp, C. Rössig, and A. Ewald, “Multisensor obstacle detection and tracking,” *Image Vis. Comput.*, vol. 18, no. 5, pp. 389–396, 2000.

- [128] F. Dellaert, D. Pomerleau, and C. Thorpe, "Model-based car tracking integrated with a road-follower," *Proc. - IEEE Int. Conf. Robot. Autom.*, vol. 3, no. May, pp. 1889–1894, 1998.
- [129] N. Kaempchen, K. Weiss, M. Schaefer, and K. C. J. Dietmayer, "IMM object tracking for high dynamic driving maneuvers," *IEEE Intell. Veh. Symp. Proc.*, pp. 825–830, 2004.
- [130] F. Lin, K. Wang, Y. Zhao, and S. Wang, "Integrated avoid collision control of autonomous vehicle based on trajectory re-planning and v2v information interaction," *Sensors (Switzerland)*, vol. 20, no. 4, 2020.
- [131] D. Ferguson, M. Darms, C. Urmson, and S. Kolski, "Detection, prediction, and avoidance of dynamic obstacles in urban environments," *IEEE Intell. Veh. Symp. Proc.*, pp. 1149–1154, 2008.
- [132] M. Gou, "LIDAR-based Multi-object Tracking System with Dynamic Modeling," 2012.

Appendices

Appendix A

A.1 A-train double parameters

The nomenclature and the parameters' values used for the dynamics model of the A-train double MTAHV are presented herein.

Symbol	Description / value	Symbol	Description / value
Y_{β_1}	$C_1 + C_2 + C_3$	l_{apij}	Distance between the i^{th} articulation point and the j^{th} vehicle unit sprung mass CG (m)
Y_{β_2}	$C_4 + C_5 + C_6$	l_{ap11}	3.865
Y_{β_3}	$C_7 + C_8$	l_{ap12}	6.760
Y_{β_4}	$C_9 + C_{10} + C_{11}$	l_{ap22}	8.240
$Y_{\dot{\psi}_1}$	$(l_{11}C_1 - l_{12}C_2 - l_{13}C_3)/U$	l_{ap23}	2.065
$Y_{\dot{\psi}_2}$	$(-l_{21}C_4 - l_{22}C_5 - l_{23}C_6)/U$	l_{ap33}	0.080
$Y_{\dot{\psi}_3}$	$(l_{31}C_7 - l_{32}C_8)/U$	l_{ap34}	6.760
$Y_{\dot{\psi}_4}$	$(-l_{41}C_9 - l_{42}C_{10} - l_{43}C_{11})/U$	l_{ij}	The distance between j^{th} ($j=1,2,3$) axle from the CG of the i^{th} ($i=1,2,3,4$) vehicle unit (m)
Y_{δ_1}	$-C_1$	l_{11}	2.145
N_{β_1}	$l_{11}C_1 - l_{12}C_2 - l_{13}C_3$	l_{12}	3.115
N_{β_2}	$-l_{21}C_4 - l_{22}C_5 - l_{23}C_6$	l_{13}	4.465
N_{β_3}	$l_{31}C_7 - l_{32}C_8$	l_{21}	3.218
N_{β_4}	$-l_{41}C_9 - l_{42}C_{10} - l_{43}C_{11}$	l_{22}	5.048
$N_{\dot{\psi}_1}$	$(l_{11}^2C_1 + l_{12}^2C_2 + l_{13}^2C_3)/U$	l_{23}	6,878
$N_{\dot{\psi}_2}$	$(l_{21}^2C_4 + l_{22}^2C_5 + l_{23}^2C_6)/U$	l_{31}	0.565
$N_{\dot{\psi}_3}$	$(l_{31}^2C_7 + l_{32}^2C_8)/U$	l_{32}	0.723
$N_{\dot{\psi}_4}$	$(l_{41}^2C_9 + l_{42}^2C_{10} + l_{43}^2C_{11})/U$	l_{41}	3.218
N_{δ_1}	$-l_{11}C_1$	l_{42}	5.048
u_i	i^{th} vehicle unit longitudinal velocity	l_{43}	6,878
v_i	i^{th} vehicle unit lateral velocity	I_i	Yaw moment of inertia of the i^{th} vehicle unit at sprung mass CG (kg.m ²)
m_i	Total mass of i^{th} vehicle unit (kg)	I_1	19,665
m_1	6,310	I_2	246,000
m_2	23,840	I_3	3750
m_3	2397	I_4	246,000
m_4	23,840	β_i	Sideslip angle for i^{th} vehicle unit at sprung mass CG
C_i	Total cornering stiffness of i^{th} axle tires (N/rad)	F_{yi}	Lateral force applied on the i^{th} articulation point
$\dot{\psi}_i$	Yaw rate of i^{th} vehicle unit at sprung mass CG		

A.2 Fundamental linear model state-space matrices

The linear fundamental yaw-plane state-space model of the A-train double is given by equation 3.6,

$$\begin{aligned}\dot{\mathbf{x}}_b &= \mathbf{A}_b \mathbf{x}_b + \mathbf{B}_b \mathbf{u} \\ \mathbf{y} &= \mathbf{C}_b \mathbf{x}_b\end{aligned}$$

Where,

$$\mathbf{A}_b = \mathbf{J}^{-1} \mathbf{K}, \mathbf{B}_b = \mathbf{J}^{-1} \mathbf{L} \text{ and } \mathbf{C}_b = \mathbf{I}_{8 \times 8}$$

The non-zero elements of matrix $\mathbf{J} \in \mathbb{R} 8 \times 8$ are:

$$\begin{aligned}J(1,1) &= l_{ap11} m_1 U_1, J(1,2) = I_{zz1}, J(2,1) = m_1 U_1, J(2,3) = m_2 U_2, J(2,5) = m_3 U_3, \\ J(2,7) &= m_4 U_4, J(3,1) = l_{ap12} m_1 U_1, J(3,4) = I_{zz2}, J(3,5) = -l_{ap22} m_3 U_3, J(3,7) = \\ &-l_{ap22} m_4 U_4, J(4,1) = l_{ap23} m_1 U_1, J(4,3) = l_{ap23} m_2 U_2, J(4,6) = I_{zz3}, J(4,7) = \\ &-l_{ap33} m_4 U_4, J(5,7) = -l_{ap34} m_4 U_4, J(5,8) = I_{zz4}, J(6,1) = 1, J(6,2) = -\frac{l_{ap11}}{U_1}, \\ J(6,3) &= -1, J(6,4) = -\frac{l_{ap12}}{U_2}, J(7,3) = 1, J(7,4) = -\frac{l_{ap22}}{U_2}, J(7,5) = -1, J(7,6) = \\ &-\frac{l_{ap23}}{U_3}, J(8,5) = 1, J(8,6) = -\frac{l_{ap33}}{U_3}, J(8,7) = -1, J(8,8) = -\frac{l_{ap34}}{U_4}\end{aligned}$$

The non-zero elements of matrix $\mathbf{K} \in \mathbb{R} 8 \times 8$ are:

$$\begin{aligned}K(1,1) &= (N_{\beta_1} + l_{ap11} Y_{\beta_1}), K(1,2) = (N_{\psi_1} - l_{ap11} m_1 U_1 + l_{ap11} Y_{\psi_1}), K(2,1) = \\ &Y_{\beta_1}, K(2,2) = (-m_1 U + Y_{\psi_1}), K(2,3) = Y_{\beta_2}, K(2,4) = (-m_2 U_2 + Y_{\psi_2}), K(2,5) = \\ &Y_{\beta_3}, K(2,6) = (-m_3 U_3 + Y_{\psi_3}), K(2,7) = Y_{\beta_4}, K(2,8) = (-m_4 U_4 + Y_{\psi_4}), K(3,1) = \\ &l_{ap12} Y_{\beta_1}, K(3,2) = (-l_{ap12} m_1 U_1 + l_{ap12} Y_{\psi_1}), K(3,3) = N_{\beta_2}, K(3,4) = N_{\psi_2}, K(3,5) = \\ &-l_{ap22} Y_{\beta_3}, K(3,6) = (-l_{ap22} Y_{\psi_3} + l_{ap22} m_3 U_3), K(3,7) = -l_{ap22} Y_{\beta_4}, K(3,8) =\end{aligned}$$

$$\begin{aligned}
&(-l_{ap22}Y_{\dot{\psi}_4} + l_{ap22}m_4U_4), K(4,1) = l_{ap23}Y_{\beta_1}, K(4,2) = (-l_{ap23}m_1U_1 + \\
&l_{ap23}Y_{\dot{\psi}_1}), K(4,3) = l_{ap23}Y_{\beta_2}, K(4,4) = (l_{ap23}Y_{\dot{\psi}_2} - l_{ap23}m_2U_2), K(4,5) = \\
&N_{\beta_3}, K(4,6) = N_{\dot{\psi}_3}, K(4,7) = -l_{ap33}Y_{\beta_4}, K(4,8) = (-l_{ap33}Y_{\dot{\psi}_4} + l_{ap33}m_4U_4), K(5,7) = \\
&N_{\beta_4} - l_{ap34}Y_{\beta_4}, K(5,8) = (l_{ap34}m_4U_4 - l_{ap34}Y_{\dot{\psi}_4} + N_{\dot{\psi}_4}), K(6,2) = -1, K(6,4) = \\
&+1, K(7,4) = -1, K(7,6) = +1, K(8,6) = -1, K(8,8) = +1.
\end{aligned}$$

The non-zero elements of matrix $\mathbf{L} \in \mathbb{R}^{8 \times 1}$ are:

$$L(1,1) = (N_{\delta_1} + l_{ap11}Y_{\delta_1}), L(2,1) = Y_{\delta_1}, L(3,1) = l_{ap12}Y_{\delta_1}, L(4,1) = l_{ap23}Y_{\delta_1}$$

And, the non-zero elements of matrix $\mathbf{T} \in \mathbb{R}^{8 \times 8}$ are:

$$\begin{aligned}
&T(2,1) = Y_{\delta_4}, T(2,2) = Y_{\delta_5}, T(2,3) = Y_{\delta_6}, T(2,4) = Y_{\delta_7}, T(2,5) = Y_{\delta_8}, T(2,6) = \\
&Y_{\delta_9}, T(2,7) = Y_{\delta_{10}}, T(2,8) = Y_{\delta_{11}}, T(3,1) = N_{\delta_4}, T(3,2) = N_{\delta_5}, T(3,3) = N_{\delta_6}, T(3,4) = \\
&-l_{ap22}Y_{\delta_7}, T(3,5) = -l_{ap22}Y_{\delta_8}, T(3,6) = -l_{ap22}Y_{\delta_9}, T(3,7) = -l_{ap22}Y_{\delta_{10}}, T(3,8) = \\
&-l_{ap22}Y_{\delta_{11}}, T(4,1) = l_{ap23}Y_{\delta_4}, T(4,2) = l_{ap23}Y_{\delta_5}, T(4,3) = l_{ap23}Y_{\delta_6}, T(4,4) = \\
&N_{\delta_7}, T(4,5) = N_{\delta_8}, T(4,6) = -l_{ap33}Y_{\delta_9}, T(4,7) = -l_{ap33}Y_{\delta_{10}}, T(4,8) = \\
&-l_{ap33}Y_{\delta_{11}}, T(5,6) = N_{\delta_9} - l_{ap34}Y_{\delta_9}, T(5,7) = N_{\delta_{10}} - l_{ap34}Y_{\delta_{10}}, T(5,8) = N_{\delta_{11}} - \\
&l_{ap34}Y_{\delta_{11}}.
\end{aligned}$$

A.3 State-space matrices of fundamental linear model extension

The fundamental linear model extension of the A-train double used in driver model design is given by:

$$\begin{aligned}
\dot{\mathbf{x}}_d &= \mathbf{A}_d \mathbf{x}_d + \mathbf{B}_d \mathbf{u} \\
\mathbf{y} &= \mathbf{C}_d \mathbf{x}_d
\end{aligned}$$

The non-zero elements of matrix $\mathbf{A}_d \in \mathbb{R}^{16 \times 16}$ are:

$$\begin{aligned}
&A_d(1,2) = U_1, A_d(1,3) = 1, A_d(1,4) = l_{11}, A_d(2,4) = 1, A_d(3,3) = \\
&A_b(1,1), A_d(3,4) = A_b(1,2)U_1, A_d(3,7) = A_b(1,3), A_d(3,8) = A_b(1,4)U_1, A_d(3,11) = \\
&A_b(1,5), A_d(3,12) = A_b(1,6)U_1, A_d(3,15) = A_b(1,7), A_d(3,16) = \\
&A_b(1,8)U_1, A_d(4,3) = A_b(2,1)/U_1, A_d(4,4) = A_b(2,2), A_d(4,7) = A_b(2,3)/ \\
&U_2, A_d(4,8) = A_b(2,4), A_d(4,11) = A_b(2,5)/U_3, A_d(4,12) = A_b(2,6), A_d(4,15) = \\
&A_b(2,7)/U_4, A_d(4,16) = A_b(2,8), A_d(5,6) = U_2, A_d(5,7) = 1, A_d(6,8) = 1 \\
&A_d(7,3) = A_b(3,1), A_d(7,4) = A_b(3,2)U_2, A_d(7,7) = A_b(3,3), A_d(7,8) = \\
&A_b(3,4)U_2, A_d(7,11) = A_b(3,5), A_d(7,12) = A_b(3,6)U_2, A_d(7,15) = \\
&A_b(3,7), A_d(7,16) = A_b(3,8)U_2, A_d(8,3) = A_b(4,1)/U_1, A_d(8,4) = \\
&A_b(4,2), A_d(8,7) = A_b(4,3)/U_2, A_d(8,8) = A_b(4,4), A_d(8,11) = A_b(4,5)/ \\
&U_3, A_d(8,12) = A_b(4,6), A_d(8,15) = A_b(4,7)/U_4, A_d(8,16) = A_b(4,8), A_d(9,10) = \\
&U_3, A_d(9,11) = 1, A_d(10,12) = 1 \\
&A_d(11,3) = A_b(5,1), A_d(11,4) = A_b(5,2)U_3, A_d(11,7) = A_b(5,3), A_d(11,8) = \\
&A_b(5,4)U_3, A_d(11,11) = A_b(5,5), A_d(11,12) = A_b(5,6)U_3, A_d(11,15) = \\
&A_b(5,7), A_d(11,16) = A_b(5,8)U_3, A_d(12,3) = A_b(6,1)/U_1, A_d(12,4) = \\
&A_b(6,2), A_d(12,7) = A_b(6,3)/U_2, A_d(12,8) = A_b(6,4), A_d(12,11) = A_b(6,5)/ \\
&U_3, A_d(12,12) = A_b(6,6), A_d(12,15) = A_b(6,7)/U_4, A_d(12,16) = \\
&A_b(6,8), A_d(13,14) = U_4, A_d(13,15) = 1, A_d(14,16) = 1 \\
&A_d(15,3) = A_b(7,1), A_d(15,4) = A_b(7,2)U_4, A_d(15,7) = A_b(7,3), A_d(15,8) = \\
&A_b(7,4)U_4, A_d(15,11) = A_b(7,5), A_d(15,12) = A_b(7,6)U_4, A_d(15,15) = \\
&A_b(7,7), A_d(15,16) = A_b(7,8)U_4, A_d(16,3) = A_b(8,1)/U_1, A_d(16,4) =
\end{aligned}$$

$$A_b(8,2), A_d(16,7) = A_b(8,3)/U_2, A_d(16,8) = A_b(8,4), A_d(16,11) = A_b(8,5)/U_3, A_d(16,12) = A_b(8,6), A_d(16,15) = A_b(8,7)/U_4, A_d(16,16) = A_b(8,8)$$

The non-zero elements of matrix $\mathbf{B}_d \in \mathbb{R} 16 \times 1$ are:

$$B_d(3,1) = B_b(1,1)U_1, B_d(4,1) = B_b(2,1), B_d(7,1) = B_b(3,1)U_2, B_d(8,1) = B_b(4,1), B_d(11,1) = B_b(5,1)U_3, B_d(12,1) = B_b(6,1), B_d(15,1) = B_b(7,1)U_4, B_d(16,1) = B_b(8,1)$$

$\mathbf{C}_d = I_{16 \times 16}$ is the identity matrix.

A.4 State-space matrices of non-linear extension of fundamental linear model

The non-linear extension of the yaw-plane dynamics model for the A-train double is given by the following equation.

$$\begin{aligned} \dot{\mathbf{x}} &= \mathbf{A}_t(\mathbf{x})\mathbf{x} + \mathbf{B}_t(\mathbf{x})\mathbf{u} + \mathbf{B}_s(\mathbf{x})\mathbf{u}_s + \mathbf{F}_s(\mathbf{x})\mathbf{d} \\ \mathbf{y} &= \mathbf{C}_t\mathbf{x} \end{aligned}$$

The non-zero elements of matrix $\mathbf{A}_t \in \mathbb{R} 18 \times 18$ are:

$$\begin{aligned} A_t(1,1) &= A_b(1,1), A_t(1,2) = A_b(1,2) \cdot V_x, A_t(1,7) = A_b(1,3), A_t(1,8) = A_b(1,4) \cdot V_x, A_t(1,11) = A_b(1,5), A_t(1,12) = A_b(1,6) \cdot V_x, A_t(1,15) = A_b(1,7), A_t(1,16) = A_b(1,8) \cdot V_x, A_t(2,1) = A_b(2,1)/V_x, A_t(2,2) = A_b(2,2), A_t(2,7) = A_b(2,3)/U_2, A_t(2,8) = A_b(2,4), A_t(2,11) = A_b(2,5)/U_3, A_t(2,12) = A_b(2,6), A_t(2,15) = A_b(2,7)/U_4, A_t(2,16) = A_b(2,8) \\ A_t(3,1) &= \psi_1, A_t(3,4) = 1, A_t(4,4) = -\frac{1}{\tau}, A_t(5,1) = 1, A_t(5,2) = l_{11}, A_t(5,3) = e_{21}, A_t(6,2) = 1 \end{aligned}$$

$$\begin{aligned}
A_t(7,1) &= A_b(3,1), A_t(7,2) = A_b(3,2)U_2, A_t(7,7) = A_b(3,3), A_t(7,8) = \\
&A_b(3,4)U_2, A_t(7,11) = A_b(3,5), A_t(7,12) = A_b(3,6)U_2, A_t(7,15) = \\
&A_b(3,7), A_t(7,16) = A_b(3,8)U_2, A_t(8,1) = A_b(4,1)/V_x, A_t(8,2) = A_b(4,2), A_t(8,7) = \\
&A_b(4,3)/U_2, A_t(8,8) = A_b(4,4), A_t(8,11) = A_b(4,5)/U_3, A_t(8,12) = \\
&A_b(4,6), A_t(8,15) = A_b(4,7)/U_4, A_t(8,16) = A_b(4,8)
\end{aligned}$$

$$A_t(9,3) = e_{22}, A_t(9,7) = 1, A_t(9,8) = -l_{ap2_2}, A_t(10,8) = 1$$

$$\begin{aligned}
A_t(11,1) &= A_b(5,1), A_t(11,2) = A_b(5,2)U_3, A_t(11,7) = A_b(5,3), A_t(11,8) = \\
&A_b(5,4)U_3, A_t(11,11) = A_b(5,5), A_t(11,12) = A_b(5,6)U_3, A_t(11,15) = \\
&A_b(5,7), A_t(11,16) = A_b(5,8)U_3, A_t(12,1) = A_b(6,1)/V_x, A_t(12,2) = \\
&A_b(6,2), A_t(12,7) = A_b(6,3)/U_2, A_t(12,8) = A_b(6,4), A_t(12,11) = A_b(6,5)/ \\
&U_3, A_t(12,12) = A_b(6,6), A_t(12,15) = A_b(6,7)/U_4, A_t(12,16) = A_b(6,8)
\end{aligned}$$

$$A_t(13,3) = e_{23}, A_t(13,11) = 1, A_t(14,12) = 1$$

$$\begin{aligned}
A_t(15,1) &= A_b(7,1), A_t(15,2) = A_b(7,2)U_4, A_t(15,7) = A_b(7,3), A_t(15,8) = \\
&A_b(7,4)U_4, A_t(15,11) = A_b(7,5), A_t(15,12) = A_b(7,6)U_4, A_t(15,15) = \\
&A_b(7,7), A_t(15,16) = A_b(7,8)U_4, A_t(16,1) = A_b(8,1)/V_x, A_t(16,2) = \\
&A_b(8,2), A_t(16,7) = A_b(8,3)/U_2, A_t(16,8) = A_b(8,4), A_t(16,11) = A_b(8,5)/ \\
&U_3, A_t(16,12) = A_b(8,6), A_t(16,15) = A_b(8,7)/U_4, A_t(16,16) = A_b(8,8)
\end{aligned}$$

$$A_t(17,3) = e_{24}, A_t(17,15) = 1, A_t(17,16) = -l_{ap2_4}, A_t(18,16) = 1$$

The non-zero elements of matrix $\mathbf{B}_t \in \mathbb{R} 18 \times 2$ are:

$$\begin{aligned}
B_t(4,1) &= \frac{1}{\tau}, B_t(1,2) = B_b(1,1) \cdot V_x, B_t(2,2) = B_b(2,1), B_t(7,2) = B_b(3,1)U_2, B_t(8,2) = \\
&B_b(4,1), B_t(11,2) = B_b(5,1)U_3, B_t(12,2) = B_b(6,1), B_t(15,2) = \\
&B_b(7,1)U_4, B_t(16,2) = B_b(8,1)
\end{aligned}$$

The non-zero elements of matrix $\mathbf{B}_s \in \mathbb{R} 18 \times 8$ are:

$$\begin{aligned}
B_s(1,1) &= B_b(1,2) \cdot V_x, B_s(1,2) = B_b(1,3) \cdot V_x, B_s(1,3) = B_b(1,4) \cdot V_x, B_s(1,4) = \\
&B_b(1,5) \cdot V_x, B_s(1,5) = B_b(1,6) \cdot V_x, B_s(1,6) = B_b(1,7) \cdot V_x, B_s(1,7) = \\
&B_b(1,8) \cdot V_x, B_s(1,8) = B_b(1,9) \cdot V_x, B_s(2,1) = B_b(2,2), B_s(2,2) = B_b(2,3), B_s(2,3) = \\
&B_b(2,4), B_s(2,4) = B_b(2,5), B_s(2,5) = B_b(2,6), B_s(2,6) = B_b(2,7), B_s(2,7) = \\
&B_b(2,8), B_s(2,8) = B_b(2,9)
\end{aligned}$$

$$\begin{aligned}
B_s(7,1) &= B_b(3,2)U_2, B_s(7,2) = B_b(3,3)U_2, B_s(7,3) = B_b(3,4)U_2, B_s(7,4) = \\
&B_b(3,5)U_2, B_s(7,5) = B_b(3,6)U_2, B_s(7,6) = B_b(3,7)U_2, B_s(7,7) = \\
&B_b(3,8)U_2, B_s(7,8) = B_b(3,9)U_2, B_s(8,1) = B_b(4,2), B_s(8,2) = B_b(4,3), B_s(8,3) = \\
&B_b(4,4), B_s(8,4) = B_b(4,5), B_s(8,5) = B_b(4,6), B_s(8,6) = B_b(4,7), B_s(8,7) = \\
&B_b(4,8), B_s(8,8) = B_b(4,9)
\end{aligned}$$

$$\begin{aligned}
B_s(11,1) &= B_b(5,2)U_3, B_s(11,2) = B_b(5,3)U_3, B_s(11,3) = B_b(5,4)U_3, B_s(11,4) = \\
&B_b(5,5)U_3, B_s(11,5) = B_b(5,6)U_3, B_s(11,6) = B_b(5,7)U_3, B_s(11,7) = \\
&B_b(5,8)U_3, B_s(11,8) = B_b(5,9)U_3, B_s(12,1) = B_b(6,2), B_s(12,2) = \\
&B_b(6,3), B_s(12,3) = B_b(6,4), B_s(12,4) = B_b(6,5), B_s(12,5) = B_b(6,6), B_s(12,6) = \\
&B_b(6,7), B_s(12,7) = B_b(6,8), B_s(12,8) = B_b(6,9)
\end{aligned}$$

$$\begin{aligned}
B_s(15,1) &= B_b(7,2)U_4, B_s(15,2) = B_b(7,3)U_4, B_s(15,3) = B_b(7,4)U_4, B_s(15,4) = \\
&B_b(7,5)U_4, B_s(15,5) = B_b(7,6)U_4, B_s(15,6) = B_b(7,7)U_4, B_s(15,7) =
\end{aligned}$$

$$\begin{aligned}
&B_b(7,8)U_4, B_s(15,8) = B_b(7,9)U_4, B_s(16,1) = B_b(8,2), B_s(16,2) = \\
&B_b(8,3), B_s(16,3) = B_b(8,4), B_s(16,4) = B_b(8,5), B_s(16,5) = B_b(8,6), B_s(16,6) = \\
&B_b(8,7), B_s(16,7) = B_b(8,8), B_s(16,8) = B_b(8,9)
\end{aligned}$$

The non-zero elements of matrix $\mathbf{F}_s \in \mathbb{R}^{18 \times 1}$ are:

$$F_s(6,1) = -V_x, F_s(10,1) = -U_2, F_s(14,1) = -U_3, F_s(18,1) = -U_4,$$

$\mathbf{C}_t = \mathbf{I}_{18 \times 18}$ is the identity matrix.